MEASURING ACID GENERATION KINETICS IN PHOTORESIST FILMS VIA CAPACITANCE TECHNIQUES

A Thesis

Presented to

The Academic Faculty

by

Cody M. Berger

In Partial Fulfillment

Of the Requirements for the Degree

Doctor of Philosophy in Chemical Engineering

Georgia Institute of Technology

August, 2004

MEASURING ACID GENERATION KINETICS IN PHOTORESIST FILMS VIA CAPACITANCE TECHNIQUES

Approved:

Clifford L. Henderson, Chair

Jeffrey D. Byers

Dennis W. Hess

Carson J. Meredith

Stephen E. Ralph

DATE APPROVED: August 17, 2004

ACKNOWLEDGEMENTS

Over the course of the past four years, numerous individuals have contributed to this work and have had an impact on my life both professionally, and personally. For their efforts, and for making the last four years as enjoyable as they were, I would like to say thank you. I would like to express my gratitude to my thesis advisor Dr. Clifford L. Henderson for his constant support and advice, and for giving me the freedom to pursue projects and ideas that I found interesting during my stay at Tech. I enjoyed the occasional golf outings tremendously and look forward to the day when my game improves enough that I can give him a true challenge on the course! I would also like to thank the other members of my thesis committee for their support and useful advice: Dr. Jeffrey Byers, Dr. Dennis Hess, Dr. Carson Meredith, and Dr. Stephen Ralph. In addition, I would like to particularly thank Dr. Jeffrey Byers and Danny Miller for their help with the interdigitated electrode sensors used in this work. Dr. Byers and Danny designed and fabricated all of the sensors used in this work and have provided countless pieces of useful information regarding them.

I would like to thank Dr. Paul Roman and Chris Huntley of DuPont/EKC Technology, Inc. for providing wonderful cross section SEM micrographs of the sensors used in this work. Many thanks are also due to Dr. Rosario Gerhardt of the School of Materials Science and Engineering at Georgia Tech for her helpful discussions of impedance spectroscopy as well as Dr. Laren Tolbert of the School of Chemistry & Biochemistry at Georgia Tech for his help with the conductivity mechanisms in polymer films.

I have been especially blessed in having met and worked with a tremendous group of graduate and undergraduate students during my stay here at Georgia Tech. I would like to thank all past and present members of the Henderson research group for their constant support. I would like to thank Kendra McCoy for helping me with QCM studies and Trevor Hoskins for suffering through a week of helping me disassemble, move, and reassemble our group cleanroom. I would like to thank Amy Meyers for her help with NMR spectroscopy. I would also like to express my gratitude for the help given to me by our undergraduate assistant, Abimbola Bolagun. Her help with synthesizing the THP protected polymers used in this work was invaluable. I also can't forget to mention the numerous friends who have helped make the stay here more enjoyable: Chris Timmons, Chris Moore, Brian White, and Mike Mckittrick. You guys provided countless laughs on the golf course, softball field, or at the lunch table, and I will always appreciate your friendship.

Last, but not least, I would like to thank my family for their unwavering support. I would like to thank my parents and sister for all they have done for me (too many things to list here!). I would also like to thank my in-laws for their constant love and support. Finally, I would like to express my utmost appreciation to my wife of five years Julie. I want to thank you for your constant love and support, and for showing extraordinary patience and understanding during the past four years. In addition, I want to thank you for giving me the best gift of all while in Atlanta, our little boy Micah. The joys of having you two around to be with have helped me make it through this last, very difficult year more than you will ever know!

TABLE OF CONTENTS

LIST OF TABLES

LIST OF FIGURES

LIST OF ABBREVIATIONS

AC – alternating current

C – Dill's C parameter

CAR – chemically amplified photoresist

CEE – Cost Effective Equipment

CMOS – complimentary metal-oxide semiconductor

CPE – constant phase element

DBU - 1,8-diazabicyclo[5.4.0]undec-7-ene, 3-piperidino-1,2-propanediol

DC – direct current

DNQ – diazonapthoquinone

DOF – depth of focus

DUV – deep ultraviolet

FTIR – Fourier transform infrared red

HF – hydrofluoric acid

HFAPNB – bis-trifluoromethylcarbinol substituted poly(norbornene)

HND-Nf – N-hydroxy-5-norbornene-2,3-dicarboximide perfluoro-1-butanesulfonate

H-NMR – proton nuclear magnetic resonance

IC – integrated circuit

IDE – interdigitated electrode

IS – impedance spectroscopy

KTFR – Kodak thin film resist

LCR – inductance, capacitance, resistance meter

LW – line width (resolution)

M_w – weight average molecular weight

NA – numerical aperture

NMOS – negative channel metal oxide semiconductor

NMR – nuclear magnetic resonance

PAC – photoactive compound

PAG – photoacid generator

PEB – post exposure bake

PGMEA – propylene glycol methyl ether acetate

PHOST – poly(hydroxystyrene)

PMOS – positive channel metal oxide semiconductor

QCM – quartz crystal microbalance

SEM – scanning electron microscope

SSE – sum squared errors

TBAH – tetrabutylammonium hydroxide

TBI-Nf – bis(4-tert-butylphenyl)iodonium perfluoro-1-butanesulfonate

TBI-Tf – bis(4-tert-butylphenyl)iodonium triflate

t-BOC – tert-butyloxycarbonyl

THP – tetrahydropyranyl

TMAH – tetramethylammonium hydroxide

TPS-Nf – triphenylsulfonium perfluoro-1-butanesulfonate

TPS-Tf – triphenylsulfonium triflate

UV - ultraviolet

SUMMARY

Chemically amplified photoresists (CARs) have served as the workhorse resist chemistry platform for the semiconductor industry for over a decade now, and all signs appear to indicate that the CAR platform will continue to serve this role well into the future. Chemically amplified photoresists transfer an image using a two-step processing sequence. First, the photoresist film is exposed to ultraviolet light. During this exposure a photoacid generator (PAG) molecule decomposes and forms a strong acid within the resist film. In the second step, the acid loaded resist film is baked at elevated temperatures in a process known as the post exposure bake (PEB). During the bake, the acid catalyzes a deprotection reaction where a protecting group on the resist's polymer matrix is removed. Prior to removal of the protecting group, the resist polymer is typically insoluble in aqueous base developer. Following deprotection, the resist becomes soluble in the developer. This solubility switch is what enables a CAR to form a latent image of the desired feature.

The work presented in this thesis focuses on our efforts to develop a new technique for characterizing what has traditionally been one of the more difficult aspects of CAR behavior to understand, the generation of photoacid from a PAG during exposure. This new technique utilizes capacitance measurements from resist coated interdigitated electrode (IDE) sensors as a mean for monitoring the production of photoacid during exposure. In this technique, the resist coated IDE is exposed to small, incremental doses of UV energy to generate small amounts of photoacid. Following each exposure dose, a capacitance measurement is made. Because the net dielectric properties

of the photoresist film have changed due to the presence of increasing amounts of photoacid, the capacitance measured from the IDE also changes after each exposure. By properly analyzing the capacitance versus exposure dose data, the kinetic rate constant that describes photoacid formation (also known as the Dill C parameter) can be calculated.

The work presented in this thesis is divided into four major areas. In the first area of work, external factors that could potentially complicate the analysis of the IDE capacitance data were examined. This involved studying three separate items. First, the spin coating capabilities of the IDE sensors used in this work were examined through SEM cross-section micrographs. Second, the effects of amine contamination from the environment were eliminated by the construction of a class 1000 "base-free" cleanroom. Finally, the effects of relative humidity upon the water sorption properties of photoresists were examined through quartz crystal microbalance studies.

The second area of work presented in this thesis focuses on the development of the measurement procedure and data analysis technique needed to obtain the Dill C parameter from IDE capacitance measurements. First, the sensitivity of the IDE sensors to photoacid was examined. Second, a means for relating photoacid concentration to IDE capacitance was determined. Third, an iterative technique was developed for calculating the Dill C parameter that is based upon fitting a model capacitance versus exposure dose curve to the experimentally obtained curves using the C parameter as the sole fitting function. Next, a means for dealing with non-homogeneous photoacid distributions was developed that utilizes a multiple thin layer approach. Finally, the appropriate optical

model for use in calculating the exposure intensity versus depth in the resist film coating an IDE was determined.

Once the basic measurement technique was developed, the next area of work focused on improvements to the technique. Two major improvements are discussed. First, the use of measurement frequency as a means for improving the capacitance response of the IDE sensor was examined. Second, a technique for normalizing the raw capacitance data that offers tremendous advantages over the original version of the IDE technique is derived and discussed.

Finally, in the last chapter of work, the ability of the IDE Dill C measurement technique to function properly in the face of two potentially troubling variables introduced by commercial photoresists is examined. First, the ability of the IDE technique to measure the Dill C parameter in a base loaded CAR film is examined. Then, the effects of low and high activation energy protecting groups upon the IDE technique are examined.

CHAPTER 1

INTRODUCTION TO MICROELECTRONICS AND MICROLITHOGRAPHY

1.1 Introduction

Merriam-Webster's dictionary defines microelectronics as, "1. A branch of electronics that deals with the miniaturization of electronic circuits and components 2. Devices, equipment, or circuits produced using the methods of microelectronics". Over the past four decades, few industries (if any) have had as significant, and as broad an impact upon global society as the microelectronics industry. In addition, few industries have experienced development and improvement at a similarly rapid pace as that experienced by the microelectronics industry.

Prior to 1947, electronic devices were composed of large, cumbersome vacuum tubes that consumed large quantities of power, produced large quantities of heat, and in general, were not very efficient. In 1947, the problems associated with using vacuum tubes were solved when Bardeen, Brattain, and Shockley demonstrated the world's first transistor at Bell Labs[1-3]. Composed of a small piece of germanium, the transistor invented by these researchers was much smaller and easier to work with than the bulky vacuum tubes, and could be more easily incorporated into electronic circuits. Despite the many advantages that the transistor provided over vacuum tubes, the problems associated with trying to greatly increase circuit feature density and performance remained. Each of the electronic circuit's components were still discrete in nature and had to be attached to the circuit individually using soldering techniques. Connecting hundreds or thousands of these discrete components to an electronic circuit using such techniques was extremely time consuming. Additionally, each of the thousands of solder joints used to connect the

devices were susceptible to mechanical fatigue that could eventually lead to device failure.

In 1960 Jack Kilby and Robert Noyce solved many of these problems and sparked the beginnings of the microelectronics industry as we know it today with their invention of the monolithic integrated circuit[4,5]. This invention allowed for a dramatic increase in device feature density (and as a result increased complexity and functionality) that was previously unthinkable. Unlike previous circuits that relied on discrete components, the monolithic integrated circuit contained all of the necessary components (passive and active) on a single piece of semiconductor material, such as silicon or germanium. Now capacitors, inductors, and transistors were all created on the same piece of silicon and did not have to be individually soldered to the circuit. Only a few connections from the integrated circuit to the outside world were necessary.

The principles and ideas upon which Kilby and Noyce's integrated circuit was created are still the foundation upon which nearly all integrated circuits created today are based, though the devices themselves are hardly comparable due to the extraordinary achievements that have been made in terms of shrinking device sizes to improve performance. Some of the first integrated circuits created in the early 1960's contained minimum feature widths on the order of tens of microns with only a handful of components per IC[5]. Today's top of the line devices have minimum feature widths of 90 nm (0.09 microns) and millions of components per IC. In addition, efforts are already well underway to develop materials and processes that would enable the production of devices with 65 nm, 45 nm, and even 32 nm minimum feature sizes[6].

What started as a simple laboratory experiment and demonstration of the world's first integrated circuit over four decades ago at Texas Instruments has now grown to monstrous proportions, with the microelectronics industry enjoying over 166 billion dollars in sales last year world-wide[7]. From complex military weaponry to satellite communications, to things as simple as a clock-radio, the impact of integrated circuits and microelectronic devices is far reaching and easy to see. With continued advances in science and technology, as well as a continued decrease in the cost of computers and other electronics devices, the proliferation of computers, the internet, and electronics in general shows no signs of stopping, meaning the microelectronics industry will only continue to grow in size, importance, and global impact in the years to come.

1.2 Microelectronic Device Fabrication

At the heart of nearly all integrated circuits lies the simple transistor. A transistor is a device in which the flow of electrons from one region to a second region is controlled by the voltage applied to a third intermediate region. When constructed in a semiconductor such as silicon, a transistor consists of two like-doped regions of silicon separated by a region of opposite doping type[5,8]. Figure 1.1 illustrates the structure of a simplified transistor in silicon.

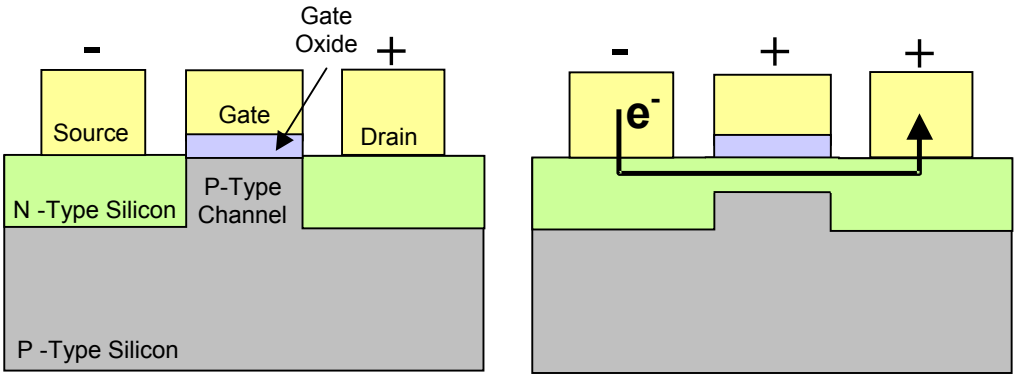

Figure 1.1 Basic configuration of an (a) transistor with no applied gate potential or current flow (OFF) and (b) transistor with a positive gate potential allowing current to flow from source to drain (ON).

As shown in the figure, two like-doped regions of silicon create the source and drain regions. In this case, these two regions are composed of n-type silicon where an excess of electrons are present to carry charge. The region separating the source and drain, the channel region, is composed of silicon with the opposite doping type. In this case, the channel is composed of p-type silicon where an excess of holes are present. Because the channel region has a different doping type than the source and drain, it is virtually impossible for current to flow from the source to the drain when a potential is applied across these two regions. Electrons flowing from the source collide with holes in the channel region and combine, eliminating their ability to carry charge. However, if a positive potential is now applied to the gate structure directly above the p-type channel region, holes are repelled and electrons are attracted to the channel becoming the majority carrier. Thus, a path consisting of excess free electrons as the majority charge carriers now exists from the source to the drain. Now, electrons (and hence current) can easily

flow from source to drain and the transistor is said to be on. By varying the dopant types and potentials applied, as well as combining NMOS and PMOS devices, it is possible to create the structures necessary to perform various logic operations.

As shown in Figure 1.1, many processing steps are required to create the structures necessary for a working transistor. Beginning with a bare silicon substrate, dopants are first introduced into the silicon to create the regions that will serve as source, drain, and channel. Next, an insulating material, such as silicon dioxide, is deposited to isolate the substrate from the gate contact and other conducting lines. Contact holes are then etched through the silicon dioxide so that conducting wires may make electrical contact with the source and drain. Finally, metal or highly doped polysilicon is deposited and etched to form the tiny wires used for applying potentials to the source, drain, and gate structures.

The processing steps discussed in the previous paragraph are often associated with what is known as "front end" processing, referring to any processing steps associated with the direct construction of the transistor itself. In an actual integrated circuit fabricated today, millions of transistors will reside on a single silicon chip. These individual transistors must be connected to one another in order to perform the various logic functions that are desired. The processing steps utilized to connect the individual transistors to one another and to bond pads connecting them to the outside world are often associated with "back end" processing. Though the exact point at which an integrated circuit is considered to have moved from "front end" to "back end" processing varies slightly from one manufacturer to another, the general ideas discussed here hold true. Figure 1.2 depicts a cross section of a more complete integrated circuit,

demonstrating the concepts of “front end” and “back end” processing, as well as the many layers of conductors, insulators, and passivation that must be deposited and patterned to create a working device.

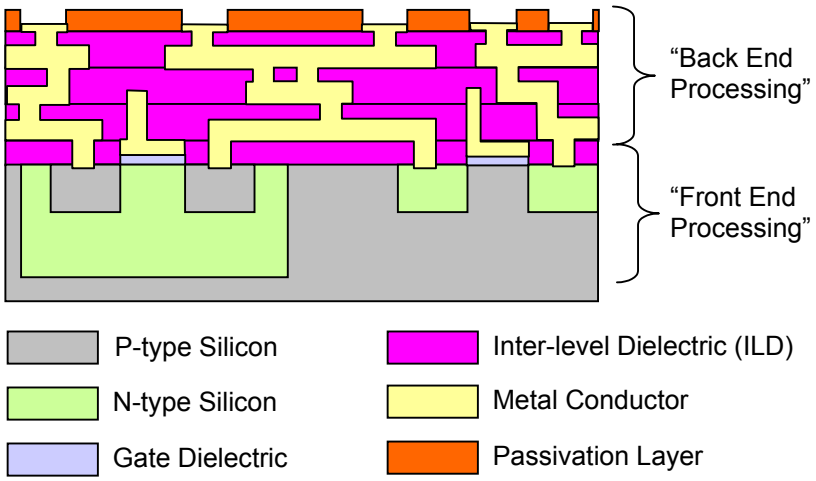

Figure 1.2 Cross section of a greatly simplified CMOS device depicting the multi-layered approach required to construct a functioning integrated circuit.

As can be seen in Figure 1.2, a completed integrated circuit is composed of numerous thin films. Each of these films (be it conductor, insulator, passivation, or even the doped regions) must be individually patterned to create the feature shapes necessary to form a working device. In a typical modern device, as many as nine separate layers of metal lines may be required to properly connect each of the transistors and form the desired circuit configuration. Each of these layers of metal must have a dielectric material deposited on and around them to isolate them from neighboring lines. In addition, each layer of dielectric must have small holes (known as vias) etched through them to allow one level of metal to reach the next. The end result of requiring so many thin films for a

working device is that as many as 25 to 30 (or more) separate patterning steps are required to create the device features from these thin films. The patterning process utilized to create circuit features from the various thin films is known as microlithography, and will be discussed in detail in the next section.

1.3 Microlithography

The process used to pattern the various thin films and doped regions used to construct an integrated circuit is known as microlithography[5,8]. This process utilizes a radiation sensitive polymer in order to create the image of a desired feature shape, and then transfers this image to the underlying thin film through a removal method such as plasma etching. Figure 1.3 below summarizes the basic processing steps involved with microlithography.

As shown in Figure 1.3, the first step in microlithography is to coat a radiation sensitive polymer thin film known as a photoresist onto the film that is to be patterned. Typically the photoresist is applied to this thin film via a spin coating process. The photoresist polymer and sensitizer molecules are first dissolved in an appropriate casting solvent (such as ethyl lactate, or propylene glycol methyl ether acetate (PGMEA)). The resulting solution is then applied to the sample and spun at a very high angular velocity. The centrifugal forces that result from the spinning motion cause the photoresist solution to spread out evenly across the sample's surface and create a relatively uniform thin film. A subsequent bake process known as the post apply bake removes most residual casting solvent from the resist film.

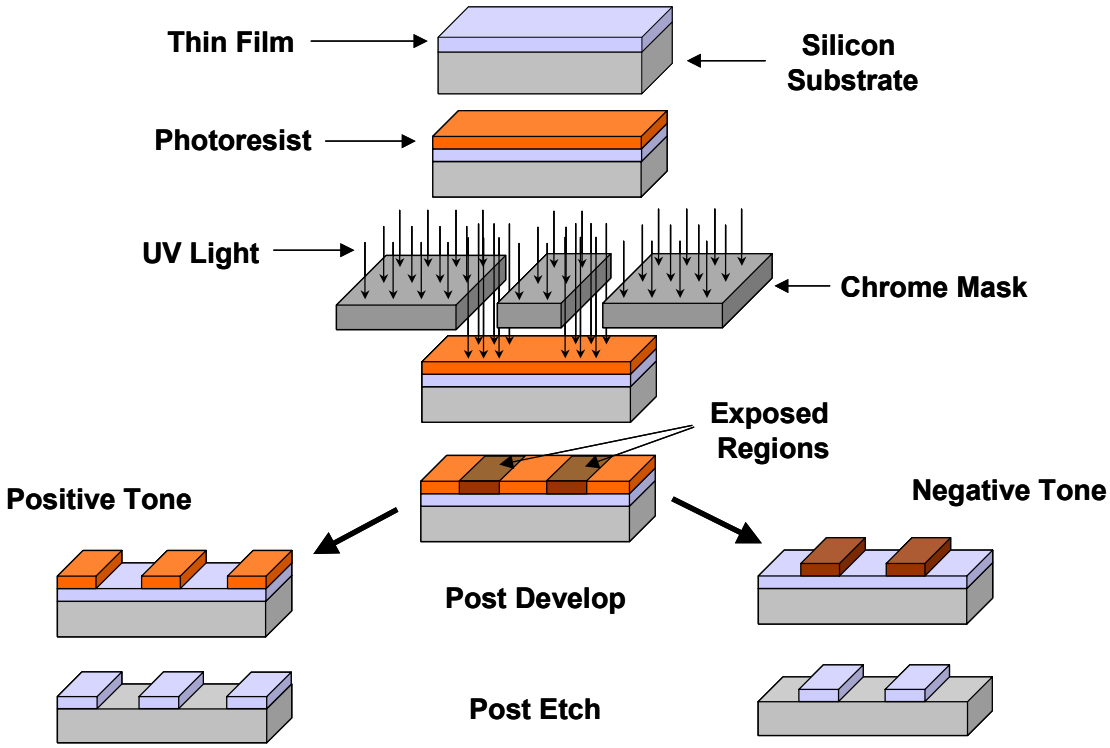

Figure 1.3 The basic processing steps utilized in microlithography.

Once the photoresist film has been properly applied to the sample's surface, the next step in microlithography is to expose the photoresist to a source of radiation to create a latent image of the desired pattern. In most high throughput manufacturing processes, the radiation is typically in the form of ultraviolet (UV) light, with most modern devices fabricated using 248 nm or 193 nm wavelength UV light. A thin, transparent plate known as a photomask (or reticle if the exposure tool is a step and repeat system) is utilized to create the pattern on the photoresist surface. This plate arrives from its manufacturer with certain portions of it coated with an opaque material (such as chromium) that blocks certain regions of the exposure radiation so that only those regions of the photoresist in the shape of the desired image are allowed to receive the exposure energy. In the process diagram shown in Figure 1.3, the photomask is designed to create the image of two lines in the photoresist film.

When the exposure radiation strikes the photoresist film, a wide variety of actions can take place to cause the solubility switch necessary for image formation, depending upon the type of photoresist that is being utilized. If the system is using a negative tone resist, the areas that are exposed to radiation become insoluble in the developer solution. Typically, these types of resists rely on cross linking, or some other means of network formation to render the resist insoluble. When the resist is exposed, the resist polymer either directly cross links, or a sensitizer is activated and catalyzes a cross linking reaction that renders the polymer matrix insoluble. If the resist system utilized is positive tone in nature, then the areas that are exposed become soluble in developer solution and are selectively removed during the development process. Typically with positive tone

systems some form of sensitizer is activated upon exposure that goes on to render the polymer matrix soluble. Often times these sensitizers act as dissolution inhibitors prior to exposure (such as in a diazonaphthoquinone/novolac system), but then do not affect, or even accelerate dissolution following exposure[5]. Other positive tone systems (such as chemically amplified photoresists) contain a sensitizer that generates a catalyst molecule upon exposure. In this case, acid is produced upon exposure that goes on to catalyze a deprotection reaction that renders the matrix polymer soluble[5].

Following the exposure and switching of the resist matrix's solubility, the resist film and sample are processed through a development sequence. In this process, a liquid developer is applied to the sample and the areas of the resist film that are now soluble in the developer are selectively removed, exposing the underlying thin film to the ambient environment. A variety of solvents have served as developer solutions in the past, while more recently, aqueous base (such as tetramethylammonium hydroxide TMAH) solutions have served as the developer of choice.

Once the resist has been properly developed, and the regions of the underlying thin film that are to be removed are now exposed, the final step in microlithography involves using a subtractive method known as etching to remove the unwanted regions of the underlying thin film. Etching can be performed using a "wet" process where the sample is immersed into a liquid etchant, such as an acid solution, or it can be performed via a "dry" process where an ionized gas, or plasma is utilized to remove the unwanted film[8]. In either case, the photoresist film serves as a protective barrier to the regions of the film that are supposed to remain on the sample while the liquid or dry etchant attacks and removes the unprotected regions. Following the etch process, the photoresist is

removed via a liquid solvent bath, or through a dry, O_2 plasma process known as ashing. The patterned sample then moves on to the next processing step, where yet another thin film is deposited and patterned using microlithography. This process of film deposition and patterning is repeated until the integrated circuit is complete, often times requiring 25 to 30 microlithography sequences, or mask levels.

The description of the microlithography process in the preceding paragraphs is somewhat generalized to give the reader a good understanding of the basic processing steps needed to pattern an integrated circuit. In reality, each of the processing steps discussed (spin coating, baking, exposure, development, etch, resist removal) are incredibly complex and a great deal of effort has been expended in attempts to understand each. The photoresist materials themselves are no exception. A wide variety of resists tailored to respond to exposure and affect solubility in many different ways have been developed. A survey of the types of resists utilized in the microelectronics industry, as well as a thorough description and discussion of the photoresist class that is the subject of the work presented in this thesis, chemically amplified photoresists, is presented in the next chapter.

CHAPTER 2

INTRODUCTION TO PHOTORESISTS

2.1 A Brief History of Photoresists

In 1826, Joseph Niepce managed to create what is thought to be the world's first known photograph[9] and in doing so became the first individual to demonstrate the concept of photosensitive materials. Niepce created his photograph by coating a pewter plate with a petroleum residue known as "bitumen of Judea", a tar-like substance that has been recovered in large chunks from the Dead Sea since ancient times. He discovered that if he exposed this coated plate to an image of his courtyard for an extended period of time (over 8 hours in this case!) the exposed regions would become less soluble in a solution of lavender oil and white petroleum. Thus by exposing his resin coated pewter plate to an image of his courtyard and then developing it in the aforementioned solution, Niepce was able to create a relief image of his courtyard on the plate's surface. Figure 2.1 illustrates the image captured by Joseph Niepce's bitumen of Judea system.

Following the work of Joseph Niepce, the next major advancement in photosensitive materials occurred in 1850 when an Englishman by the name of William Henry Fox Talbot created the first practical photoresist system consisting of ammonium dichromate in a gelatin material[9]. This "photoresist" was easily cast into thin films from water and was water developable following exposures. This system was orders of magnitude more sensitive to light exposure than Niepce's bitumen of Judea systems, and was so successful at transferring images Talbot was awarded one of the first British patents (No. 565) for his invention in 1852. In the late 1800's and early 1900's the

Figure 2.1 Courtyard image captured by Joseph Niepce, the world's first photograph (reprinted with permission from: Harry Ransom Humanities Research Center, The University of Texas at Austin).

printing industry grew dramatically and during these years dichromated gelatins continued to serve as the primary image transfer material for creating printing plates made of metal or stone.

When workers at Bell Laboratories attempted to make the first integrated circuits in the early to mid 1950's they, too, turned to dichromated gelatins as their choice of imaging material[9]. These materials were readily available and had been used extensively for the previous century in the printing industry. Unfortunately, these researchers soon discovered that the strong hydrofluoric acid etches used in their processing sequence destroyed the gelatins and left little or no structure in the circuit. In addition, considerable "dark reactions" occurred where the gelatin began to slowly crosslink in the

presence of the dichromate even when not exposed. To solve these problems the Bell workers turned to Louis Minsk of the Eastman Kodak Research Laboratory. Minsk created a resist composed of poly(vinylcinnamate), as shown in Figure 2.2[5,9].

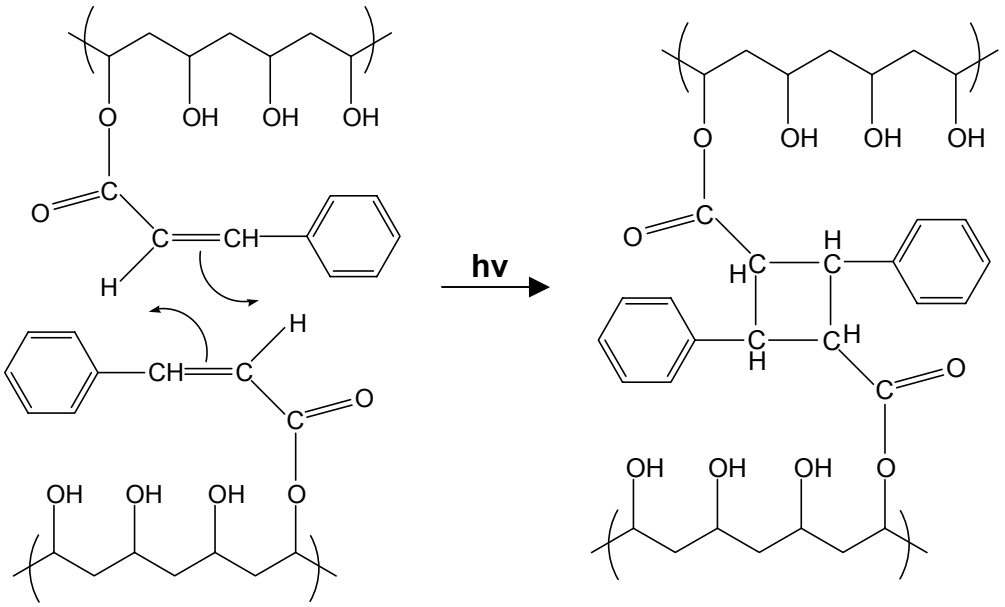

Figure 2.2 Poly(vinylcinnamate) based resist system created by Louis Minsk.

Upon exposure to UV light the cinnamoyl groups dimerize and form a cross-linked network of polymer chains. In the cross-linked regions of the resist the polymer is insoluble in a developer solution. In the uncross-linked regions the polymer is quite soluble. Minsk essentially created one of the very first negative-tone photoresists. The poly(vinylcinnamate) was very sensitive to light, withstood the harsh conditions imposed by HF etching, and in addition, the cinnamoyl groups were not susceptible to any dark reactions, making the poly(vinylcinnamate) based resist quite stable during storage. Unfortunately, the thin films of poly(vinylcinnamate) experienced problems with

adhesion to the silicon dioxide films that are critical to the construction of an integrated circuit. In order to create high quality, functional devices, a means of improving the adhesion of the poly(vinylcinnamate) resist to SiO_2 had to be found, or an alternate resist chemistry had to be developed. Though work was poured into improving the poly(vinylcinnamate)'s adhesion, the latter approach was eventually taken and resulted in the first true workhorse resist system of the microelectronics industry – the Kodak Thin Film Resist, or KTFR for short[5,9,10].

The creation of the Kodak Thin Film Resist is credited to two gentlemen working at Kodak at the time – Martin Hepher and Hans Wagner. The resist chemistry they developed consisted of a bis(arylazide) sensitizer dispersed in a cyclized poly(cis-isoprene) rubber. Figure 2.3 below illustrates the generic structures used.

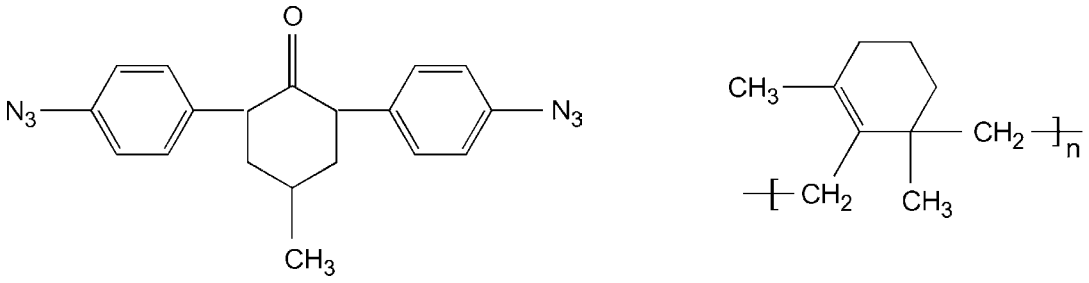

(a) (b)

Figure 2.3 (a) Typical bis(arylazide) sensitizer and (b) cyclized poly(cis-isoprene) matrix

The bis(arylazide) sensitizer has a strong absorption peak centered at approximately 360 nm wavelength light. Thus, these particular sensitizers are highly sensitive to the I-line (365 nm) mercury lamp emission line. Upon exposure to 365 nm UV light, the arylazide group will become excited and N_2 is removed, leaving behind an extremely reactive nitrene intermediate. This reactive species can undergo a variety of other reactions, including insertion into the double bond located on the cyclized poly(cis-isoprene). Because insertion into double bonds can take place on both ends of the bis(arylazide), the result of exposure is a highly crosslinked poly(cis-isoprene) network. The un-networked rubber matrix that was previously soluble in non-polar organic solvents is now crosslinked and quite insoluble. This solubility switch upon exposure is of course what makes the KTFR system capable of transferring an image. As mentioned earlier, the KTFR resist system served as the first true "work horse" resist platform for the microelectronics industry and served this function well from 1957 until around 1972 when the features printed on an integrated circuit reached the resolution limit of KTFR, around 2 microns.

As KTFR's usefulness declined it became necessary for lithographers to search for a new resist material with even better resolution capabilities[5,9,10]. The search ended with the Kalle Corporation (later Hoescht AG) in Germany. In the early 1900's a German monk by the name of Gustav Kogel had been assigned the tedious task of duplicating by hand hundreds of medieval documents from the library in his monastery's basement. Needless to say, Gustav grew tired of painstakingly copying each document by hand. After a great deal of experimentation he discovered that if he coated the blank papers

with a specific diazonium salt manufactured by the nearby Kalle Corporation he could duplicate the documents utilizing sunlight as his exposure source. Gustav continued working with the Kalle chemists and together they developed a refined duplication process whose principles are still used today to create engineering blue prints.

In the 1930's and 1940's Kalle continued research into the usefulness of diazonium salts under the guidance of Otto Suss. They began to look at utilizing a form of diazonium salt known as diazonapthoquinones (DNQ). To serve as a matrix material for the photoresist the Kalle chemists began looking at a novolac resin produced by the Albert Chemical Company, ironically, just across the street from the Kalle Corporation. Suss and his chemists combined the photosensitive DNQ molecules with the novolac matrix to produce the first DNQ-Novolac resist system, a positive-tone system. Figure 2.4 below demonstrates the basic components of a DNQ-Novolac resist system.

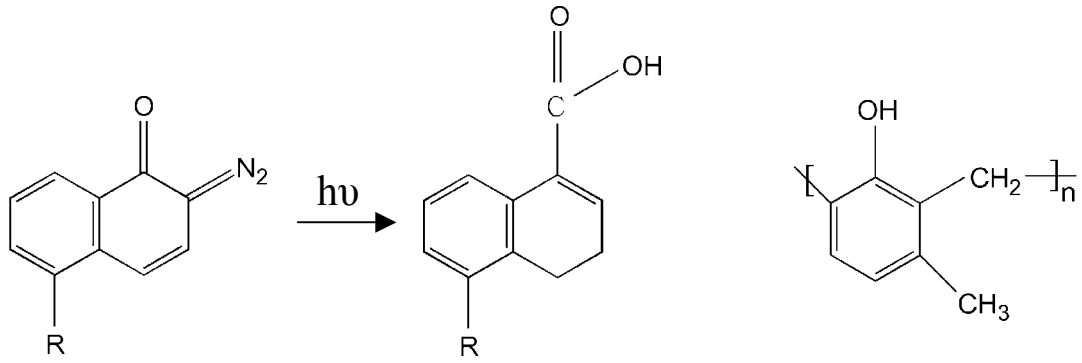

(a) (b)

Figure 2.4 (a) Generic structure of a diazonapthoquinone (DNQ) sensitizer and (b) novolac matrix polymer.

By itself, the novolac resin utilized in DNQ-Novolac systems is quite soluble in aqueous base developer solutions. However, the addition of 10 to 20 wt% DNQ to the novolac matrix causes the resist to dissolve orders of magnitude more slowly in aqueous base solution than the novolac matrix alone[5,10]. Upon exposure, these dissolution characteristics can be altered. When the DNQ molecule is exposed to UV light, the absorption of photons excites the molecule and results in the evolution of nitrogen, forming a reactive carbene intermediate. This carbene intermediate rearranges to form a ketene which further reacts with trace amounts of water within the resist film to form a carboxylic acid. The carboxylic acid group renders the DNQ (and thus the DNQ-Novolac system) soluble in aqueous base solution, creating the solubility switch necessary to form an image.

DNQ-Novolac resist systems provide many advantages over their predecessors including increased resolution capabilities and decreased swelling during development. These systems served as the workhorse resist platform for nearly a quarter century, from 1972 until the early to mid 1990's when chemically amplified resists began seeing increased use in production lines. DNQ-Novolac resist systems are still being used in many applications today.

2.2 Chemically Amplified Photoresists (CARs)

From the invention of the first integrated circuit in 1960, the driving force behind lithography innovation has ultimately been the desire to print smaller and smaller features so that device feature density can be increased and allow for increased device performance at a lower cost. It was this desire that led to the replacement of the KTFR

resist system in 1972 by the DNQ-Novolac system, and it was this desire that ultimately led to the creation of chemically amplified photoresists (CARs) as a replacement for the DNQ-Novolac systems.

The absolute minimum feature size that an be resolved with a particular photolithography system is termed the resolution, and is described by the following equation for an array of lines and spaces of equal width[5]:

$$LW = \frac{k_1 \lambda}{NA} \qquad [2.1]$$

Here LW refers to the minimum line width that can be resolved, λ refers to the wavelength of the exposure source radiation, NA refers to the numerical aperture of the exposure lens system, and k_1 refers to a process constant that depends on the specific resist technology that is being applied, such as the specific resist materials used, the exposure techniques used (such as off-axis illumination, etc.), and the masking techniques used (such as optical proximity correction, phase shifting masks, etc.). Traditionally, the two most common ways to reduce the resolution have been to shrink the exposure wavelength or to increase the numerical aperture. However, doing so does not come without a cost. In order to print a high quality line within a specified critical dimension tolerance, it is important that the line's image projected into the resist film from the photomask remain in focus throughout the thickness of the resist film. Of course, the true image focal point lies within a single plane within the resist film and the quality of the image decreases as one moves away from this focal point. Fortunately,

there is usually a small distance on either side of the focal point where the image will still meet specifications. This distance on either side of the focal point where the projected image is still focused (within specified tolerances) is referred to as defocus tolerance, or depth of focus (DoF) and is described by equation 2.2[5]:

$$DoF = \pm \frac{k_2 \lambda}{NA^2} \qquad [2.2]$$

Here k_2 is again a constant associated with the specific resist and exposure system being used while λ and NA are used as defined previously for the resolution relationship. It is desirable to have as large a depth of focus as possible. A large depth of focus means that a thick resist film can be used and still have a focused image within it. If the depth of focus shrinks, a thinner resist film must be used. The lithographer must then be concerned with issues such as etch resistance as the thinner film may not provide an adequate barrier against plasma or wet etch processes.

Examination of equation 2.2 makes it easy to see the cost that one pays for decreasing resolution by decreasing wavelength or increasing numerical aperture. Performing both activities results in a corresponding decrease in the depth of focus. However, because of the power of 2 dependence upon numerical aperture, increasing numerical aperture has a more significant detrimental effect upon depth of focus. For this reason, and because numerical aperture has a physical limit in an air-based projection lens system of 1.0 (efforts aimed at developing immersion lithography techniques are attempting to change this), the typical path taken to minimize resolution has been to shrink the exposure wavelength. This has been the trend in recent years and the reason

for moving into the deep - UV exposure region (240 - 260 nm light) from the mid - UV region (300-365 nm). The industry is now moving to 193 nm lithography for this same reason and may possibly consider moving to 157 nm lithography in the future[9].

When lithographers moved from 365 nm exposure sources to 248 nm sources, a new problem was soon encountered. The traditional mercury lamp sources that had been used in nearly all 365 nm stepper systems simply did not provide a high enough emission output at 248 nm to be useful in a manufacturing process[5,10,11]. Figure 2.5 illustrates the emission spectrum from a mercury arc lamp used in a common 365 nm stepper tool, illustrating the much lower intensity provided at 248 nm wavelength[5].

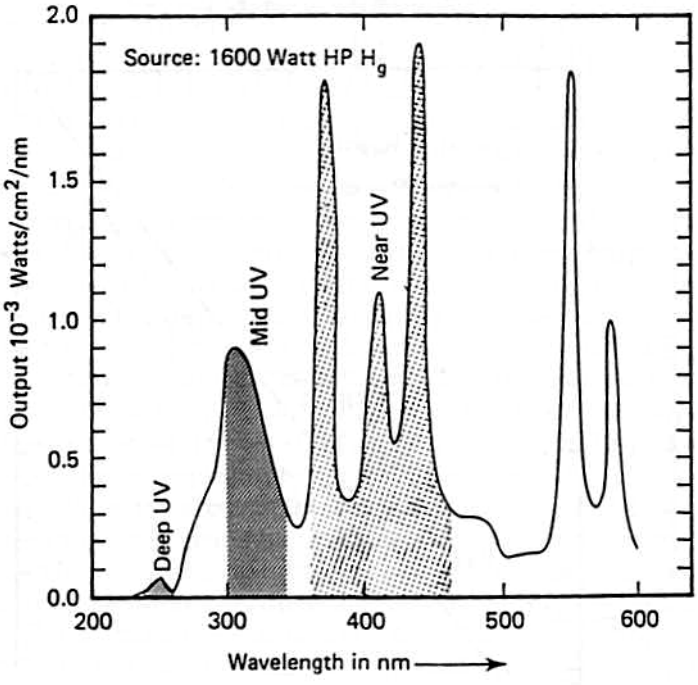

Figure 2.5 Mercury lamp output from a common I-line stepper tool (Reprinted with permission from Introduction to Microlithography, 2nd edition. Copyright 1994 American Chemical Society.)

In previous photoresist chemistries (such as the DNQ-Novolac systems), one photon was required to initiate one chemical reaction that led to a solubility switch. For a given set of process conditions, a certain threshold number of photochemical reactions must have taken place (and thus a threshold amount of photons must have been absorbed) in order for a high quality image to be produced. Because of the lower emission intensity at 248 nm, to receive the same number of photons necessary to produce an image at 365 nm a photoresist must be exposed to 248 nm radiation from a mercury lamp for a much longer exposure time (over 100 times longer!). Wafer throughputs using conventional resist chemistries at 248 nm simply were not acceptable and a new resist platform had to be developed. The answer was chemical amplification[5,9-11].

In the original non-chemically amplified photoresists (such as DNQ-novolacs), one photon is required to perform one photochemical event that leads to image formation. The concept of chemical amplification works on a slightly different principle where the chemical reaction responsible for the polymer's solubility switch is not directly caused by the absorption of photons. Instead, exposure of the resist will cause the generation of a catalyst molecule (typically an acid). This catalyst molecule will then go on to catalyze the reactions responsible for the resist polymer solubility switch. By selecting appropriate catalyst molecules that can regenerate themselves and catalyze more than one reaction, it is possible to greatly increase the net sensitivity of the resist to exposure. Thus, in a chemically amplified system, the absorption of one photon will generate one catalyst molecule, but each catalyst molecule may initiate multiple chemical reactions leading to the solubility switch.

Most positive-tone chemically amplified photoresists (CARs) are composed of at least two components: a protected polymer matrix and a photoacid generator (production quality CARs will typically contain other additives such as base quenchers and these additives will be discussed in detail later in Chapter 6). Prior to exposure, an acid labile protecting group on the matrix polymer renders the polymer insoluble in aqueous alkaline developer solutions. When UV light strikes the resist during the exposure process, energy from the photons excites the photoacid generator (PAG) and causes it to decompose and form an acid. Following exposure, the CAR film is processed through a post exposure bake (PEB) step during which the acid goes on to catalyze a deprotection reaction that removes the protecting group from the polymer matrix and renders the matrix soluble in developer solution. The acid is regenerated during the deprotection reaction making it possible for one photo-generated acid molecule to catalyze many deprotection reactions. In this manner the original photochemical reaction is "amplified" into a much larger series of reactions in the material, thus resulting in extremely high effective sensitivities for these materials.

The oldest known documentation of the concept of a chemically amplified photoresist can be found in a United States patent describing the work of Smith and Bonham at 3M in 1973[12]. In this system, Smith utilizes a novolac resin protected by a tetrahydropyranyl (THP) ether group and an iodonium salt photoacid generator. Unfortunately for Smith (and for 3M!), this work was never published and was essentially allowed to remain hidden within the United States patent database for many years. It wasn't until the early 1980's that chemical amplification began receiving serious consideration for use in microlithography[5,9-11]. Around this time, researchers Jean

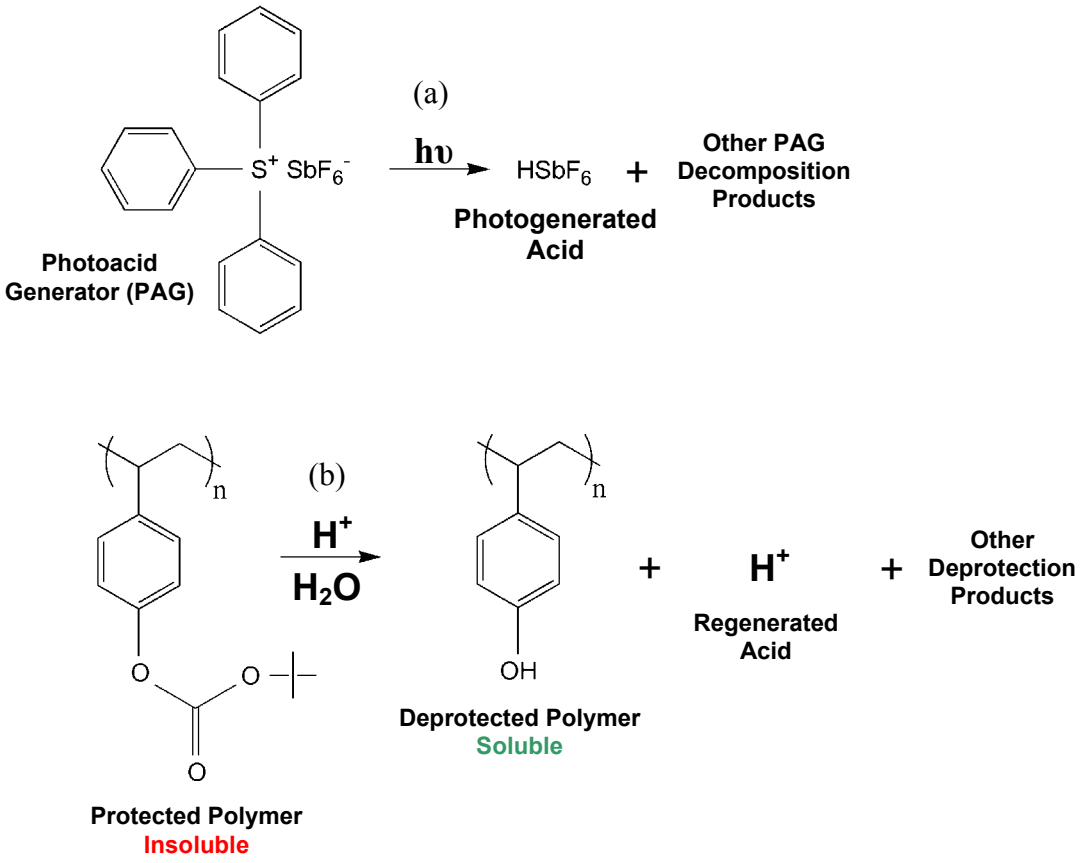

Figure 2.6 (a) Exposure and (b) acid catalyzed deprotection process for a system consisting of t-BOC protected PHOST and triphenylsulfonium hexafluoroantimonate PAG.

Frechet, Grant Willson, and Hiroshi Ito had come together at IBM's Almaden Research Center in San Jose, California. Together they developed the industry's first practical chemically amplified photoresist system consisting of a t-butyloxycarbonyl (t-BOC) protected poly(hydroxystyrene) (PHOST) matrix and an onium salt PAG (in this case, triphenylsulfonium hexafluoroantimonate was utilized). Figure 2.6 above depicts the materials utilized in this system, as well as the two step processing sequence used for imaging with the CAR platform.

While the t-BOC protected PHOST system is illustrated in Figure 2.6, it is important to point out here that a great number of other chemically amplified systems have also been developed and used in the industry. The resist chemist can try a large number of combinations of protecting groups, matrix polymers, and PAGs in a search for the resist system that meets all of their individual performance requirements. To attempt to review and mention each and every one of the individual chemically amplified systems that have been studied in this chapter would be impractical. Instead, the reader is encouraged to consult several review articles and general reference texts along with references contained within[5,9-11].

2.3 CAR Characterization and Simulation

The basic t-BOC protected PHOST system illustrated in Figure 2.6, and other slight variations of this system have served as the workhorse CAR system for 248 nm lithography[5,9-11]. The PHOST polymer used as the resist matrix is well suited for 248 nm deep-UV lithography due to a minimum in absorbance at and near the 248 nm wavelength. As next generation lithography techniques are developed, the chemically

amplified resist platform will more than likely continue to be the technique of choice for lithographers throughout the industry due to continued issues with wafer plane UV flux from modern exposure sources. The matrix polymers utilized in the resists will have to change due to absorbance considerations, but the basic idea of using a protected polymer matrix and a photoacid generator will remain the same. For this reason, developing techniques to characterize CAR behavior and enable accurate lithography simulations are of the utmost importance.

Lithography simulation capabilities are important to the microelectronics industry for a variety of reasons. First, simulations save the lithographer a significant amount of time. Typical product lifetimes in the microelectronics industry today usually last on the order of 18 months to two years[13]. Thus, the sooner a manufacturer can develop the processing sequences needed to create a new generation of products, the sooner he/she can start producing them in mass and therefore maximize the amount of profit that can be drawn from the latest generation products. However, in order to develop useful lithography processes, a wide variety of experiments and tests must be performed. If these experiments have to be performed using actual wafers in a production line, it may take weeks before a single set of test wafers can proceed through the manufacturing line and test results can be obtained. Using simulations for these same experiments can deliver similar results on the order of a few hours, or at most, a few days, drastically reducing the process development time. Similarly, by performing experiments through simulations, the total amount of raw materials required (such as test wafers, photoresists, developers, etc.) is greatly reduced. Finally, simulations make it possible to develop processes using materials that may not even exist yet. A process development engineer

can utilize simulations to determine how a material needs to behave to deliver the desired performance for his process, and then have the material custom made to meet his performance specifications. In the end, all of these benefits ultimately lead to what every manufacturer wants to hear: accurate simulations save the user a great deal of money, and can deliver them a competitive edge!

Figure 2.7 illustrates the five basic processing characteristics typically included in a lithography simulation, along with the various parameters required as inputs to the models used to simulate each step[14].

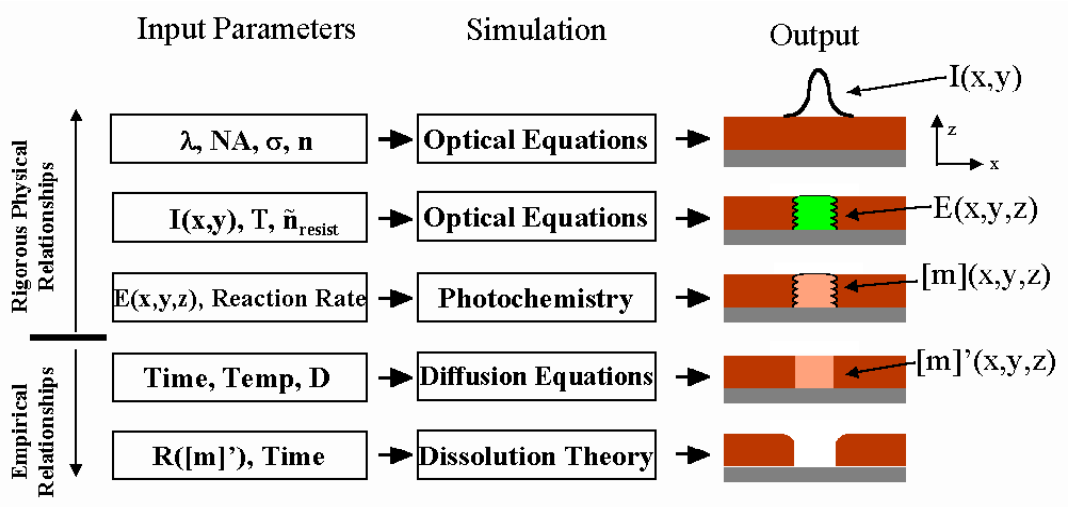

Figure 2.7 The five basic aspects of microlithography from a simulation standpoint. (Reprinted with permission from Advances in Photoresist Characterization and Lithography Simulation copyright 1998 Cliff Henderson).

In order to have an accurate simulation of the overall lithographic process, it is imperative that each of the five steps be modeled correctly, and therefore, that each of the

models' input parameter sets be as accurate as possible. Traditionally, for chemically amplified photoresists, one of the more difficult aspects of the lithography process to characterize and model has been the photochemistry, or the photo-initiated decomposition of a PAG into acid. This process is the focus of the work presented in this thesis.

The photolysis of a PAG, particularly the onium salt PAGs typically employed in chemically amplified photoresists, is a complicated, yet well studied phenomenon[15-17]. A photoacid generator can follow a variety of pathways to produce its photoproducts. For instance, a PAG molecule can receive its energy for excitation via two different mechanisms – direct absorption of a photon or matrix sensitization in which the matrix resin absorbs a photon and passes the energy on to the PAG via electron transfer or some other means[15-17]. In addition, once the PAG molecule becomes excited it can then proceed down even more reaction pathways depending upon the type of bond cleavage that occurs and whether or not the initial decomposition products become trapped within a solvent cage or manage to escape[15-17].

To attempt to model and incorporate each of the various decomposition paths separately into an exposure model for a lithographic simulation would be time consuming and require an extensive amount of experimental work. Furthermore, from a practical point of view, the only piece of information that is typically required for creating an accurate simulation is the amount of photoacid produced for a given exposure dose, regardless of the reaction pathways that led to the photoacid generation. Therefore, a far simpler approach is commonly utilized for the purposes of lithography simulation, where

a generic first order rate expression is assumed to properly describe the kinetics of PAG decomposition, as shown below in equations 2.3 – 2.6[18-28].

$$PAG + h\upsilon \xrightarrow{C} Acid \qquad [2.3]$$

$$\frac{d[PAG]}{dt} = -C \cdot [PAG] \cdot I_{h\upsilon} \qquad [2.4]$$

$$[PAG] = [PAG]_O \cdot \left(e^{-C \cdot I \cdot t}\right) = [PAG]_O \cdot \left(e^{-C \cdot E}\right) \qquad [2.5]$$

$$[Acid] = [PAG]_O - [PAG] = [PAG]_O \cdot \left(1 - e^{-C \cdot E}\right) \qquad [2.6]$$

In these equations, *[Acid]* refers to the concentration of photoacid, or PAG photoproducts that has been generated, *[PAG]* refers to the concentration of PAG, $[PAG_0]$ is the initial PAG loading in the resist matrix, *I* is the incident exposure intensity, *E* is the incident exposure dose (I*t), and *C* is a first order PAG photolysis rate constant, commonly known as the Dill C parameter.

The origins of the Dill C parameter come from the early work by Frederick Dill, William Hornberger, Peter Hauge, and Jane Shaw at the IBM T.J. Watson Research Center in Yorktown Heights, New York[29]. These researchers set out to develop a means for mathematically describing the imaging behavior of photoresists and the result was a set of three model input parameters, the Dill A, B, and C parameters that can be used to

characterize resist behavior. In resists used prior to the development of CARs, significant changes in the absorption properties of the resist occurred upon exposure due to the destruction of the sensitizer molecules utilized. Thus, in order to properly model their imaging behavior, the parameters A (an exposure dependent absorption term) and B (an exposure independent absorption term) were developed. The C parameter was developed as an "optical sensitivity term" to describe how sensitive the sensitizer molecules were to the exposure source. It was essentially used as a first order rate constant for describing the destruction of sensitizer molecules (such as DNQ) upon exposure. For most typical CAR systems that have been developed thus far, no significant changes in absorption (a phenomenon known as bleaching) have been observed upon exposure[19,21,28,30]. Thus the Dill A and B parameters are not as critical to the success of a lithography simulation as they previously were for non-CAR systems. However, the C parameter is still quite relevant and is used to quantify how sensitive PAG molecules are to UV radiation, as evidenced by its use as a first order rate constant in the PAG decomposition kinetics equations shown earlier in equation 2.6. It is important to point out again at this point that the C parameter takes into account all forms of energy transfer to the PAG, and all potential pathways for PAG decomposition. As a result, the C parameter is not an intrinsic property for a PAG alone, but rather is dependent upon both the PAG and the matrix in which it is being studied.

A closer look at the resulting first order expression for PAG decomposition (equation 2.6) reveals that all one needs to know in order to understand the amount of acid that has been produced is the initial PAG loading [PAG_0], the exposure dose E, and the Dill C parameter. Exposure dose E will always be known, as the lithographer is

almost always interested in modeling the response of the PAG to a given exposure dose. The term [PAG_0] is often known, however even if it is not, most simulation packages typically are interested in a normalized PAG conversion, or the expression [Acid]/[PAG_0] rather than a true acid concentration. Thus, the only true unknown of the expression is the Dill C rate constant. Unfortunately, the Dill C parameter is also the most difficult of the input parameters to measure, and has been the subject of a great deal of research effort[19,21-24,28,31-40]. This difficulty stems from the incredibly small amount of acid that is generated in a chemically amplified photoresist. A typical chemically amplified photoresist will contain approximately 2 to 4 weight percent PAG by solids. Thus, assuming a modern 300 mm wafer is coated with a 500 nm thick resist film (and assuming a density of the resist of 1.15 g/cm^3, the approximate density of PHOST), 0.04 grams of resist are contained on the wafer surface, 0.8 – 1.6 x 10^{-03} grams of which is PAG. At 100% conversion, this amounts to only micro-moles of photoacid for detection over the entire wafer's film. If the surface area is further reduced to a value more realistic for acid measurement sampling techniques (say on the order of 10 cm^2), then the amount of acid is further reduced to tens of nanomoles. Needless to say a very sensitive quantitative technique must be utilized to measure such small amounts of acid (more will be said regarding this sensitivity in Chapter 4). A description of the various techniques that have been utilized to measure the Dill C parameter for photoacid generator decomposition is provided in the following sections.

2.4 Previous Techniques Used to Measure Dill's C Parameter in CARs

Several different experimental techniques have been used in attempts to measure Dill's C parameter for chemically amplified photoresists. These techniques include an ionic conductivity technique[31] where photoacid is generated in an aqueous solution and the conductivity of that solution is monitored as a function of dose; a spectroscopic ellipsometery technique[24]; several different spectroscopic techniques that utilize either acid sensitive fluorescent molecules or acid sensitive molecules whose absorbance properties change upon exposure to acid[23,34-38,40]; and a standard addition technique similar to an acid base titration[19,21-23,28,32,33,39]. Of these techniques, those that employ acid sensitive molecules whose absorbance or fluorescence properties change in the presence of acid have been most often employed by industry[23,40]. More recently, the standard addition technique has been developed and has received a significant amount of attention. A more detailed discussion of the spectroscopic techniques as well as the standard addition method follows.

2.4.1 Solution – Based Spectroscopic Techniques

Solution-based spectroscopic techniques are by far the most commonly employed methods and have been the semiconductor industry's method of choice for characterizing PAGs[23,34,36-38]. This technique involves four basic steps. First, chemically amplified resists containing the desired PAG are coated onto a series of wafers. Second, each wafer is flood exposed at a different exposure dose to generate varying quantities of acid. Next, the resist films (now loaded with photoacid) are washed off of the silicon substrates with an appropriate solvent and collected in quartz cuvettes. Finally, an acid sensitive dye

molecule is added to the cuvettes and optical measurements, such as absorbance or fluorescence, are taken to determine how much acid was generated for the given dose. These acid sensitive molecules have included such things as rhodamine B, tetrabromophenol blue sodium salt, N-(9-acridinyl)acetamide, coumarin 6, sulfonapthaleins, merocyanines, monazines, xanthenes, and benzothiazoles. When in the presence of an acid, these molecules' absorbance, or fluorescence properties change in a predictable manner, thus allowing the user to determine the amount of photoacid within the resist solution based on the measured absorbance or fluorescence. By analyzing the acid concentration versus dose relationship determined from the absorbance or fluorescence versus dose data, the Dill C parameter can be extracted.

2.4.2 On Wafer Spectroscopic Techniques

The on-wafer fluorescence spectroscopy technique is similar in nature to the solution technique, only the amount of time and effort involved is greatly reduced. In this technique, acid sensitive fluorescent dyes are introduced into the photoresist solution prior to its casting onto silicon substrates[34,35,40]. Resist films containing the fluorophores are coated onto silicon wafers and exposed to varying doses of UV radiation. The fluorescence of the exposed regions is then measured to determine the amount of acid produced by the exposure energy. The fluorescent dyes typically decompose when they encounter an acid, so the degree of fluorescence is indicative of the acid concentration.

2.4.3 Standard addition techniques

The final technique to be discussed, the standard addition method, is one of the most recent developments in efforts to measure the Dill C parameter[19,21-23,28,32,33,39]. This technique is similar to an acid/base titration. In a typical chemically amplified photoresist, a threshold dose of UV energy (known as the dose to clear) is required to generate enough acid that the resist film will deprotect and completely clear to silicon during development. Providing too little exposure energy results in too little acid being generated and there will be resist film remaining in the exposed regions after development. The dose to clear is the exact exposure dose value at which just enough acid has been generated to catalyze deprotection reactions and allow the resist film to clear to the silicon wafer beneath the film. The standard addition technique involves adding small quantities of a base quencher to the resist solution prior to coating and exposure. When acid is generated within the film, the base present within the film neutralizes acid molecules and renders them useless in the deprotection reaction. In order to overcome this acid deficiency, the UV exposure dose must be increased. A new "dose to clear" is observed, where the acid produced by the additional exposure dose is assumed to be directly proportional to the amount of base added to the resist film. The amount of base is subsequently increased, resulting in even higher "dose to clear" values. This process is repeated until the amount of base present in the film is so high that the resist film will no longer clear to silicon regardless of the exposure dose provided. By examining the relationship between dose to clear and added base, it is possible to extract the Dill C parameter for PAG photolysis.

2.5 Thesis Project Motivation

Though all three techniques discussed here have experienced reasonable success in measuring the Dill C parameter, they each suffer from a variety of shortcomings. For instance, the solution-based techniques require an extremely large amount of effort, wet chemistry, and raw materials. Multiple wafers must be coated and exposed, and then a large amount of wet chemistry must be performed to extract the resist films and prepare the solutions for absorbance or fluorescence measurements. In addition to the effort and materials involved, the various pieces of equipment and processing steps required to perform this technique are typically not found in or associated with a wafer fabrication facility. Finally, washing resist films on the order of 1 micron in thickness off of the silicon wafers for collection in cuvettes is a difficult, destructive technique that can serve as an additional source of error in this measurement technique.

The on wafer technique attempts to alleviate some of the error and problems associated with washing off resist films in the solution-based technique by adding the acid sensitive fluorescent molecules directly to the resist solution prior to spin coating and then coating the fluorophore loaded solution onto the silicon wafer. Nevertheless, it, too, has its flaws. The introduction of dye molecules into the resist film can potentially cause changes in the UV absorption properties of the film as well as the energy transfer mechanism within the film, both of which in turn change the effective dose of energy the PAGs receive. The exact nature of these interactions between the dye molecules and the PAG are presently unknown. Thus, utilizing such an invasive method for Dill C measurement introduces many questions as to the accuracy of the Dill C parameter obtained from this technique.

Finally, like the two spectroscopic techniques, the standard addition technique is not without its share of problems. The main disadvantages with this technique include the time, materials, and effort involved to generate the dose to clear versus base content relationship, as well as the invasive nature of the experiments. Wet chemistry must be performed prior to spin coating any wafer in order to prepare multiple resist solution samples, each with an incrementally increasing amount of base added to it. Then, multiple wafers must be coated and exposure dose arrays printed onto their surface in order to determine the dose to clear for each different resist solution sample. Like the on-wafer fluorescence technique described earlier, the added base in the resist solutions could possibly alter the absorbance characteristics of the resist film or the energy transfer mechanisms between the matrix and PAG, resulting in additional error in the Dill C estimation.

As can be seen from the descriptions provided above, the techniques commonly employed for measuring the Dill C parameter for a photoacid generator are less than desirable. In general they are invasive, possibly destructive techniques that are laborious and not at all fab-friendly. Thus, it was desired to develop a new means of measuring the Dill C parameter for PAG decomposition that eliminated many of these problems. The work presented in this thesis describes our efforts to develop such a technique for measuring the Dill C parameter that utilizes electrical measurements (capacitance) from small, interdigitated electrode sensors coated with the chemically amplified resist of interest. This new technique is quick, easy to perform, non-invasive and non-destructive, and can be readily performed using the equipment already found in a fab environment. A

detailed description of the work performed to develop this technique and test its applicability will be found in the following chapters.

CHAPTER 3*

INTERDIGITATED ELECTRODE SENSORS AND POTENTIAL CONFOUNDING VARIABLES

3.1 Introduction

As mentioned at the end of the previous chapter, the electrical-based measurement technique proposed in this thesis for measuring the Dill C rate constant for photoacid generator (PAG) photolysis relies on capacitance measurements taken from interdigitated electrode (IDE) sensors coated with the chemically amplified photoresist being studied. This technique exploits the changes in the net dielectric constant of the photoresist film that occur as photoacid is generated within the film due to exposure. Prior to exposure, the resist film coating the IDE sensor has a baseline net dielectric constant leading to a specific, baseline capacitance value that is measured from the IDE sensor. As photoacid is produced during exposure, the presence of the acid leads to a change in the net dielectric constant of the photoresist film resulting in a corresponding change in the capacitance that is measured from the interdigitated electrode sensor. As will be shown later in Chapter 4, by properly analyzing the capacitance versus exposure dose curves that

---

* Material presented in this chapter has appeared in part in previously published articles:

Berger C, Henderson C, *The effect of humidity on water sorption in photoresist polymer thin films*, Polymer, **44**, 2101 – 2108, 2003.

Berger C, Henderson C, *Equilibrium sorption and rate of diffusion of water into photoresist thin films*, Proceedings of SPIE, **5039**, 984 – 985, 2003.

Berger C, Henderson C, *Measurement of photoacid generation kinetics in photoresist thin films via capacitance techniques*, Proceedings of SPIE, **5039**, 322 – 333, 2003.

Berger C, Byers J, Henderson C, *Using interdigitated electrodes for measuring photoacid generator kinetics in chemically amplified resists*, Journal of the Electrochemical Society, **151(2)**, G119 – G130, 2004.

are collected from the IDE sensors it is possible to extract the Dill C rate constant for the PAG.

The use of interdigitated electrode structures as sensors is not a completely novel concept. Over the years this type of electrode configuration has been used to study a wide range of subject matters and IDEs have served a variety of roles in those studies (more will be said later in this chapter regarding their prior uses). Their usefulness often stems from their incredible sensitivity and their simple geometry. However, this usefulness (and in particular the sensitivity) does not come without a price. Often times understanding exactly what the IDE sensor is sensing becomes quite complicated due to confounding variables such as changes in environmental conditions, or baseline IDE characteristics. The information presented in this chapter will describe in detail efforts that have been taken to understand several of these complicating factors, as well as the work that has been done to minimize their effects. The reader will first be introduced to the IDE sensors that have been utilized for all work presented in this thesis so that he/she may become familiar with their specific geometry, as well as several other uses of such sensors. Then, information will be provided detailing experimental work used to study three complicating issues: base contamination, relative humidity, and IDE spin coating.

3.1.1 Interdigitated Electrode (IDE) Sensor Geometry

Interdigitated electrode sensors (often referred to as comb electrodes, or array electrodes) consist of two sets of conductive electrode fingers with each set of fingers attached to a separate bond pad. The fingers protruding from the two bond pads are intertwined (or interdigitated) amongst one another, as shown in Figure 3.1a. Typically,

the users of IDE sensors will exploit measurements of resistance or capacitance between the two IDE finger sets as a means of detecting some form of a chemical change in the material coating the electrode fingers. More specific details of IDE uses can be found later in this chapter.

All of the interdigitated electrode sensors that were utilized in this work were fabricated at International SEMATECH in Austin, Texas, by Dr. Jeffrey Byers and Daniel Miller. Figure 3.1 provides detailed information about the structure of the sensors used in this work.

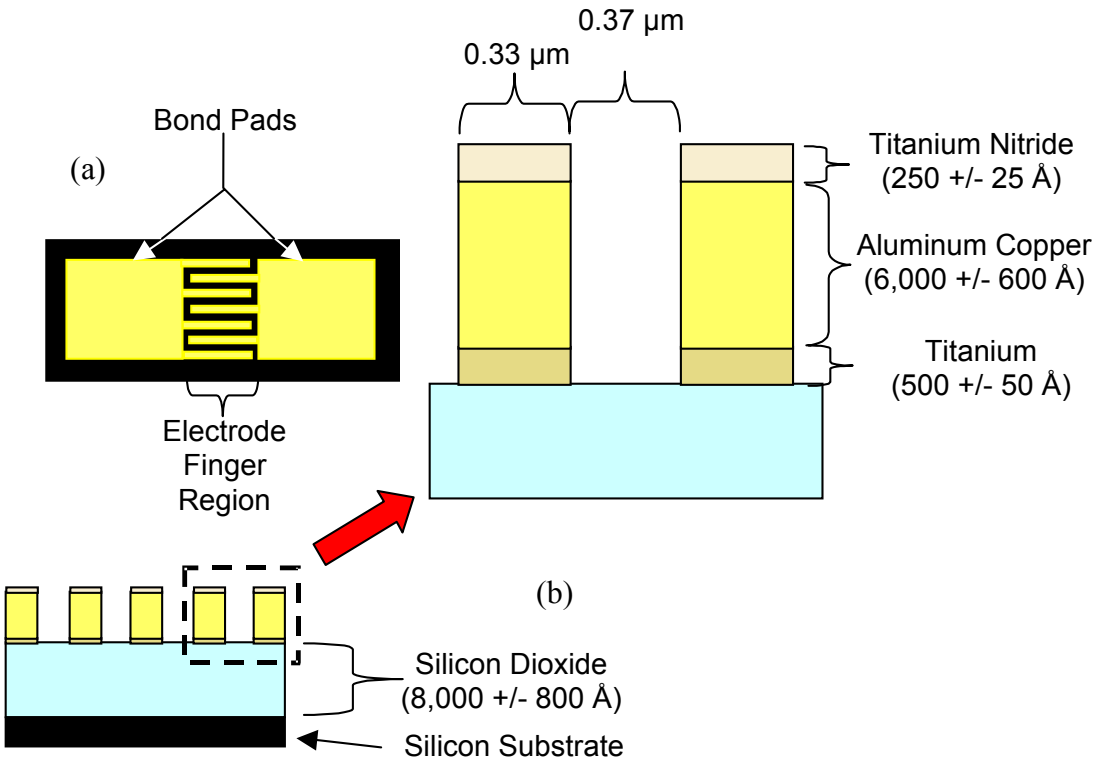

Figure 3.1 (a) Top down view of a typical interdigitated electrode (IDE) structure used in this work (b) cross section view of IDE detailing the specific dimensions of each material and structure used in the IDE

As can be seen from Figure 3.1, the IDE sensors that were utilized in this work are relatively simple structures composed of conducting fingers that reside on an insulating silicon dioxide substrate - all initially fabricated on an 8 inch diameter silicon wafer. The silicon dioxide layer deposited onto the silicon substrate is 8,000 Å thick, and serves to isolate the IDE's bottom fringe electric fields from the semi-conducting substrate. The IDE fingers and bond pads consist of three separate metal layers deposited on top of the silicon dioxide layer. First, a 500 Å thick blanket layer of titanium was deposited. Next, the bulk of the IDE fingers was deposited in the form of a 6,000 Å thick layer of an aluminum/copper alloy. Finally, a thin top layer of 250 Å of titanium nitride was deposited. In all processing steps utilized to fabricate the IDE fingers, a process tolerance of +/- 10% was allowed.

Once the blanket films of silicon dioxide and metal were deposited, photolithography was utilized to pattern the metal films into the shapes of the IDE fingers and bond pads. For the sensors used in this work, a finger pitch of 0.70 μm was used, with a target 1:1 finger width to finger spacing ratio. Analysis of SEM micrographs indicates that the true finger width is not quite the same as the spacing, with the width measuring approximately 0.33 μm while the spacing measures 0.37 μm. In addition, the target finger height was 6,750 Å (0.675 μm) while SEM analysis indicates that the actual height is approximately 0.7 μm. The entire sensor measures 3 cm from the end of one bond pad to the other and measures 0.8 cm wide. The IDE finger region between the two bond pads is 0.8 cm square. Based on the dimensions of this finger region and the finger pitch, there are approximately 11,400 IDE fingers located within the IDE finger region, giving over 90 meters of finger length. This large number of fingers and total finger

length provides excellent sensitivity to any changes in the material that is coating the IDE sensor, and will prove quite useful for sensing the small amounts of photoacid typically produced by a PAG. However, it should also be noted that such tiny finger dimensions combined with the sheer number of fingers present makes the IDE sensors quite vulnerable to contamination issues. Particulate contamination can easily bridge two or more fingers resulting in an electrical short and a defective sensor. Great effort is taken to ensure that the IDE sensors are protected from particulate contamination, including only using the sensors in a cleanroom environment.

3.1.2 Interdigitated Electrodes as Sensors

Interdigitated electrode sensors provide many advantages over traditional electrode configurations for sensing applications. First, the incredible number of electrode fingers that can be fabricated within the IDE sensing region allows for increased sensitivity to the material that is coating them. Second, in order to measure the electrical properties of a material, that material typically needs to be sandwiched between two separate electrodes. Typically, a parallel plate capacitor configuration is constructed with two large, flat pieces of metal sandwiching the material of interest. Unfortunately, this type of configuration is often very difficult to utilize. A bottom electrode must first be deposited. This is followed by deposition of the material under study, and then finally, deposition of a top metal electrode. During the process used to deposit the top electrode, the thermal, electrical, and chemical processing utilized could potentially alter the properties of the material being studied. In addition, this type of configuration is limited to a single use. The sensor cannot be reclaimed for future use due to the electrode plate

that resides on top of the material of interest. Unlike a parallel plate configuration (with a "horizontal" orientation), the IDE configuration has a "vertical" orientation. Both electrodes are already deposited in the form of the two finger sets. The material of interest is then simply deposited onto the sensor's finger region and fills the gaps between the IDE fingers and the areas above the fingers. There is no further processing required that could potentially alter the properties of the material being studied. In addition, removal of the material is relatively easy, allowing for repeated uses of the same IDE sensor. For the photoresist samples studied in this work, removal is achieved through a simple solvent wash where the IDE sensor is soaked successively in acetone, methanol, and finally, isopropyl alcohol. A quick rinse with de-ionized water is followed up by a short bake on a hot plate to dry the sensor and the sensor is ready to be used again in only a few minutes. Finally, the use of interdigitated electrodes provides one last obvious advantage over other configurations in terms of studying photosensitive materials. In order to measure the kinetics of PAG photolysis it is imperative that data be collected as the resist is exposed to incremental doses of UV radiation. A parallel plate configuration would not allow for proper exposure of the CAR film. The film would have to be fully exposed and then covered with a top electrode. The IDE sensor configuration allows for simultaneous exposure and measurement of electrical properties.

Because of the many advantageous qualities that IDE sensors possess, they have been used in a wide variety of applications. These applications include such things as surface acoustic wave (SAW) devices[41] , photodectors[42-44], and chemical or biological sensors[45-59]. The range of substances, or chemicals that have been "sensed" using IDE sensors is quite broad and ranges from biological applications to things as simple as

measuring relative humidity. For instance, Van Gerwen and co-workers demonstrated that IDEs could be utilized to sense the presence of antigens or antibodies as they bind to selective probe molecules near the surface of IDE fingers[47]. Hofmann and co-workers studied the use of IDEs to analyze the composition of mixtures of various alcohols in water[48]. Finally, Pan and co-workers used IDE sensors to monitor the curing of polyimide films[57]. In all of these applications, either the resistance or the capacitance of the IDE sensor (or both in the form of impedance) is monitored to detect the presence of the species under study.

A large amount of work has recently been poured into developing simple relative humidity sensors using interdigitated electrode sensors coated with a polymer film that is capable of absorbing water to some degree[50,52-55,58]. In these applications, as the relative humidity of the measurement environment changes, the amount of water absorbed into the polymeric film changes accordingly. As the film's water content changes, the resistance, as well as the net dielectric constant of the polymer film also change. By monitoring the measured resistance or capacitance of the IDE sensor, a simple, usually quite accurate relative humidity sensor can be realized. The ideas and concepts behind the use of IDEs as relative humidity sensors are very similar in nature to the technique proposed in this thesis for measuring the Dill C parameter. Like the relative humidity sensors, a polymer film (the CAR film) is coated onto the IDE sensor. As photoacid is produced during exposure, the dielectric constant of the film changes, resulting in a change in the measured capacitance. The capacitance versus exposure data collected from the IDE sensor is subsequently used to determine the Dill C parameter.

3.1.3 Potential Confounding Variables

As just mentioned, the Dill C measurement technique discussed in this work exploits changes in the net dielectric properties of the CAR film that occur as acid is generated from the PAG molecules within it. Using the highly sensitive IDEs, the change in dielectric constant is then quite easily observed through changes in measured IDE capacitance. However, because changes in the dielectric constant of the CAR film are used as the measuring stick for quantifying PAG decomposition, the IDE Dill C measurement technique is exposed to several potentially troubling issues. Essentially any foreign substance or processing sequence that may alter the net dielectric constant of the CAR film will also alter the capacitance and may potentially cause problems with the capacitance data analysis used to extract the Dill C parameter.

Unfortunately, there are several such items that exist in a typical laboratory setting. The first of these is base contamination. If ambient base is present in high enough levels, and is absorbed into the CAR film, the base can neutralize the photoacid and alter the observed capacitance, severely complicating the analysis technique used to obtain Dill's C parameter. The second potential problem encountered is relative humidity. As relative humidity varies from one day to another within our laboratory, the amount of water absorbed into the resist film can vary significantly. Water has a very high dielectric constant (~ 80 at 1kHz measurement frequency)[60] compared to the low value associated with resist polymers (typically on the order of 2 – 5)[61] and as a result, introducing water into the resist film varies the net dielectric properties of the films significantly, introducing error into the measured capacitance and once again complicating the Dill C analysis. Finally, the third potentially troublesome quality of the

technique that must be studied is the ability of the IDE to be spin coated with resist. It was unknown initially whether resist would adequately fill the tiny spaces between the IDE fingers, and to what degree the overlying resist film would be planar. Voids of air within the resist coating, or significant topography on the resist surface could lead to problems analyzing the measured capacitance and calculating the UV intensity throughout the resist film during exposure respectively.

A detailed description of the efforts taken to understand and eliminate the effects of these three issues is provided in the next sections of this chapter. To eliminate the effects of base contamination, a "base-free" cleanroom environment was constructed and supplied with the appropriate equipment for the Dill C measurement technique. To understand the effects of relative humidity upon the water content of the CAR films, quartz crystal microbalance (QCM) techniques were utilized to measure the amount and rate of water sorption into three common photoresist matrix polymers at various relative humidities. Finally, to understand the quality of the films coating the IDE sensors a series of SEM micrographs were collected showing cross sections of the resist coated IDE sensor fingers. Each of these efforts will now be discussed in detail.

3.2 Experimental Methods

3.2.1 Materials

A series of electronic grade photoresist resin polymers were obtained from commercial electronic material suppliers as follows: poly(p-hydroxystyrene) (PHOST, M_w = 11,800) was obtained from DuPont Electronic Materials (formerly Triquest Chemical Company); novolac sample #1 (M_w = 1,615, PDI = 2.283) was obtained from

Shipley Company; novolac sample #2 ($M_w \approx 22{,}000$, PDI ≈ 25) was obtained from AZ Electronic Materials, and two bis(trifluoromethyl)carbinol substituted poly(norbornene) resins (HFAPNB-1: $M_w = 8{,}882$, PDI = 2.25 and HFAPNB-2: $M_w = 94{,}159$ PDI = 9.21) were obtained from Promerus Electronic Materials. Figure 3.2 shows the generic structure of all three polymer types. Both the HFAPNB and PHOST samples are known to be linear homopolymers. In the case of novolacs, it is common to polymerize mixtures of meta and para-cresols with small amounts of other co-monomers that introduce some degree of branching in the material. Such detailed structural information for the novolac samples used in this work is not available. Ethyl lactate (98%) and propylene glycol methyl ether acetate (PGMEA) (99%) were purchased from Aldrich Chemical Co. and used as casting solvents for the various polymers. The polymers and solvent were used as received.

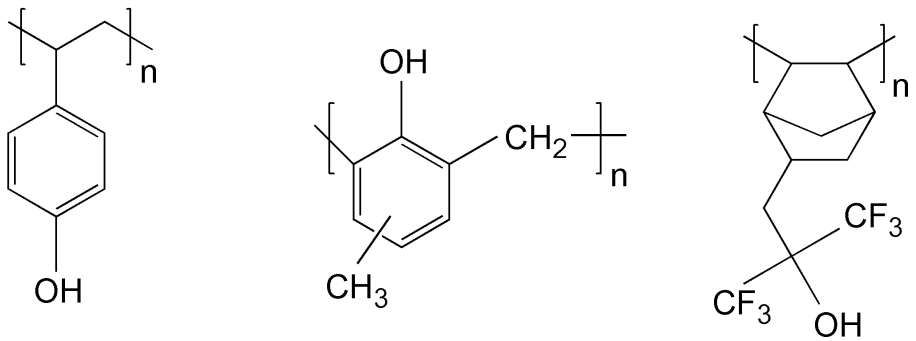

(a) (b) (c)

Figure 3.2 (a) poly(p-hydroxystyrene) (PHOST), (b) novolac, and (c) bis-trifluoromethylcarbinol substituted poly(norbornene) (HFAPNB).

3.2.2 Water Sorption Measurement Procedures

Two separate experimental methods were used to study the effects of relative humidity upon the photoresist polymers studied. First, a quartz crystal microbalance (QCM) was used to study the effects of relative humidity upon the equilibrium water content of the resist polymers as well as the rate of water sorption. A QCM utilizes oscillating quartz crystals as a means for mass measurement[62]. When an electric potential is applied to the uncoated quartz crystal, the piezoelectric nature of quartz will cause the crystal to oscillate at a baseline resonance frequency. The result is the formation of a standing wave within the quartz known as a shear wave that is centered along the centerline of the quartz slice. As mass is added to the crystal's surface, the effective thickness of the quartz increases, increasing the shear wave's wavelength and effectively lowering the oscillation frequency. By monitoring the changes in the oscillation frequency of the resist coated quartz crystal, it is possible to monitor the absorption and desorption of water from the film. More will be said in the results and discussion section of this chapter regarding QCM theory and in particular, the Sauerbrey equation used to convert frequency to mass. Finally, in a second set of water sorption experiments, IDE sensors were used to study the effects of relative humidity upon the measured capacitance and hence the net dielectric constant of the resist polymers.

For the QCM experiments, all water sorption measurements were conducted using a Maxtek quartz crystal microbalance (PLO-10 Phase Lock Oscillator, 5 MHz gold plated quartz crystals model # SC-501-1). PHOST (13.2 wt% solids in ethyl lactate) was spin coated onto the QCM crystals at 1000 rpm for 30 seconds using a CEE Model 100 CB spin coat/bake system to create a film approximately 1.1 μm in thickness. Novolac-1

(14.8 wt% in PGMEA) and novolac-2 (19.8 wt% in PGMEA) were spin coated at a similar rate and time to create films approximately 0.8 μm and 1.4 μm thick respectively. Finally, the HFAPNB-1 (24.9 wt% in PGMEA) and HFAPNB-2 (15.7 wt% in PGMEA) were spin coated at 1000 rpm for 30 seconds to create films 1.1 μm and 0.6 μm thick respectively. All solutions were filtered through 0.2 micron Teflon filters prior to coating to remove particulates, and all films were subjected to a 115°C soft bake for three minutes following spin coating to remove the majority of residual casting solvent.

Two small humidity chambers were custom designed and constructed for the water sorption measurements. Nitrogen gas from the headspace of a liquid N_2 cylinder was used to purge the humidity chambers and provide a low humidity environment. Nitrogen gas and/or room air was bubbled through a water reservoir at varying flow rates to adjust the humidity level inside the chambers. A hygrometer probe (Omega, model #RH411) was inserted into the chamber near the location of the polymer coated samples and was used to provide real-time monitoring of the chamber's relative humidity. Figure 3.3 illustrates the basic experimental setup that was utilized for the QCM experiments.

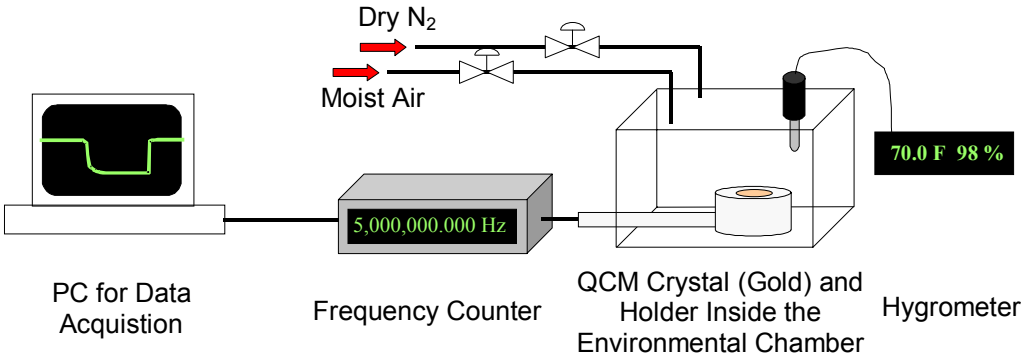

Figure 3.3 Basic experimental setup used for QCM water sorption experiments. Only one of the two environmental chambers is shown.

Initially, one humidity chamber was allowed to stabilize at a low relative humidity value (6 - 9 %) while the other chamber stabilized at a high humidity value (93 – 98 %). To obtain the dynamic water sorption data, the oscillation frequency of the polymer coated QCM crystal was recorded as the QCM crystal and holder were transferred from one chamber to the other. For example, to obtain dynamic data for water absorption the QCM crystal was first placed inside the low humidity environment and allowed to equilibrate as water left the polymer film. Then, the crystal and holder were immediately transferred into the high humidity chamber. As water was absorbed into the polymer film the recorded oscillation frequency dropped due to the added mass of the water on the crystal. Dynamic data for water desorption was obtained in a similar manner, only by starting in the high humidity chamber and moving to the low humidity chamber. Under these circumstances, the recorded frequency increased due to loss of mass on the QCM crystal. The process of transferring from one chamber to the other was repeated several times to ensure the dynamic data's reproducibility.

Static equilibrium crystal frequency values were also measured for intermediate humidity values by adjusting the humidity of one of the environmental chambers and allowing the coated crystal to equilibrate in the chamber at each desired humidity level. These equilibrium frequency values for each humidity were recorded and used to determine a relationship between mass of water absorbed and the humidity. The temperature inside the chamber was held relatively constant at 22.8 +/- 1.2 ºC during all of these experiments.

For the IDE sensor experiments, all capacitance measurements were conducted using a two-point probe station (Micromanipulator, #6200) and an Agilent LCR meter

(model 4284A). Measurements were conducted at a frequency of 1 kHz using a 50 mV bias on interdigitated electrodes (IDEs) coated with PHOST, HFAPNB-1, and novolac-2 polymer samples. The polymer films were spin coated onto the IDE sensors using the same CEE spin coater described above at 1000 rpm for 30 seconds. A soft bake of 115ºC for 3 minutes was used immediately following coating to remove residual casting solvent. Capacitance measurements were performed by applying two probe tips attached to the LCR meter onto the bond pad regions of the IDEs illustrated earlier in Figure 3.1. The polymer coated IDE along with the electrical probes were placed directly inside the same humidity chamber used for the QCM experiments (shown above in Figure 3.3) and exposed to various relative humidity conditions achieved through similar means as the QCM experiments described above. As the polymer films absorbed/desorbed water, the measured capacitance of the IDE would change. The measured capacitance of the IDE was monitored until it was clear that no further change in capacitance would occur (i.e. the polymer film had absorbed its equilibrium water content for the respective relative humidity value). The capacitance for this point was recorded and used to determine a relationship between capacitance and film water content.

3.2.3 IDE Sensor Spin Coating Study

To study the quality of the films that are spin coated onto the IDE sensors, PHOST (15.0 wt% in ethyl lactate) was spin coated onto an IDE sensor at 900 rpm for 30 seconds using the CEE spin coater/bake plate system. A soft bake of 115ºC for 60 seconds was used to remove residual casting solvent following coating. The resist coated IDE sensor was then cleaved in half using a diamond tipped wafer scribe. SEM

micrographs were taken of the IDE cross sections to determine the quality of the coating process.

3.2.4 Film Thickness Measurements

A variable angle spectroscopic ellipsometer (V-VASE from J.A. Woollam Inc.) was used to measure the thicknesses of the different resist films used in these experiments. For these measurements, the materials of interest were cast onto plain silicon <100> wafers (Nova Electronic Materials) or onto the gold plated QCM crystals. The ellipsometry parameters, Ψ and Δ, were collected over the wavelength range from 500 nm to 1000 nm at angles of 65º, 70º, and 75º. The Ψ and Δ data were analyzed using the WVASE-32 analysis software (J.A. Woollam Inc.) by fitting the ellipsometry data using a film stack model composed of a Cauchy layer model for the polymer film on top of a 15 angstrom thick SiO_2 layer, all on a semi-infinite layer of silicon. For the QCM crystal film thickness, a Cauchy layer model was used on top of a semi-infinite layer of gold.

3.3 Results and Discussion - Construction of a "Base-Free" Work Environment

The effects of base contamination upon chemically amplified photoresist performance are well studied and well documented[63-68]. It has been found that small amounts of ambient base, on the order of only a few ppb (in some cases as low as 1-2 ppb[63,64]), can cause significant degradation of CAR performance. The base molecules from the ambient environment are absorbed into the CAR film and neutralize the photoacid molecules that have been generated to catalyze the deprotection reactions

responsible for switching the solubility of the matrix polymer. In a chemically amplified resist, a threshold number of deprotection reactions must take place in order for the solubility of the exposed region to switch from insoluble to soluble. Accordingly, a threshold amount of photoacid must be present to initiate these deprotection reactions. If enough acid molecules are neutralized by the absorbed base, an insufficient number of deprotection reactions will take place and the polymer will remain insoluble in aqueous base developer. This phenomenon is especially problematic at the resist surface where the base is absorbed the fastest, resulting in a feature distortion known as "T-topping", where the tops of features are spread out, similar to the shape of the letter "T", as illustrated in Figure 3.4 below[63,65,66].

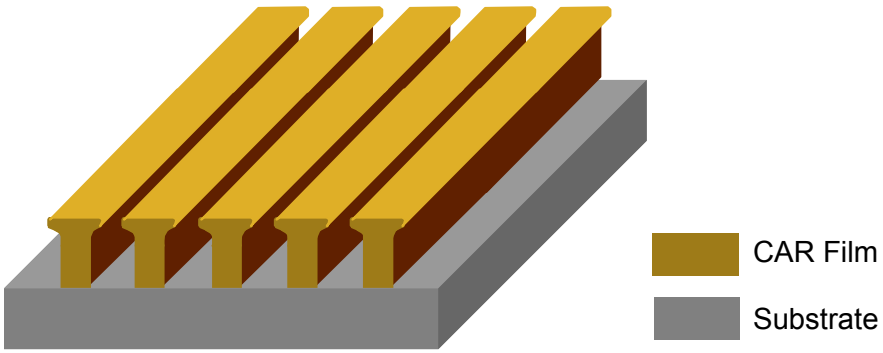

Figure 3.4 "T-Topping" of printed lines due to base neutralization of photoacid.

In typical room air, anywhere from 10 to over 50 ppb of base can exist[63,69], depending upon the location, time of day, and time of year (in agricultural areas base levels can spike during planting season due to the heavy use of nitrogen-based fertilizers). This level of base is more than enough to cause substantial problems with CAR performance

during lithographic imaging processes. As one could easily imagine, base contamination is also a big concern for anyone trying to measure the Dill C parameter. All of the techniques used to measure Dill's C rely on some form of acid sensitive indicator. In the spectroscopic based techniques, acid sensitive dyes that change absorbance or fluorescence properties in the presence of acid are used. In the standard addition technique, the dose to clear is used where the dose to clear is directly dependent upon the amount of acid available for deprotection. The IDE technique is no exception. The presence of acid within the CAR film directly affects the net dielectric constant of the film and causes a change in the capacitance values measured from the IDE. If ambient base is absorbed into the film and neutralizes the photoacid, this neutralization would no doubt alter the observed capacitance response. The effects of base neutralization would overlap with the acid generation response, introducing error into the measurement technique. For this reason, efforts must be taken to eliminate ambient base from the Dill C measurement environment.

Two potential options were explored for creating a "base-free" work environment to perform the IDE sensor measurements of the Dill C parameter. The first option explored consisted of a custom built enclosure that would contain all of the necessary equipment needed for a Dill C measurement. Essentially, this plan called for construction of a large box from some type of transparent material (such as Plexiglas) and mounting of a base filter to an air inlet into the enclosure. All of the equipment would be contained inside the enclosure and glove access as well as a pass through window would be provided similar to a glove box enclosure. Unfortunately, this type of configuration proved to be impractical, as too many pieces of equipment would ultimately be required

to perform a Dill C measurement. The second option for a "base-free" environment, and the option utilized, was to build a cleanroom and fit the cleanroom's HEPA fan units with base filtration. An Airlock Modular Cleanroom package was purchased from Simplex Isolation Systems and erected in the laboratory. This cleanroom structure measures 8 feet wide by 16 feet long and is constructed from non-outgassing materials to minimize the chances that any bases are outgassed into the cleanroom from the wall material. Five HEPA fan units are located on top of the cleanroom and provide particle free, laminar flow to the cleanroom. With this fan configuration the cleanroom is rated a class 1000 cleanroom, meaning less than 1000 particles 0.5 microns in diameter or larger in size will be found in every cubic foot of air. Yellow light covers were installed over the fluorescent lights inside the cleanroom to filter out UV radiation and prevent unwanted PAG decomposition due to secondary exposure sources. Figure 3.5 below depicts the "base-free" cleanroom.

(a) (b)

Figure 3.5 (a) Outside view of "base-free" cleanroom (b) View of HEPA fan unit on cleanroom roof.

The most common bases typically found in the ambient environment include nitrogen containing compounds such as ammonia, various amines (methylamine, dimethylamine, trimethylamine, cyclohexylamine, morpholine, ethylamine, etc.), n-methyl pyrrolidone, and the common aqueous base developers such as tetramethylammonium hydroxide[63-69]. In order to establish "base-free" working conditions, filter units designed to remove these particular types of base from the ambient air were installed on top of the HEPA fan units (in the light blue region in Figure 3.5b above) and served as pre-filters for the main HEPA filters. The base filters selected for this purpose were Vaporsorb II Rooftop Lithography-Chemical Air Filters (part number ESI001462) purchased from Extraction Systems, Inc. These filters contain a recently developed polymeric filtration media that offers removal efficiencies 3-5 times better than that typically achieved using a charcoal media. The Vaporsorb II filters are designed to remove 99.99% of total molecular base contamination providing downstream base levels less than 1 ppb, more than adequate for Dill C measurements.

Inside the cleanroom all of the necessary equipment needed to perform the IDE sensor measurements of the Dill C parameter was installed. This equipment included the 2 point probe station (Micromanipulator, #6200), the LCR meter (Agilent model 4284A), the CEE model 100 CB spin coat and bake system, and an Oriel Instruments 248 nm flood exposure source (model # 87530-1000). Figure 3.6 below shows the equipment inside the cleanroom structure.

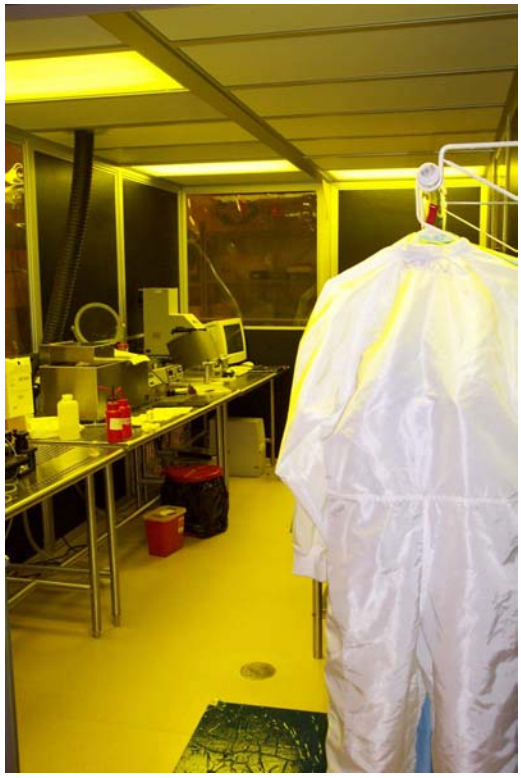

(a)

(b)

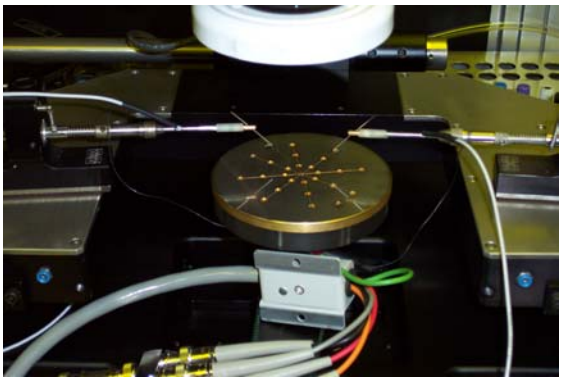

(c)

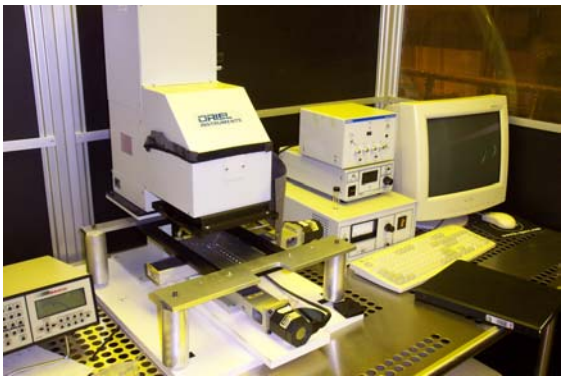

(d)

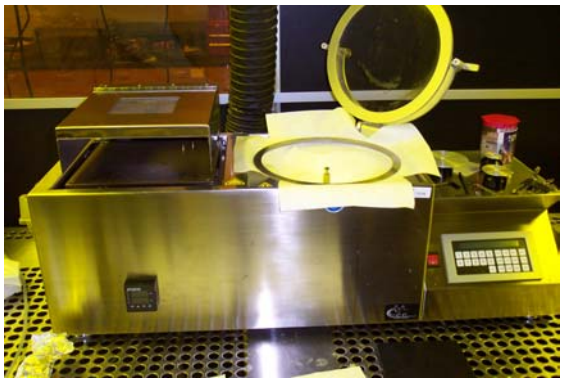

(e)

Figure 3.6 (a) View through entry way of "base-free" cleanroom (b) Agilent LCR meters and two point probe station (c) close-up view of two point probe platform and probes (d) Oriel Instruments 248 nm flood exposure source and x-y stepper stage (e) CEE model 100 CB spin coat/bake system.

As shown in the photographs, all equipment was placed onto perforated stainless steel tables to minimize particulate contamination and maximize laminar air flow. A closer look at Figure 3.6a reveals that the base-free HEPA fan units are placed directly over the equipment to be certain that the base-free air flows into the work environment around the equipment where the CAR films will be processed. Cleanroom garments such as those illustrated in Figure 3.6a are worn to further minimize particulate contamination and base contamination from the human occupants.

Once the cleanroom was erected and all equipment was installed, a simple test was performed to determine if significant levels of base were present inside the filtered cleanroom. The dose to clear of a commercial chemically amplified resist (AX1020P, AZ Electronic Materials) was monitored at two different times. This measurement required several simple processing steps. First, the CAR was spin coated onto a silicon wafer. Next, a dose array was exposed onto the wafer, where many (16 – 25) regions of different exposure intensity were exposed in an incremental fashion, starting from near zero mJ/cm^2 and working up to over 30 mJ/cm^2 dose. A post exposure bake of 110°C for 60 seconds was then used to initiate the deprotection reactions that remove the protecting groups from the matrix polymer and switch the solubility. Finally, the wafers were developed in an aqueous solution of base developer (such as tetramethylammonium hydroxide (TMAH)). The region of the CAR film that was exposed to the least amount of UV energy, and yet still dissolves completely to reveal the underlying silicon indicates the dose to clear, where the minimum threshold amount of acid is produced.

This dose to clear measurement was performed for two different samples, with slightly different processing times. The first wafer was exposed, immediately baked, and

then developed. The immediate bake following exposure allowed minimal time for base to be absorbed into the CAR film and neutralize acid. The second wafer was exposed, and then allowed to sit out in the cleanroom for over 1 hour, providing ample time for ambient base to absorb into the film and neutralize the acid. If base levels inside the cleanroom were indeed high, the second wafer should have displayed a noticeable increase in the dose to clear due to the need for increased exposure dose to produce excess acid to compensate for the acid neutralized by base. This was not the case. Both wafers indicated a dose to clear of 8.6 mJ/cm^2. This appears to indicate that the base filtration was working properly, and that Dill C measurements could be performed with minimal concerns of base contamination.

3.4 Results and Discussion - The Effect of Relative Humidity upon Water Sorption

As described in section 3.1.2, IDE sensors coated with polymer films are often used as relative humidity sensors[50,52-55,58]. The addition of water to a polymer film dramatically changes the resistance as well as the net dielectric constant of the polymer allowing the IDE user to monitor the level of water in the polymer film by examining the IDE sensors' measured resistance or capacitance. As relative humidity changes the water content within the polymer film also changes resulting in a corresponding resistance or capacitance change, allowing one to easily monitor relative humidity via resistance or capacitance measurements taken from the polymer coated IDE sensor.

While the sensitivity of polymer coated IDEs to relative humidity is a blessing in terms of creating humidity sensors, the capacitance changes that are caused by varying relative humidity are troublesome for Dill C measurements. Any change in capacitance

not caused by the addition of photoacid to the polymer matrix adds new complexity to the Dill C analysis. Data collected in a laboratory environment at one relative humidity value cannot be compared to data collected in an environment at a second relative humidity value due to a shift in the baseline capacitance from differences in background water content. All work presented in this thesis was performed in laboratories located in Atlanta, Georgia. Relative humidity is known to vary greatly from one day to another at this location. It is not uncommon for the environment to be relatively dry one day (relative humidity of around 25%) and then be quite wet the next day (relative humidities of more than 80%). Because of the potential for such rapid, large swings in relative humidity, and due to the potential for baseline capacitance changes to introduce error into the Dill C analysis, it is important that the water sorption properties of the resist materials studied using IDEs be understood. A detailed study of the effects relative humidity has upon the equilibrium water uptake as well as the rate of water sorption was performed.

3.4.1 The Effect of Relative Humidity on Equilibrium Water Uptake

The effect of ambient relative humidity on water sorption in three photoresist polymers was investigated by measuring the frequency shift of polymer coated QCM crystals exposed to varying relative humidity environments. The QCM oscillation frequency versus relative humidity data was then used to calculate a relationship between water mass in the thin film versus water partial pressure in the environment. Water partial pressure was chosen as the independent variable rather than relative humidity so that the data presented here can be used in any laboratory anywhere on earth. The relative humidity measured in one location is not necessarily the same as that measured in

another location due to differences in atmospheric pressure and ambient temperature. Partial pressure is a "true" measurement of the concentration of water in the air regardless of location.

Obtaining the water partial pressure is a simple calculation that only requires knowledge of the water vapor pressure at the experimental temperature of 22.8°C (20.777 mm Hg) and the relative humidity in the measurement environment[60]. Relative humidity is the partial pressure of water divided by the vapor pressure of water. Thus to obtain the partial pressure of water one has to simply multiply the relative humidity by the vapor pressure of water.

The next step in obtaining water uptake versus water partial pressure data was to convert the equilibrium QCM frequency data into mass or percent water uptake. Initially, the QCM frequency data was plotted against water partial pressure and a linear least squares fit was used to model the data. A representative example of such a plot is illustrated in Figure 3.7 for PHOST.

As can be seen from Figure 3.7, the linear fit of the PHOST data captures the trend in the data well with an R^2 value of approximately 0.97. The y-intercept of the linear fits should in principle be the frequency of the polymer coated crystal in a completely dry environment, and thus it is used later to calculate the "dry" mass of the polymer thin film. It should be noted, however, that it is quite likely that there are small quantities of water tightly bound to the polymer matrices that would remain in the film even in completely dry environments. Thus the absolute mass of the completely water-free polymer film may be slightly lower than that calculated from the method used here.

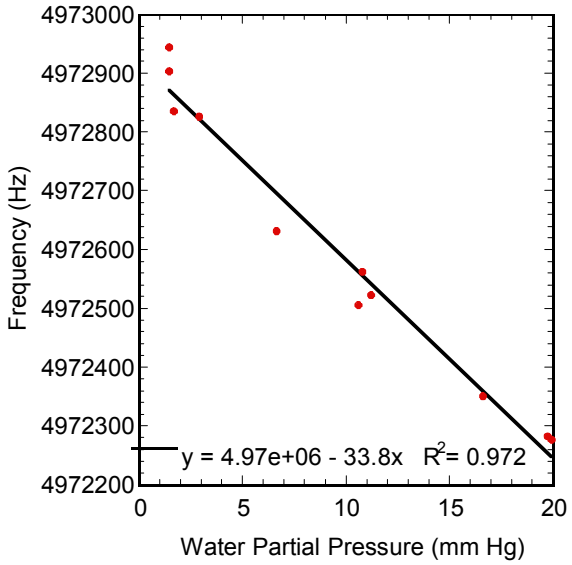

Figure 3.7 Linear relationship between QCM crystal frequency and water partial pressure used to find the "dry" mass of the polymer film.

For the purposes of this work, the calculated "dry" mass is used to estimate the overall mass gain due to water sorption rather than actual water content of the film. The water content values reported later are probably reasonable estimates of actual water content, however, it should be noted that the actual total water content in the materials may be slightly higher than that reported in this thesis due to the effect of bound water.

The natural frequency of the QCM crystal used in each experiment was measured prior to being coated with the polymer film. The mass of material on the crystal can then be calculated from the various QCM frequency values using equation 3.1, which is simply a variation of the Sauerbrey equation[62] .

$$m_{added} = \frac{(f_{uncoated} - f_{measured})}{C_f} \qquad [3.1]$$

In this equation, m_{added} is the mass added to the crystal per unit area, $f_{uncoated}$ is the natural frequency of the clean crystal, $f_{measured}$ is the frequency of the crystal after some mass is added to the crystal's surface, and C_f is a constant calculated using equation 3.2 below[62].

$$C_f = \frac{2f_q^2}{(\rho_q v_q)} \qquad [3.2]$$

Here f_q is the resonant frequency of the bare crystal (nominally 5.0 MHz), ρ_q is the density of the quartz crystal (2.649 g/cm^3), and υ_q is the shear wave velocity of the AT cut quartz crystals used in this study (332,200 cm/s). It is important to note that the Sauerbrey equation shown above is only valid for thin films that can be considered rigid masses as the Sauerbrey equation assumes that the small amounts of mass added to the quartz crystal can be treated as equivalent thicknesses of quartz. If the film is not a rigid mass, the shear wave in the QCM crystal will lose a significant amount of energy through visco-elastic losses in the non-rigid mass. This energy loss will in turn affect the frequency measurement and the crystal behavior can deviate strongly from the Sauerbrey relationship. The rigid mass requirement for the Sauerbrey equation is especially important for high mass loadings on the QCM crystal. A good indicator of the elastic behavior of the quartz crystal/polymer film system is the ratio of the acoustic impedance (Z) of the respective materials[62]. As the elastic behavior of the polymer film changes, the value of Z will change as well. It has been discussed by Lu and Czanderna that for high mass loadings on a QCM significant deviations from the Sauerbrey equation can occur for small changes in Z[62]. This could mean the potential for calculation errors as water is

absorbed into the polymer films, plasticizes them, and changes their elastic behavior (Z value). Fortunately, any changes in the elastic behavior of the polymer films studied in this paper should not create a significant deviation from the Sauerbrey equation. While demonstrating that changing Z at high mass loadings created significant measurement errors, Lu and Czanderna also demonstrated that at low mass loadings or crystal frequency shifts, (i.e. delta frequency due to mass addition divided by crystal resonant frequency is less than 0.05) the mass/frequency relationships for essentially all values of Z will converge upon the Sauerbrey relationship[62] . The frequency shift ratios observed in the experiments reported here were very small (0.001 - 0.002), and thus the use of the Sauerbrey relationship to calculate mass added to the crystal from the crystal's frequency shift should introduce insignificant error.

Using equations 3.1 and 3.2, as well as the QCM frequency data, it is possible to calculate equilibrium water uptake data for various water partial pressures. Figure 3.8 illustrates this data for all five polymer samples studied in this work. As expected, the water content of the polymer films increases with increasing ambient water content (i.e. relative humidity, or water partial pressure). In fact, in this case the water uptake exhibits a linear relationship with water partial pressure over the entire range of measured polymer water contents, similar in nature to that observed for ideal liquid-vapor systems described by Henry's Law.

Table 3.1 lists the equilibrium water uptake in a saturated environment for these polymers. All three polymer types used in this study contain hydroxyl functional groups that are hydrophilic and capable of hydrogen bonding to some degree with sorbed water molecules. Due to the hydrophilic nature of these groups, all of the polymers studied are

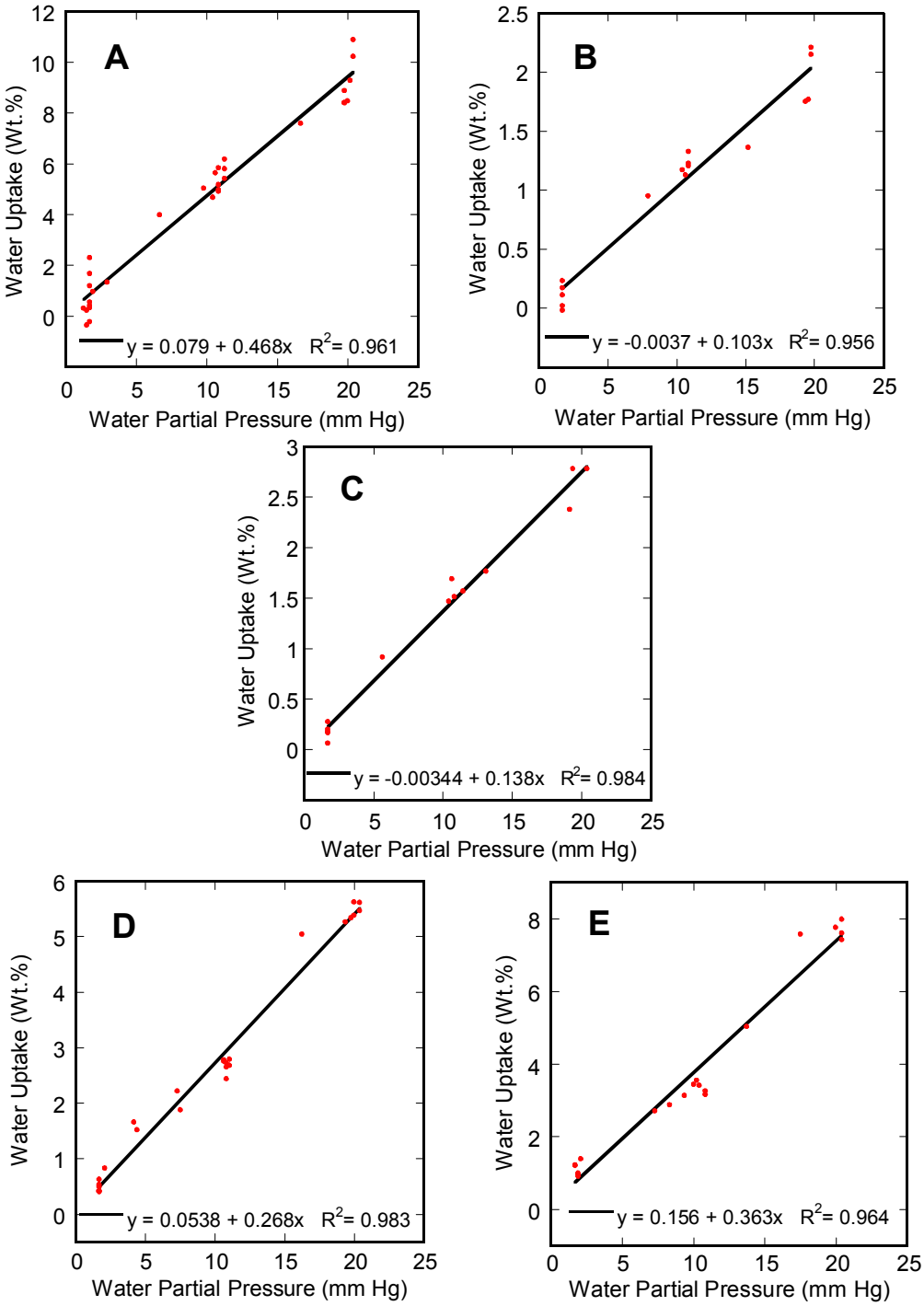

Figure 3.8 Equilibrium water uptake data versus water partial pressure for (a) PHOST, (b) Novolac - 1, (c) Novolac - 2, (d) HFAPNB – 1, and (e) HFAPNB - 2.

Table 3.1 Summary of equilibrium and dynamic water sorption data for all samples.

Polymer	Molecular Weight (M_w)	Maximum Water Uptake at Saturation (Wt.-%)	Estimated Diffusion Coefficient (x 10^{-9} cm^2/s) For Water Sorption
PHOST	11,800	9.8	1.8
HFAPNB-1	8,882	5.6	3.5
HFAPNB-2	94,159	7.7	1.9
Novolac-1	1,615	2.2	0.31
Novolac-2	~22,000	2.9	0.28

capable of absorbing significant quantities of water. Nevertheless, there are sharp differences in the amount of water sorbed at saturation between the novolac resins (~ 2 – 3 wt.%), HFAPNB resins (~ 5 – 8 wt.%), and the PHOST (9 – 10 wt.%). This difference in the amount of water sorbed in these materials can be a result of various factors including free volume differences between the materials and differences in the affinity or solubility of water in the polymers. Based on knowledge of the behavior of these polymers in their use as photoresist resins, it is believed that one contributor to these differences in water uptake is the ability of these polymers to exhibit hydrogen bonding between hydroxyl groups on the same polymer chain or between chains. Such hydrogen bonding could then effectively reduce the ability of these hydroxyl groups to bind to as many or as strongly to sorbed water molecules, thus lowering the capacity of the polymer to absorb water. Novolac and HFAPNB polymers are known to form hydrogen bonds between hydroxyl groups adjacent to one another on the same polymer chain or on neighboring chains[70,71], while little evidence has been found for hydrogen bonding in PHOST matrices. This fact is supported by the ability of researchers to develop dissolution inhibitors that function through hydrogen bonding for HFAPNB type

materials and novolac, while attempts to make such inhibitors for PHOST have been unsuccessful[70-72].

In order to further test this hypothesis, water sorption in two different molecular weight HFAPNB polymers was measured. HFAPNB–1 had a low molecular weight of 8,882 while HFAPNB-2 had a much higher molecular weight of 94,159. It is known that the poly(norbornene) materials used in this work, which were made using Pd catalysts, form an unusual rigid-rod like helix-kink morphology[71,73]. This polymer secondary structure results in a number of unusual physical properties for these materials. As the molecular weight of the HFAPNB is increased, it has been observed through fourier transform infrared spectropscopy studies that the level of hydrogen bonding between hydroxyl groups in thin films of this material decreases[71]. The higher molecular weight HFAPNB samples have a much higher probability of having a "kink" in the polymer structure. These kinks effectively space the hydroxyl groups further apart, preventing them from hydrogen bonding with one another to form intermolecular links. Therefore, with more hydroxyl groups free for hydrogen bonding with water one might expect the amount of water uptake in higher molecular weight HFAPNB polymers to increase as the molecular weight of the material increases. Thus, the ultimate equilibrium water uptake for HFAPNB-2 was expected to be higher than that of HFAPNB-1. As illustrated in Table 3.1, this increase in water uptake with molecular weight has been observed. The higher molecular weight HFAPNB absorbed 7.7 wt.% while the lower molecular weight version absorbed only 5.6 wt.%. It should be pointed out that this increase in molecular weight for the HFAPNB films may also result in a slight increase in the polymer free

volume, which may also contribute to this increase in the polymer's ability to absorb water.

3.4.2 The Rate of Water Diffusion into Photoresist Polymer Films

Besides the equilibrium water uptake of the resist polymers at various water partial pressure values, the rate at which the water is absorbed and reaches its equilibrium uptake is also of significance for the Dill C measurement technique. A typical Dill C measurement experiment that involves coating an IDE with a CAR film, exposing the film and sensor to incremental exposure doses, and then collecting capacitance data will usually require experimental times on the order of 30 minutes. If the diffusion of water into the resist polymer is very slow, then it is entirely possible that on the time scale of the experiment very little water will diffuse into or out of the polymer film as the relative humidity changes, causing minimal changes in the measured capacitance. Likewise, if the diffusion of water in the polymer films is quite rapid, then any change in relative humidity will have an immediate impact on the observed capacitance values measured from the IDE sensor.

Thus, the dynamic frequency data collected as the QCM crystal was transferred from the "dry" chamber to the "wet" chamber was examined to determine the rates of water absorption and diffusion during the sorption and desorption experiments. Figure 3.9 illustrates a typical set of sorption-desorption QCM frequency data from these experiments.

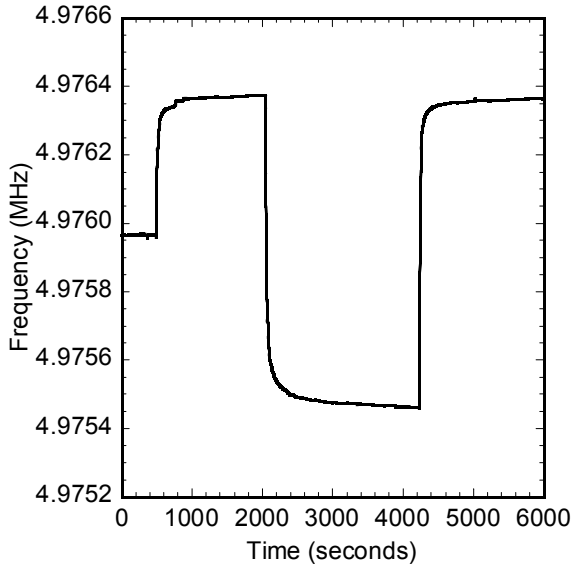

Figure 3.9 Typical sorption and desorption QCM frequency response.

As shown in Figure 3.9, the polymer coated QCM crystals were initially allowed to reach equilibrium at room conditions, as indicated by the initial flat line. Then, the QCM holder and crystal were transferred into the dry chamber and allowed to equilibrate. Upon doing so, water vapor within the film immediately began to leave, resulting in a decrease in total mass on top of the crystal surface as indicated by the rapid rise in frequency and eventual plateau. After reaching equilibrium at dry conditions, the QCM holder and crystal were immediately transferred into the wet chamber, where at this time water from the environment was rapidly absorbed into the polymer film, increasing the total mass on the quartz crystal. This increase in mass was indicated by the rapid drop in frequency as shown in Figure 3.9. After reaching equilibrium at wet conditions, the QCM holder was transferred back to the dry chamber and the process was repeated several times.

In all cases, the frequency data indicated that qualitatively the sorption-desorption processes are quite rapid, with the majority of the water gain or loss occurring during the first few seconds after the environmental conditions are changed. In fact, all polymers sorbed or desorbed at least 80% of their final equilibrium water uptake within the first three minutes of exposure to the new environment.

If purely Fickian diffusion was occurring during these processes, the diffusion behavior and water uptake could be modeled using the following equation for mass uptake into a thin, semi-infinite slab of material from one face[74-80].

$$\frac{M_t}{M_\infty} = 1 - \frac{8}{\pi^2}\sum_{n=0}^{\infty}\frac{1}{(2n+1)^2}\exp\left[-\frac{(2n+1)^2\pi^2 Dt}{4L^2}\right] \qquad [3.3]$$

where M_t is the mass uptake at time t, M_∞ is the ultimate mass uptake at time $t = \infty$, D is the diffusion coefficient (cm^2/s), and L is the film thickness. For the initial phases of the sorption process ($M_t/M_\infty < 0.6$), the water uptake for these polymers is observed to follow a linear relationship versus the square root of time as would be expected for a Fickian diffusion process. Thus, a simplified version of equation 3.3 can be used that describes mass uptake into a thin, semi-infinite slab from one face[75,76,79,81,82] during the initial uptake times.

$$\frac{M_t}{M_\infty} = \frac{2}{L}\left(\frac{Dt}{\pi}\right)^{\frac{1}{2}} \qquad [3.4]$$

This equation is often referred to as the "short time" approximation and was used here to estimate a Fickian diffusion coefficient for water in the various polymers studied. Fractional mass uptake (M_t/M_∞) was calculated from the QCM frequency data and plotted against $t^{1/2}$ and the slope of the resulting plot from $M_t/M_\infty = 0$ to $M_t/M_\infty = 0.6$ was used to evaluate D. Figure 3.10 illustrates the fractional mass uptake versus the square root of time for novolac sample #2, which was typical for the polymers studied in this work.

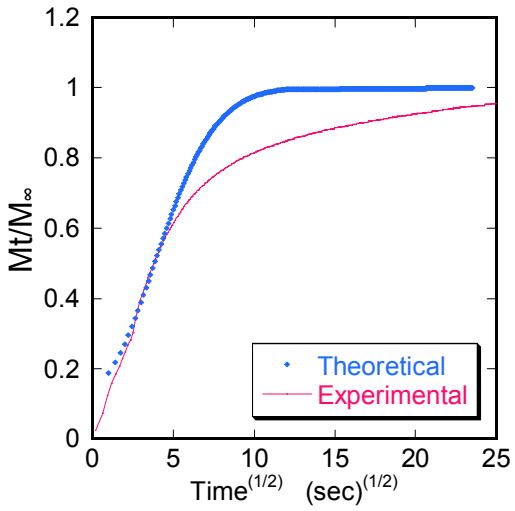

Figure 3.10 Relative water mass uptake versus the square root of time for novolac-2. Also shown is the theoretical Fickian mass uptake versus the square root of time calculated using the diffusion coefficient found from the "short time" approximation.

Table 3.1 shown earlier lists the estimated Fickian diffusion coefficient values for the polymers studied in this work. These diffusion coefficients are applicable generally for water uptake values where $M_t/M_\infty < 0.6$. PHOST and the HFAPNB polymers absorbed water quite rapidly with diffusion coefficient values between 1.8×10^{-09} and 3.5

x 10^{-09} cm^2/s. The novolac resins were somewhat slower with values near 0.3 x 10^{-09} cm^2/s.

While no other diffusion coefficient data for water sorption could be found in the literature for PHOST or the HFAPNB samples, data was located for novolac for comparison to the values found here. It is interesting to note that the estimated diffusion coefficient for the novolac resins (0.3 x 10^{-09} cm^2/s) is somewhat smaller than that found in previous work with novolac resist systems (1.0 - 1.3 x 10^{-09} cm^2/s)[83-85]. Though it is not certain, it is possible that this difference in diffusion rate is due to differences in composition of the novolac materials studied. In particular, each of the three previous studies examined water sorption in commercial positive type novolac resists (AZP4620 and AZ 9260 from Clariant[83] , HPR 204 from Hunt Chemical[84] , and OFPR 800 from Tokyo Ohka Kogyo[85]). In addition to the novolac matrix polymer, these systems were undoubtedly loaded with a sensitizer compound (most likely some form of diazonapthoquinone (DNQ) dissolution rate inhibitor) and other dissolution rate modifiers. The system studied here consisted only of a pure novolac polymer matrix (i.e. no sensitizers or other additives) cast from a single solvent. It is possible that these additives could be partly responsible for the faster diffusion observed in the commercial resists. For example, it is possible that the DNQ and other additives may act as plasticizers and allow for faster rates of diffusion (although it must also be noted that DNQ could also potentially lessen the rate of diffusion due to hydrogen bonding with the hydroxyl groups on novolac). It is also possible that film additives and variations in the film preparation conditions (such as bake temperatures) could lead to varying amounts of residual casting solvent in the film. Such film composition and thermal history

differences could also then lead to changes in the diffusion behavior of the films due to plasticization and other effects.

As seen in Figure 3.10, the fractional mass uptake data exhibited Fickian diffusion behavior in the initial "short time" phases of the sorption process. This is indicated by the initially linear trend in mass uptake versus the square root of time. Fickian behavior in the initial "short times" was observed for all of the polymers examined. Figure 3.10 also illustrates theoretical Fickian mass uptake calculated from equation 3.3 using the diffusion coefficient found from the "short time" Fickian approximation (i.e. the short time approximation was used to find the diffusion coefficient from the linear portion of the mass uptake curve, and then this diffusion coefficient was used in equation 3.3) found for that particular novolac sample. Obviously a significant deviation from Fickian diffusion occurs at high mass uptake values. This type of deviation was observed to varying degrees for all of the polymers used in this work and is indicative of a concentration dependent diffusion coefficient[76,78].

3.4.3 The Effect of Humidity Upon IDE Capacitance Measurements

As discussed earlier in section 3.1.1, the geometry of the IDEs used to measure the Dill C rate constant renders them incredibly sensitive to small changes in the dielectric properties of the coated film. This sensitivity is what is exploited in the proposed Dill C measurement routine, where changes in the dielectric constant of the CAR film caused by the generation of photoacid will serve as a measuring stick for PAG photolysis. Because IDEs are so sensitive to changes in dielectric properties of the film coating them, and because the QCM results discussed in sections 3.4.1 and 3.4.2

demonstrated that small changes in relative humidity can cause significant changes in the equilibrium water content of common resist polymers, it is necessary to determine exactly to what extent relative humidity changes can alter the measured capacitance, or the net dielectric properties of a resist coated IDE. Thus, capacitance measurements of polymer coated interdigitated electrodes were utilized to determine the effect of humidity upon the polymer's dielectric properties. Three separate IDE sensors were spin coated with a photoresist polymer and then placed inside the relative humidity chamber described in section 3.2.2. The capacitance of the IDE sensor was recorded after the sensor had reached equilibrium at a particular water partial pressure value. Figure 3.11 illustrates the individual capacitance measurements collected for the three polymer samples studied at each water partial pressure value. In an effort to conserve the interdigitated electrodes used, only three of the five polymer samples studied using the QCM were measured using the IDE sensors: PHOST, HFAPNB-1, and novolac-2. In all cases, a linear relationship was found between measured capacitance and water partial pressure, similar to that found in previous studies that utilized polymer coated interdigitated electrodes as humidity sensors[52].

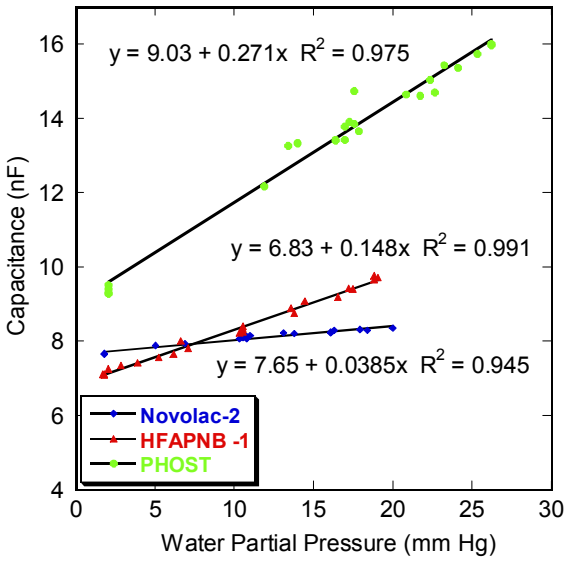

Figure 3.11 Capacitance of resist coated IDEs versus the partial pressure of water for novolac-2, HFAPNB-1, and PHOST.

The importance of maintaining a constant humidity environment when performing acid measurement experiments is readily apparent after examining Figure 3.11. PHOST, which was shown earlier to absorb the most water, also exhibits the strongest dependence of measured capacitance (i.e. film dielectric constant) on water partial pressure. The PHOST film showed roughly a 6 nF increase in measured capacitance, representing a change of almost 70 percent for the film between dry and humid conditions. The other polymer films also showed significant changes in capacitance as water partial pressure varied from near 0 to over 25 mm Hg. The HFAPNB coated IDE fluctuated from near 7 nF to near 10 nF, while novolac displayed a capacitance change of near 1 nF.

In addition to capacitance, the relationship between the film's water content and the net dielectric constant of the polymer films was also of direct interest. The dielectric

constant of the polymer films was derived from the IDE capacitance measurements through a technique known as conformal mapping that is described elsewhere[48] and discussed further in Chapter 4. In this technique, the geometry of the IDE electrode fingers are mathematically manipulated so that they can be treated as an equivalent parallel plate capacitor, greatly simplifying the analysis of the IDE fingers' electric fields. Without the transformations, modeling the capacitance of IDE fingers becomes extremely difficult due to the presence of the fringe fields located above and below the fingers. More will be said about conformal mapping equations later in Chapter 4 section 3.3.

By using the relationships derived earlier in section 3.4.1 for equilibrium water content versus water partial pressure, it was possible to calculate data for the net dielectric constant of the polymer films versus water content as shown below in Figure 3.12. These relationships were in turn used to investigate the applicability of common dielectric mixing rules to the water/resist matrix system. It was initially hoped that the capacitance data collected in these water sorption experiments for each polymer system could be described by a single, common dielectric mixing rule. If this turned out to be the case, it might then be possible to use the mixing rule along with our knowledge of resist water content at various relative humidities to predict shifts in the baseline capacitance data recorded for the PAG kinetics studies. In other words, the mixing rule could be used to account for variations in capacitance data due to changes in relative humidity in the laboratory without having to run experiments and collect data to measure this effect each time. To test this idea, one of the most common, and more general mixing rules was applied to the collected capacitance data. This rule is a simple power-law mixing rule with one adjustable parameter, n, as show in equation 3.5 [86,87].

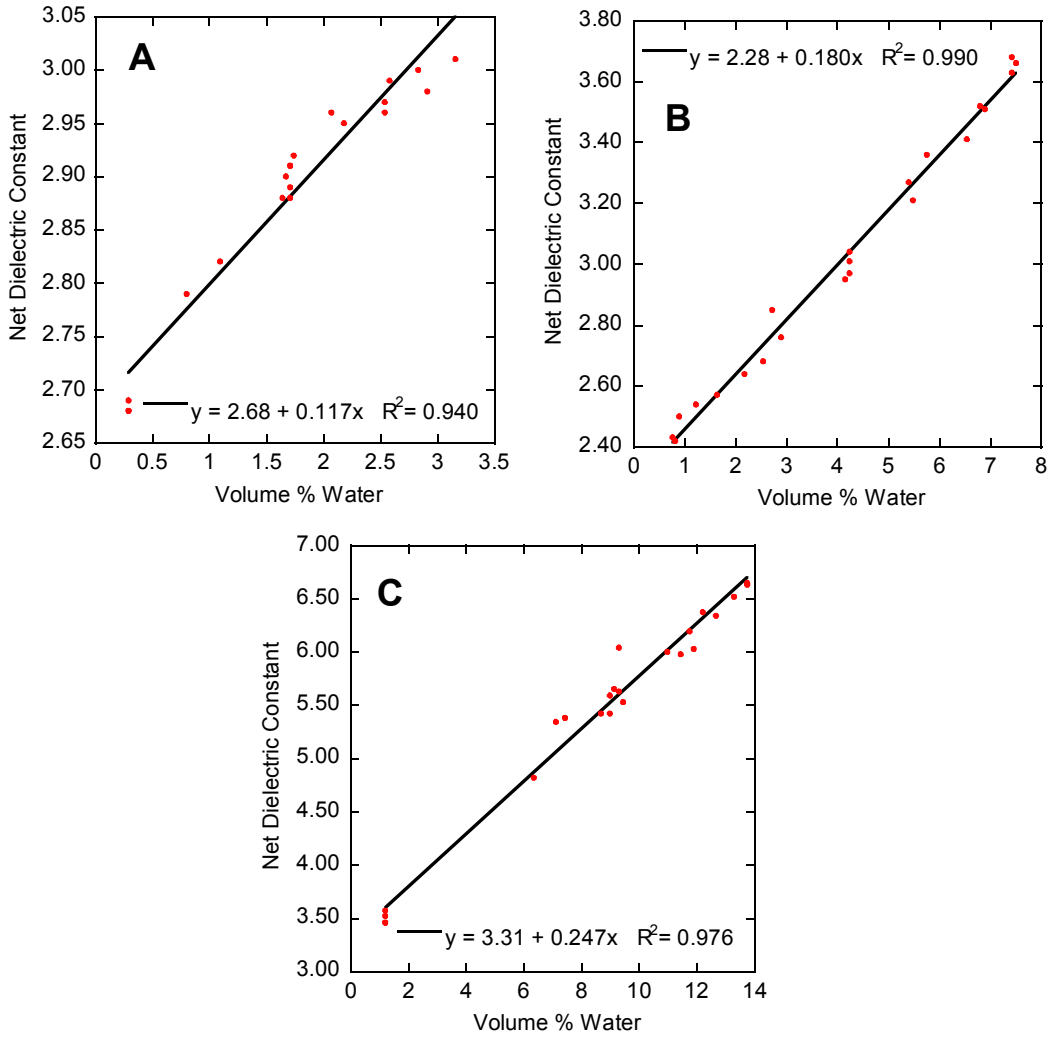

Figure 3.12 Net dielectric constant versus water content (in volume %) for (a) Novolac-2, (b) HFAPNB-1, and (c) PHOST.

$$k_{effective}^{n} = v_1 k_1^{n} + v_2 k_2^{n} \qquad [3.5]$$

Here, $k_{effective}$ is the net, or effective dielectric constant of the film, k_1 and k_2 are the dielectric constants of components 1 and 2 in the mixture, and v_1 and v_2 are the volume fractions of each component in the mixture. "n" is an adjustable parameter that should vary from -1 to 1 (known as the Wiener bounds[86,87]) for all dielectric mixtures, depending upon the type of mixing that takes place between the two components within the film. An n value of +1 is equivalent to capacitors connected in parallel, while an n value of –1 is equivalent to capacitors connected in series. Figure 3.13 shows the results of fitting the power-law equation to the effective dielectric constant data collected for the three polymer systems. Similar fits were obtained for all three polymers. The power-law equation proved to be quite successful at accurately describing the dielectric mixing of all three polymer samples. The best fit n values found for the samples were 0.33, 0.37, and 0.12 for HFAPNB-1, PHOST, and novolac-2 respectively. It was desired that one common value of n could be used to describe the effects of mixing water into all resist polymers so that the power-law could be universally applied. The low n value of novolac-2 in comparison to the higher, more equivalent values for PHOST and HFAPNB-1 indicates that this may not be possible. The interaction between water and the novolac matrix polymer in terms of dielectric properties is obviously somewhat different than that in PHOST and HFAPNB.

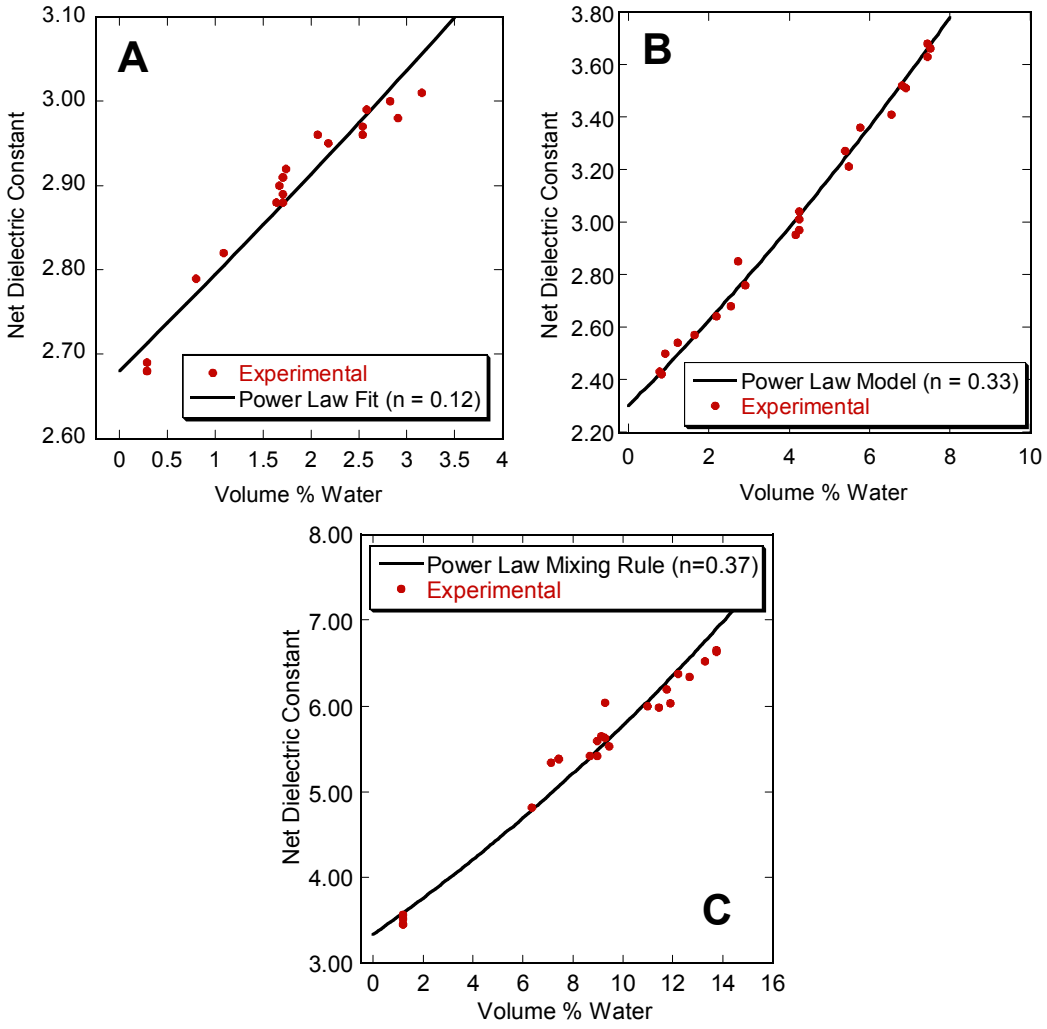

Figure 3.13 Best fit of power-law dielectric mixing rule for (a) Novolac-2, (b) HFAPNB-1, and (c) PHOST.

3.5 Results and Discussion – Spin Coating Film Quality

One of the first potential problems encountered while working with the IDE sensors was the task of uniformly coating the electrode fingers by spin coating. It was unclear how well polymer thin films would coat the sensor fingers and fill the regions between each finger. It is important that three criteria be met when coating the IDE

sensors. First, the polymer film needs to fill the regions between the fingers with near zero void formation. Voids of air between the electrode fingers would alter the net dielectric constant of the polymer film in this region due to the low dielectric constant of air (~ 1) as compared to the dielectric constant of the PHOST film (~ 3 – 4). It is important that only the PHOST film loaded with PAG contribute to the measured capacitance of the IDE, and not air voids between the fingers, in order to properly model the capacitance behavior of the IDE sensor. In addition, since the amount of acid typically produced by a PAG is incredibly small, it is important that all of the electric field regions be exposed to the photoacid so that as much signal change as possible can be obtained. Voids of air would essentially lower the sensitivity of the IDE fingers to the production of acid.

The second criteria that must be met involves the thickness of the resist film over the top of the electrode fingers. As depicted in Figure 3.14a, there are electric fringe fields located above and below the electrode fingers. These fields contribute significantly to the overall measured capacitance, and thus it is important that these fields be contained entirely within the resist film above the fingers, as well as the SiO_2 layer below the fingers. If significant portions of the fringe fields were allowed to escape out of the resist or SiO_2, the dielectric properties of air and silicon would then influence the measured capacitance and the exact distance over which these fringe fields propagated into these semi-infinite media would be important in order to properly model the capacitance response. Thus, failure to contain the fringe fields in the resist and oxide layers adds confounding variables to the Dill C analysis of the capacitance response. Therefore, it

was desirable to have a film thickness above and below the fingers that would capture essentially all fringe fields. Most literature sources agree that a thickness equivalent to the

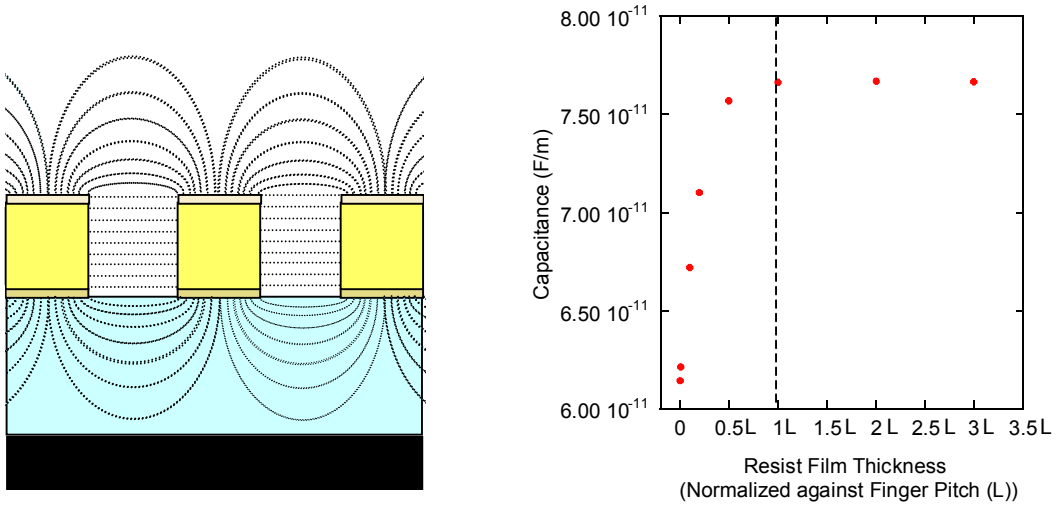

(a) (b)

Figure 3.14 (a) Cross section view of IDE showing fringe electric fields and (b) finite element simulation results demonstrating that the fringe fields extend a distance above the electrode fingers equivalent to the electrode pitch (L).

electrode pitch should be sufficient to capture virtually all of the electric fringe fields.[47,52] This number was confirmed through two dimensional finite element simulations of the electromagnetic fields using Maxwell 2D simulation software from Ansoft Corporation, as depicted in Figure 3.14b. In these simulations, a two dimensional model consisting of the cross section of two electrode half-widths separated by the electrode spacing was utilized. Symmetric boundary conditions were used to take advantage of the periodicity found in interdigitated structures. Inputs to the model included the electrode width,

electrode spacing, electrode height, SiO_2 film thickness, and polymer film thickness. In addition to these geometric parameters, appropriate material property sets also were applied to the different structures. For this model, materials that closely resemble the true system were chosen: aluminum for the electrodes, silicon dioxide for the SiO_2 layer, silicon for the substrate, and a polyimide film was chosen to serve as a generic polymer film. In each simulation, the thickness of the polyimide film was varied and the effect that this thickness variation had upon the total measured capacitance was recorded. As can be seen in Figure 3.14b, once the thickness of the resist over the electrode fingers reaches that of the electrode pitch (L), no further significant change in capacitance occurs. This indicates that the film thickness has essentially captured all of the fringe electric fields above the electrode fingers. When the thickness is less than L, the fringe fields are influenced by the dielectric properties of air (k~1) and the capacitance value drops.

The third and final objective of the spin coating process involves the planarity of the resist film. It was desirable, though not absolutely necessary, that the coated resist film over the electrode fingers be as planar as possible, and not duplicate the underlying topography. A planar film makes subsequent analysis of the light propagation and exposure dose profiles within the resist film substantially less complex.

In order to determine how well the coating process met these three criteria, a series of scanning electron micrographs were taken of cross sections of resist (PHOST) coated IDEs using the standard coating process described in section 3.2.3. An example of such an SEM micrograph of a resist coated IDE is shown in Figure 3.15.

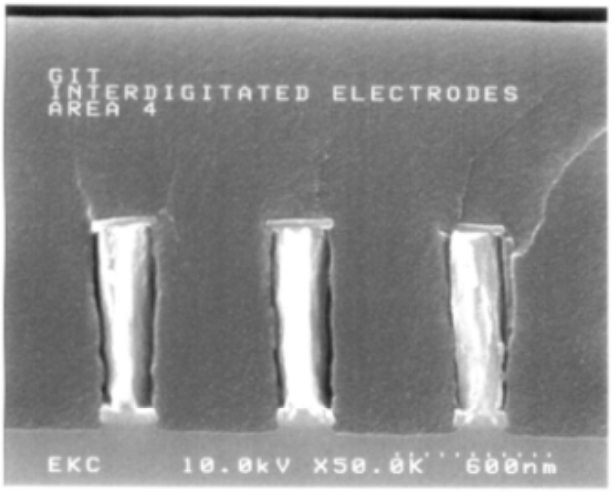

Figure 3.15 Cross section of resist coated IDE sensor.

The information provided from the SEM photos indicates that all three criteria were met by the coating process. The photos indicate that the polymer fills the space between the electrode fingers in a uniform fashion with no noticeable voids. Also, the top surface of the resist film is quite planar, with very little indication of the underlying topography. Finally, measurements taken from the SEM photos indicate a film thickness above the electrode fingers of approximately 0.8 microns, which is indeed thicker than the 0.7 micron electrode pitch. The thickness of the SiO_2 layer below the fingers was fabricated to be 0.8 microns. Therefore, these thicknesses should be sufficient to capture essentially all of the electric fringe fields above and below the electrode fingers.

3.6 Conclusions and Recommendations

The geometry of the interdigitated electrode sensors used for the work presented in this thesis is such that the IDE sensors are very sensitive to any changes in the

chemical makeup of the material that is coating them. The individual fingers themselves are 0.33 μm wide with 0.37 μm spacing between adjacent fingers. At such size scales, an incredibly large number of fingers (over 11,000) can be inserted into a very small area, such as the 0.8 cm square sensing region of the IDEs used in this work. Because of their tremendous sensitivity, it is imperative that a thorough review of any potentially complicating issues be made, and that these issues are well understood. Three such issues are particularly important for the use of IDE sensors as Dill C measurement tools. First, it is important that any ambient base be removed from the measurement environment due to concerns of acid neutralization. Second, with relative humidity potentially changing on a daily basis, it is important that the effects relative humidity has upon water sorption and the net dielectric constant of the resist films be understood. Finally, for Dill C modeling purposes, it is very important that the resist film coats the IDE sensor with a high quality, void-free film. The information provided in this chapter reported the results of our efforts to understand these three potentially complicating issues.

A "base-free" class 1000 cleanroom was constructed and supplied with the equipment necessary for performing a Dill C measurement using IDE sensors. This cleanroom was built from non-outgassing materials and is supplied particle free, laminar air flow from five HEPA fan units. Each HEPA fan is equipped with a base filter unit designed to remove 99.99% of all ambient base from the incoming air. A simple dose to clear experiment was performed to test whether or not the cleanroom's air contained minimal base. The results of this experiment indicated that no significant shift in the CAR film's dose to clear was observed after exposure to the cleanroom's air for an

extended period of time, indicating that the cleanroom was acceptable for chemically amplified resist work. No significant neutralization of the photoacid is expected.

To understand the effect of varying relative humidity, water sorption data were collected for five different polymers at various relative humidity values using a quartz crystal microbalance. Based on the frequency data collected from the QCM system, a number of conclusions can be drawn. First, a linear relationship was found for water uptake versus water partial pressure for all polymers studied. All polymers absorbed significant quantities of water in a saturated environment with PHOST absorbing the most (9.8 wt.%) followed by high molecular weight HFANB (7.7 wt.%), low molecular weight HFANB (5.6 wt.%), and the novolac resins (2 – 3 wt.%). The ability of hydroxyl groups on the polymer to hydrogen bond with water is suspected to play a major role in the ability of the polymer to absorb water. Second, the rates of sorption and desorption in all of the polymers studied were rapid, with the majority of the water uptake occurring within the first few seconds of exposure to the humid environment. The diffusion of water into the polymers at low water uptakes (i.e. $M_t/M_\infty < 0.6$) followed Fickian behavior as exhibited by the linear relationship between fractional mass uptake and the square root of time for these materials. At high mass uptake values, all polymers deviated from Fickian behavior and exhibited trends indicative of concentration dependent diffusion. Finally, a linear relationship was found between measured capacitance of polymer coated interdigitated electrodes and water partial pressure. The sorption of water into polymer thin films caused significant shifts in measured capacitance, with PHOST changing by nearly 6 nF (nearly 70% of the original baseline value). A common power-law dielectric mixing rule was shown to accurately predict the

net dielectric constant of water/polymer mixtures in various relative humidity environments, though a common power law exponential factor (n) was not observed.

Finally, the ability of the IDE sensors to be spin coated with polymer films was investigated by taking cross section SEM micrographs of resist coated sensors. The SEM photos indicated three important qualities of the spin coating process. First, the films that coated the IDE were planar. Little to none of the underlying topography was evident in the top surface of the film, greatly simplifying modeling efforts of the exposure intensities within the film. Second, the polymer appears to adequately fill the regions between IDE fingers with little or no void formation. Finally, the thickness of the film over the IDE fingers was found to be thick enough to contain nearly all of the IDE sensor's top fringe fields.

Based upon the findings from the experiments performed in this work, the following recommendations can be made for minimizing the effects of the three confounding variables discussed in this work. First, all work should be performed inside the "base-free" cleanroom to minimize the effects of acid neutralization. The cleanroom's base filtered HEPA fans should be turned on and allowed to run for at least 30 minutes prior to use. Based on the air flow from the HEPA fans this time should allow for several complete purgings of the room's air, eliminating most of the ambient base and greatly reducing particle counts. Second, to minimize the effects of water sorption, all Dill C measurements for a particular PAG/polymer combination should be conducted on a single day in as small of a time scale as possible. Limiting the experimental time to a single day and short experimental period lessens the chances of relative humidity dramatically changing and affecting the baseline capacitance values

measured for the resist coated IDEs. Relative humidity should also be monitored using a hygrometer during each set of Dill C measurements to make certain the relative humidity does not change dramatically during the course of a set of experiments. More will be said later in Chapter 5 about ways to minimize the effects of relative humidity, when a new data analysis technique will be introduced.

CHAPTER 4*

INTERDIGITATED ELECTRODE SENSORS A DILL C MEASUREMENT TOOL

4.1 Introduction

Having established a suitable "base-free" working environment for chemically amplified resist research, and freshly armed with a better understanding of the spin coating capabilities of IDEs and water sorption properties of photoresist materials, the next logical step in this work was to begin developing the electrical measurement procedure and data analysis technique that would be used to obtain the Dill C rate constant from IDE sensor electrical measurements. The information presented in this chapter focuses on this task in great detail.

In order for the Dill C parameter to be measured via IDE sensors, two critical goals must be met. First, an electrical measurement procedure must be demonstrated that is both easy to facilitate with the IDE sensors and capable of detecting the presence of photoacid in the small amounts typically found in chemically amplified photoresists. Second, once it has become obvious that such a technique exists and that some form of electrical data can be collected that is directly related to photoacid within the polymer film, the next goal is to determine an effective means of analyzing the raw electrical data

* Material presented in this chapter has appeared in part in previously published articles:

Berger C, Henderson C, *Measurement of photoacid generation kinetics in photoresist thin films via capacitance techniques*, Proc. of SPIE, **5039**, 322 – 333, 2003.

Berger C, Byers J, Henderson C, *Using interdigitated electrodes for measuring photoacid generator kinetics in chemically amplified resists*, Journal of the Electrochemical Society, **151(2)**, G119 – G130, 2004.

so that photoacid generation kinetics data can be extracted from it. The work presented in this chapter demonstrates the efforts taken to accomplish both of these goals through the results obtained from a series of experiments with a model chemically amplified resist system composed of a poly(p-hydroxystyrene) matrix loaded with triphenylsulfonium triflate PAG. Other PAG/polymer systems will be discussed in later chapters.

4.1.1 Capacitance, Dielectric Constant, and Dill C Measurements

In order to use IDE sensors to measure Dill C parameters some form of electrical measurement must be taken from the sensor that indicates photoacid's presence. For the measurement technique proposed and discussed in this thesis, IDE capacitance is the parameter that was chosen for photoacid detection.

Consider the geometry of a parallel plate capacitor as depicted in Figure 4.1 below. Two parallel conducting plates each with area A are separated by a distance d. The space between the two plates is a vacuum. If a potential difference is applied across the two conducting plates, charge of equal and opposite sign will build up on each of the plates. The ratio of the magnitude of the charge (Q) stored on either plate to the magnitude of the potential difference across the two plates (V) is termed the capacitance (C) as shown in equation 4.1[61,88,89]. The capacitance of a parallel plate capacitor with vacuum separating the two plates is shown in equation 4.2 with A and d defined as before and ε_0 the permittivity of free space[61,88,89].

$$C = \frac{|Q|}{|V|} \qquad [4.1]$$

$$C = \frac{A \cdot \varepsilon_0}{d} \qquad [4.2]$$

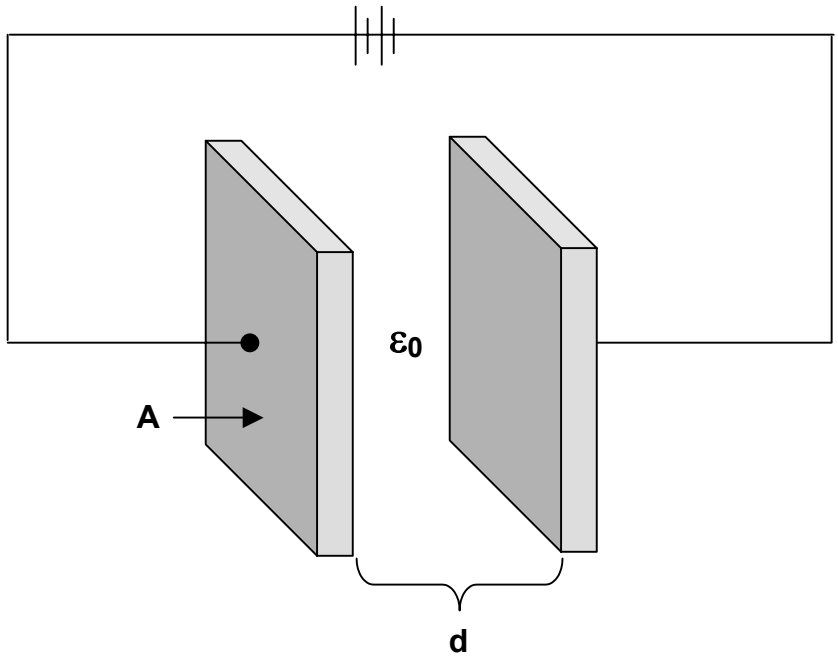

Figure 4.1 Layout of a parallel plate capacitor filled with a vacuum.

Thus, capacitance is the ability to store electric charge. Now consider the same parallel plate capacitor filled with a dielectric media such as a polymer film with dielectric constant k. If the same potential difference is now applied across the two conducting plates, charge will not only accumulate on the plate surface as before, but the dielectric media will also "charge up". Charged species within the dielectric media will attempt to

align themselves with the electric field established between the two plates by the potential difference. This alignment or orientation essentially allows more charge to be stored between the two plates and the dielectric media serves as a charge reservoir. Because the magnitude of charge increases for the same potential difference, the capacitance of this system increases by a factor of k, the dielectric constant of the media filling the space between the two conducting plates. The dielectric constant is essentially the ratio of a capacitor's capacitance filled with a dielectric to the capacitance of the same capacitor filled with a vacuum[61,88,89]. The capacitance of a parallel plate capacitor such as that in Figure 4.1 filled with a dielectric media with dielectric constant k is now the following[61,88,89].

$$C = \frac{A \cdot k \cdot \varepsilon_0}{d} \qquad [4.3]$$

The geometry of the IDE sensors (shown earlier in Figure 3.1) is very similar in structure to that of a parallel plate capacitor. For each finger pair, two conducting plates are separated by a dielectric media (polymer film). If a potential difference is applied across the IDE fingers, the polymer film between the fingers "charges up" and charge is stored leading to a specific capacitance. Like the parallel plate capacitor, the capacitance measured from an IDE sensor is proportional to the geometry of the IDE fingers and the dielectric constant of the polymer film filling the inter-finger spaces:

$$C = f(geometry, k) \qquad [4.4]$$

The exact equation for IDE capacitance is a bit more complicated than that of a simple parallel plate geometry due to the large number of fingers and the much greater influence of the fringe electric fields at the top and bottom of the IDE fingers. However, it is the general idea that the IDE's capacitance value is a function of the dielectric media's k value that is critical to the success of the IDE sensors as photoacid detection devices. In the proposed Dill C measurement technique, the capacitance of the IDE sensor is monitored as the photoresist polymer coating the fingers is exposed to UV light. Initially, this polymer film has a net dielectric constant of k_0. After exposure, some of the photoacid generator loaded into the polymer film will decompose to form a strong acid among other decomposition products. Because the contents of the resist film have now changed due to exposure, the net dielectric constant will also have changed to a new value, k_1. Since the IDE capacitance value is a function of the polymer film's net k value, the expected result of PAG decomposition is a change in the measured capacitance of the IDE sensor. It will be shown later in this chapter that this change in measured capacitance can be exploited as a means for detecting and quantifying the presence of photoacid, similar to the use of IDE sensors as relative humidity sensors described earlier in Chapter 3 section 1.2.

4.2 Experimental Methods

4.2.1 Materials

Electronic grade poly(p-hydroxystyrene) (PHOST, M_w = 11,800) was obtained from DuPont Electronic Materials (formerly Triquest Chemical Company) and used as

the matrix polymer for all experiments. Triphenylsulfonium triflate (TPS-Tf) and ethyl lactate (98%) were purchased from Sigma Aldrich and used as the photoacid generator and casting solvent for all solutions used in the work presented in this chapter. The polymer, PAG, and solvent were all used as received. Figure 4.2 illustrates the structure of both the PHOST matrix and the TPS-Tf PAG.

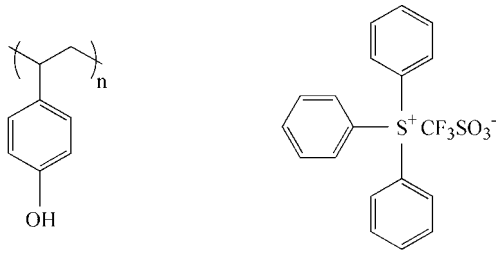

(a) (b)

Figure 4.2 (a) poly(p-hydroxystyrene) and (b) triphenylsulfonium triflate.

The PHOST matrix and TPS-Tf PAG were mixed to create solutions ranging from 13 to 15 wt.% solids, with PAG loadings ranging from 0 to 5 wt.% by solids. All solutions were filtered through 0.2 μm Teflon filters and spin coated at 900 rpm for 30 seconds onto interdigitated electrode sensors (described earlier in Chapter 3 Section 1.1) using a CEE Model 100 CB spin coat and bake system. These spin coat and bake conditions resulted in films approximately 1.5 microns in thickness. A contact hotplate soft bake at 115ºC for one minute was performed after spin coating to remove residual casting solvent from the film. Following the spin coating process, the polymer thin film covered the entire IDE finger region, as well as most or all of the two bond pads. To facilitate electrical probing, a small portion of a lint free cloth was soaked in acetone and

used to wipe away the polymer film covering the edges of the two bond pads. Care was taken to avoid getting the cloth or acetone near the IDE finger region. In addition, a contact hotplate bake of 10 to 15 seconds at 115°C was performed to insure that no residual acetone made its way into the IDE finger region.

4.2.2 Capacitance Measurements for Acid Detection

The presence of photoacid in the PHOST film was monitored by recording the capacitance of the polymer coated IDE sensors as the exposure dose was slowly increased. All capacitance measurements were performed using a two-point probe station attached to an Agilent model 4284A precision LCR meter. The two probe tips from the probe station were applied to the two bond pads located on opposite sides of the electrode finger region, as depicted previously in Figure 3.1. All capacitance values reported for the work in this chapter were recorded for a measurement frequency of 1 kHz and a 50 mV applied bias (other measurement frequencies will be examined in Chapter 5). All 248 nm wavelength exposures were performed using an Oriel Instruments flood exposure source (model # 87530-1000) equipped with a 248 nm bandpass filter (bandwidth is approximately 11nm at full width, half-max).

A typical measurement routine for the IDEs consists of a series of steps, as depicted in Figure 4.3. First, the baseline capacitance was measured for the IDE sensor coated with the PHOST/TPS-Tf film prior to any exposure. Next, the polymer coated IDE was exposed to a small dose of 248 nm radiation (typically 2 to 3 mJ/cm^2) to decompose a small amount of the photoacid generator and produce photoacid. The capacitance of the IDE sensor was then measured again, where at this time the presence

of a small amount of photoacid in the film results in a change in the measured capacitance. The dielectric properties of the TPS-Tf photoproduct molecules are now slightly different from those of the original TPS-Tf PAG molecules. This difference results in a small shift in the net dielectric constant of the polymer film that ultimately is reflected through a small shift in the capacitance that is measured from the IDE sensor.

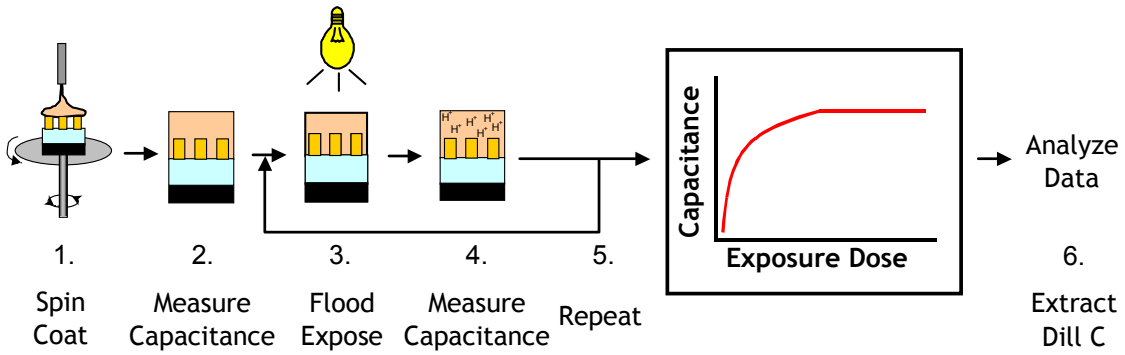

Figure 4.3 Standard IDE Dill C measurement routine.

Next, the process of exposing and measuring capacitance is repeated until no further change in capacitance is recorded for the IDEs. The lack of change in capacitance should indicate that essentially 100% of the TPS-Tf PAG molecules have decomposed into their photoproducts. By properly analyzing the recorded capacitance versus exposure dose data, as shown later in this chapter, it is possible to extract the Dill C parameter for the TPS-Tf PAG (and others).

4.2.3 Photoresist Optical Properties

As will be shown later in this chapter, in order to properly model the exposure intensity received by the PAG molecules at various depths throughout the polymer film, it is necessary to have detailed information available regarding the polymer film's optical constants (n and k) at the exposure wavelengths of interest. A variable angle spectroscopic ellipsometer (V-VASE from J.A. Woollam Inc.) was used to measure the optical constants of the different resist films used in these experiments. For these measurements, the materials of interest were cast onto plain silicon <100> wafers (Nova Electronic Materials). The ellipsometry parameters, Ψ and Δ, were collected over the wavelength range from 200 nm to 1000 nm at angles of 65º, 70º, and 75º. The Ψ and Δ data were analyzed using the WVASE-32 analysis software (J.A. Woollam Inc.) by fitting the ellipsometry data using a film stack model composed of a Cauchy layer model for the polymer film on top of a 15 angstrom thick SiO_2 layer, all on a semi-infinite layer of silicon. The optical constants, n and k, obtained from these measurements were subsequently used in calculations of the exposure intensity profile within the resist film.

4.3 Results and Discussion – The Development of the Basic Dill C Measurement Technique

The development of the basic IDE sensor Dill C measurement technique was accomplished through a series of experiments that were designed to address five primary requirements. First, the sensitivity of the IDE sensors to the incredibly small amounts of

photoacid that are typically produced in a chemically amplified photoresist was examined. Once an appropriate level of sensitivity was established, a means for relating the raw IDE sensor capacitance to the amount of photoacid and/or PAG that is contained within the resist film was determined. Next, the algorithm used to calculate the Dill C parameter from IDE capacitance was determined. Finally, the last two areas addressed in the development of this technique are related to needs and complications that are associated with the Dill C calculation algorithm. First, a means for dealing with non-homogenous concentration gradients was determined and then, the appropriate optical model was determined for properly describing the exposure intensity versus depth within the resist film. Each of the five areas just mentioned are equally important for measuring the Dill C parameter from IDE sensor capacitance. Failure to complete any one of the five renders the other four essentially useless. A detailed discussion of each of these areas follows in the next few sections.

4.3.1 Determination of IDE Sensor Sensitivity to CAR Photoacid

The amount of photoacid generated in a chemically amplified photoresist is typically quite small. As an example, consider a system such as the one studied in this work that consists of triphenylsulfonium triflate PAG mixed into a poly(p-hydroxystyrene) matrix. A typical CAR system will contain PAG at loadings ranging from approximately 2 to 4 weight percent by solids. Based on these loadings, the molecular weight of the PAG and hydroxystyrene mer unit, and a resist film that is 1 micron thick, this equates into the presence of only 3 to 8 nanomoles of photoacid in a 1 cm by 1 cm square exposure region at 100% PAG conversion. On the molecular scale,

this corresponds to approximately 3 to 9 molecules of photoacid per 1000 hydroxstyrene mer units at 100% PAG conversion. Of course in order for a photoacid sensor to be useful in practical applications, it should be able to detect the presence of photoacid at conversion values far less than 100% (such as 2%). At 2%, this corresponds to roughly 6 to 18 molecules of photoacid per 100,000 hydroxystyrene mer units. In other words, nearly ppm level sensitivity is required in order to create a useful photoacid sensor.

Before any attempt can be made to measure the Dill C parameter, or develop a technique for analyzing raw capacitance data, it is necessary to first prove that the IDE sensors are capable of detecting such tiny quantities of acid that are generated by the PAG. This process involves two steps. First, it is necessary to prove that any changes in measured capacitance are the result of changes in the photoacid generator and not from exposure induced changes in either the sensor or the PHOST matrix. Thus, the first experiment performed involved coating an IDE sensor with a PHOST film that contained no PAG and monitoring the capacitance of the sensor as it was exposed to 248 nm ultraviolet light. If there was truly no change occurring in the coated IDE sensor then there should be no measurable change in capacitance, and the plot of capacitance versus exposure dose should be a flat line with zero slope. Figure 4.4 displays the results of exposing a plain PHOST film to 248 nm light.

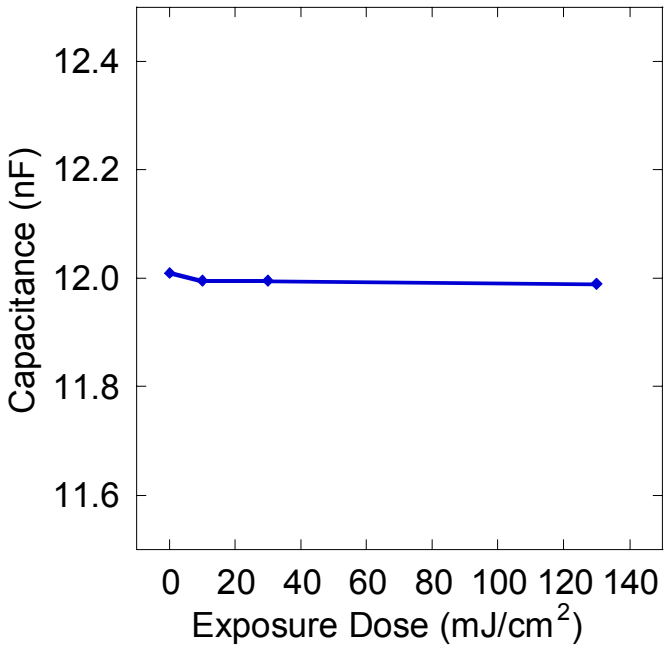

Figure 4.4 Capacitance response of a plain PHOST coated IDE to 248nm exposure.

PHOST with zero loaded PAG was exposed until a dose of 130 mJ/cm^2 was realized. From Figure 4.4 it is obvious that no significant change in capacitance of the PHOST coated IDE occurred as a result of exposure. A very small drop is evident between the first two measurement points, but the magnitude of this drop should in now way influence the analysis of PAG loaded films' capacitance data, and is very likely simply due to noise. Thus, PHOST will serve as an inert matrix material with any measured changes in capacitance stemming from changes in the dielectric properties of the PAG only.

Satisfied that PHOST and the IDE sensor were essentially photochemically inert in terms of dielectric behavior, the next required test was to determine if the IDE sensor

could in fact detect the presence of small amounts of photoacid. This was accomplished by measuring the capacitance response of IDE sensors coated with PHOST films containing different PAG loadings. For this particular experiment, loadings of 0.81, 2.50, and 4.56 wt.% TPS-Tf with respect to solids were mixed into PHOST solutions and coated onto several different IDEs. The results of exposure of these samples to 248 nm radiation are depicted in Figure 4.5.

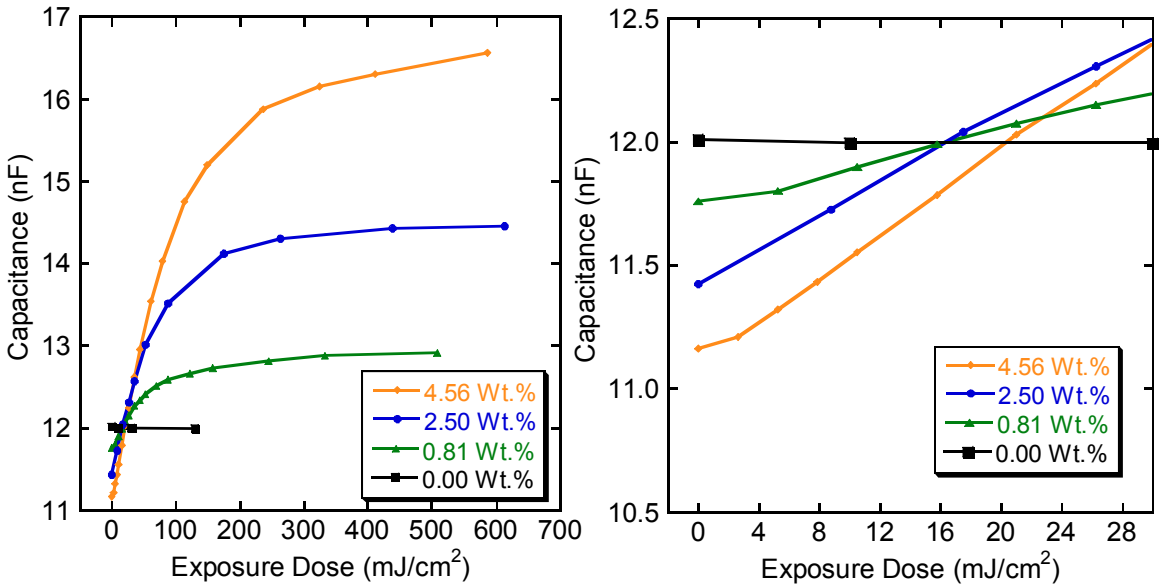

Figure 4.5 (a) Capacitance response of IDE coated with four different loadings of TPS-Tf PAG and (b) close-up view of dose zero.

Several encouraging pieces of information can be gained from this experiment. First, it is apparent that the IDEs are easily capable of detecting the tiny amounts of acid generated by a PAG. A shift of nearly 6 nF in measured capacitance was observed for

the 4.56 wt% loading of TPS-Tf, representing over a 50% change in the baseline capacitance. Even for the smaller loading of 2.50 wt%, the shift in capacitance was over 25% of the baseline value. As indicated in Figure 4.5, the IDEs are capable of detecting much smaller loadings of PAG than those tested here, and therefore should easily be capable of detecting the quantities of acid typically employed in commercial chemically amplified photoresists.

The second promising aspect of the data displayed in Figure 4.5 is the shape of the capacitance response curve. As mentioned in Chapter 2 Section 2.3, the decomposition of a PAG into its photoproducts is generally accepted to be a first order kinetics process that can be described by equation 2.6. If one were to plot the acid concentration versus exposure dose for this first order process, a curve of similar shape to that obtained in Figure 4.5a is observed. Thus, at first glance it would appear that the capacitance response is indicating PAG decomposition into photoacid upon exposure.

The final and most important result displayed in Figure 4.5 is reflected in the magnitude of the capacitance readings at both zero exposure dose and at the final large exposure dose. Assuming nearly 100% conversion of the PAG to its photoproducts takes place as a result of the extensive exposure, essentially only the PAG photoproducts should be present within the PHOST matrix at the final large exposure dose. Thus, the final measured capacitance values are indicative of the different loadings of the photoproducts, whose dielectric properties will be dominated by the generated acid, within the matrix. The capacitance values observed at large exposure doses do appear to scale proportionally with photoproduct loading. Likewise, at zero exposure dose (Figure 4.5b), no PAG decomposition is expected and thus the capacitance measured at zero dose

should be indicative of the effect that PAG loading has upon the dielectric constant of the film and the measured capacitance of the sensor. A close examination of the data displayed in Figure 4.5b reveals that once again, the measured capacitance values scale proportionally with PAG loading. Thus, it was confirmed that the IDEs are not only capable of detecting the tiny quantities of acid and PAG present in a chemically amplified resist, but are also capable of quantifying their amounts within the film. This ability becomes critical to the success of the Dill C measurement routine and will be discussed in further detail in the next sections of this chapter.

4.3.2 The Dill C Calculation Algorithm

Once it was proven that the IDE sensors used in this work were in fact capable of detecting photoacid in polymer thin films, and appeared to also be capable of quantifying the level of photoacid contained within the film, it was then possible to begin work on the calculation algorithm that would be used to extract the Dill C parameter from raw IDE capacitance data.

It is obvious based on the data presented in the previous section that the IDE sensors are capable of detecting the generation of photoacid from a PAG in thin polymer films and generating a capacitance signal that is related to PAG and acid concentration. However, quantifying photoacid generation kinetics using the IDE sensor data requires an analytical method that: (1) relates the measured capacitance data to photoacid concentration and (2) provides a method for properly modeling the exposure process and extracting rate constants and Dill C parameters from this data. In this work, it was assumed that the reaction of the photoacid generator is first order and can be described

using a kinetic expression of the form shown earlier in equation 2.6. The analytical approach used to extract the Dill C rate constant from the raw capacitance data is illustrated in Figure 4.6 below.

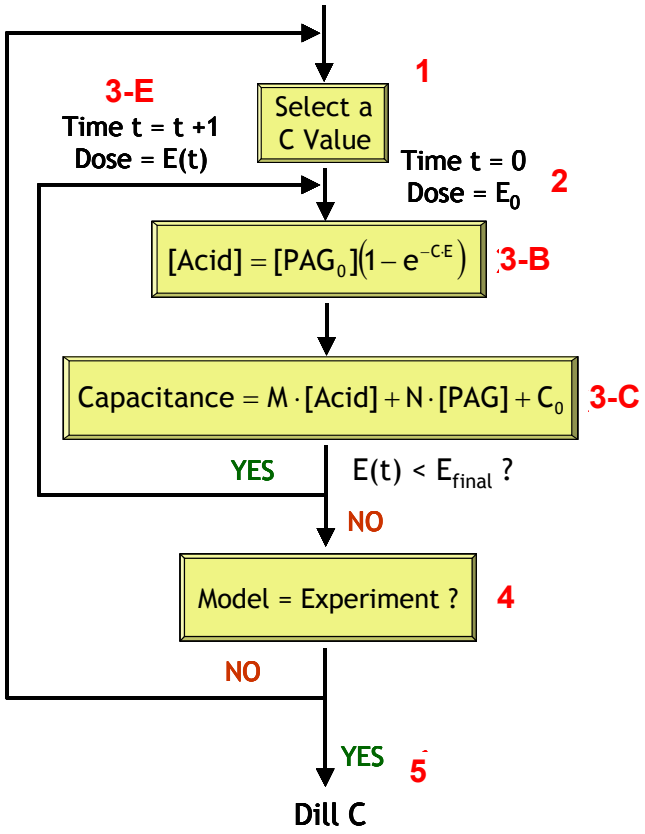

Figure 4.6 Dill C calculation algorithm for IDE capacitance data.

As shown in Figure 4.6, the analytical approach used to extract Dill's C from the raw IDE capacitance is an iterative technique that involves the creation of simulated capacitance versus exposure dose curves and then fitting these simulated, or model curves to the

experimentally obtained capacitance versus exposure dose curves using the Dill C parameter as the only fitting function. The basic steps in the algorithm are as follows:

[1] Select a Dill C parameter value for use in the first order kinetics expression for photoacid generation.

[2] Set the initial film composition and optical properties as a function of depth at appropriate uniform starting values (i.e. at time zero, exposure dose (E) is zero, acid concentration is zero, and the PAG concentration is equivalent to $[PAG]_0$).

[3] Produce a simulated capacitance versus exposure dose curve by:

A. Modeling the intensity profile *I(z)* as a function of depth within the resist film using the current film composition as a function of depth profile.

B. Using the current Dill C parameter and some incremental exposure dose ΔE, calculate the new PAG and photoproduct concentrations at each depth z in the resist film using the first order kinetics equation shown in Figure 4.6 and equation 2.6.

C. Based on the calculated concentrations of PAG and photoproduct within the film, calculate the expected measured capacitance contribution for each depth z within the resist film using an appropriate dielectric or capacitance mixing rule.

D. Sum the capacitance contributions from each depth z to calculate the predicted total measured capacitance of the IDE sensor at the current total exposure dose E.

E. Increment the total exposure dose E by an increment ΔE and repeat steps A – D to generate a complete capacitance versus exposure dose curve.

[4] Compute an appropriate measure of fit error, such as the sum squared error (SSE), between the modeled capacitance curve and the experimentally obtained data.

[5] Pick a new Dill C value and repeat steps 3 and 4 until the fit error between the modeled and experimental data set is minimized.

In general, the overall procedure discussed in steps 1 through 5 is quite straightforward, but the detailed calculations associated with each step warrant further discussion. In particular, a more in depth description of parts A through D in step 3 is needed. The following sections describe the details associated with each of these steps in more detail, and are presented in an order which makes the connection between these calculations most obvious.

4.3.3 Relating IDE Sensor Capacitance to Polymer Film Contents

In order to create a simulated capacitance versus exposure dose curve, it must be possible to relate the IDE sensor's capacitance to the quantities of PAG and photoproducts that are generated within the resist film due to exposure. In other words, some form of dielectric, or capacitance mixing rule needs to be determined between IDE sensor capacitance and PAG and photoproduct concentration within the resist film.

Two potential avenues can be explored for selecting the best mixing rule for this application. First, a wide variety of dielectric mixing rules already exist for use in many common applications[86,87,90-103]. These rules can be examined and tested for applicability to the IDE sensor Dill C technique. Second, an empirical approach can be explored where known amounts of PAG and photoacid are loaded into the polymer film coating

the IDE sensor and the effects of varying loading upon IDE capacitance can be observed. Thus a relationship can be directly measured for each PAG/matrix polymer system.

Initially dielectric mixing rules were tested for applicability to the IDE/chemically amplified photoresist system. The dielectric mixing theory method required a two step process. First, the capacitance data from the IDE sensor was used to determine an effective dielectric constant for the polymer film on the electrodes. Then the dielectric constant data was used in conjunction with dielectric mixing rules to back out an acid concentration of the film for each exposure dose. Several papers have been written that discuss predicting capacitance of an interdigitated electrode structure[42,45-48,104,105]. Typically these predictions rely on a technique known as conformal mapping to approximate the stray electric fields that exist from the top (or bottom) of one electrode finger to the next. This technique transforms the complex geometric shape of these electric fields into that of a simple field between two parallel plate capacitors that can be described by the typical equation for capacitance between two parallel plates. Unfortunately, the equations used to perform these transformations are ellipsoid integrals that cannot be solved analytically. Thus some form of numerical approximation is typically used that incorporates the interdigitated electrodes' geometric parameters and the overlying film's dielectric constant to predict the capacitance that would be measured for the electrode structure. Equations 4.5 – 4.7 are examples of one such approximation by Hoffman and coworkers that may be used to estimate the resist films' effective dielectric constants for the interdigitated structures used in this work[48].

$$C_{meas} = (N-1)\varepsilon_o\varepsilon_{meas}\left[\frac{1}{2}\frac{\sum_{i=0}^{n}\left(\frac{(2i)!}{2^{2i}(i!)^2}\right)^2\left(\sqrt{1-k^2}\right)^{2i}}{\sum_{i=0}^{n}\left(\frac{(2i)!}{2^{2i}(i!)^2}\right)^2 k^{2i}}+\frac{h}{d}\right]L \qquad [4.5]$$

$$C_{offset} = (N-1)\varepsilon_o\varepsilon_{offset}\frac{1}{2}\frac{\sum_{i=0}^{n}\left(\frac{(2i)!}{2^{2i}(i!)^2}\right)^2\left(\sqrt{1-k^2}\right)^{2i}}{\sum_{i=0}^{n}\left(\frac{(2i)!}{2^{2i}(i!)^2}\right)^2 k^{2i}}L \qquad [4.6]$$

$$C_{Total} = C_{meas} + C_{offset} \qquad [4.7]$$

Here C_{meas} is the capacitance of the field between and above the electrodes, C_{offset} is the capacitance contribution from the fringe fields within the silicon dioxide substrate, N is the number of electrode fingers, ε_o is the permittivity of free space, ε_{meas} is the permittivity of the polymeric material on and between the fingers, ε_{offset} is the permittivity of the silicon dioxide, k is the ratio of space between electrodes to electrode pitch, h is the height of the electrode fingers, d is the spacing in between the fingers, and L is the length of a single finger. By using equations 4.5 – 4.7, the net dielectric constant of the polymer film coating the IDE can be calculated based on the capacitance value measured from the IDE.

Once a relationship between polymer film net k and exposure dose has been established, attention moves towards using dielectric mixing rules to determine acid concentration in the film based on the net k value. In practice either the true acid

concentration could be found using an appropriate mixing rule, or knowledge of the proper mixing rule could simply be used to re-scale the capacitance data into a linear mapping with acid concentration. A tremendous amount of effort has been expended trying to understand and model the effects of mixing two or more substances upon the net dielectric constant of that mixture[86,87,90-103]. Mixtures ranging from impurities mixed in snow or soil to polymer/ceramic composites used in packaging applications have been modeled by dielectric mixing rules. However, no single dielectric mixing rule has been found that can effectively model all systems. For this reason, many different rules have been proposed that relate the volume fraction of two (or more) mixed substances, their individual dielectric constant, and the net dielectric constant of the mixture[86,87,90-103]. Equation 4.8 displays the most general form of dielectric mixing rule, the power law rule[86,87,94].

$$\varepsilon^n = \sum_{i=1}^{m} \left(\upsilon_i \varepsilon_i^n \right) \qquad [4.8]$$

Here ε is the effective dielectric constant of the mixture, ε_i is the dielectric constant for component i, and v_i is the volume fraction of component i. In theory, the true value of the effective dielectric constant for a mixture should lie between the values determined by n =1 and n = -1 known as the Wiener bounds[86,87,94]. The most commonly used mixing rule is a special case of equation 4.8 as n approaches zero known as the Lichtenecker rule, or logarithmic mixing rule[86,87,94].

$$\log \varepsilon = \nu_1 \log \varepsilon_1 + \nu_2 \log \varepsilon_2 \qquad [4.9]$$

As mentioned earlier, no mixing rule can effectively model the dielectric behavior of all mixtures. For this reason, a great number of mixing rule variations exist for a large variety of situations. In addition, there are many situations where known dielectric mixing rules do not adequately predict the net dielectric constant for the systems under study. The photoacid/polymer film systems appear to be such a system. Numerous versions of the dielectric mixing rules (including equations 4.8 and 4.9) were tested with the capacitance data collected from the IDE sensors, and no one rule could be found that universally applied to the PAG/polymer films. In addition to this failure, the dielectric mixing rules were less than desirable for one other reason. Using dielectric mixing rules requires calculation of the polymer film's net dielectric constant from the raw capacitance data prior to actually making use of the mixing rule. This calculation adds an additional step to the capacitance data analysis and one more potential source of error. Thus, it was more desirable to pursue a simpler empirical capacitance mixing relationship for use with the IDE sensor data.

To determine this mixing relationship, known quantities of PAG and photoproduct molecules must be loaded into the polymer matrix and the resulting IDE capacitance observed. The nature of this relationship was determined using the data displayed earlier in Figure 4.5 for the IDE sensitivity test where IDE capacitance was measured with several different loadings of TPS-Tf. A closer look at the observed capacitance response reveals the secret to developing a relationship between measured capacitance and PAG/photoproduct concentration. The measured capacitance values at zero exposure dose (refer to Figure 4.5b) correspond to the PHOST film which contains

only PAG molecules. There is no photoproduct present within the film at this time. Thus, it is possible to determine the relationship between measured capacitance and PAG concentration by comparing the measured capacitance values for each different PAG loading at zero exposure dose. Likewise, the final measured capacitance value should correspond to a PHOST film where only the photoproducts of the PAG decomposition are present. Thus, by comparing the final measured capacitance values (refer to Figure 4.5a) to the initial PAG loadings it is possible to obtain a relationship between measured capacitance and photoproduct concentration within the resist film. Figure 4.7 displays the results of this observation for the TPS-Tf loaded PHOST films. It should be noted that the error bars associated with these capacitance measurements, and for all capacitance measurements reported in this thesis, are so small that the markers used to indicate the data points on the plots are actually larger than the error.

As can be seen in Figure 4.7, linear relationships were observed between measured capacitance and both PAG and photoproduct concentrations. As PAG concentration within the PHOST film increases, the measured capacitance of the PHOST/PAG mixture decreases. As acid or photoproduct concentration increases within the PHOST film, the measured capacitance also increases. Physically, these two observations are exactly as expected. The TPS-Tf PAG molecules are highly fluorinated, and as such, potentially have a lower dielectric constant than the polarizable PHOST matrix. Therefore, as PAG content increases within the PHOST, the net dielectric constant of the PHOST-PAG mixture decreases which results in a decrease in total measured IDE capacitance. Likewise, when the TPS-Tf decomposes into its photoproducts, it essentially creates two smaller ionic species within the PHOST film that

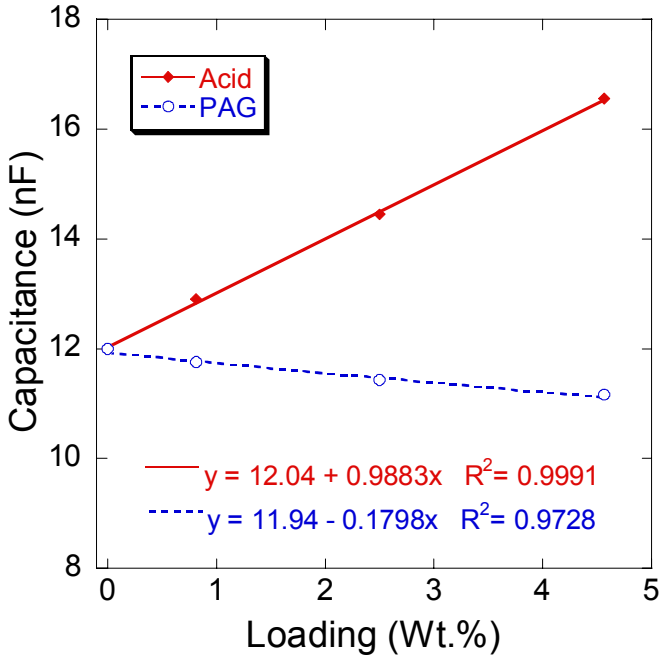

Figure 4.7 Linear relationships observed between TPS-Tf loading and measured IDE capacitance.

are much more polarizable than the TPS-Tf PAG molecule as a whole. The dielectric constant of the photoproducts is much higher than the dielectric constant of the PHOST, and thus as photoproduct content increases the measured IDE capacitance also increases. However, though the shifts in capacitance are reasonable based on the structure of the PAG and photoproducts respectively, the linear trends that are observed may be somewhat surprising when first observed. As discussed earlier in this section, dielectric mixing rules are commonly employed to predict the net dielectric constant of a mixture of two or more substances with known dielectric constants. If one were to examine these dielectric mixing rules and create a plot of the effective dielectric constant of a mixture

consisting of two components ($k_1 = 2$, $k_2 = 100$) from 0 to 100 volume % of component 2 (such as in Figure 4.8a for the power law mixing rule shown earlier in equation 4.8) the resulting curves would reveal that the relationship between net k and the content of component 2 should in general be far from linear.

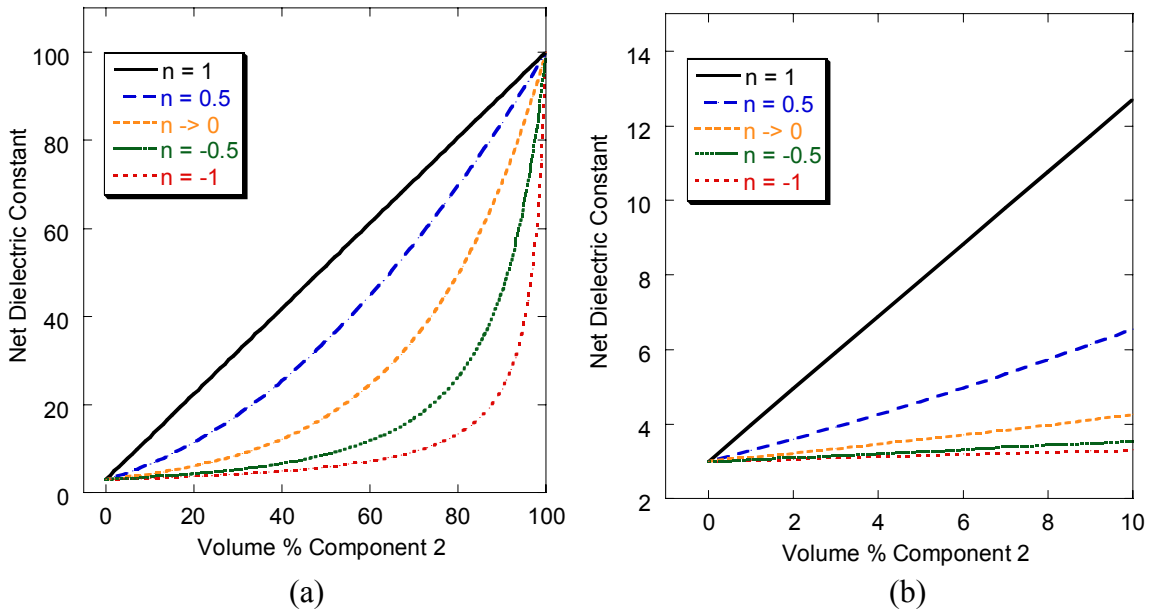

Figure 4.8 (a) Power law mixing relationship between two components of vastly different dielectric constant. Component 1 has a k value of 2 and component 2 has a k value of 100 (b) close-up view of the low loading region for component 2.

The capacitance of an IDE is directly proportional to the effective dielectric constant of the film coating it, thus one would expect the capacitance of a mixture to follow a non-linear relationship as well. However, it is important to remember that the loadings of PAG and photoproduct typically encountered with a chemically amplified photoresist are quite small (typically far less than 5 wt%). A closer look at Figure 4.8a reveals that in

low concentration regions (Figure 4.8b) the relationship between net k (and hence IDE capacitance) and the content of component 2 can be approximated as linear. Therefore, the linear relationships observed in Figure 4.7 are in fact very reasonable. This assumption of linearity in the dielectric mixing behavior should however be kept in mind if one were to attempt to apply the techniques discussed in this paper to mixtures with significantly larger additive loadings.

By combining the two linear relationships observed in Figure 4.7, it is possible to generate an empirical mixing relationship between measured IDE capacitance for a given exposure dose (C_{IDE}) and the PAG/photoproduct content within the matrix at the same dose as depicted in equation 4.10.

$$C_{IDE} = M \cdot [Photoproduct] + N \cdot [PAG] + C_0 \qquad [4.10]$$

Here M is the slope of the relationship between photoproduct concentration and measured capacitance (0.9883 from Figure 4.7 for TPS-Tf in PHOST), N is the slope of the relationship between PAG concentration and measured capacitance (-0.1798 from Figure 4.7 for TPS-Tf in PHOST), and C_0 is the common capacitance intercept for both relationships. In this case C_0 corresponds to the capacitance of a pure PHOST film with zero PAG or photoproducts present (11.99 from Figure 4.7 for TPS-Tf in PHOST). It should be noted that the values given here for these parameters are valid only for TPS-Tf in PHOST as measured using IDEs of the dimensions and specifications given in this work. For different IDE sensor geometries or resist chemistry mixtures, the type of dielectric mixing calibration curve shown in Figure 4.7 must be generated.

Given equations for light propagation and photoacid generator reaction kinetics (such as equation 2.6), the decomposition of the PAG into photoproducts can be calculated to yield the concentration of the different species in the film. The PAG and photoproduct concentrations that result from these calculations can then be used to predict the capacitance that would be measured from an IDE using equation 4.10.

4.3.4 Calculating IDE Capacitance in the Presence of a Non-Homogeneous Media

Steps 3-C and 3-D of the Dill C extraction algorithm require calculation of the predicted capacitance of the IDE based on the calculated PAG and photoproduct concentrations within the thin film. If a uniform distribution of PAG and photoproduct existed within the film, this calculation would be trivial. All that would be required for such a calculation in a homogenous medium is a relationship between the concentration of PAG and photoproducts within the film and the dielectric constant, or capacitance, of the material (such as that displayed in equation 4.10 of the previous section). This relationship could then be used to compute the capacitance expected from the IDE sensor. Unfortunately, the true distribution of PAG and photoproducts throughout the film is far from uniform. The intensity of light that reaches different points within the resist film changes from point to point due to various optical phenomena including absorbance and standing waves[5,106-113]. Thus, the amount of PAG decomposition that occurs at each point within the resist film changes spatially within the film.

In this work, it is assumed that the 248 nm exposure source being used produces highly uniform and perfectly collimated light, and that this collimated source is used to illuminate the film coated sensor in a direction normal to the sensor surface. The use of

such a collimated source permits the assumption that light propagation in the x and y directions within the plane of the resist film and sensor are negligible. Thus, only factors that influence the propagation of light in the vertical z direction with respect to the film surface must be considered. This means that each point z throughout the depth of the resist film can possess varying exposure intensities and will thus have different rates of reaction. This variation in rate of reaction leads to concentration variations in both PAG and photoproducts along the z direction. These concentration variations in the direction normal to the film surface result in different net dielectric properties at each point vertically through the film and ultimately lead to different capacitance contributions from each strata or layer of the film. Therefore, to predict or model the overall capacitance measurement of the IDE (i.e. the value recorded from a measuring instrument such as the LCR meter used in this work), a means must be determined for appropriately dealing with the non-homogenous distribution of PAG and photoacid within the resist film. The solution developed in this work utilizes a thin, multilayer approximation, where the resist film is effectively divided into a large number of slices in the vertical z direction, and the light intensity and resulting film composition in each slice must be computed and tracked individually. The individual capacitance contributions based on these properties calculated for each slice can then be summed together appropriately to determine the expected total capacitance of the IDE.

Therefore, a procedure must be determined for calculating and appropriately summing together the capacitance contribution from each individual slice or layer in the thin film coating the IDE sensor to obtain the predicted total capacitance of the IDE. To perform this task, the capacitance mixing rule displayed in equation 4.10 is used to model

each thin slice of the device by assuming that the compositions and properties of the polymer film in the thin slice are uniform. The concentrations of PAG and photoproduct are first calculated for each thin slice based upon the local exposure intensity received by the resist slice and equation 2.6 (the first order kinetics equation). Equation 4.10 is then used to calculate the predicted capacitance for each slice ($C_{slice\ i}$) based on each slice's PAG and photoproduct concentrations. In other words, equation 4.10 can be rewritten for each slice as:

$$C_{slice\ i} = M \cdot [Photoproduct] + N \cdot [PAG] + C_0 \qquad [4.11]$$

It is important at this point to remember that the slope and intercept values in equations 4.10 and 4.11 provide a capacitance value based on the composition of each slice that would be observed if the **entire** IDE sensor were coated with a homogeneous polymer film loaded with the same concentrations of PAG and photoproduct as those in the thin slice. This capacitance value $C_{slice\ i}$ is obviously much larger than the actual capacitance contribution the thin slice would contribute alone. Thus, it is necessary to properly adjust the individual capacitance values calculated for each slice to reflect their true individual contribution to the total IDE capacitance. In other words, if an entire IDE were coated with a polymer film that resulted in a given measured capacitance for the IDE, what would be the thin slice's contribution to that total IDE sensor capacitance? This small capacitance value would be the true capacitance contribution of the thin slice to the total IDE measured capacitance for a film with non-homogenous properties, such as that encountered in this work. To obtain the total IDE capacitance for any given exposure

dose, one would then have to properly sum together each of these small capacitance values.

To determine these individual slice contributions and the appropriate manner in which to sum them together, the IDE sensor as a whole must be considered. The capacitance measurement obtained from an IDE originates from three separate electric field regions as shown previously in Figure 3.14: a top fringe field located in the resist film, an inter-electrode field located between the electrode fingers (also in the resist film), and a bottom fringe field located in the silicon dioxide layer on the silicon substrate. The total capacitance measured for the IDE sensor is simply the sum of the capacitance contributions from these three separate electric field regions. The polymer thin film slices, whose properties change during exposure, each reside in one of the first two electric field regions. Thus, in order to determine what contribution each slice in the different regions make, the contribution of each region to the total IDE capacitance must first be determined.

Fortunately as alluded to previously, the bottom fringe fields of the IDE are located entirely within an inert silicon dioxide substrate (refer to section 3.5 and Figure 3.14 which discuss the spin coating capabilities of the IDE sensors, and the thickness of film required to fully capture the fringe fields). This substrate's dielectric properties remain constant throughout the exposure process, and hence the contribution from the bottom fringe fields to the total IDE capacitance will also remain constant. Thus, in terms of dielectric media with changing properties, only the regions whose electric fields are located within the changing resist film require more careful analysis. The capacitance contribution of the bottom fringe fields is still, however, accounted for through the

constant capacitance offset, C_0, utilized in equations 4.10 and 4.11 to predict capacitance based on film composition. This constant contains the capacitance contribution of the bottom fringe fields as well as the inter-electrode fields and top fringe fields for an IDE coated with the pure polymer matrix, which in these experiments is PHOST.

As mentioned earlier, through conformal mapping techniques it is possible to generate equations that describe the expected capacitance of an IDE based on the IDE's geometry and the dielectric constants of the substrate and coated film. Through the use of such an equation generated by Hoffman and coworkers[48] (described earlier in section 4.3.3), and based upon the particular geometric structure of the IDEs used in this work, it was calculated that the top fringe fields (i.e. those propagating above the electrode fingers) of the IDE structures contribute approximately 23% of the total capacitance attributed to the electric fields residing above the silicon dioxide substrate (i.e. the fields that will be responsible for sensing resist composition changes.) The remaining 77% of the capacitance attributed to the electric fields residing above the silicon dioxide substrate is attributed to the regions between the electrode fingers. Thus, with knowledge of each region's contribution to the measured IDE capacitance, it is now only necessary to determine a procedure for calculating the capacitance of the two "sensing" regions of the IDE device (the top fringe fields above the electrode fingers and the regions between electrode fingers).

The total capacitance contribution of the region between electrode fingers ($C_{inter-electrode}$) is calculated by dividing the electrode fingers into thin slices of equal thickness to the resist film slices, such as shown in Figure 4.9. The combination of the thin slices of

the electrode fingers and the resist dielectric material sandwiched between them are then treated as tiny capacitors in parallel.

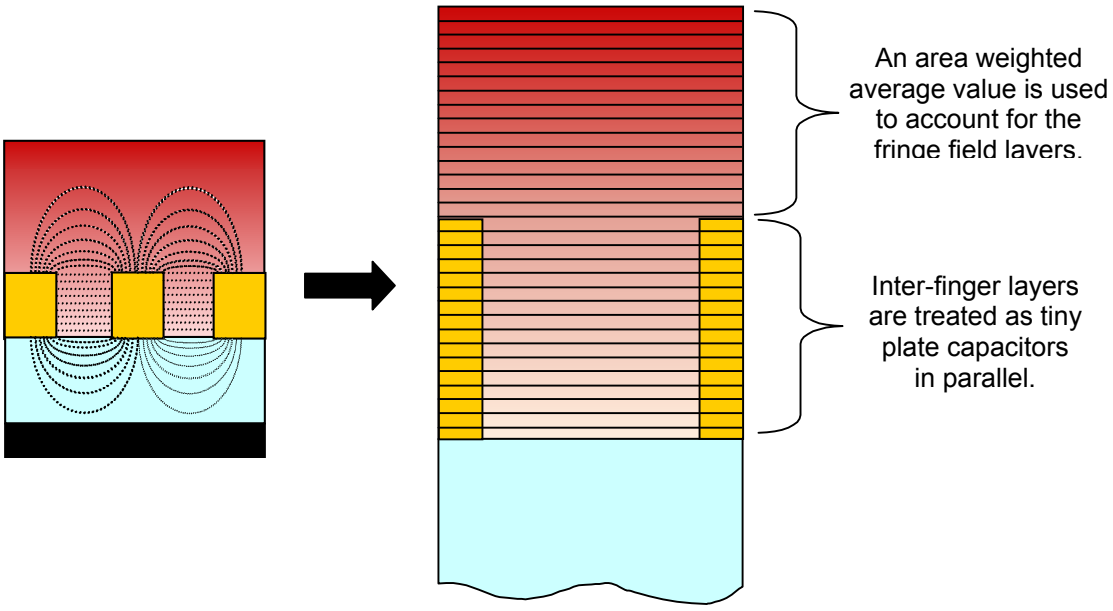

Figure 4.9 Thin layer treatment of polymer coated IDE sensor.

The total capacitance contribution from the region between the electrode fingers, which is divided into *n* equal thickness slices, is then simply the sum of each individual slice's capacitance. Of course, by using equation 4.11 to calculate each individual slice's capacitance ($C_{slice\ i}$), the sum of the individual slice capacitance values represents a value that would be measured for the sum of *n* different and complete IDEs. Thus, division by the number of slices *n* is required to normalize the capacitance contributions from the inter-electrode slices to account for the fact that the $C_{slice,i}$ value is the capacitance for an

entire IDE coated with the material of the composition in slice *i*. Equation 4.12 displays the equation utilized to obtain the capacitance contribution of the inter-electrode region to the total IDE capacitance. The 0.77 multiplier accounts for the 77% contribution to the total "sensing region" capacitance as described earlier.

$$C_{\text{inter-electrode}} = \left(\sum_{i=1}^{n} \frac{C_{slice\ i}}{n} \right) \cdot 0.77 \qquad [4.12]$$

The process of dividing the electrode fingers into thin layers works quite well for the electric field between the electrode fingers. However, this technique is not applicable for the fringe fields above the electrode fingers. Due to the curved shape of the fringe fields, these fields propagate through several different resist film slices with different dielectric properties (as seen in Figure 4.9), and thus one single capacitance value from a single film slice cannot accurately describe the true capacitance generated by these electric fields. At this time, a rigorous technique that can be used to account for the non-homogenous dielectric properties encountered by the electrode fringe fields could not be identified in the literature. Thus, as a first approximation, an area weighted average of PAG and photoproduct concentrations observed in the fringe field regions was used to estimate the capacitance contribution from this electric field region. Simulations have shown that the majority of the contributions due to the top electric fringe fields of an IDE occurs in the portion of the fringe fields nearest the top of the electrodes (i.e. the bottom portion of the fringe fields adjacent to the electrode fingers)[46,47]. Therefore, averages of PAG and photoproduct concentrations were calculated for the bottom half of the fringe

field region in the resist film layers. The expected capacitance based on this average concentration ($C_{top\ fringe}$) was then calculated using the capacitance mixing rule given in equations 4.10 and 4.11, and then multiplied by 0.23 to properly weight the contribution of the top fringe fields to the total IDE capacitance. A combination of the capacitance contributions calculated for each of the two regions of the resist film yields the following expression for the total predicted capacitance for the IDE at any given exposure dose.

$$C_{IDE} = \left(\sum_{i=1}^{n} \frac{C_{slice\ i}}{n} \right) \cdot 0.77 + C_{top\ fringe} \cdot 0.23 \qquad [4.13]$$

Here C_{IDE} refers again to the capacitance one would expect to see measured for the IDE on an LCR meter at any given exposure dose, $C_{slice\ i}$ refers to the capacitance calculated for a particular slice between the electrode fingers using equation 4.11 and the concentrations of PAG and photoproducts for a given exposure dose, n is the number of slices that the electrode fingers have been divided into (i.e. the number of capacitors in parallel), and $C_{top\ fringe}$ is the average capacitance from the fringe field portion of the IDE.

As mentioned earlier, the capacitance of an IDE is composed of a contribution from the bottom electric fringe fields, the top fringe fields, and the inter-electrode region. At first, it is not readily apparent that the capacitance contribution from the bottom fringe fields, which propagate in the silicon dioxide layer, is accounted for in equation 4.13. However, as mentioned earlier, a closer inspection reveals that this contribution is in fact included. The capacitance values for $C_{top\ fringe}$ and $C_{slice\ i}$ are calculated using equation

4.11 along with the composition of the slice or region in question. Equation 4.11 contains a constant capacitance offset C_0 that corresponds to the capacitance measured for an IDE coated with pure PHOST. This constant automatically contains the capacitance contribution from the bottom fringe fields. Since these fields are located in an inert oxide substrate, this contribution remains constant and is therefore accounted for throughout the capacitance calculations by the C_0 term in equations 4.10 and 4.11.

4.3.5 The Effects of Resist Optical Models upon the Dill C Analysis

Up to this point, methods for dealing with the acid concentration gradients that will be developed within the resist film, as well as a method for relating measured capacitance to PAG and photoproduct concentration have been discussed. The last piece of information required, and perhaps the most important, is the exposure intensity profile within the resist film. The exposure intensity at each point *z* within the resist film is needed to calculate the extent of PAG decomposition at that point, which is in turn used to predict the capacitance of the IDE. In order to examine the importance of properly modeling the exposure intensity profile within the resist film, a series of exposure models were explored, with each successive model progressively incorporating a more realistic representation of the real optical phenomena that occur during exposure of the IDE sensors.

As the first and simplest case, consider an exposure model that incorporates no absorbance effects or any other optical phenomena. The incident dose of UV radiation at the resist film's surface is assumed to be constant throughout the resist film from the surface to the substrate as depicted in equation 4.14 and Figure 4.10**.** As a result, the

concentrations of PAG and photoproduct will be uniform throughout the entire resist film at any given exposure dose, also shown in Figure 4.10.

$$I(z) = I_0 \qquad [4.14]$$

Here *I(z)* is the exposure intensity at any depth *z* throughout the resist film, and I_o is the light intensity at the film surface.

This approach to modeling the exposure dose within the IDE resist film was incorporated into the Dill C computation algorithm and used to generate a best fit modeled capacitance curve. This best fit model curve is displayed for two different loadings of TPS-Tf along with the experimentally obtained data for the same loadings in Figure 4.10. Figure 4.10 appears to show a reasonable fit of the experimental capacitance curves. However, the "knee" region near 200 to 300 mJ/cm^2 exposure dose shows significant disagreement between the model predicted curve and the experimental data. This deviation stems directly from the use of an inaccurate exposure intensity model. With the incident dose exposure model used here, all PAG molecules receive the same exposure dose at the same time. Thus all PAG molecules should complete decomposition at approximately the same time. The result is a curve with a sharper knee transition region, such as the model curve in Figure 4.10c. In reality, a wide range of exposure intensities are likely experienced by the PAG molecules due to absorbance and other optical phenomena. Thus, some PAG will complete decomposition at an early time, while others take much longer. The result of this distribution of completion times is a

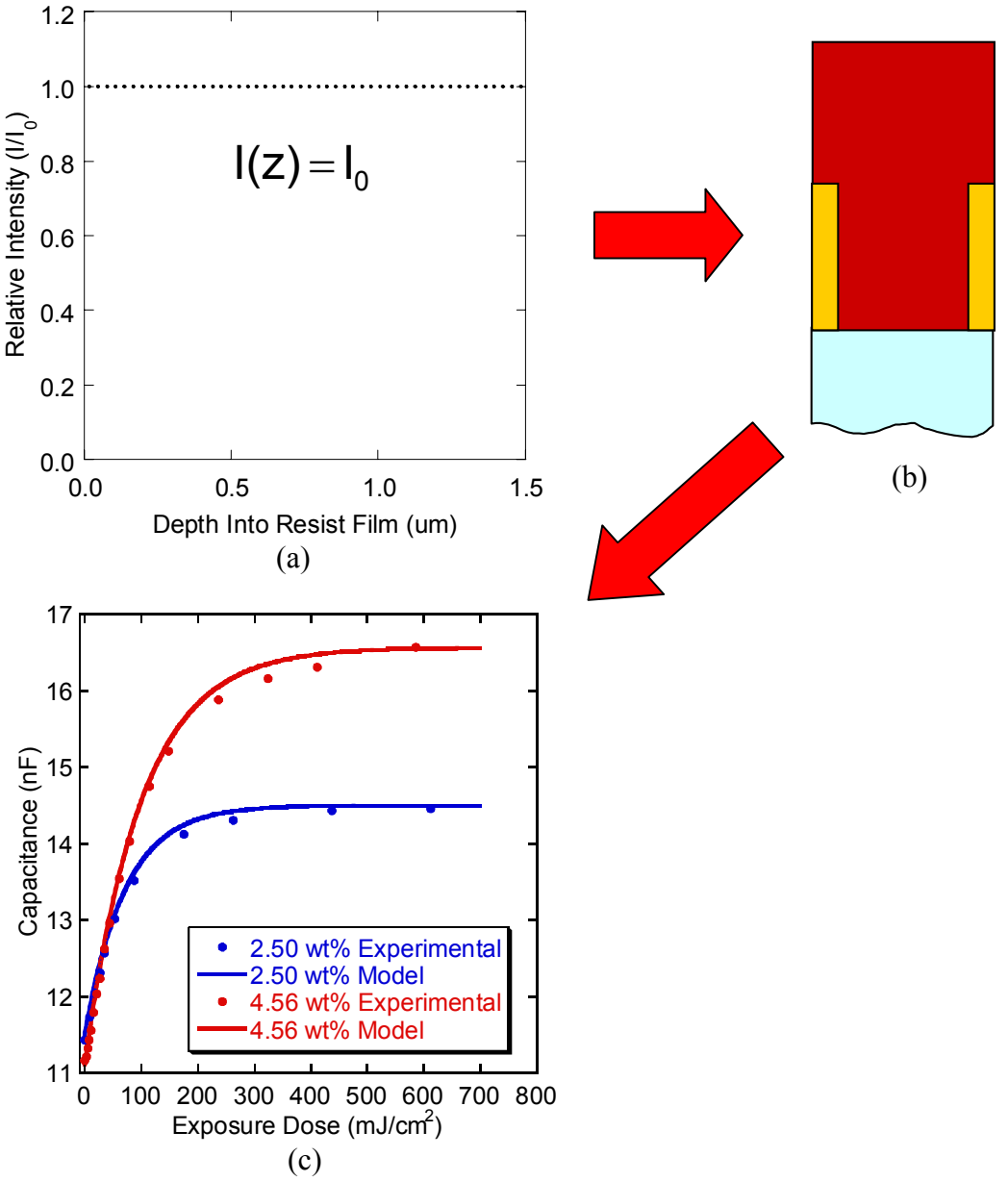

Figure 4.10 **(a) Exposure intensity distribution through resist film (b) schematic representation of acid concentration that results from exposure profile in Figure 4.10a and (c) resulting model fit to experimental data curves using exposure intensities in Figure 4.10a.**

flattening of the knee transition region. This flattening effect will become more evident as different exposure models are tested and discussed in the next few paragraphs. The best fit Dill C value for this incident model curve was 0.01 cm^2/mJ for the 4.56 wt% solution and 0.014 cm^2/mJ for the 2.50 wt% solution. These values are considerably lower than the range of literature Dill C values typically reported for TPS-Tf PAG in a PHOST-like matrix (0.037 – 0.055 cm^2/mJ)[22,32,39] and the values obtained for the two loadings differ by approximately 40 percent.

Obviously, the optical model just described is far from being an accurate representation of the true exposure intensity profile within the resist film. A better model can be obtained by accounting for the absorption properties of the resist. Thus, Beer's Law can be used to calculate the exposure intensity versus depth into the resist film due to absorption by the resist material as depicted in Figure 4.11 and equation 4.15[109].

$$I(z) = I_0 e^{-\alpha z} \qquad [4.15]$$

As in equation 4.14, I(z) is the exposure intensity at any depth z in the resist film, Io is the intensity at the surface of the film, and α is the absorbance of the resist film at the exposure wavelength. The absorbance is calculated from the optical constants n and k collected through spectroscopic ellipsometry, as described in section 4.2.3. Specifically, equation 4.16 is utilized to calculate the film absorbance[28,112].

$$\alpha = \frac{4 \cdot \pi \cdot k}{\lambda} \qquad [4.16]$$

It should be noted at this point that it is assumed that the extinction coefficient k, and thus the absorbance for the resist film remains constant throughout the exposure process[19,21,28,30]. Therefore, it is only necessary to measure one value of k for the PAG loaded film, and not a pre-exposure and post-exposure value. In fact, it is this lack of "bleaching" during PAG conversion that has made it necessary to develop new techniques for monitoring photoacid production and measuring Dill's C parameter. In most non-chemically amplified resist systems, a large change in film absorbance occurs as the photoactive compound (PAC) is decomposed or otherwise reacts to create the solubility switch necessary for image formation. Thus, in these systems, monitoring film absorbance has been a useful means for measuring the Dill C parameter for PAC's. For accurate modeling of such systems, Dill's A and B parameters must also be determined to account for the changes in film absorbance that occur as the exposure takes place[29]. Fortunately, as alluded to earlier, no significant changes in absorbance are typically observed for CAR systems, and thus one measured value of k will typically suffice.

For this Beer's Law model of exposure intensity, the exposure dose decreases as you traverse from the surface of the film toward the substrate due to the film absorbance. As a result, more PAG decomposition will have occurred at the top of the resist film than at the bottom for any given exposure dose, and thus PAG molecules at the top of the film will reach complete conversion before those at the bottom of the film. This distribution of completion times will result in a flattening of the model capacitance versus dose curve and an increase in the Dill C value needed to match the experimental curve. The best fit model capacitance curves generated by using this exposure model are depicted in Figure

4.11 along with the exposure intensity profiles and a schematic representation of the acid distribution within the polymer film.

Three important pieces of information can be gained from this model. First, the best fit Dill C value for this model curve was found to be 0.024 cm^2/mJ for both PAG loading solutions. Obviously, the magnitude of the Dill C value has increased tremendously. This increase makes perfect sense when one considers the absorbance of the resist. By accounting for intensity loss in the film due to absorption, the Dill C rate constant must show a corresponding increase to compensate for this loss and still fit experimental data. However, despite the increase, the Dill C values are still considerably lower than those reported in literature[22,32,39].

The second piece of information gained from the absorbance model relates again to the best fit Dill C value. In the first model described, two substantially different Dill C values were obtained for the two different loadings of PAG. However, when absorbance is considered the best fit Dill C values for both loadings conveniently converge onto one common Dill C. This attribute stems from the absorbance of the PAG molecules themselves. The PAG used here is strongly absorbing at the 248 nm wavelength (0.101 $\mu m^{-1}wt\%^{-1}$). Thus, as the loading of TPS-Tf increases in the PHOST, the net absorbance of the film increases which in turn lowers the intensity received by the PAG molecules and requires larger Dill C values to compensate and match the experimental data. By accounting for the absorbance of the PAG in this second model, one common Dill C value is calculated as expected. The final piece of information gained from the absorbance model relates to the shape of the model curve. The best fit curve generated by the first "incident" light only model showed significant deviation from the

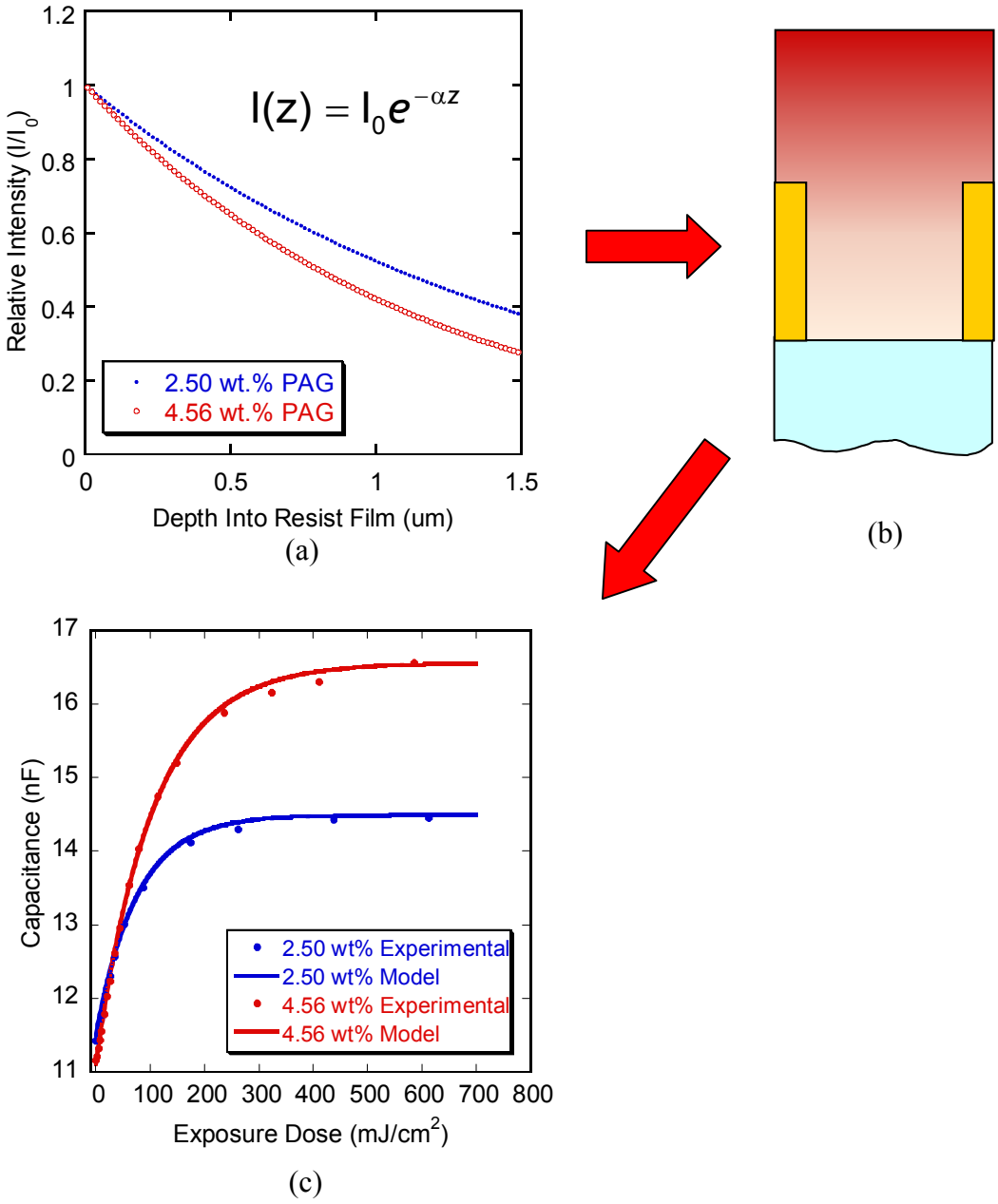

Figure 4.11 (a) Exposure intensity distribution through resist film using Beer's Law (b) schematic representation of acid concentration that results from exposure in Figure 4.11a and (c) resulting model fit to experimental data curves using exposure intensities in Figure 4.11a.

experimental curves in the "knee" transition region where the capacitance curve begins to flatten. The absorbance model shows deviation in the same region, however the magnitude of the deviation has decreased considerably. The importance of accurately modeling the exposure intensity within the resist film that coats the interdigitated electrode is readily apparent after examining the two previous model cases. Absorbance plays a tremendous role in the observed behavior of the capacitance response measured from the IDEs. However, absorbance is not the only optical phenomenon that occurs in these systems. The resist films coated onto the IDEs used in this work are coated directly onto the thick layer of SiO_2. No anti-reflective coating has been applied beneath the resist film. Because of this, standing waves should be present within the film[5,106-113]. These standing waves in the intensity profile in the film significantly alter the capacitance response of the IDE due to the nodes and antinodes of high and low intensity that lead to regions of high and low PAG decomposition. Thus, it is imperative that standing waves be incorporated into the intensity model used for the Dill C algorithm. In this work, the standing wave model discussed by Mack was used to calculate the relative intensity profile within the resist film based on the resist and silicon dioxide substrate's thicknesses and their complex refractive indices[111-113].

The intensity profile calculated for the resist coated IDE is shown in Figure 4.12. Figure 4.12 demonstrates that standing waves dramatically affect the dose of 248 nm radiation received throughout the resist film, as indicated by the periodic swing in intensity versus depth into the film. This periodic intensity profile was therefore used to calculate PAG decomposition in our Dill C algorithm and to generate predicted capacitance curves. The best fit model capacitance curves are displayed in Figure 4.12d.

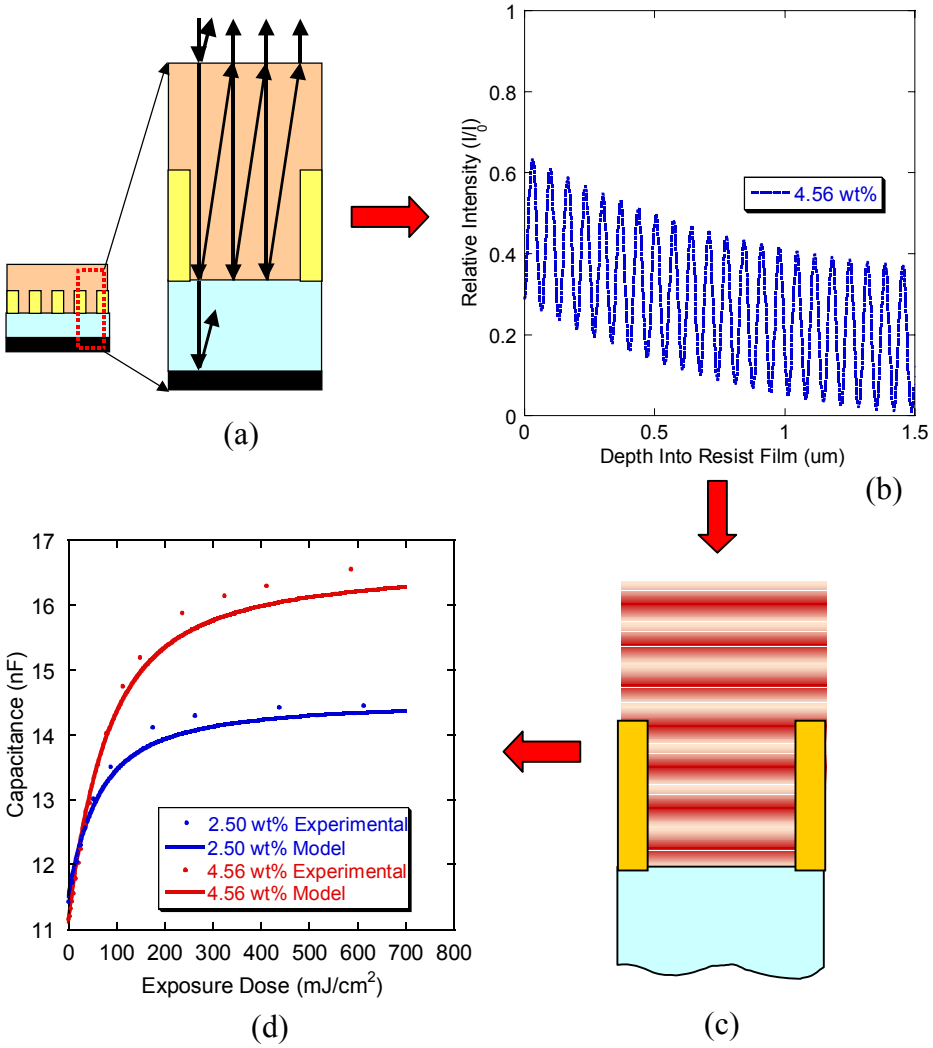

Figure 4.12 **(a) Schematic representation of the multiple interfacial reflections that take place and lead to the formation of standing waves within the resist film (b) complex standing wave intensity profile calculated for the TPS-Tf loaded PHOST film using Mack's model (c) schematic representation of the acid concentration profile within the resist film as a result of standing waves (d) best fit of model capacitance curves to experimental data using standing wave exposure profile.**

A best fit Dill C value of 0.0475 cm^2/mJ was obtained from the fit shown in Figure 4.12d. This value is significantly greater than that calculated for the simple absorbance model, and is in reasonable agreement with values reported in literature (0.037–0.055 cm^2/mJ)[22,32,39]. However, it is obvious from Figure 4.12d that the capacitance curve predicted using this standing wave model does not accurately capture the true behavior of the experimental system, based on the deviation between the model curve and experimental curve after the transition "knee" region. The source of this difference was thought to be caused by the collimated flood exposure source that was used in this work to expose the IDEs to 248 nm radiation. All of the calculations discussed thus far have assumed monochromatic light at 248 nm wavelength. Therefore, absorbance values and refractive indices at 248 nm were utilized in the intensity calculations. However, the flood exposure source utilized in this work is not a perfectly monochromatic source. In fact, the 248 nm bandpass filter used has a full width, half max value of approximately 11nm. The transmission spectrum of the 248nm filter is displayed in Figure 4.13b. Though the majority of the exposure radiation is centered at 248 nm, there are obviously significant contributions from surrounding wavelengths as well. Each of these contributing wavelengths will generate a different standing wave pattern within the resist film due to the difference in wavelength itself as well as variation in the resist's n and k values with wavelength. These standing wave patterns for each wavelength will be superimposed within the film to generate a single complex intensity profile within the resist film that determines the true dose received by the PAG molecules. The intensity profile generated by the polychromatic source should contain less modulation between the relative intensities for the nodes and antinodes in the

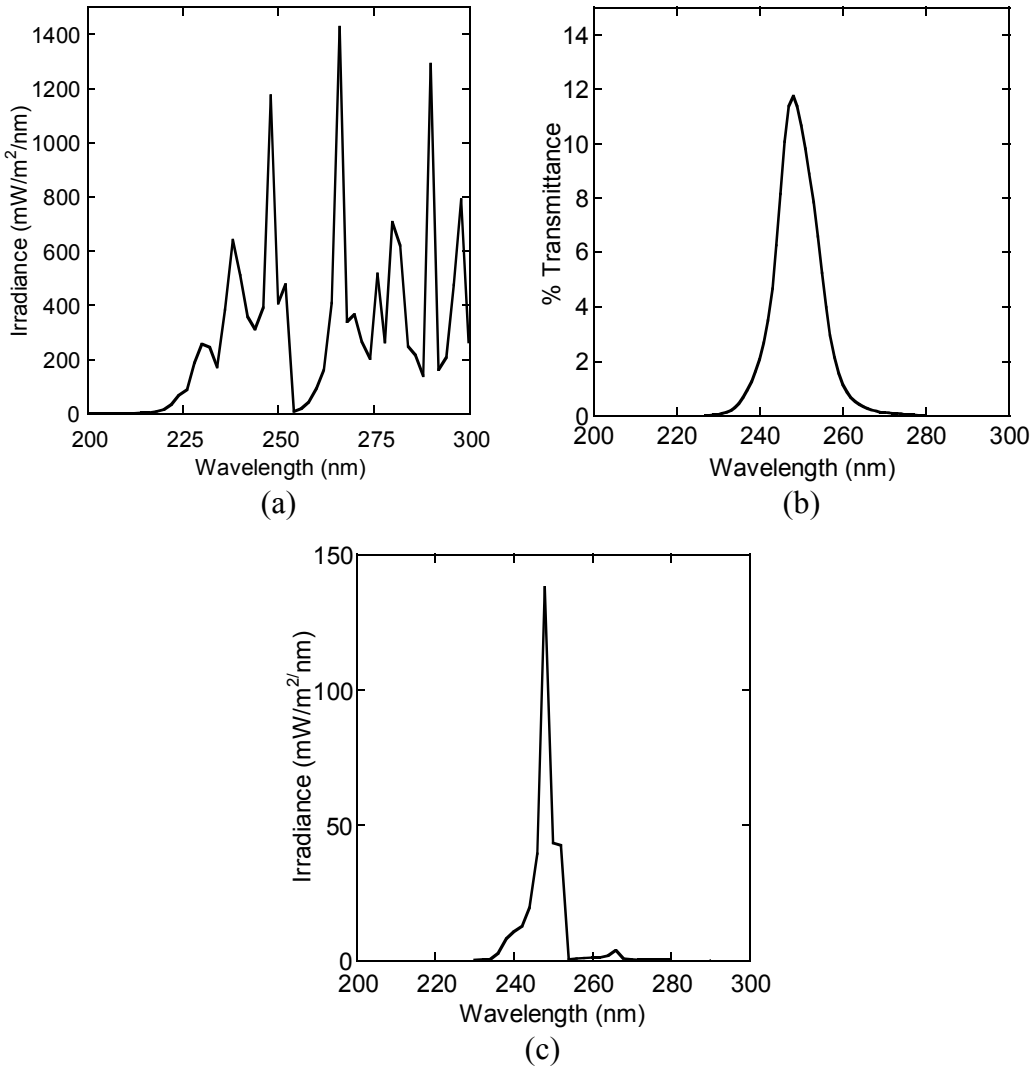

Figure 4.13 (a) Emission spectrum of the Hg(Xe) arc lamp used in the flood exposure source (b) transmission spectrum of the 248nm bandpass filter (c) "true" intensity spectrum received at the resist film surface as result of overlaying the bandpass filter spectrum onto the Hg(Xe) lamp spectrum.

standing wave pattern than a monochromatic source, resulting in a standing wave pattern that more closely resembles the behavior of a simple absorbance system, and allowing for a model predicted capacitance curve that more closely fits the experimental data. In order to best approximate the true exposure intensity profile received by the IDE samples, the transmission spectrum of the 248nm filter was overlaid onto the emission spectrum of the Hg(Xe) arc lamp used in the flood exposure tool. The Hg(Xe) emission spectrum as well as the resulting "true" emission spectrum are displayed in Figures 4.13a, and 4.13c respectively. The spectrum in Figure 4.13c is the true emission spectrum to which the IDEs were subjected. The area underneath this emission spectrum curve was then used to calculate the relative dose contribution of each wavelength to the overall emission. The percent dose contribution of each wavelength to the overall exposure was then used with the model for standing waves to generate the true polychromatic exposure profile within the resist film. A standing wave pattern was first generated for each wavelength using the optical properties of the resist at each particular wavelength. Each standing wave pattern was then weighted based on that wavelength's percent contribution to the "true" emission spectrum, and then summed together to generate the polychromatic intensity profile, as indicated in equation 4.17.

$$I(z)_{polychromatic} = \sum_{\lambda=230nm}^{270nm} I(z)_{\lambda} \cdot Y_{\lambda} \qquad [4.17]$$

In equation 4.17, $I(z)_{polychromatic}$ refers to the exposure intensity profile versus depth into the film (z) generated by our polychromatic 248nm exposure tool, $I(z)_{\lambda}$ refers to the individual standing wave intensity profiles generated at each wavelength λ, and Y_{λ} is the

weighting factor for each wavelength's contribution to the net polychromatic exposure profile. Wavelength (λ) varies from 230nm to 270nm in the equation because this range sufficiently captures the wavelengths that contribute significantly to the 248nm filtered Hg(Xe) lamp output. The polychromatic intensity profiles for the 2.50 wt.% and 4.56 wt.% loadings of TPS-Tf are displayed in Figure 4.14a.

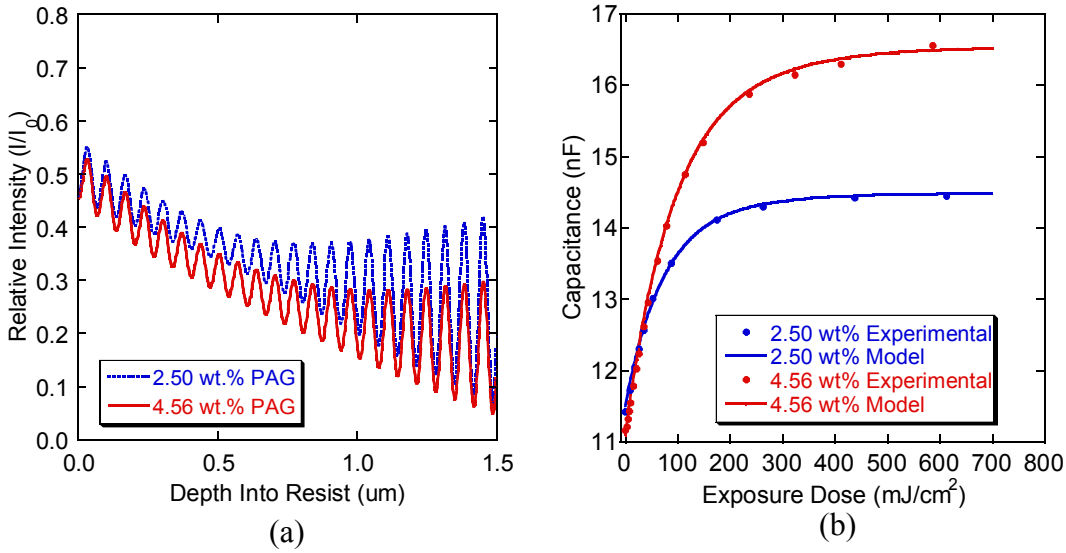

Figure 4.14 (a) Polychromatic standing wave intensity profiles and (b) model fits based upon intensities calculated in 4.14a.

Obviously the intensity profile generated through this method is considerably different from that generated by monochromatic standing waves (Figure 4.12b). The difference between the intensity of the nodes and antinodes is much smaller than that in the monochromatic data shown in Figure 4.12 and also increases with depth into the resist film. The impact that these differences will have upon the shape of the modeled

capacitance curve are significant, and the best fit capacitance curves generated using this more advanced exposure model are displayed in Figure 4.14b.

In the case of the monochromatic standing wave model, the very low intensity of the nodes results in a large portion of the PAG within the resist film decomposing at a very slow rate. This means that one portion of the resist will decompose completely at an early time, while the large portion of the resist that experiences the low intensity of the nodes will reach complete decomposition at a much later time. As a result, the height of the knee transition region drops considerably, and the model curve shows significant deviation from the experimental curve as displayed in Figure 4.12d.

For the polychromatic case, the node regions of the standing wave pattern do not provide intensities as low as that in the monochromatic case. In addition, the difference between the intensity of the nodes and antinodes is not as great as that in the monochromatic case. These two attributes cause the PAG molecules throughout the resist to complete decomposition on more similar time scales, resulting in the increase in the height of the "knee" region and a closer match to the experimental capacitance curve. As displayed in Figure 4.14b, the model capacitance curve calculated using the polychromatic standing wave intensity profile displayed in Figure 4.14a very closely matches the true behavior observed for the PHOST coated IDE. The best fit Dill C for this case was 0.045 cm^2/mJ, well within the range of literature reported C values (0.037 – 0.055 cm^2/mJ)[22,32,39]. Based on the excellent fit of the model curve to the experimental data, the fact that the intensity profile generated in this case should closely approximate the true intensity experienced by the IDEs, and the excellent agreement between this value of the Dill C and literature reported values, it is believed that this value of 0.045

cm^2/mJ represents the true value of the Dill C parameter for the triphenylsulfonium triflate photoacid generator using 248nm exposure and a PHOST matrix. In addition, it appears that the capacitance measurement routine, as well as the data analysis technique developed to obtain the Dill C discussed in this chapter is suitable for measuring accurate Dill C parameters for PAGs loaded into polymer thin films. This technique will be put to the test in later chapters as different PAG/polymer systems are studied and documented.

4.4 Conclusions and Recommendations

In this chapter, the steps taken to develop a complete measurement technique and data analysis routine suitable for measuring PAG decomposition kinetics via interdigitated electrode sensors has been presented and discussed. The use of interdigitated electrodes to measure the kinetics of photoacid generation in chemically amplified resist films can provide a number of advantages over previous techniques including: (1) the method is non-invasive, (2) the method is non-destructive, (3) the method has the potential to produce a Dill C measurement with a single resist coated IDE, and (4) the technique can easily be performed in both laboratory and wafer fab environments.

In this chapter, the feasibility of using such interdigitated electrodes to measure the Dill C rate constant has been examined. The initial results from this work indicate that IDEs are capable of both detecting the small quantities of acid generated by PAGs at loadings typical of those found in chemically amplified resists and quantifying the amount of acid generated during exposure. Linear mixing relationships were observed between measured IDE capacitance and the concentrations of both PAG and the PAG

photoproducts. These relationships were utilized to determine the Dill C parameter from the measured IDE capacitance response versus exposure dose data sets for model CAR systems consisting of triphenylsulfonium triflate (TPS-Tf) in a poly(hydroxystyrene) matrix. A Dill C value of 0.045 cm^2/mJ was measured for TPS-Tf in PHOST which is in excellent agreement with previous literature values for similar PAG-polymer systems.

Initial efforts to measure the Dill C parameter using this IDE based method have demonstrated that the quality of the Dill C parameter obtained from data fitting is heavily dependent upon the quality of the optical model used to predict the intensity profile within the resist film. It was shown that optical models that account for resist absorption, standing waves, and the bandwidth of the exposure source can be used to accurately model the exposure process on the IDE sensors and thus produce accurate Dill C values.

CHAPTER 5*

IMPROVED DILL C MEASUREMENT THROUGH NORMALIZED, MULTI-FREQUENCY IDE CAPACITANCE MEASUREMENTS

5.1 Introduction

At this point in this thesis, a functional technique has been developed for measuring the Dill C parameter for PAG decomposition in a chemically amplified photoresist film via interdigitated electrode sensor capacitance measurements. The basic capacitance measurement procedure as well as the data analysis technique used to extract Dill's C from the raw capacitance data have been developed and described in detail. In addition, many issues that could potentially harm or complicate the IDE Dill C measurement technique have been studied, such as the effects of relative humidity upon water sorption in photoresist films, the effects of ambient base contamination, and the spin coating abilities of the IDE sensor fingers. It is safe to say that the Dill C parameter can now be accurately measured for PAG molecules in polymer thin films through capacitance measurements from IDE sensors. However, like any process or device encountered in life, room always exists for improvement. This chapter focuses on two very important improvements made to the IDE Dill C measurement technique: (1) the

* Material presented in this chapter has appeared in part in previously published articles:

Berger C, Henderson C, *Improved method for measuring photoacid generator kinetics in polymer films using normalized interdigitated electrode capacitance data*, J. Vac. Sci. Technol. B, **22(3)**, 1163 – 1173, 2004.

Berger C, Henderson C, *Chemically amplified photoresist characterization using interdigitated electrodes: An improved method for determining the Dill C parameter*, Proc. of SPIE, **5376**, 995 - 1006, 2004.

Berger C, Henderson C, *Advances in a novel technique for measuring photoacid generator kinetics*" Proc. of RETEC: The 13th International Conference on Photopolymers, In Press, 2003.

use of multiple measurement frequencies for capacitance collection and (2) the development of a capacitance normalization technique. The significance of these improvements will be discussed in detail along with experimental examples.

5.1.1 Multi-Frequency Measurements for Increased Sensitivity

When the IDE Dill C technique was first proposed, one of the first major questions to answer was whether or not the IDE sensors would in fact be sensitive enough to detect the presence of tiny amounts of PAG photoproducts. As shown in chapter 4 section 3.1, this question was answered by the data collected for TPS-Tf PAG in PHOST measured at 1 kHz frequency. For this particular system, the PAG photoproducts were easily detected, even at small loadings, at 1 kHz frequency. Unfortunately, as different PAG systems were examined following the developmental work performed with TPS-Tf, it was soon learned (as will be shown later in this chapter) that not all PAG photoproducts are as easily detected at 1 kHz as those of the TPS-Tf system. For some systems, very small capacitance changes occur during exposure and PAG decomposition. Such small changes can be very difficult to interpret due to background noise and other complicating factors, such as subtle relative humidity changes. As a result, it was highly desirable to determine a means for improving the capacitance response of the IDE sensors to PAG decomposition. The first logical possibility that was explored was to change the measurement frequency.

As discussed in Chapter 4 Section 1.1, the capacitance that is measured from the IDE sensors is a function of both the geometry of the IDE fingers and the dielectric constant of the polymeric media coating the fingers. The dielectric constant of a material

is a measure of that material's net polarizability, or ability of its components to orient themselves in the presence of an electric field[61,89]. Three different mechanisms contribute to a material's net polarizability, with the net value corresponding to the sum of each mechanism's contribution[61,89]:

1. **Electronic Polarization** – shifts in the location of electron clouds with respect to the positively charged nucleus as a result of an electric field.

2. **Ionic Polarization**- the relative displacement of ions in a polar covalent bond due to the influence of an electric field.

3. **Orientational or Dipole Polarization**- rotation or orientation of an entire molecule, or dipole as the result of forces exerted on the permanent dipoles by the electric field.

Figure 5.1 illustrates the concept of polarization. In this case, permanent dipoles are polarized by the presence of an electric field.

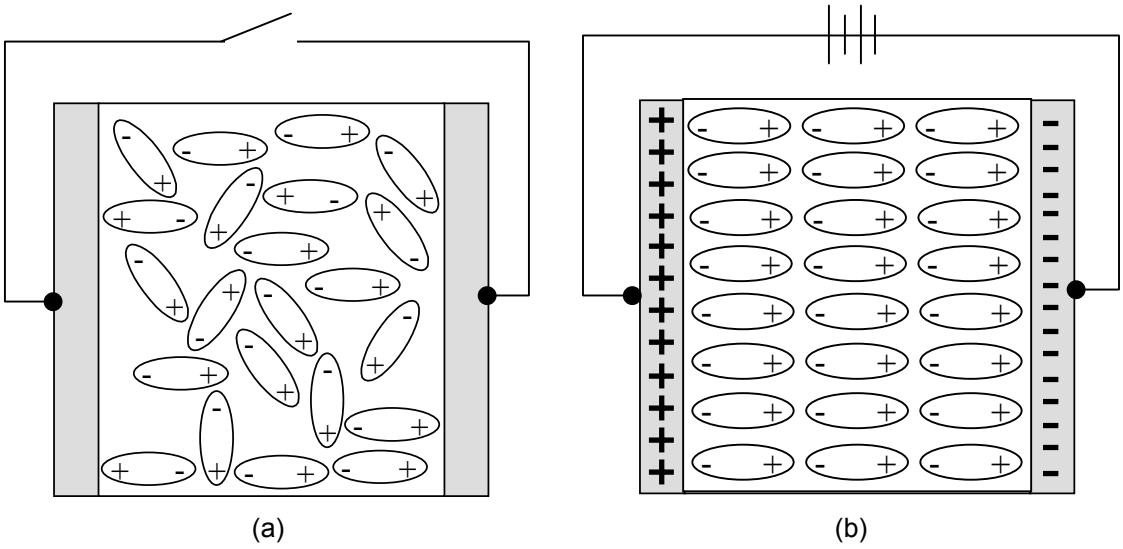

Figure 5.1 (a) Random orientation of dipoles with no electric field applied (b) orientation of permanent dipoles with applied electric field.

In a dielectric media such as a polymeric film, if no electric field is present the charged species within the film, such as the permanent dipole moments in Figure 5.1, will randomly orient themselves in a manner that maintains charge neutrality and also minimizes the energy within the system. Figure 5.1a illustrates this concept. However, if an electric field is applied across the polymer film, the permanent dipole moments within the film will now try to orient themselves with the direction of this field, as illustrated in Figure 5.1b. If the field is in place long enough, such as for a DC system, all of the dipole moments and other sources of charge will properly orient themselves with the electric field.

Of course, for the measurements taken with this work, an alternating current system is used where the direction of the electric field changes periodically. The measurement frequency used determines the rate at which the electric field changes direction. As mentioned earlier, the net polarizability of the material subjected to the electric field depends upon the ability of the electrons, ions, dipoles, and molecules within that material to rotate and properly align themselves with the electric field direction as it changes. It is readily apparent that the frequency at which the alternating current field changes polarity can play a large role in net polarizability[61,89]. At low frequencies, the time scale of the electric field's direction change is large, and so most of the material's electrons, atoms, and dipoles have enough time to properly orient themselves with the electric field before it changes direction again. However, at higher frequencies, the electric field changes direction so quickly that the larger species in the material, such as molecules with strong permanent dipoles, cannot orient themselves completely before the field changes direction again. Thus, only the faster responding

species, such as electron clouds, contribute to the net polarizability. Therefore, it is typically observed that materials have higher net polarizabilities, and hence higher dielectric constants at lower frequencies. Based on this concept, it should be clear that one possible means for enhancing the capacitance signal produced during photoacid generation is to change and optimize the capacitance measurement frequency. This concept is explored in detail later in this chapter.

5.1.2 Normalized Capacitance for Increased Accuracy and Efficiency

As shown in Chapter 4, the IDE Dill C measurement technique is heavily dependent upon the linear relationships that are measured between IDE capacitance and PAG/photoproduct concentration within the resist film. The slopes of these linear fits allow for the creation of a capacitance mixing rule that is directly used to predict IDE capacitance for any given extent of PAG conversion (see Figure 4.7 and Equation 4.10). For the TPS-Tf system that was initially used to develop the IDE Dill C measurement technique, the quality of these linear fits was excellent, with very little deviation of the raw capacitance data points from the linear fits. Because of this, excellent fits were also obtained between the experimental capacitance versus exposure dose curves and the model capacitance versus dose curves. As new PAG systems were tried with the IDE technique, it was soon discovered that not all systems provide linear fits of as high quality as that found with the TPS-Tf system. Due to a variety of different possibilities (discussed later in this chapter), many of the capacitance values used to determine the capacitance mixing rule deviated substantially from the linear fits. The ultimate result of these deviations is that the slope and intercept values used in the capacitance mixing rule

will not accurately predict all of the raw capacitance data points, leading to significant deviations between raw capacitance versus exposure dose curves and the modeled curves. In the end, this leads to unwanted error in the Dill C value extracted from this data.

To eliminate this problem, it was decided that a means for normalizing the raw capacitance data collected from the IDE sensor must be determined. The work presented in this chapter details the efforts taken to develop such a normalization scheme. A detailed derivation of the normalized capacitance expression is presented, along with examples of its use and dramatic improvement of the model curve fits. In addition, a discussion of the many advantages that normalization provides over the original measurement procedure is provided.

5.2 Experimental Methods

5.2.1 Materials

Electronic grade poly(p-hydroxystyrene) (M_w = 11,800) was obtained from DuPont Electronic Materials (formerly Triquest Chemical Company) and used as the matrix polymer for all experiments. Triphenylsulfonium triflate (TPS-Tf), triphenylsulfonium perfluoro-1-butanesulfonate (TPS-Nf), bis(4-tert-butylphenyl)iodonium triflate (TBI-Tf), bis(4-tert-butylphenyl)iodonium perfluoro-1-butanesulfonate (TBI-Nf), and N-hydroxy-5-norbornene-2,3-dicarboximide perfluoro-1-butanesulfonate (HND-Nf) were used as the photoacid generators (Sigma Aldrich) while ethyl lactate (Sigma Aldrich, 98%) was used as the casting solvent for all solutions used

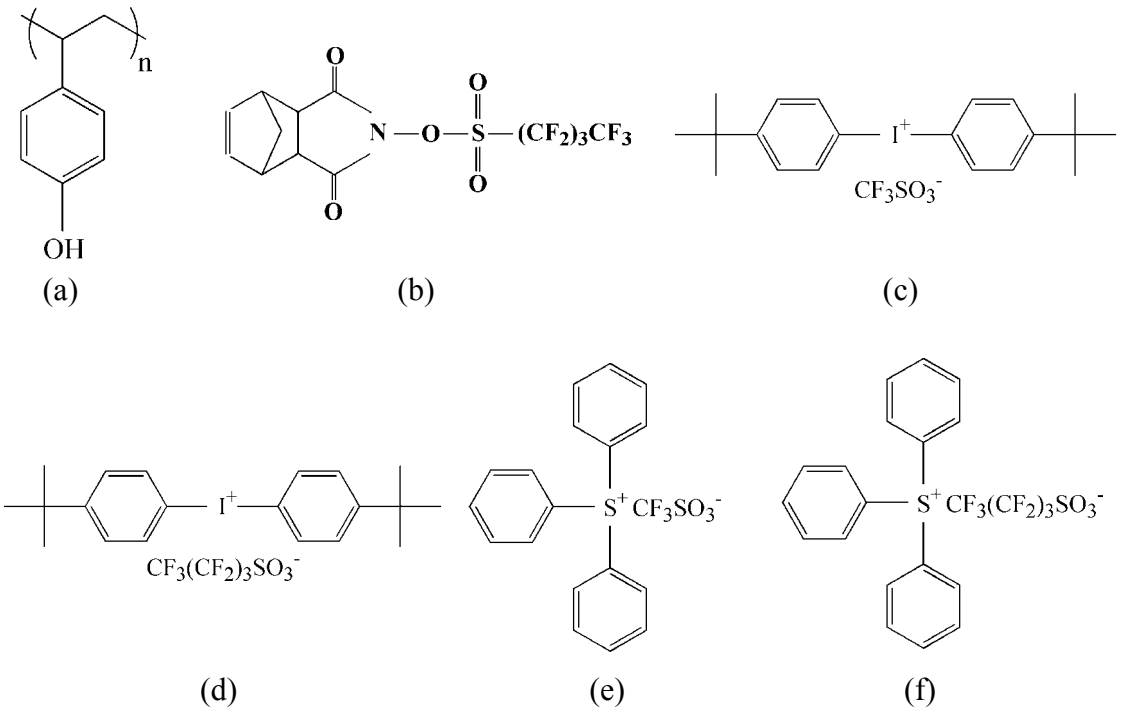

Figure 5.2 Chemical structures of (a) poly(p-hydroxystyrene) (PHOST), (b) N-hydroxy-5-norbornene-2,3-dicarboximide perfluoro-1-butanesulfonate (HND-Nf), (c) bis(4-tert-butylphenyl)iodonium triflate (TBI-Tf), (d) bis(4-tert-butylphenyl)iodonium perfluoro-1-butanesulfonate (TBI-Nf), (e) triphenylsulfonium triflate (TPS-Tf), and (f) triphenylsulfonium perfluoro-1-butanesulfonate (TPS-Nf).

in this work. The polymer, PAGs, and solvent were all used as received. Figure 5.2 above illustrates the structure of both the PHOST matrix and the PAGs used in this work. Other than the PAGs utilized, all other sample preparation techniques and experimental methods used in this chapter are identical to those used in Chapter 4. Identical spin coat and bake conditions, IDE geometries, exposure equipment, ellipsometry, and capacitance measurements were performed. The only exception to the measurement conditions used in Chapter 4 was the measurement frequency and applied bias used in this chapter. For this chapter, a range of measurement frequencies from 20 Hz up to 1 MHz was used with an applied bias of 20 mV, as opposed to a single 1 kHz frequency and 50 mV bias used in the previous chapter.

5.3 Results and Discussion – Multi-Frequency Measurements

As shown in Chapter 4 in Figures 4.5a and 4.5b, the TPS-Tf PAG provides an excellent capacitance signal upon conversion from PAG to photoproducts when measured at 1 kHz. The 4.56 wt% loaded sample resulted in an increase of 5.5 nF upon exposure, or a capacitance change of over 49% of the original baseline capacitance value. Even the small loading of 0.81 wt% provided a response of approximately 10% of the original baseline value. It is obvious from these figures that TPS-Tf photoproducts are easily detected using IDE capacitance measurements taken at 1kHz. Unfortunately, not all PAG decomposition products provide such a large capacitance signal at 1 kHz measurement frequency. For instance, consider the 1 kHz data collected for TBI-Nf displayed in Figure 5.3.

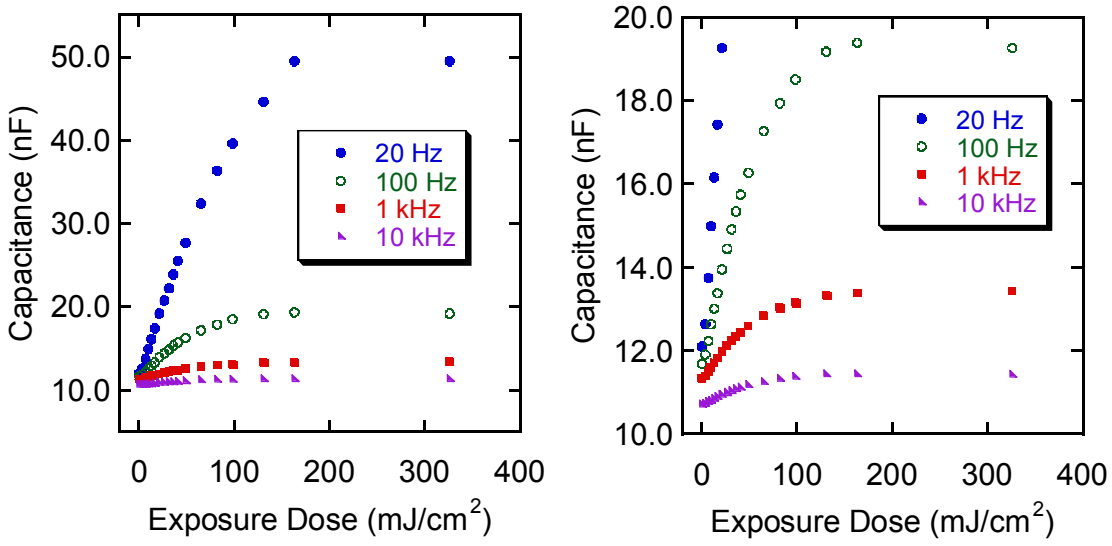

Figure 5.3 (a) Effect of measurement frequency upon measured capacitance for 3.66 wt% TBI-Nf in PHOST (b) Close up view of high frequency capacitance measurements for 3.66 wt% TBI-Nf in PHOST.

Unlike the 1 kHz data collected for TPS-Tf, the TBI-Nf PAG provides a much smaller capacitance response to exposure. The 3.66 wt% loaded sample data at 1 kHz displayed in Figure 5.3 only resulted in a capacitance change of 2.1 nF, less than half of that the TPS-Tf would have provided at a similar loading. At smaller loadings, the capacitance response becomes even smaller, and results in a noisy capacitance versus dose curve that is more difficult to accurately interpret. The variation in magnitude of capacitance responses observed for the TPS-Tf and TBI-Nf PAGS undoubtedly stems from differences in the dielectric properties at 1 kHz of the photoproducts of these different PAGs. With a wide variety of other PAGs available for use in chemically amplified photoresists, the capacitance responses that may be experienced during IDE measurement will no doubt range from easily detected to virtually un-detectable upon exposure and

measurement at 1kHz. Thus, to make the IDE measurement technique more applicable to a wider variety of PAGs with different dielectric properties, it was desired to optimize the method to maximize its sensitivity in detecting photoacid generation.

As mentioned in the introduction section, the capacitance of the IDE sensor is directly proportional to the net dielectric constant of the polymer film coating the IDE fingers. It is widely known that the dielectric properties of materials vary with frequency[61,89]. Anytime a dielectric constant is reported for a material in literature, the corresponding measurement frequency must also be reported in order to make the data useful. As alluded to earlier in section 5.1.2, this frequency dependence of dielectric constant is due to the changes in net polarizability that occur as the frequency changes. At higher measurement frequencies, species within the dielectric media have less time to orient themselves with the alternating electric field. Thus, bulkier species that take longer to rotate and orient themselves contribute less to the net polarizability and the net dielectric constant of the media lowers. At lower measurement frequencies, more time is allowed for orientation and thus more of the species within the media contribute to the net polarizability, increasing the polarizability and the net dielectric constant. Since the IDE capacitance is directly proportional to the net dielectric constant of the dielectric media coating the fingers, it should be possible to vary measurement frequency and tailor the capacitance obtained from the IDE fingers in order to increase or decrease the sensitivity of the IDE sensor to changes in the film contents.

This idea was tested for several different PAGs and similar results were obtained for all of the materials tested. At low measurement frequencies, the capacitance change measured upon exposure is much greater than that observed at high frequencies. Figures

5.3a and b illustrate this concept using data collected at frequencies ranging from 20 Hz to 10 kHz for the TBI-Nf PAG. As can be seen, at frequencies of 1 kHz and higher, the capacitance change upon exposure is relatively small. However, if frequency is lowered, the capacitance change is dramatically increased.

It is obvious from Figure 5.3 that by varying measurement frequency it is possible to both increase and decrease the measured capacitance response. However, in order for this method to be a viable technique for improving the capacitance signal, it must be shown that the same Dill C value is found for each measurement frequency. Table 5.1 lists the Dill C values calculated for several PAGs studied in this work at a variety of measurement frequencies. The TPS-Tf data presented in Chapter 4 was not included because its data was only collected at 1kHz measurement frequency. Because the TBI-Nf, TBI-Tf, and HND-NF PAGs produce a capacitance change that is much smaller than the TPS-Nf, the capacitance change recorded at 100 kHz was simply too small, and too noisy to yield a usable Dill C value.

As can be seen in Table 1, the Dill C values calculated at all measurement frequencies are essentially the same within statistical significance except for very low frequency values approaching 20 Hz in some cases. It is was somewhat unexpected that the Dill C values calculated at 20 Hz for the nonaflate PAGs are slightly lower than the values observed at the other four frequencies. The specific origin of this effect is not yet clear, though it is speculated that perhaps this drop is an artifact of the measurement instrument itself. 20 Hz is the bottom measurement frequency that the LCR meter used in this work is capable of. Though more work needs to be done in terms of investigating

Table 5.1 Calculated Dill C values versus frequency for TBI-Nf, TPS-Nf, TBI-Tf, and HND-NF PAGs (Intervals shown are 95% confidence intervals).

Frequency	20 Hz	100 Hz	1 kHz	10 kHz	100 kHz
TBI-Nf Dill C (cm^2/mJ)	0.040 +/- 0.028	0.059 +/- 0.018	0.055 +/- 0.022	0.054 +/- 0.027	too noisy
TPS-Nf Dill C (cm^2/mJ)	0.023 +/- 0.007	0.038 +/- 0.004	0.040 +/- 0.004	0.041 +/- 0.009	0.043 +/- 0.011
TBI-Tf Dill C (cm^2/mJ)	0.053 +/- 0.014	0.059 +/- 0.016	0.053 +/- 0.022	too noisy	too noisy
HND-NF Dill C (cm^2/mJ)	0.015 +/- 0.006	0.017 +/- 0.009	0.019 +/- 0.009	0.020 +/- 0.011	too noisy

the stability and accuracy of the frequency generator at low frequencies near 20 Hz, it is clear from the data that for measurement frequencies greater than 20 Hz the Dill C values calculated are in agreement with one another, and thus varying measurement frequency is a potential tool for generating greater capacitance responses that are more easily interpreted for PAG photolysis kinetics.

5.4 Results and Discussion – Normalization Technique

5.4.1 Need for a Normalization Scheme

As was shown in Chapter 4, the ability to measure the Dill C parameter depends heavily upon the linear mixing relationship obtained between measured capacitance and the content of PAG and photoproducts within the resist film as described in equation 4.10 and 4.11. This relationship is essentially responsible for permitting generation of the model predicted capacitance versus exposure dose curves for comparison to the

experimental data. The quality of this linear mixing relationship obtained for a particular PAG-polymer system has a significant impact upon the accuracy of the measured Dill C value. If the slopes and intercept calculated from the linear fit of the experimental data do not adequately describe all of the experimental data, it is likely that the model capacitance versus dose curve generated using these slope values will also fail to capture all of the experimental capacitance versus dose curve data points, resulting in potentially large errors in the calculated Dill C parameter.

Unfortunately, there are many external factors that can influence the baseline capacitance of the IDEs and introduce error into the measured linear relationship, especially when measurements on multiple IDE sensors and data collected at different times are involved. For instance, as discussed in Chapter 3, the polymer films typically used for photoresists (such as PHOST) are known to absorb significant quantities of water, and the amount of water absorbed can change considerably as the relative humidity of the ambient environment of the polymer changes. This sorbed water can alter the net dielectric constant of the polymer film resulting in significant changes in the measured capacitance of the resist coated IDE as relative humidity changes. For example, the capacitance of an IDE coated with PHOST (which has been shown capable of absorbing nearly 10 wt% water at 100% relative humidity) has been observed to vary linearly from 9 nF at 0% relative humidity to nearly 16 nF at 100% relative humidity (refer to Figure 3.11). Thus, the baseline capacitance of a resist coated IDE measured at one time may be different from the baseline capacitance measured at a different time for the same identical resist coated IDE simply due to differences in the ambient relative humidity. This shift in baseline capacitance can create problems when one tries to use

experimental data collected at different times and create a linear mixing relationship. To combat the problem of shifting IDE baseline capacitance with relative humidity, all IDE experiments can be performed in a very short time period on the same day in order to minimize such humidity variations. Nevertheless, the relative humidity in our laboratories has been observed to change by as much as 5% (resulting in a baseline capacitance shift of around 0.3 nF for a PHOST coated IDE) during the course of a set of several consecutive Dill C measurement experiments in the worst cases. For PAGs that do not produce large capacitance responses, this 0.3 nF change could be catastrophic.

In addition to environmental factors such as relative humidity, other factors such as small geometry variations from IDE to IDE can influence the baseline capacitance. The IDE sensors utilized in this work were all fabricated at the same time using identical process recipes with the goal of producing sensors that would all be essentially identical. Nevertheless, wafer to wafer, as well as center to edge variations within a wafer can result in small geometric differences from one IDE to another, such as the width of the IDE fingers. At the dimensions at which the IDE sensors used in this work were fabricated, there are over 11,000 fingers used to sense the dielectric properties of the media coating them. Any small change in finger width or height will cause significant changes in the baseline capacitance for that IDE sensor. For instance, through the use of conformal mapping equations discussed earlier in Chapter 4, it is possible to calculate the capacitance measured from an IDE sensor based upon the dimensions of the sensor and the dielectric constants of the materials surrounding its fingers. Using such equations as described by Hoffman and coworkers[48], it is possible to simulate the effects of changing the geometry of the finger width and height of the IDE sensors used in this work. The

IDE sensors used here were fabricated using process tolerances of 10%. In other words, the finger height and width could vary +/- 10% from the target value. If such variations were in fact realized, the conformal mapping equations indicate that the baseline capacitance of the uncoated IDE in air ($k \approx 1$) could vary from 3.89 nF up to 4.27 nF (actual values measured for the IDEs in this work typically range from near 4.05 up to approximately 4.25 nF). For some PAG/polymer systems, such as TBI-Tf, the magnitude of the capacitance change recorded during photolysis is only on the order of 1 nF using these sensors. Thus, if multiple IDEs with different baseline values are utilized to obtain the linear capacitance mixing relationship, significant error could be introduced into the calculated slopes and intercept values for such systems with small capacitance changes.

Figures 5.4a through 5.4f illustrate the type of variation in the linear capacitance relationships that is believed to originate from differences in baseline capacitance, either due to humidity changes, IDE geometry differences, or some other factors.

The mixing relationships observed in Figures 5.4 a, c, and e were observed for IDE's coated with different loadings of TPS-Nf (10kHz), TBI-Tf (1kHz), and TBI-Nf (100 Hz) in PHOST respectively. Due to the deviations of the experimental data from the best fit line, the slopes calculated from the best fit of the data points in Figures 5a, c, and e do not allow for a perfect modeling of the capacitance versus exposure dose curve needed to obtain the Dill C. Figures 5.4 b, d, and f illustrate this problem. For example, at a loading of 1.95 wt% TBI-Tf (Figure 5.4 c and d), the experimental capacitance for the PAG loaded sample (dose zero) lies well below the best fit line, while the capacitance recorded for the exposed sample (dose final) was well described by the best fit. When

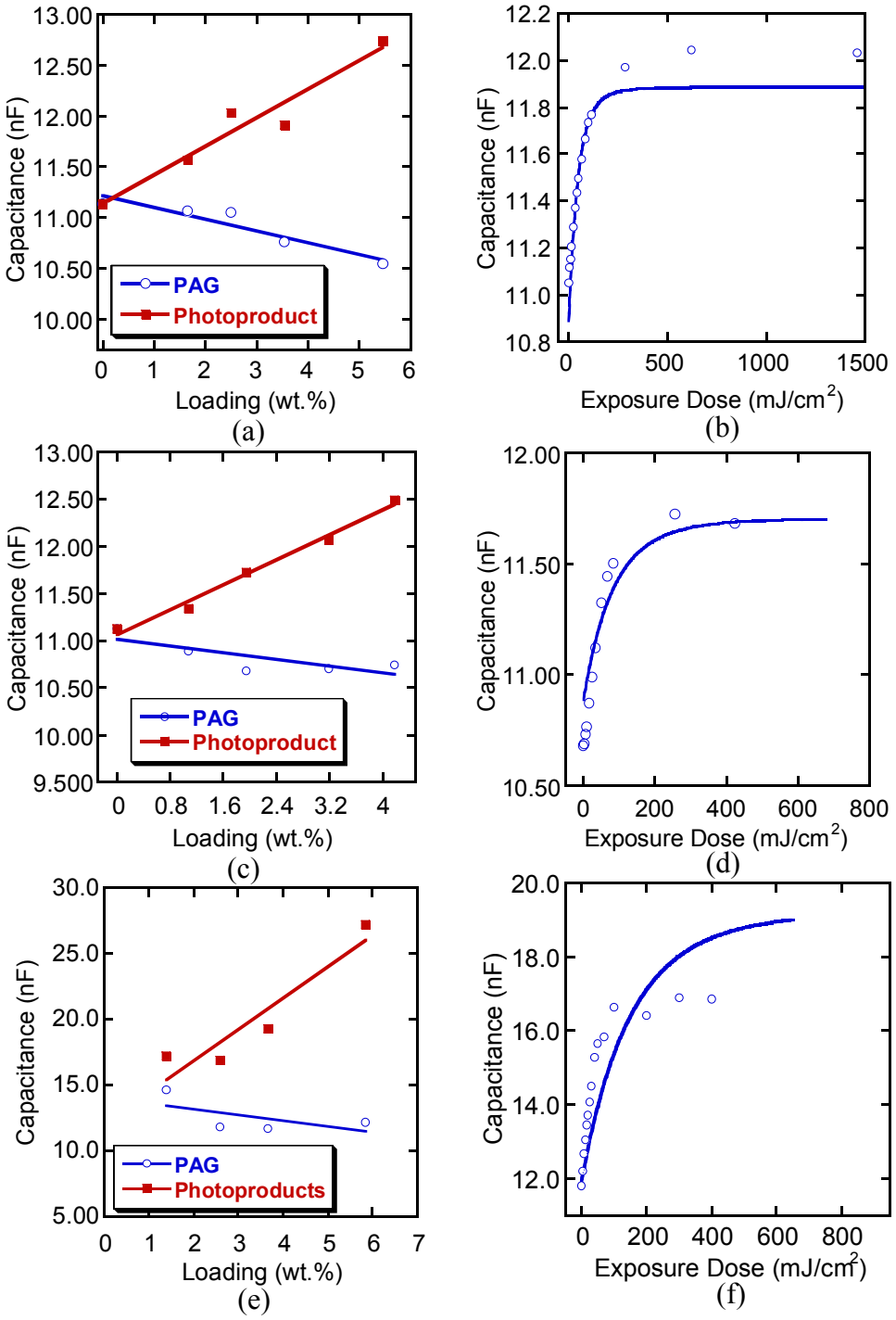

Figure 5.4 (a) Linear mixing relationship for TPS-Nf at 10kHz (b) model curve fit for 2.50 wt% TPS-Nf at 10 kHz (c) mixing relationship for TBI-Tf at 1 kHz (d) model curve fit for 1.95 wt% TBI-Tf at 1 kHz (e) mixing relationship for TBI-Nf at 100 Hz (f) model curve fit for 2.59 wt% TBI-Nf at 100 Hz.

the slopes and intercept calculated using the best fit lines of this data are used to create model capacitance curves (Figure 5.4d), the deviations observed in Figure 5.4c are transferred into the model fit. The model curve deviates significantly from the experimental data at exposure dose zero and is described quite well at the final dose values. Similar deviations are observed in the data displayed in the other graphs in Figure 5.4. In Figures 5.4 a and b, the 2.50 wt% TPS-Nf loaded sample's dose zero and dose final data points deviate to the high side of the linear best fit. Likewise, this deviation is transferred into the model curve in Figure 5.4b. In Figure 5.4e, the 2.59 wt% TBI-Nf sample deviates to the low side of the linear fit. In Figure 5.4f, the model curve deviates slightly below the experimental data for the dose zero point, and significantly below at dose final, leading to a horrible model curve fit whose Dill C value is without question in error. Due to this introduction of error into the Dill C as a result of deviations to the linear mixing rule caused by shifts in baseline capacitance, it would be desirable if a means of normalizing the capacitance data could be determined so that variations in baseline capacitance due to IDE geometry differences, or other external factors such as relative humidity changes, could be eliminated.

The third, and perhaps most important, reason for deriving a normalization technique for the capacitance data stems once again from the required linear capacitance versus resist film composition calibration curves described in equations 4.10 and 4.11, and shown earlier in Figure 5.4. In order to determine this relationship, it is necessary to load known quantities of a desired PAG into the resist matrix. In general, obtaining these calibration data sets is itself a time consuming and material intensive task, requiring the preparation and measurement of a number of different IDE samples. Additionally, if it

became necessary to determine the Dill C of an unknown PAG in a resist solution of an unknown composition, there would not be enough information available to generate the capacitance versus film composition calibration relationship required by the previous IDE data analysis method. Therefore, a means of normalizing the capacitance data that can eliminate this need for such a capacitance versus composition calibration curve would prove to be invaluable in both saving time and material and by enabling the analysis of "unknown" samples such as commercial photoresist materials.

5.4.2 Derivation of a Capacitance Normalization Technique

The normalization technique proposed in this work is based upon the linear relationships between capacitance and PAG and photoproduct content discussed earlier in equation 4.10 and 4.11. This type of relationship has been observed for all PAG-polymer systems studied thus far in our work, and it is assumed for the purposes of this derivation that a similar linear relationship will be observed for essentially all subsequent PAG systems studied. Thus, the derivation of our proposed normalization technique begins with equation 4.10, restated here for convenience as equation 5.1.

$$C_{IDE} = M \cdot [Photoproduct] + N \cdot [PAG] + C_0 \qquad [5.1]$$

As discussed earlier, the relationship shown in equation 5.1 was determined by examining the capacitance values measured on the IDE at the initial and final exposure doses, as depicted in Figure 5.5a. Figure 5.5a displays an example of a typical capacitance versus exposure dose curve generated for a specific loading of PAG in a polymer coated IDE. The initial capacitance value, C_{min} corresponds to the capacitance

measured for the polymer film at exposure dose zero with all of the PAG molecules initially loaded still present, and zero photoproducts present. The final capacitance value, C_{max}, corresponds to the capacitance measured for the polymer film at the final exposure dose value once all of the PAG has been converted into its photoproducts. By plotting the C_{min} and C_{max} values for this particular loading of PAG, as well as for IDE sensors coated with films containing different amounts of PAG, linear relationships that can be used as capacitance versus concentration calibration curves such as those displayed in Figure 5.5b are typically observed. In this particular case, it appears that as photoproduct content increases the measured capacitance of the IDE also increases. Likewise, as PAG content of the film increases, the measured capacitance of the IDE decreases.

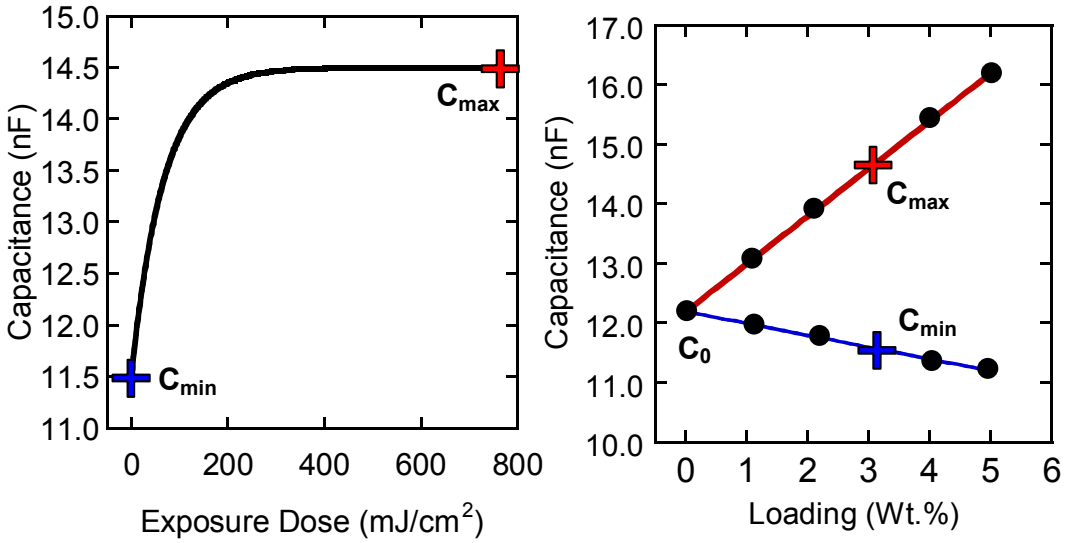

Figure 5.5 (a) Typical capacitance versus exposure dose curve obtained for PAG decomposition (b) Typical linear mixing relationships observed for various PAG loadings samples.

Both linear relationships converge upon a common y intercept, C_0, that corresponds to the PHOST film with no added PAG or photoproducts. At this time, it is important to point out that these particular slope trends (i.e. PAG content increases, capacitance decreases; photoproduct content increases, capacitance increases) may not hold true for every PAG that exists due to differences in the dielectric properties from PAG to PAG and their respective photoproduct molecules. For instance, depending upon the PAG and polymer used, the PAG molecules may be more or less polarizable than the pure matrix polymer. As a result, as PAG content increases, the capacitance measured may increase or decrease. Nevertheless, what should be observed in all cases regardless of the PAG and photoproduct's dielectric properties are linear relationships between capacitance and the PAG or photoproduct content. Thus the measured IDE capacitance can be predicted using an equation such as equation 5.1 with the slopes M and N varying from one PAG system to another depending upon the particular dielectric properties of the PAG.

As just mentioned, equation 5.1 contains two slope values, M and N, that correspond to the slopes of the relationships between measured capacitance, C_{IDE}, and the content of photoproducts and PAG respectively. A closer look at Figure 5.5b reveals that these two slopes can be rewritten in terms of capacitance values and the concentrations of PAG and photoproducts using the simple equation for the slope of a line as follows:

$$slope = \frac{y_2 - y_1}{x_2 - x_1} \qquad M = \frac{C_{\max} - C_0}{[Photoproduct_\infty] - 0} \qquad N = \frac{C_{\min} - C_0}{[PAG_0] - 0} \qquad [5.2]$$

Here C_{max} and C_{min} are the capacitance values at the final exposure dose and exposure dose zero for a given loading of PAG and photoproducts as defined earlier, C_0 is the

common y intercept at a PAG/photoproduct loading of zero, *[Photoproduct$_\infty$]* refers to the loading of photoproducts at the final exposure dose (i.e. where C_{max} is measured), and *[PAG$_0$]* refers to the initial loading of PAG at exposure dose zero (i.e. where C_{min} is measured). The slopes *M* and *N* are calculated from the slope of a line running from the y intercept at C_0 to the point C_{max} or C_{min}. It is important to remember that every raw capacitance versus exposure dose curve collected contains a C_{max} and C_{min} value, as well as a *[Photoproduct$_\infty$]* and *[PAG$_0$]* value. This stems from the fact that each curve generated is for an IDE coated with a resist film with a different initial loading of PAG.

The term *[Photoproduct$_\infty$]* can now be re-written as *[PAG$_0$]* for the slope *M* equation if it is assumed that at the final large exposure dose (where C_{max} is measured) all of the initial PAG molecules have been converted into their photoproducts. Thus, the value of *[Photoproduct$_\infty$]* is equal to the value of *[PAG$_0$]*. Equation 5.1 can now be rewritten as the following after inserting the slope values from equation 5.2:

$$C_{IDE} = \frac{C_{\max} - C_0}{[PAG_0]} \cdot [Photoproduct] + \frac{C_{\min} - C_0}{[PAG_0]} \cdot [PAG] + C_0 \qquad [5.3]$$

As was just mentioned, it is assumed that essentially all of the initial PAG molecules, or *[PAG$_0$]*, convert to photoproducts on a one to one molar basis. Thus, the concentration of photoproducts at any exposure dose can be described by the following equation:

$$[\text{Photoproduct}] = [\text{PAG}_0] - [\text{PAG}] \qquad [5.4]$$

$$[\text{PAG}] = [\text{PAG}_0] - [\text{Photoproduct}] \qquad [5.5]$$

Here *[Photoproduct]* is the concentration of photoproducts at a given exposure dose, $[PAG_0]$ is the initial concentration of PAG molecules, and *[PAG]* is the concentration of PAG molecules at a given exposure dose. After substituting equation 5.5 into equation 5.3 and performing some algebraic manipulations, it is possible to derive the following expression:

$$\frac{C_{IDE} - C_{\min}}{C_{\max} - C_{\min}} = \frac{[Photoproduct]}{[PAG_0]} \qquad [5.6]$$

Thus by inserting expressions for the slopes *M* and *N* into equation 5.1, it is possible to show that the raw capacitance data can be normalized into an expression equivalent to the concentration of photoproducts at any given exposure dose divided by the initial PAG loading. The raw capacitance values are essentially being normalized against the total change in capacitance that occurs between exposure dose zero and the final exposure dose, or from 100% PAG to 100% photoproducts within the resist film. Recall once again the first order kinetics expression for the decomposition of a PAG into its photoproducts:

$$[\text{Photoproduct}] = [\text{PAG}_0]\left(1 - e^{-C \cdot E}\right) \qquad [5.7]$$

If the photoproduct concentration in equation 5.7 is normalized against the initial PAG loading, and compared to equation 5.6, the following simple normalized relationships are obtained.

$$\frac{[Photoproduct]}{[PAG_0]} = \left(1 - e^{-C \cdot E}\right) = \frac{C_{IDE} - C_{\min}}{C_{\max} - C_{\min}} \quad [5.8]$$

$$\left(1 - e^{-C \cdot E}\right) = \frac{C_{IDE} - C_{\min}}{C_{\max} - C_{\min}} \quad [5.9]$$

With equation 5.9, it is now possible to directly compare the raw capacitance data (in normalized form) to the first order kinetics equation. The Dill C parameter can be found by simply computing a curve of the normalized photoproduct value ($1 - e^{-CE}$) versus dose E and adjusting C until this curve best fits the experimentally obtained curve for normalized capacitance versus exposure dose.

If a uniform dose of exposure energy were received throughout the resist film that coats the IDE, this calculation would be trivial. Unfortunately, as alluded to in Chapter 4 sections 3.3 – 3.5, the exposure intensity throughout the film is far from uniform. Optical phenomena such as standing waves and absorbance create complex intensity profiles within the resist film that change in the vertical z direction. Thus, the exposure dose E utilized in equation 5.9 changes from point to point in the z direction. This changing dose means that the normalized concentration of PAG and photoproducts predicted by the expression ($1-e^{-CE}$) in equation 5.9 also changes in the z direction. To account for these changes, an analytical technique similar to that discussed in Chapter 4 for the original data analysis method is employed. The resist film coating the IDE is divided into thin slices and the exposure intensity along with normalized concentration is then calculated for each thin slice. The normalized concentrations from each slice are then appropriately summed together to determine the overall normalized concentration that would reside

within the film coating the IDE for comparison to the normalized capacitance data. The method for calculating the exposure intensities that result from polychromatic standing waves is performed in the same fashion as that described in the previous chapter. In addition, the method used to sum the normalized concentration values from each individual slice is the same as that used to sum the individual slice capacitance values in the previous chapter. Each slice's normalized concentration value is multiplied by an appropriate weighting factor depending upon the region of the IDE electric fields from which it originates. Again, the details of this method are also described in Chapter 4 in the report of the un-normalized original technique.

The advantages of the normalization expression shown in equation 5.9 are numerous. First, variations in sensor to sensor baseline capacitance values caused by humidity fluctuations, or from differences in geometry or other electrical properties, are eliminated. The data from each sensor, regardless of baseline capacitance, should always collapse into the normalized relationship varying from 0 to 1 as described by equation 5.9. More importantly, this technique totally eliminates the need for determining the linear calibration relationship described earlier in equation 5.1 and shown in Figure 5.4. This linear mixing relationship is automatically lumped into the normalized expression as shown during its derivation. Therefore, it is no longer necessary to coat several IDEs with different loadings of PAG and record capacitance versus exposure dose curves, saving large amounts of material, and preserving the life of our valuable IDE sensors. Finally, because it is no longer necessary to measure the linear mixing relationships, no prior knowledge of the contents inside the resist film is necessary. In theory, it is now possible to coat a single IDE with a resist solution of unknown PAG content and

composition and subsequently determine the Dill C parameter from a single capacitance versus exposure dose curve – a tremendous improvement over the prior version of this technique.

5.4.3 Application of the Normalization Technique to Previously Collected Data

In order to test the validity of this new normalization technique, the method was used to analyze capacitance data collected from a series of resist coated IDEs. First, the normalization method was used to analyze the capacitance data reported in Chapter 4 for TPS-Tf and the Dill C values obtained from both the original (referred to here as the "original IDE analysis method") and new normalization methods were compared. Additionally, several new polymer-PAG systems were analyzed using both the original IDE analysis method and the new normalization technique for data comparison.

Consider first the data previously collected for TPS-Tf in PHOST. Figure 5.6a illustrates both the best fit model predicted capacitance versus exposure dose curves and the experimental capacitance versus exposure dose curves for loadings of 2.50 wt.% and 4.56 wt.% TPS-Tf in PHOST (also displayed in Figure 4.14b). As can be seen, the original IDE data analysis method worked quite well for modeling the capacitance behavior of the TPS-Tf system, producing a Dill C value of 0.044 cm^2/mJ for the 4.56 wt.% data, and a Dill C of 0.045 cm^2/mJ for the 2.50 wt.% data, in excellent agreement with C values reported for a similar TPS-Tf/PHOST system by others[22,32,39]. The model predicted curves and experimental data curves are in excellent agreement. The high quality of fits obtained using the original IDE data analysis method stems directly from the excellent linear relationship obtained for TPS-Tf capacitance versus film composition

calibration plot displayed earlier in Figure 4.7. There is essentially no deviation from the linear fit for any of the data points. Thus, the model predicted curve based upon these relationships should, and does, capture the true behavior very well.

Now, consider the same data sets modeled using the new normalization approach. Figure 5.6b illustrates the same two data sets analyzed after normalization. Once again, the model predicted curves fit the experimental data curves quite well, this time producing a Dill C value of 0.044 cm^2/mJ for the 4.56 wt.% data and 0.046 cm^2/mJ for the 2.50 wt.% data.

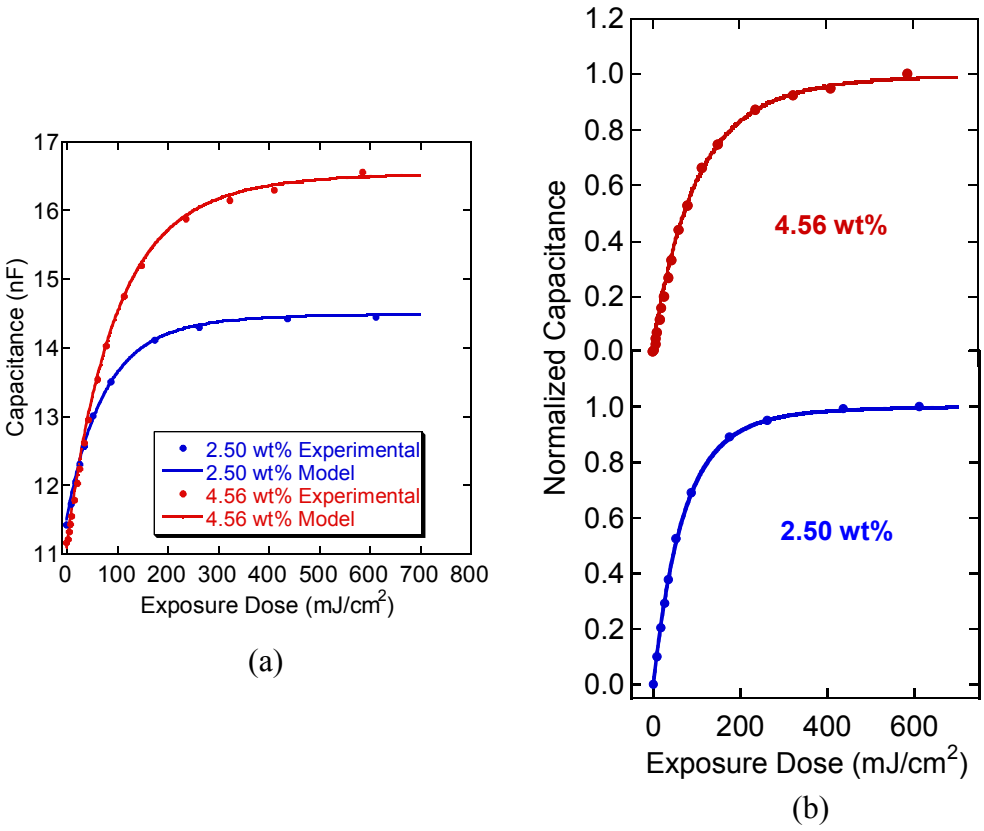

Figure 5.6 (a) Model curve fits for TPS-Tf using the original data analysis method (b) model curve fits using the normalized approach.

Two significant pieces of information are provided by the data examined above. First, the Dill C values obtained by the original data analysis method and the new normalization methods are in nearly perfect agreement with one another. This indicates that the normalization based model is predicting the same type of capacitance behavior predicted by the original data analysis method, and thus using the normalized capacitance data in place of the raw, un-normalized capacitance data is an acceptable substitution. Second, it is obvious from examining the two figures comparing the model predicted data to the experimental data that there is no significant difference in the quality of the model fits based on the normalized versus the un-normalized model. This again is due to the high quality of the linear relationships obtained between the measured IDE capacitance and PAG and photoproduct content in the TPS-Tf/PHOST system, as illustrated in Figure 4.7. As can be seen, the linear relationship measured for TPS-Tf predicts the capacitance for all IDE's loaded with different amounts of PAG. Because this relationship already captures the behavior of the IDE's well, with no significant deviations, there is no significant improvement in quality of fit for the model curves generated with the un-normalized method versus the normalized method.

Now consider data collected for the TBI-Tf PAG in PHOST. The linear relationship between measured IDE capacitance and TBI-Tf/photoproducts concentration, as well as the resulting model fit to the experimental data for a 1.95 wt% loaded sample, were displayed previously in Figures 5.4c and 5.4d. As can be seen, there are small deviations at various points on the curve between the linear model and the experimental data. As a result, when the original IDE data analysis method is used to predict the capacitance versus exposure dose curves, significant deviations occur between the model

predicted curves and the experimental curves, particularly at the starting and ending points (dose zero and dose final). Because of the deviations, determining a best fit of the model to the capacitance curve using a quality of fit parameter such as sum squared error (SSE) results in less than satisfactory agreement between the model and the experimental data. This in turn results in very little confidence in the Dill C parameters extracted from this data. The use of SSE minimization and other similar fitting techniques result in a Dill C parameter that causes the least deviation from modeled data points to experimental points, regardless of what effect this may have upon the shape of the model predicted capacitance curve. This problem was also displayed earlier in Figure 5.4d (and for TBI-Nf in 5.4f). The rate of increase in capacitance versus exposure dose (i.e. the slope of the curve) is different from the experimental data, but this shape is the best fit through the SSE method because the deviations between model data and experimental data are minimized. The best fit Dill C parameter for this data set (5.4d) was found to be 0.041 cm^2/mJ using the original IDE analysis method on the raw capacitance data set.

Despite the deviations displayed for the data in Figure 5.4, there were also model predicted curves generated for TBI-Tf in PHOST through the original data analysis method that did not exhibit such large deviations from the experimental curves. Two such curves are displayed in Figure 5.7 for 3.19 and 4.18 wt.% TBI-Tf in PHOST measured at 1 kHz. The average best fit Dill C value found for all of the acceptable model fit cases for TBI-Tf was 0.056 cm^2/mJ using the original IDE analysis method.

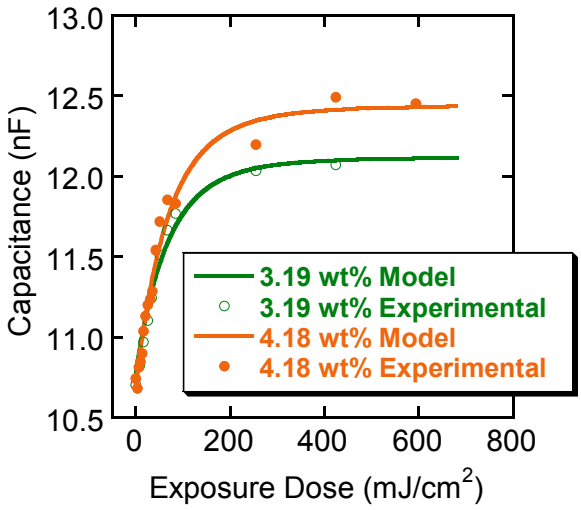

Figure 5.7 Model curve fits for 3.19 and 4.18 wt% TBI-Tf in PHOST.

Now, consider the same TBI-Tf data from Figures 5.4d and 5.7 with the new normalization technique applied. The best fit curves for this data are displayed in Figure 5.8. From this figure, it is easy to see that the normalization approach has improved the quality of fit tremendously for the 1.95 wt.% data, as indicated by the lack of deviation between model predicted curves and experimental curves. In addition, an average Dill C of 0.055 cm^2/mJ was found using the best fit results of the normalized technique to all of the TBI-Tf data curves collected, in excellent agreement with the average found using the original technique (0.056 cm^2/mJ). These values are also in agreement with C values found for TBI-Tf in a PHOST like matrix using other Dill C measurement techniques[22,32,39] Figure 5.9 below offers further proof of the improvement in quality of model fit achieved through normalization for the other two PAGs displayed earlier in Figure 5.4, TPS-Nf (Figure 5.4b) and TBI-Nf (Figure 5.4f).

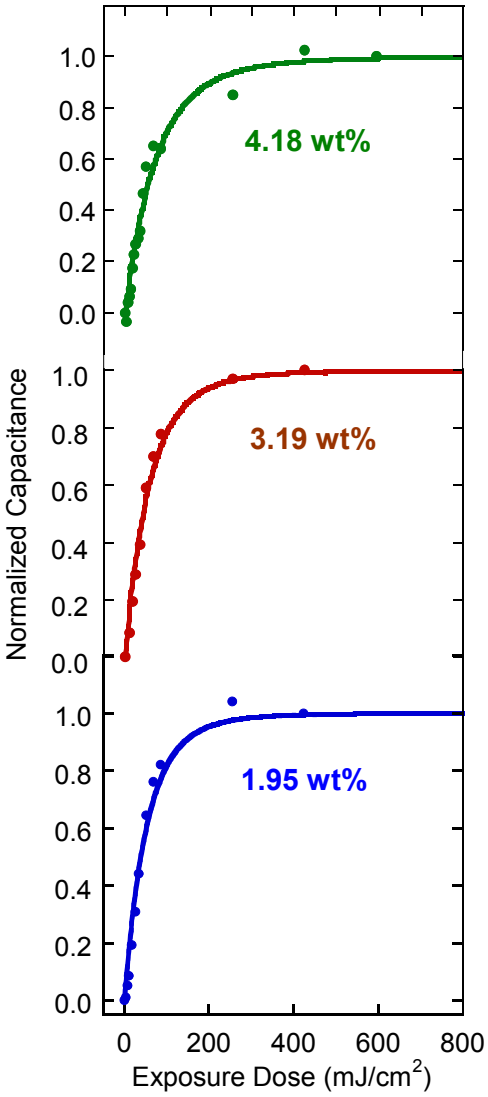

Figure 5.8 Model curve fits for three loadings of TBI-Tf in PHOST using the normalization technique.

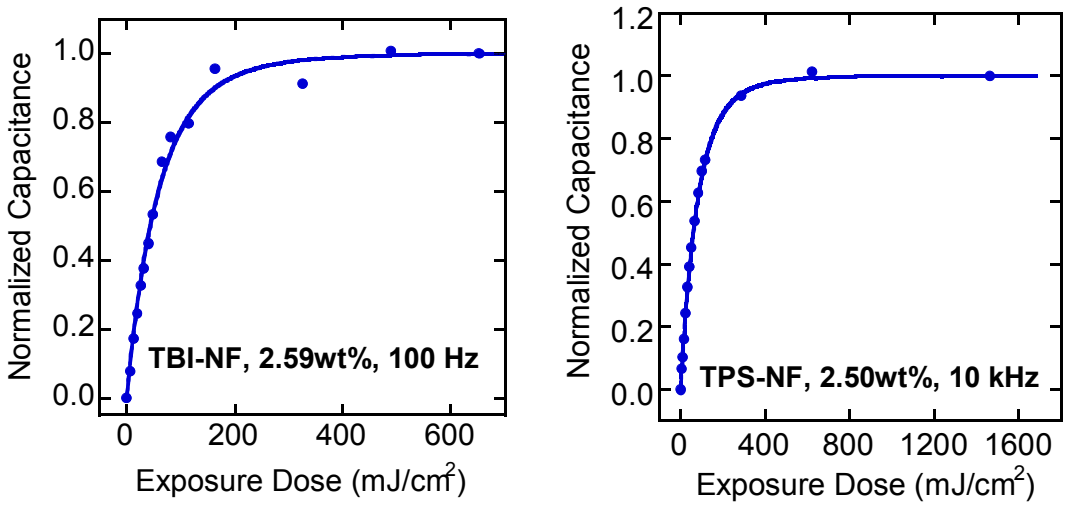

Figure 5.9 (a) model curve fit achieved through normalization for 2.59 wt% TBI-Nf in PHOST measured at 100 Hz frequency and (b) model curve fit achieved through normalization for 2.50 wt% TPS-Nf in PHOST measured at 10 kHz frequency.

The ability of the normalization technique to create such excellent fitting curves stems from its derivation from the linear capacitance relationship. Unlike the original IDE analysis method, which relies on experimentally measured values of this relationship, the normalized approach automatically assumes such a relationship exists, without having to actually measure it experimentally. The slope values that create the mixing relationship are automatically lumped into the normalized capacitance expression. Thus, IDE specific deviations due to baseline fluctuations, etc., are automatically accounted for in the normalized data set.

As mentioned earlier, in order for the newly derived normalization technique to be proven viable, two important criteria must be met. First, improvement in the quality of the model fits must be shown. This criteria was obviously met as shown by the dramatic improvement in quality of fit in Figures 5.8 and 5.9 over the fits obtained using

the original technique shown in Figure 5.4 b, d, and f. Second, it must be shown that the normalization technique is predicting the same type of behavior that the original technique predicts (i.e. the same Dill C values are obtained using both techniques). The data discussed for TPS-Tf and TBI-Tf have proven that such a condition exists with the normalization technique, as C values obtained using both methods are in agreement. Nevertheless, the specific capacitance curves for TPS-Tf, TBI-Tf, TPS-Nf, and TBI-Nf shown and discussed in the previous paragraphs were just a few specific representative examples of how error introduced into the linear mixing relationships can wreak havoc upon the quality of model fits obtained through the original IDE measurement technique, and how normalization can minimize this problem. In reality, for each PAG studied, three to four IDEs are each coated with a PAG/polymer sample of different PAG loadings, and then data is collected from each IDE at three to four different measurement frequencies. This means that there are typically anywhere from 9 to 16 raw capacitance versus dose curves collected for each PAG studied. The average of the 9 to 16 best fit Dill C values is taken and reported as the PAG's Dill C value. The average Dill C values (along with 95% confidence intervals) calculated using the original IDE method and the new normalized method on all TBI-Tf curves (not just those shown in the figures in this chapter), as well as for all data curves collected for TPS-Tf and three other PAGs (TBI-Nf , TPS-Nf, and HND-NF) are reported in Table 5.2. Obviously, several of the model curves generated using the original technique were in significant disagreement with the experimental curves and could not produce reliable Dill C values (hence the need for normalization!). To calculate the average values for the "un-normalized data" in Table

5.2, only data from curves demonstrating an acceptable model fit were used. Data from curves showing significant model deviation were omitted from these calculations.

Table 5.2 Summary of Dill C values calculated using un-normalized and normalized data analysis techniques.

PAG	Dill C via Un-normalized Data	Dill C via Normalized Data
TPS-Tf	0.045 +/- 0.001 cm^2/mJ	0.046 +/- 0.007 cm^2/mJ
TPS-Nf	0.039 +/- 0.008 cm^2/mJ	0.040 +/- 0.002 cm^2/mJ
TBI-Tf	0.056 +/- 0.011 cm^2/mJ	0.055 +/- 0.007 cm^2/mJ
TBI-Nf	0.054 +/- 0.018 cm^2/mJ	0.056 +/- 0.009 cm^2/mJ
HND-Nf	0.016 +/- 0.003 cm^2/mJ	0.018 +/- 0.002 cm^2/mJ

From Table 5.2, it is apparent that both techniques predict the same Dill C value within statistical significance, and thus using the normalized capacitance expression to predict capacitance is an acceptable variation upon the original IDE technique. Table 5.2 also demonstrates one other important quality of the IDE Dill C measurement technique in terms of Dill C accuracy. The values reported for TPS-Tf, TBI-Tf, and HND-Nf are all in agreement with C values reported by others using different measurement techniques[22,32,39]. In addition, the values reported for TPS-Nf and TBI-Nf also appear reasonable. This statement is based upon the similar structures of these PAGs to others in Table 5.2. For instance, TPS-Tf and TPS-Nf are very similar in structure except for the number of CF_2 groups located in the anionic portion (the acid portion) of the PAG. The cationic triphenylsulfonium portion, the segment that contains the primary chromophores of the PAGs, are identical. It has been reported in the past that the chromophore portion of the PAG, rather than the anionic acid portion contributes more to the photolysis

behavior of the PAG, and that PAGs with similar chromophores tend to have similar C values[20,22]. Thus, one would expect TPS-Tf and TPS-Nf to have similar Dill C values. This trend holds true here, where TPS-Tf and TPS-Nf have very similar C values. Likewise, the TBI-Tf and TBI-Nf PAGs also have similar C values.

5.5 Conclusions and Recommendations

Two significant improvements to the original IDE Dill C measurement technique have been presented in this chapter. First, measurement frequency has been investigated as a potential means for improving the capacitance response generated by PAG decomposition, making it possible for PAG molecules that are not easily detected at 1kHz measurement frequency to be easily monitored. It was shown that the frequency dependence of a material's net polarizability can be exploited to allow for an increase or decrease in the magnitude of that material's net dielectric constant, which ultimately leads to an increase or decrease in the capacitance measured from the IDE sensor. This concept was demonstrated for a system consisting of TBI-Tf PAG in a PHOST matrix, where the capacitance response varied significantly with measurement frequency. In addition, it was demonstrated through several different PAG systems that the capacitance versus dose curves recorded at all frequencies were predicting the same behavior, and hence the same Dill C value. The lone exception to this rule may possibly be at the lowest possible measurement frequency, 20 Hz. The data at this frequency seemed to indicate an unexpected lessening in the Dill C value extracted from the data. Based on these observations, it is recommended that all future Dill C measurements be performed at frequencies ranging from 100 Hz up to 10 kHz. Frequencies higher than 10 kHz

appear to provide capacitance responses that are too small and noisy to be useful for data interpretation. Frequencies less than 100 Hz, as just mentioned, may possibly provide Dill C values that are inaccurate.

The second improvement made to the IDE Dill C technique discussed in this chapter was the development of a normalized capacitance expression for use in analyzing the raw IDE capacitance data. The normalized data analysis method is a natural extension of the previously demonstrated linear capacitance mixing rules that can be used for describing the dielectric constant of polymer films containing low loadings of photoacid generator.

The use of normalized IDE capacitance data to measure photoacid generator kinetics provides many advantages over the method previously presented for directly using the capacitance data from IDEs to measure the Dill C parameter for PAGs. First, the normalized data eliminates the variations in baseline capacitance that can occur due to differences in IDE geometry such as finger width, height, etc. Thus, data can now be collected on IDEs of varying sizes (i.e. without requiring exacting fabrication tolerances for the IDEs) and used universally for measuring photoacid generation kinetics. Second, the normalized approach to measuring the Dill C eliminates the influence of many of the fluctuations in baseline capacitance caused by changing environmental conditions such as relative humidity. Thus, data collected from an IDE exposed to 50% relative humidity can now be compared to data collected at 10% relative humidity without worrying about the changes in baseline capacitance that such an environmental difference will cause. It was shown experimentally that the new normalized IDE analysis method provides superior model fit quality, and thus in turn can extract more accurate and precise Dill C

parameters, in the face of noise and error sources such as varying environmental conditions and natural variations in the size of the IDEs used to make such measurements. Finally, and most importantly, the normalized data approach can in theory allow for the characterization of a Dill C parameter for a resist without any prior knowledge of the resist composition or PAG loading. A capacitance versus exposure dose curve generated for a single resist coated IDE, coupled with the resists optical properties, is now sufficient to enable determination of the Dill C parameter for the polymer-PAG system, significantly reducing the amount of time and effort needed to characterize the kinetics of a chemically amplified photoresist.

CHAPTER 6

PHOTORESIST COMPOSITION EFFECTS UPON DILL C MEASUREMENTS: BASE QUENCHERS AND PROTECTING GROUPS

6.1 Introduction

Chapters 4 and 5 of this thesis focused on the development of the IDE Dill C measurement technique and improvements of the technique in the form of a normalization scheme and multi-frequency measurements. To perform the work in these chapters, model versions of chemically amplified photoresists were utilized that consisted of an unprotected poly(p-hydroxystyrene) matrix loaded with varying amounts of several different PAG molecules. The model resist systems chosen were purposely simplified to enable a quick development of the Dill C measurement technique. True commercial resist systems typically have many additional components other than the matrix and a PAG, such as base quencher molecules and protecting groups[5,10,11,33,114]. These components participate in reactions within the resist that can ultimately lead to changes in the resist's overall chemical makeup, and potentially to changes in the film's net dielectric constant. For instance, base quencher molecules are often used to neutralize acid that diffuses outside of the exposed regions and thus minimize line width spread[33,114]. With the IDE Dill C measurement technique heavily dependent upon capacitance measurements of IDEs coated with such films, any component of the resist that can potentially change the net dielectric constant of the film is of great concern. These changes introduce confounding variables that must be dealt with during the IDE capacitance data analysis used to extract the Dill C. As alluded to earlier, until now model systems lacking many of these additional components have been used to develop

the basic IDE Dill C measurement routine and data analysis technique. The work in this chapter now focuses on the various effects that adding such components to a chemically amplified resist system can have upon the IDE Dill C technique, and how the data analysis routine must be modified to account for such components. In particular, work will be presented that focuses on base quenchers and protecting groups commonly used in CAR systems.

6.1.1 Protecting Groups

As discussed in Chapter 2, Section 2, chemically amplified photoresists must contain at least two components in order to form an image: a protected polymer matrix and a photoacid generator[5,11]. When a CAR film is exposed to UV light, the photoacid generator decomposes to form an acid. In a subsequent bake step, the acid catalyzes a deprotection reaction where the protecting group on the polymer matrix is removed, rendering the polymer matrix soluble in developer solution (see Figure 6.1). Up to this point in this thesis, only an unprotected matrix polymer (PHOST) has been utilized. This unprotected polymer matrix was purposely chosen to facilitate the development of the Dill C measurement routine and data analysis routine. With an unprotected matrix polymer, the chemical changes that take place on the polymer chain in the presence of photoacid are minimal, or non-existent. The polymer chain for all practical purposes is inert to the photoacid. Thus, the only change that occurs within the matrix during exposure is the decomposition of the PAG into photoacid. Furthermore, since the PAG decomposition is the only change occurring in the polymer matrix during exposure, it is quite easy to correlate any changes in IDE capacitance (from net dielectric constant

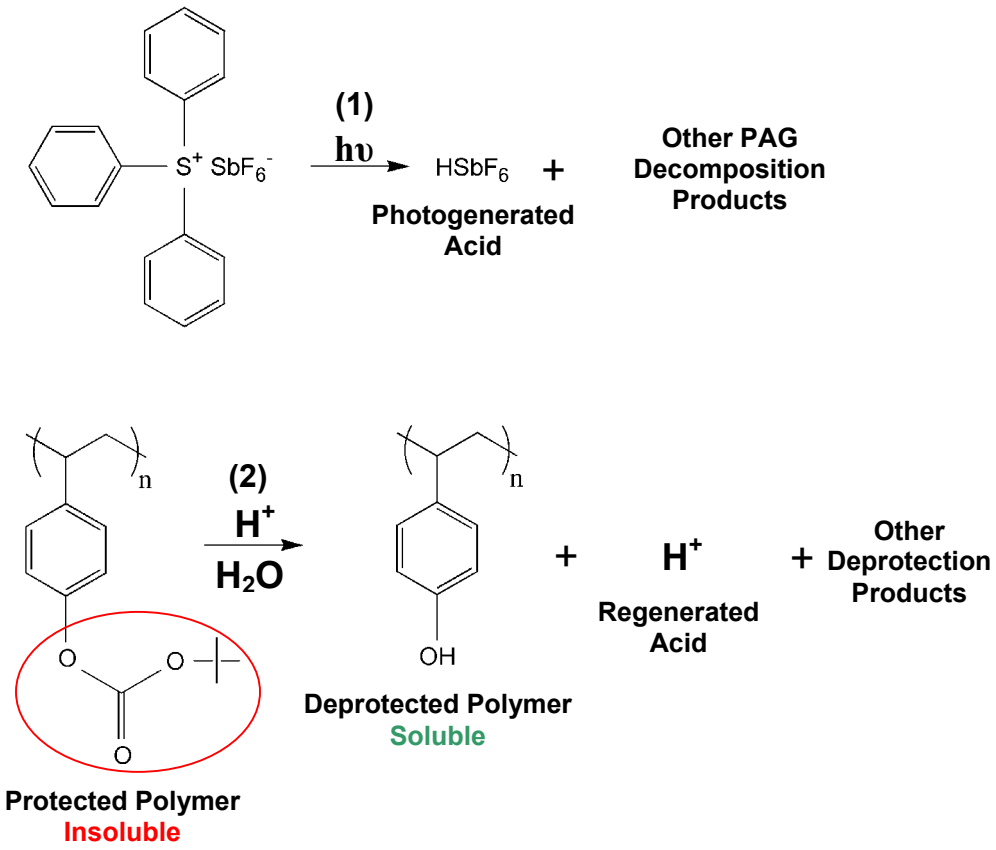

Figure 6.1 Typical chemically amplified photoresist. (1) Exposure to produce photoacid and (2) acid catalyzed deprotection to render the matrix polymer soluble.

changes) to the production of photoacid within the film. Thus, by using an unprotected matrix polymer it is easier to correlate IDE capacitance to the presence of photoacid and develop an appropriate data analysis routine for extracting the Dill C parameter. Unfortunately, true chemically amplified photoresists contain protected polymer matrices. Figure 6.1 provides an example of a very common protected polymer matrix, poly(p-t-butyloxycarbonyloxystyrene)[5,9-11,115]. Here, the t-butyloxycarbonyl (t-BOC) protecting group (circled in red) has been added to a PHOST matrix and renders the matrix insoluble in aqueous base developer. The amount at which a protecting group is added to an unprotected polymer varies widely from system to system, but the most common range of protecting ratios ranges anywhere from 15 to 40% protection[116], depending upon the specific performance requirements of the photoresist. The t-BOC group shown here is just one example of an acid labile protecting group that can be added to a resist matrix polymer. This particular group was part of the first deep-UV chemically amplified resist to be used in full scale manufacturing[5,9-11], and has been used extensively in the semiconductor industry for the construction of integrated circuits. However, there are many other protecting groups available for use in a CAR system. These include such groups as tetrahydropyranyl[5,10,11,117-124] trimethylsilyl[5,10,11], tert-butyl[5,10,11], cyclohexnyl[5,10,11], and tetrahydrofuranyl[124], among many others[5,10,11].

Despite the differences that these protecting groups have from one group to another, they can in general be classified into one of two groups: high activation energy protecting groups and low activation protecting groups[122,125]. High activation energy groups, such as esters and carbonates (such as t-BOC) require high amounts of energy, even in the presence of photoacid, to enable the deprotection reaction to take place[122].

Thus, a bake process performed at elevated temperatures (typically over 100°C) must be performed before any deprotection reactions can take place. If left at room temperature, even in the presence of photoacid, the protected matrix would essentially remain unchanged. Low activation energy systems on the other hand, such as those with acetal-based protecting groups, require much less energy for the deprotection reaction to take place in the presence of acid[122]. Low activation energy systems are known to deprotect even at room temperature in the presence of acid[124]. Thus, immediately after the exposure process has started and a small amount of acid has been generated, deprotection is taking place within the low activation energy resist system. A post exposure bake process will undoubtedly accelerate the deprotection process, but is not entirely necessary in order for deprotection to take place.

Because of the differences in their behavior, these two classes of protecting groups are expected to have drastically different impacts upon the IDE Dill C measurement routine. The IDE capacitance measurements required for measuring the Dill C parameter are performed during the exposure process at room temperature. No elevated temperature bake step is required, and the resist coated IDE is never subjected to such elevated temperatures following exposure. Thus, if a polymer matrix protected by a high activation energy group is utilized in the CAR system being measured using the IDE technique, one would expect that zero deprotection reactions will take place and that the polymer will remain protected throughout the duration of the exposure and measurement process. Thus, the only chemical or compositional change taking place within the CAR system during this time should be the generation of acid from PAG decomposition, and this change should be easily correlated to the measured IDE capacitance. On the other

hand, if a low activation energy protecting group is utilized in the CAR system being studied, it is very likely that deprotection will occur during the exposure and capacitance measurement process at room temperature. Thus, in addition to an increase in acid concentration due to PAG decomposition, the polymer matrix will also be changing while the capacitance measurements are being recorded. This change in the polymer matrix structure will no doubt affect the net dielectric properties of the resist film in some manner, and ultimately lead to changes in the capacitance. There will now be two different mechanisms responsible for changing the IDE capacitance. In order to obtain the Dill C, a means must be determined for deconvoluting the overall capacitance response that results from these two factors so that a capacitance versus exposure dose curve can be generated for the PAG decomposition alone.

Obviously low activation energy protecting group systems have the potential to introduce a new confounding variable into the IDE Dill C technique. Therefore, it is critical that such as system be studied using the IDE technique so that a means for properly dealing with this type of system can be determined. In this chapter, work will be presented that deals with each type of protecting group. First, the capacitance response of a high activation energy group will be examined. For this system, a t-BOC protected PHOST was utilized. Second, a low activation energy system that utilizes an acetal based resist composed of a tetrahydropyranyl ether protected PHOST was studied. The capacitance response of both systems to exposure were studied in order to determine the applicability of the IDE Dill C technique to protected matrices.

6.1.2 Quencher Molecules

As discussed in Chapter 2 section 2, the performance of a chemically amplified photoresist is heavily dependent upon the presence of photoacid within the matrix. The acid is responsible for catalyzing the deprotection reactions that take place to render the matrix polymer soluble. Unfortunately, this catalytic nature of the photoacid can often be problematic in terms of achieving finely resolved features. It has long been known that the photoacid generated during exposure is quite capable of diffusing outside the regions of high acid concentration to the surrounding polymer where no acid is present[127,128]. This diffusion of photoacid can ultimately lead to image distortion. Figure 6.2 illustrates this concept.

As can be seen in Figure 6.2, when the photoresist is initially exposed, a relatively uniform distribution of photoacid is generated within the bounds of the exposed region. However, immediately after exposure photoacid molecules will begin to diffuse from the high concentration exposed region to the surrounding matrix where little, or zero photoacid is present. This diffusion is especially problematic during the post exposure bake process where the elevated temperatures dramatically increase the mobility of the acid molecules. Unfortunately for the lithographer, the acid molecules that diffuse outside the exposed region are still quite capable of catalyzing deprotection reactions that alter the resist film's solubility. Thus, deprotection takes place outside of the desired exposed region and ultimately, this leads to an increase in the width of the developed region over the desired width initially printed during exposure.

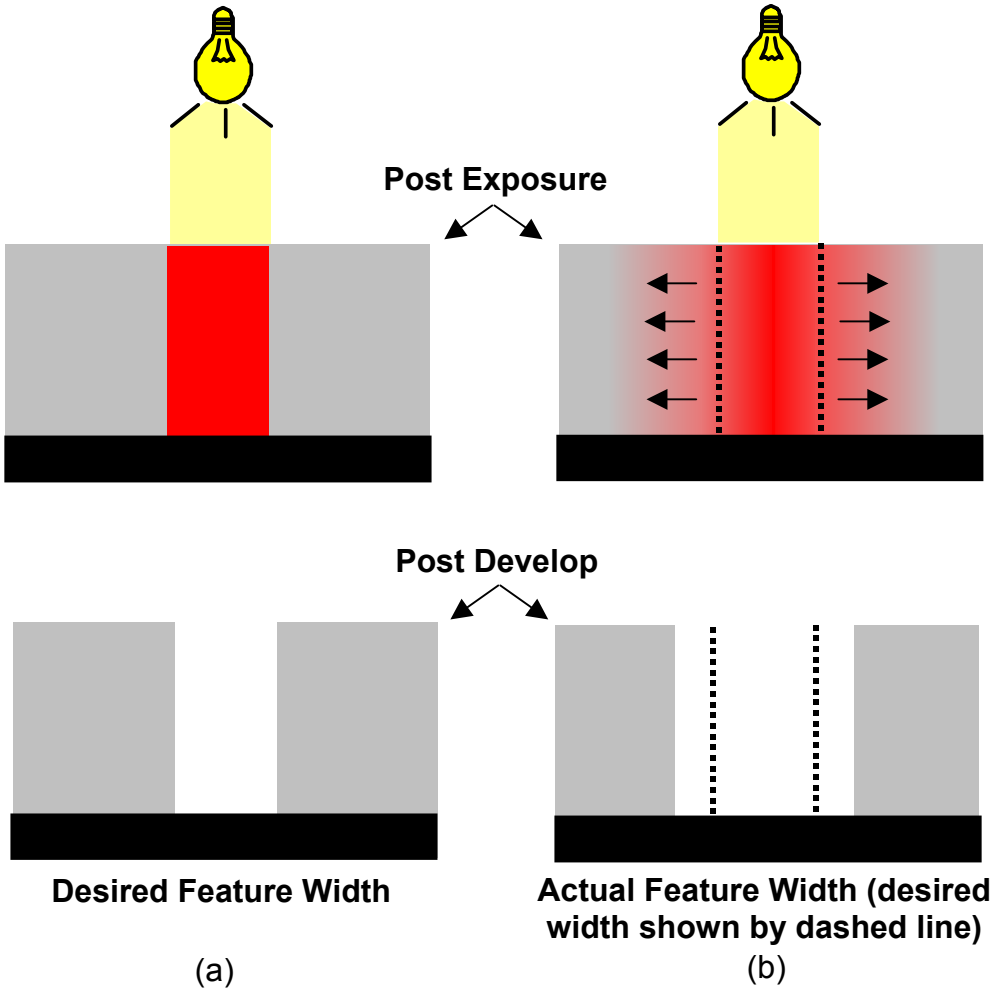

Figure 6.2 (a) Ideal case of exposure and feature formation in a resist system with no acid diffusion (b) Image distortion due to acid diffusion in the resist matrix.

With critical dimension tolerances continuing to shrink tremendously, feature broadening due to acid diffusion is of great concern and must be minimized in order to enable precise manufacturing of today's top of the line devices. Obviously, one method that could be used to counter these effects is to initially print an exposed region that is purposely smaller than desired and allow the feature to then broaden due to diffusion. This method requires a good understanding of the diffusion properties of the particular matrix and PAG being used, as well as their behavior as a function of bake temperature. Such information is not easily obtained. A second alternative that many resist manufacturers have utilized is to load the resist solution with various base materials designed to neutralize the photoacid and render it useless in terms of catalyzing a deprotection reaction[33,114]. Common bases that have been used for this purpose include 1-piperidineethanol, 1,8-diazabicyclo[5.4.0]undec-7-ene, 3-piperidino-1,2-propanediol, and tetrabutylammonium hydroxide[33,114]. Figure 6.3 illustrates the ideas behind this approach.

As shown in Figure 6.3, a chemically amplified resist film that is loaded with a base quencher initially has a uniform distribution of base throughout the film prior to exposure, as indicated by the blue circles. Upon exposure, a large quantity of photoacid is generated in the exposed regions (indicated by the red circles). When the photoacid comes into contact with the base quencher molecules, it is neutralized and rendered incapable of catalyzing a deprotection reaction (purple circles). As acid molecules attempt to diffuse outside of the exposed region, they will likely come into contact with a base quencher within a short distance of the exposed region and become neutralized. Thus, useful acid catalyst (and hence deprotection reactions) are confined to the initial

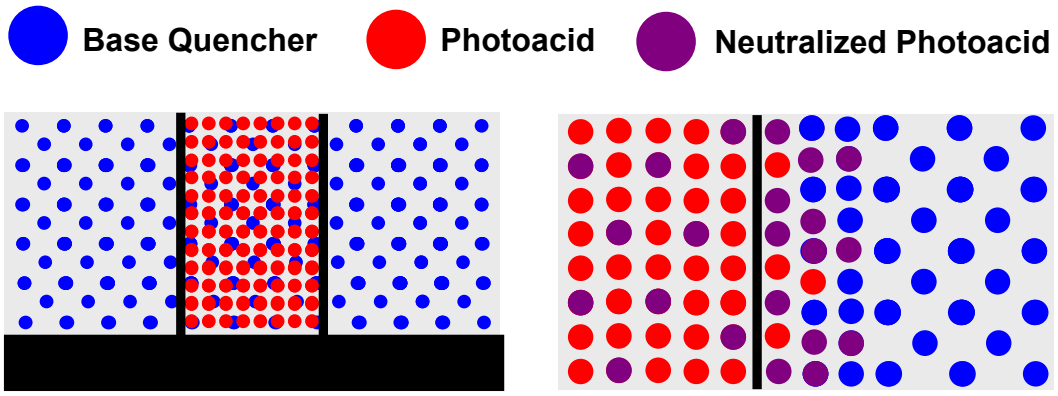

Figure 6.3 Depiction of the use of base quencher molecules to neutralize diffusing photoacid. (a) resist film immediately following exposure (b) close up view of the boundary between the exposed region and the unexposed region.

exposed region and the final feature width retains its desired size. In this type of system, it is apparent that many acid molecules will also be neutralized within the desired exposed region in addition to the unexposed film. However, the photoacid molecules are present in much greater numbers than the base quencher molecules within the exposed region, providing plenty of un-neutralized photoacid to catalyze deprotection and alter the solubility of the resist film.

Attempting to measure the Dill C parameter in a CAR system loaded with a base quencher presents a unique set of potential problems. As discussed throughout this thesis, the IDE Dill C technique relies on capacitance measurements that change due to predictable changes in the resist film's net dielectric constant as the PAG decomposes and forms photoacid. In a system loaded with base quencher, many of these photoacid

molecules will become neutralized immediately after they are formed due to PAG decomposition. This neutralized acid/base pair will undoubtedly have different polarizability properties than the photoacid alone. As a result, the change in net dielectric constant of the film that occurs with photoacid production can no longer be predicted and the linear capacitance mixing relationships that serve as the basis for the IDE technique no longer apply. The resist system essentially becomes a four component system with matrix, PAG, acid, and acid/base neutral species rather than the usual three component system. A new analytical approach must be developed to deal with such a system and the development of this technique will be discussed later in this chapter.

6.2 Experimental Methods

6.2.1 Materials and Methods – Base Quencher Study

To study the effects of using a CAR system loaded with a base quencher upon our IDE Dill C technique, a Dill C measurement was performed using an IDE sensor coated with a film consisting of a polymer matrix loaded with a photoacid generator and a common base quencher. Electronic grade poly(p-hydroxystyrene) (PHOST, M_w = 11,800) was obtained from DuPont Electronic Materials (formerly Triquest Chemical Company) and used as the matrix polymer for all base quencher experiments. Triphenylsulfonium triflate (TPS-Tf) and ethyl lactate (98%) were purchased from Sigma Aldrich and used as the photoacid generator and casting solvent for all solutions used in the base quencher study. 1,8-Diazabicyclo[5.4.0]undec-7-ene (1,5-5) (DBU, Sigma Aldrich) was selected for use as the base quencher molecule in this study. Figure 6.4 illustrates the structure of these three compounds.

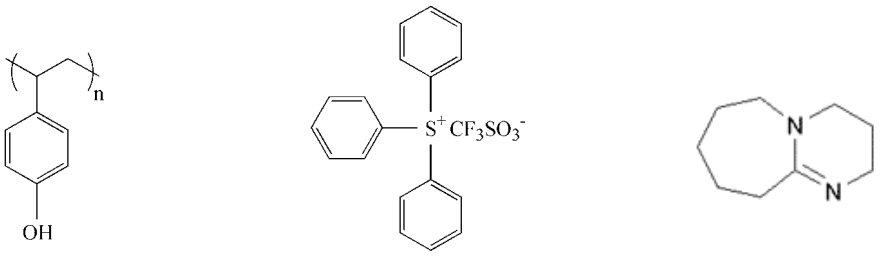

(a) (b) (c)

Figure 6.4 Chemical structures of (a) poly(p-hydroxystyrene) (PHOST), (b) triphenylsulfonium triflate (TPS-Tf), and (c) 1,8-Diazabicyclo[5.4.0]undec-7-ene (1,5-5) (DBU).

Due to the incredibly small amounts of acid produced in a CAR film, a dilute stock base solution was first created. DBU was diluted in ethyl lactate solvent to form a stock solution consisting of 2.18 wt% DBU. Next, a resist solution was created consisting of PHOST, TPS-Tf, ethyl lactate, and DBU. The completed solution was 15.11 wt% total solids, 5.31 wt% TPS-Tf by solids, and 0.30 moles of DBU per mole of TPS-Tf. The solution was stirred extensively until all components were dissolved and mixed thoroughly.

The base loaded resist solution was filtered through 0.2 μm Teflon filters and spin coated onto an IDE structure using similar spin and bake conditions as discussed in chapters 4 and 5. The spin coating process was conducted at 900 rpm for 30 seconds. A contact hotplate bake of 115ºC for 60 seconds was performed to remove residual casting solvent. All other experimental details are identical to those reported in Chapter 4. A standard IDE Dill C measurement routine was followed using the same probe station, exposure tool, and equipment settings as those described in Chapter 4. In addition,

similar ellipsometry experiments were performed to determine the base loaded resist's optical constants for use in the Dill C analysis routine.

6.2.2 Materials and Methods – Protecting Group Study

Two different protecting groups were studied to determine the effects of using a high activation energy protecting group versus a low activation energy protecting group. For the high activation energy group, tert-butyloxycarbonyl (t-BOC) protected PHOST was utilized[122,125]. The t-BOC protected PHOST was donated by DuPont Electronic Materials (formerly Triquest Chemical Company). This sample arrived premixed in a solution that consisted of 29.9 wt% t-BOC/PHOST dissolved in propylene glycol methyl ether acetate (PGMEA) solvent. The molecular weight (M_w) of the PHOST polymer prior to being blocked was reported as 12,020. Once blocked, the polymer was reported to consist of 26.4% t-BOC protected styrene units and 73.6% unprotected hydroxystyrene units[116]. Figure 6.5 below illustrates the structure of the t-BOC protected PHOST polymer discussed in this chapter.

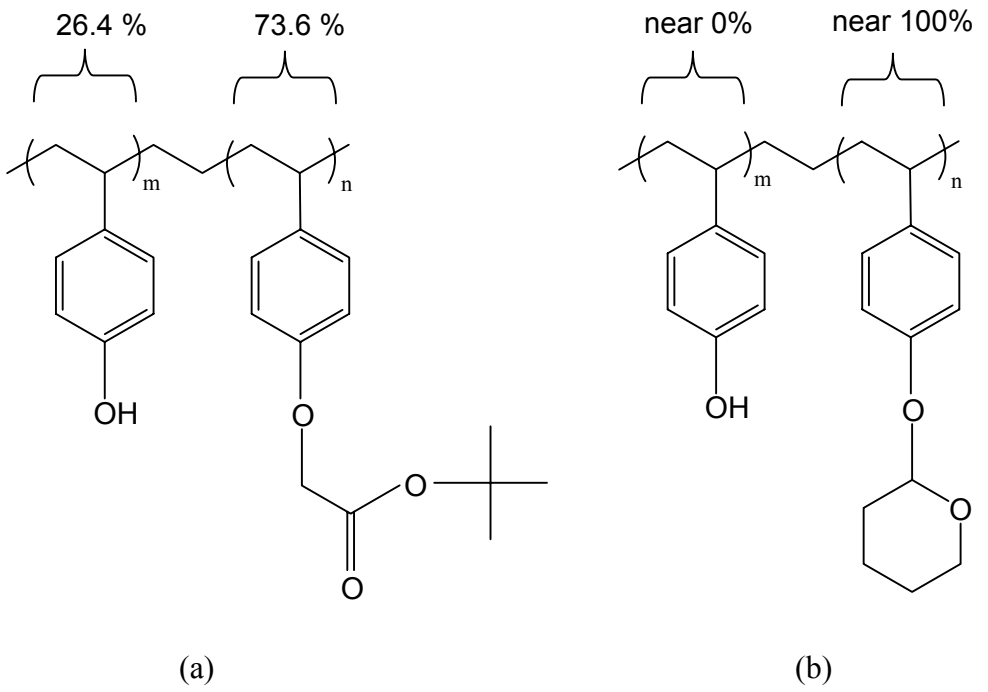

Figure 6.5 (a) Structure of tert-butyloxycarbonyl (t-BOC) protected PHOST and (b) structure of tetrahydropyranyl (THP) protected PHOST.

For the low activation energy protecting group, a common acetal protected polymer was chosen, tetrahydropyranal ether (THP) protected PHOST[122,125]. Figure 6.5 above illustrates the structure of this protected polymer. For this protected polymer, no commercial suppliers could be located. Thus, this polymer system was synthesized in our laboratory for this work. Several different methods exist for the preparation of THP protected PHOST[117-124]. The method used to prepare the material discussed in this work is based upon the procedure described by Shiraishi and coworkers[117]. 5.04 grams of the same PHOST described in section 6.2.1 were dissolved in 70 mL of ethyl acetate (Sigma Aldrich) in a round bottom flask. To this solution, 14.02 grams of 3,4-dihyrdro-2H-pyran (Sigma Aldrich) and two drops of 12M HCl (Fisher Scientific) were added. The solution was allowed to sit at room temperature for 13 days. Next, the solution was washed (using

a separation funnel) with a saturated aqueous solution of sodium bicarbonate (Sigma Aldrich) to neutralize the HCl present in the solution. Following this wash, the solution was dried over 5.33 grams of anhydrous sodium sulfate (Sigma Aldrich) for 19 hours. The THP/PHOST polymer was then precipitated from the dried solution by addition of the solution to fresh petroleum ether (Sigma Aldrich). The resulting polymer was placed under a vacuum for 8 hours to remove residual solvent following precipitation. 6.03 grams of the THP protected PHOST were obtained.

To determine if in fact THP protected PHOST was obtained from the above reaction, and to approximate the degree of protection, proton NMR and FTIR spectroscopy were performed on a sample of the dried polymer. For the H-NMR spectra, samples were processed on a Varian Mercury Vx 300 instrument using $CDCl_3$ as the solvent. For the FTIR spectra, a Bruker IFs66vS FTIR/Raman system was utilized. Figure 6.6 below illustrates the proton NMR spectrum obtained for the THP protected polymer.

As can be seen in the figure, four broad peaks are present: a set of peaks centered near 6.5 ppm (4H) that correspond to the four hydrogen atoms located on the benzene ring (refer to Figure 6.5 earlier), a single peak located at 5.3 ppm (1H) that represents the hydrogen on the CH-Ar group connected to the polymer backbone, a doublet centered at 3.8 ppm (2H) that corresponds to the CH_2 group's hydrogen atoms, and finally, a quartet of peaks centered near 1.8 ppm (9H) that represent the nine hydrogen atoms on the THP group[119,124]. There are also several very narrow, tall peaks scattered throughout the spectrum. These peaks are the result of residual ethyl acetate that was not successfully removed during the vacuum drying process.

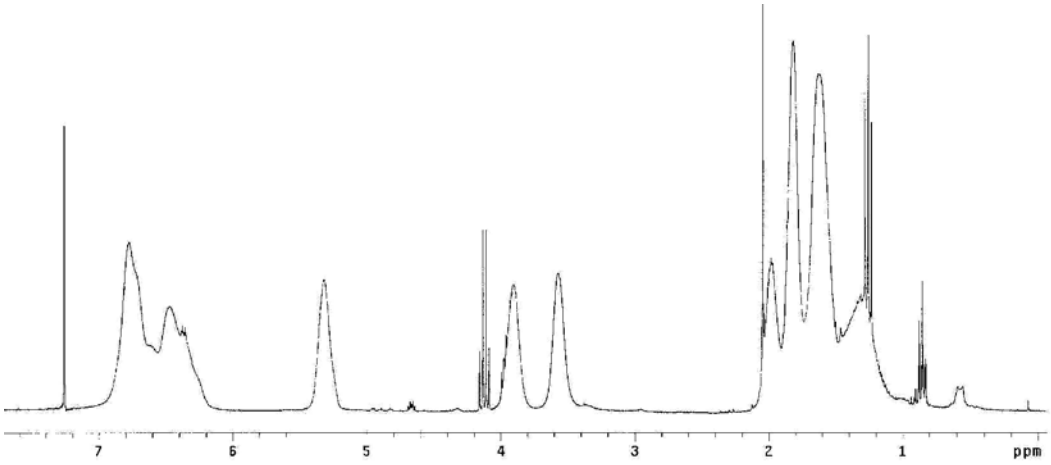

Figure 6.6 H-NMR spectrum collected for the THP protected PHOST polymer.

The locations and relative sizes of the peaks observed in Figure 6.6 agree perfectly with those discussed and presented with other H-NMR spectra of THP-PHOST in various literature sources[119,124]. Based on this information, it is believed that the desired THP protected PHOST polymer was in fact synthesized.

The degree of THP protection can also be estimated from the H-NMR spectra. In this case, the integrated areas underneath the peaks are compared to one another to determine the relative number of one hydrogen type versus another. Using this information for the peaks in Figure 6.6, it is believed that the polymer formed here is nearly 100% protected. The FTIR spectrum recorded for this polymer shown in Figure 6.7 further supports this assertion.

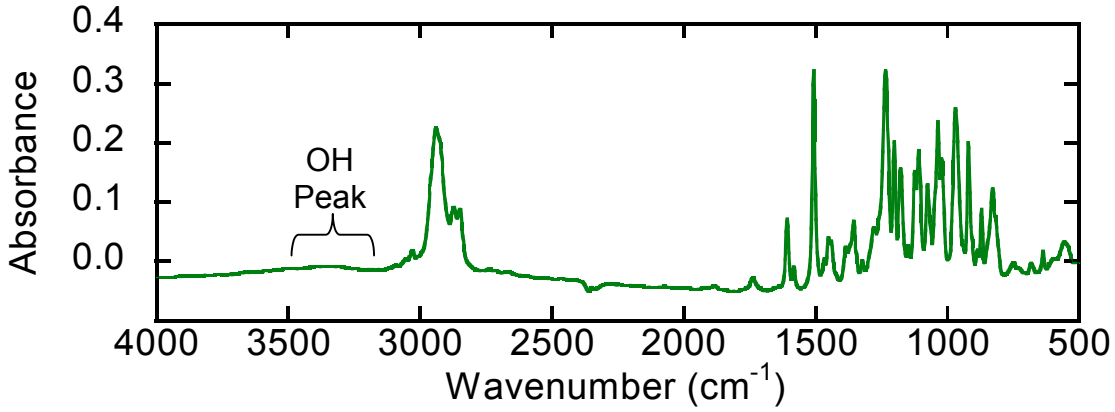

Figure 6.7 FTIR spectrum for THP protected PHOST

The structure of unprotected PHOST, as shown in Figure 6.5 earlier, contains a hydroxyl group attached in the para position of the benzene ring. This hydroxyl group is easily detected in FTIR spectroscopy[118,120,121,123,124] in the form of a broad peak located in the wavenumber range from 3200 to 3500 cm^{-1}. In fact, this peak is one of the most commonly used peaks in deprotection kinetics studies due to the direct correlation between the size of the peak and the number of hydroxyl groups present on the resist polymer. As is easily seen in Figure 6.7, this peak is not present (or is very small) in the spectrum recorded for the THP protected polymer made in this work. Thus, it would appear that very few hydroxyl groups are present on the polymer chain, and thus the majority of the mer units are protected by the THP group. The use of FTIR to monitor deprotection will be discussed in more detail later in this chapter.

Once the two protected polymers were obtained, PAG loaded resist solutions were prepared. The concentrated t-BOC/PHOST solution was first diluted with PGMEA (Sigma Aldrich) from 29.9 wt% solids to a more manageable 15.1 wt% solids. TPS-Tf

PAG was added to this solution to create a final mixture that was 3.7 wt% TPS-Tf by solids and 15.6 wt% total solids in PGMEA. The THP protected PHOST and TPS-Tf PAG were dissolved in ethyl lactate (Sigma Aldrich) to create a resist solution that was 4.1 wt% TPS-Tf by solids and 15.7 wt% total solids in ethyl lactate. All solvents and PAG were used as received.

Two different sets of experiments were performed with each protected polymer. First, FTIR spectroscopy was utilized to determine the stability (or lack thereof) of the protecting groups at room temperature in the presence of photoacid. For these experiments, the resist solutions were spin coated onto blank ZnSe crystals (SpectraTech) at 700 rpm for 30 seconds and then contact hotplate baked at 130ºC for 60 seconds to remove residual casting solvent. The polymer coated ZnSe disks were then scanned using the FTIR instrument at the following times: post spin coat, post exposure (with varying doses), and post post exposure bake. All FTIR scans were performed in transmission mode using a Bruker IFs66vs FTIR/Raman system using a KBr beam splitter and a standard mid-IR measurement routine.

Once the FTIR experiments were complete, the second set of experiments consisted of observing the capacitance behavior of IDE sensors coated with the protected resins during exposure (and hence acid formation). Resist solutions were spin coated onto IDE sensors using a CEE Model 100 CB spin coat and bake system (Brewer Science) and then baked at 130ºC for 60 seconds to remove residual solvent. Capacitance measurements were performed using an Agilent LCR meter (model 4284A) and the standard measurement and data anlaysis routines discussed in Chapters 4 and 5. For Dill C calculations, spectroscopic ellipsometry was performed to determine the optical

constants of the various resins. The standard measurement procedure and data analysis routine discussed in Chapter 4 was utilized for these measurements.

6.3 Results and Discussion – Base Quencher Study

6.3.1 Capacitance Versus Exposure Dose Curves for Base Loaded CAR Films

The DBU loaded TPS-Tf/PHOST solution was spin coated onto an IDE sensor and capacitance versus exposure dose curves were collected at 5 different frequencies. The raw data curves collected during this experiment at each measurement frequency are displayed in Figure 6.8 below. Each of the graphs in Figure 6.8 also contains an inset showing a close up view of the low exposure dose capacitance data values. The data collected at 100 kHz measurement frequency is displayed, however the data proved to be too noisy to allow for an accurate measurement of the Dill C parameter.

The effects of the base quencher upon the capacitance curve are immediately apparent for all data curves collected. In a typical capacitance versus dose curve collected for a polymer film loaded only with PAG and no base quencher, the capacitance rises immediately after the first exposure and continues to rise until eventually all of the PAG molecules have been converted to their photoproducts. A good example of this behavior for comparison to the base loaded sample can be found previously in Figure 4.5 for TPS-Tf loaded PHOST films. The only difference between the films used to produce the curves in Figure 4.5 and those displayed in Figure 6.8 is the addition of the base quencher DBU. Unlike the capacitance curves in Figure 4.5 for a system with no base quencher, the DBU loaded samples' curves contain an intial lag in the rise of capacitance

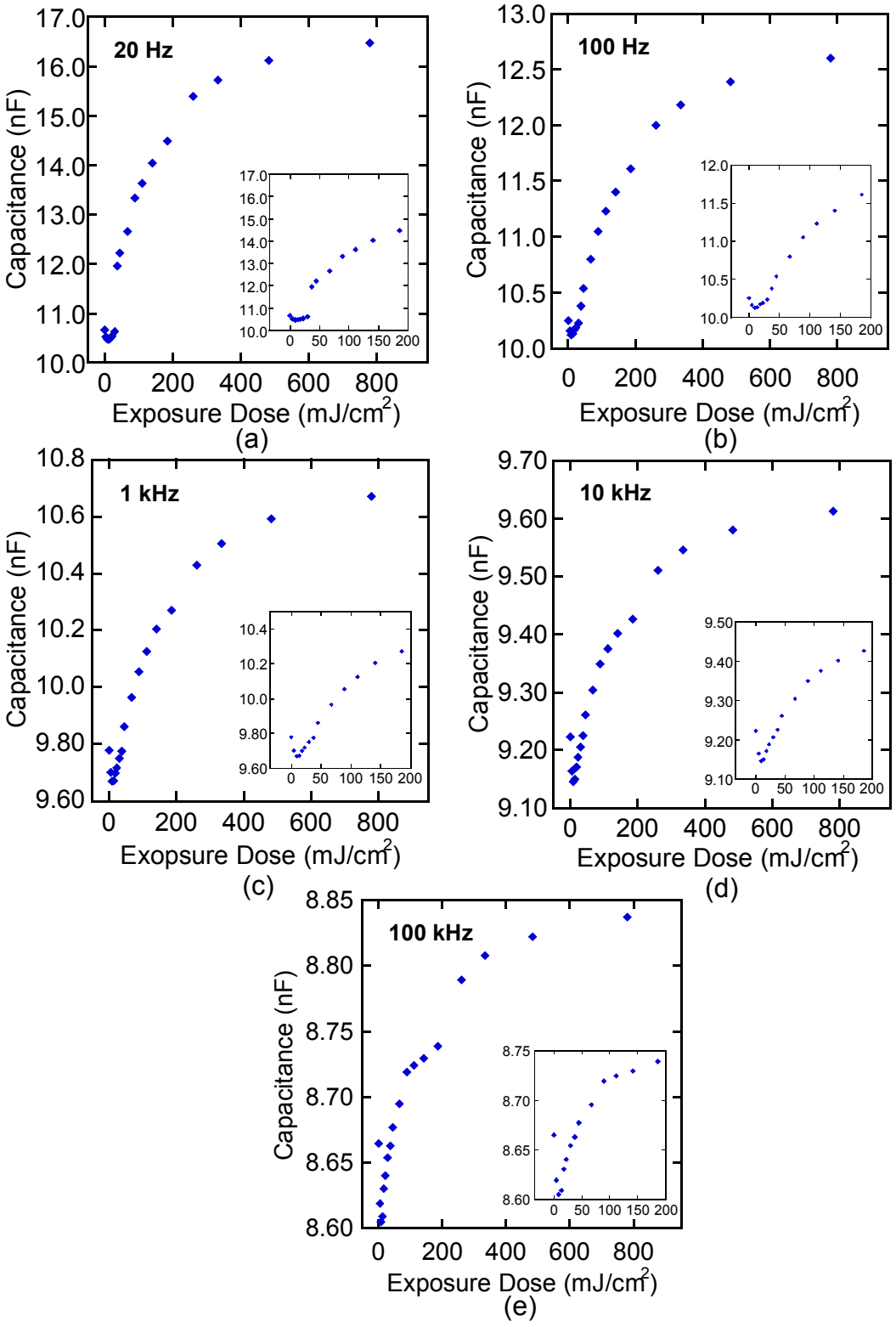

Figure 6.8 Raw capacitance curves collected for the DBU loaded TPS-Tf/PHOST solution at (a) 20 Hz (b) 100 Hz (c) 1 kHz (d) 10 kHz (e) 100 kHz.

versus dose. Following the baseline capacitance measurement at exposure dose zero, a small drop in capacitance was observed for the first two exposure doses (corresponding to a total dose of 8.9 mJ/cm^2). A slow increase in capacitance is observed following the first two data points, although it requires nearly 30 mJ/cm^2 of dose before the capacitance reaches the initial baseline value recorded at dose zero. The magnitude of the capacitance drop and rise in the dose range 0 to 30 mJ/cm^2 was observed to be proportional to the measurement frequency. At 20 Hz, this drop and then rise was very small, with the capacitance values in the entire range from 0 to 30 somewhat resembling a flat line. At 100 Hz, the dip in capacitance is more pronounced. Likewise, at 1 kHz, even more dip is evident. At 10 kHz and 100 kHz, the dip becomes quite large compared to the total capacitance change for acid generation. Nevertheless, despite the size of the drop, the capacitance returns to the initial baseline value at or near 30 mJ/cm^2 for all measurement frequencies.

The origin of the capacitance drop (or lag in the capacitance increase typically observed for a PAG loaded film) undoubtedly comes from the presence of the DBU base quencher. As acid is produced due to PAG decomposition, the DBU neutralizes the acid creating a neutral species within the film. This neutral species has different dielectric properties than the acid molecules alone and thus the capacitance responds differently (even decreasing) from the usual acid response. As discussed in chapters 4 and 5, in order to measure the Dill C parameter a linear mixing relationship must be determined that is based on capacitance values that correspond to a film loaded with 100% PAG and 100% photoproducts (C_{min} and C_{max}). The normalization technique discussed in Chapter 5 is also based upon these values with the normalized capacitance expression being

derived directly from these values. Unfortunately, the presence of base quencher skews the true magnitude of these capacitance values. The C_{max} value corresponds to an acid concentration that has been artificially lowered due to base neutralization. Likewise, C_{min} would be altered due to the presence of base in addition to the PAG molecules at dose zero. Thus, a new means for analyzing films loaded with base quenchers must be determined.

6.3.2 Measuring Dill's C in a Base Loaded Film

The secret to analyzing capacitance data that has been collected for a film loaded with a base quencher is to use a modified version of the normalization technique discussed in Chapter 5. Ordinarily, a Dill C measurement would require using all of the collected capacitance data from dose zero to dose final to generate the normalized capacitance curve. However, due to the dip or lag in capacitance discussed in the previous section, the initial capacitance data collected for a base quencher loaded system cannot be used to create such a curve. Thus, the data immediately following this lag (around 30 mJ/cm^2 as shown in Figure 6.8) must be used to measure the Dill C for a base loaded system.

One of the attractive features of the normalized capacitance expression discussed in Chapter 5 is that one can start analyzing capacitance collected from any point during PAG conversion (i.e. start analyzing at an exposure dose after zero) and the normalized capacitance response will match the normalized response created from any other starting point. For example, consider the normalized capacitance curves shown in Figure 6.9 below. To create these curves, a capacitance versus exposure dose curve was first

generated from the linear mixing relationship described in equation 4.10 using the following parameters: C_0 = 10.5 nF, M = 0.4 nF/wt% acid, N = -0.05 nF/wt% PAG, [PAG_0] = 3 wt%, and C = 0.02 cm^2/mJ. From the capacitance versus dose data created using these values, a normalized capacitance versus dose curve was created as described in Chapter 5. This curve is displayed in Figure 6.9 as the "0" data points from dose 0 to 500 mJ/cm^2. Now consider what occurs when one generates a normalized curve starting with capacitance data not at dose zero on the initial raw capacitance curve. Suppose that one starts with the capacitance value at dose 20 mJ/cm^2 and creates a normalized capacitance curve from this dose value to dose final - assuming that the capacitance value at dose 20 mJ/cm^2 now corresponds to dose zero and adjusting all dose values by the necessary 20 mJ/cm^2 difference.

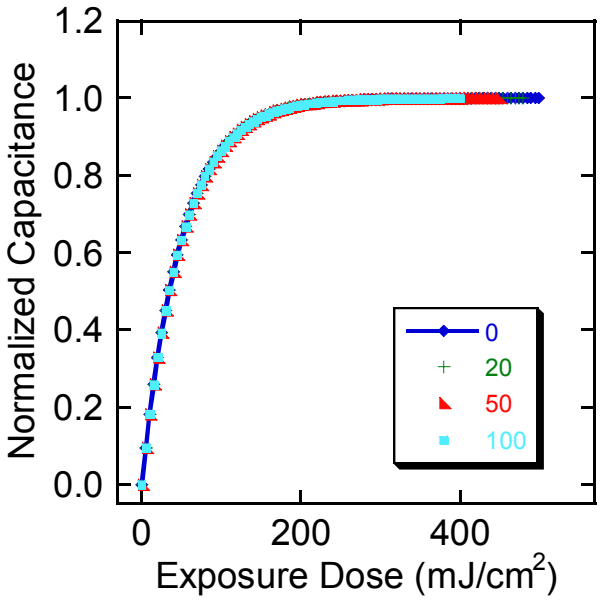

Figure 6.9 Normalized capacitance curves created using raw capacitance data from various starting dose values.

In other words, it is assumed that the PAG decomposition that has occurred up to dose 20 mJ/cm^2 simply creates a new baseline capacitance and that the remaining PAG molecules within the film that have not yet decomposed will decompose due to exposure from dose 20 mJ/cm^2 onward in a normal fashion. The capacitance response from this point on is simply due to the decomposition of the remaining PAG molecules in the film. The capacitance value collected at dose 20 mJ/cm^2 is now assumed C_{min} with the dose final value still C_{max} and the normalized capacitance expression is created. Figure 6.9 illustrates the results of creating this new adjusted normalized curve, as well as the results of starting at even further points along in the original curve, such as 50 mJ/cm^2 and 100 mJ/cm^2. These latter two capacitance values were originally located far into the capacitance response measured from dose zero (so much so that the 100 mJ/cm^2 capacitance value was located near the knee transition region) and yet the normalized curves created using these latter values as starting points still duplicate the original normalized curve with zero deviations.

Having determined that one can start at any point on the raw capacitance versus dose curve and create identical normalized capacitance curves makes it possible to now analyze the base loaded films' data for Dill C values. As mentioned earlier (and shown in Figure 6.8), an initial dip or lag in the capacitance response occurs for the base loaded films until around dose 30 mJ/cm^2, where it is assumed that all of the base quencher has been used up and the PAG decomposition proceeds in a normal fashion. Thus it was decided to start the normalized data analysis at dose 37.2 mJ/cm^2, the first capacitance data point collected after the initial "dip" region at all measurement frequencies. Instead of starting at dose zero and using all capacitance data points, this later dose value was

used as the starting point. Basically, it was assumed that at this point, all of the base quencher had been used up, and therefore acid generation following this point should proceed normally. The normalized Dill C analysis was performed normally from this point on as if we were simply starting with a different, smaller initial loading of PAG.

Exposure dose 37.2 mJ/cm^2 was set as dose zero and all subsequent dose values were adjusted accordingly by subtracting 37.2 mJ/cm^2 from that particular dose value. The capacitance value at dose 37.2 mJ/cm^2 was assigned as C_{min} and the final dose's capacitance value was C_{max}, per the usual technique. The capacitance data points between C_{min} and C_{max} were then normalized per the normal procedure described in Chapter 5 and equation 5.9. Following the creation of a normalized capacitance curve, the Dill C parameter was measured by using the normal routine of selecting a Dill C value and generating model normalized capacitance curves. The Dill C value was adjusted until these model curves matched the experimental capacitance versus dose curve. Again, the details of this part of the analysis are identical to those described in Chapters 4 and 5. Figure 6.10 below illustrates the model fits obtained for the capacitance data collected at 20 Hz, 100 Hz, 1 kHz, and 10 kHz. As shown in Figure 6.10, excellent fits were obtained for the model capacitance curves to the experimental curves. For the 1 kHz data, a best fit Dill C of 0.031 cm^2/mJ was found. For 20 Hz, 100 Hz, and 10 kHz measurement frequencies, best fit Dill C values of 0.031, 0.030, and 0.030 cm^2/mJ were found respectively, giving an average value of 0.0305, or 0.031 cm^2/mJ with a 95% confidence interval of +/- 0.001. As mentioned earlier, the data recorded at 100 kHz was simply too noisy to be of any use in the Dill C analysis.

In Chapters 4 and 5 the Dill C of TPS-Tf PAG in PHOST was measured and found to be 0.045 cm^2/mJ. It is interesting that the average value obtained here of 0.031 cm^2/mJ for a base loaded PHOST film is quite a bit lower than the C value measured in the plain PHOST film. Though the exact cause of this change in the C value for TPS-Tf is not known, it is highly suspected that the presence of the DBU base quencher acts to retard the rate of PAG decomposition. The research group of Pawloski and coworkers at the University of Wisconsin have done extensive amounts of work aimed at measuring the Dill C parameter using the standard addition technique discussed in Chapter 2[19,22,32,33,114]. In two of their reported sets of experiments, they used the same base quencher (DBU) in their standard addition method to measure the Dill C parameter for TPS-Tf at 248 nm wavelength[22,32]. DBU was added in amounts ranging from 0 to 10 mol% during the standard addition process. The C values calculated for TPS-Tf in PHOST using their method were 0.037 and 0.044 cm^2/mJ. The confidence intervals for the first number were not given, while for the second number they were 0.026 to 0.062 cm^2/mJ. These two values are in reasonable agreement with the 0.045 cm^2/mJ value measured here in Chapter 4, but nevertheless appear to be slightly less than this value. Perhaps the lessening in acid generation rate is dependent upon the quantity of base present. As mentioned earlier, Pawloski utilized between 0 and 10 mol% DBU, whereas the experiments discussed here utilized 30 mol% DBU. Perhaps the greater amount of DBU present within the resist films here led to a more dramatic retardation of PAG decomposition.

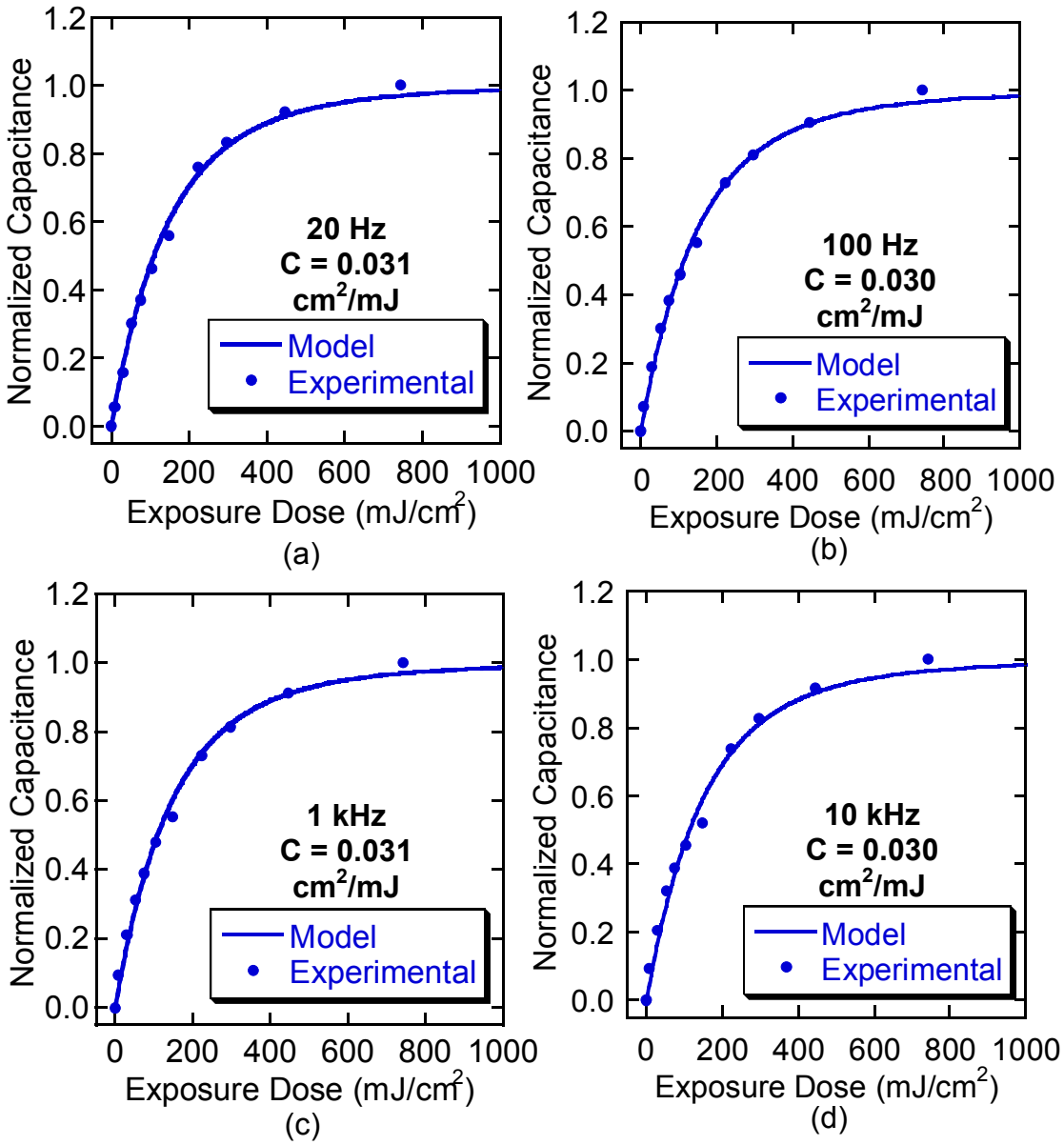

Figure 6.10 Model capacitance curve fits to experimental capacitance recorded at (a) 20 Hz, (b) 100 Hz, (c) 1 kHz, and (d) 10 kHz.

Further evidence that the base quenchers added to a resist film may alter the rate of PAG decomposition is provided again by Pawloski and co workers[33]. In a recent paper they study the effects of two different base quenchers upon the apparent rate of photoacid generation. The two base quenchers were 1-piperidineethanol (1PE) and 3-piperidino-1,2-propanediol (3P12PD). Unfortunately they did not study the exact DBU base quencher used here. They found that resist formulations that were otherwise identical except for the type of base quencher had Dill C values statistically different from one another. They speculated that the base is somehow capable of participating in the complex reactions that take place during the formation of photoacid or during the transfer of energy from the matrix to the PAG. They suggest that perhaps the base quencher consumes radicals or ions that serve as intermediates during the transformation from PAG to photoacid. Perhaps this same sort of behavior can explain the lower C value obtained for DBU loaded samples that were measured here. If the DBU is scavenging radicals or ions and preventing some of the PAG molecules from converting, it would serve to effectively slow down the conversion and lessen the Dill C value.

6.3.3 Determining Base Loading From Capacitance Data

A second useful piece of information that could potentially be gained from the raw capacitance data collected for a base loaded CAR film could be the exact loading of base within the film. It was just demonstrated that the Dill C parameter can be measured for a base loaded film. Once this C value is known, it is then possible to calculate the exact amount of photoacid that has been produced within the resist film to within reasonable accuracy for any exposure dose. Thus, assuming a 1:1 stoichiometric

neutralization of the base by the photoacid, it should be possible to accurately determine how much base was present within the resist film by examining the raw capacitance versus dose curve.

For example, consider the raw capacitance data shown previously in Figure 6.8. In these curves it is apparent that between the capacitance data points located at dose 29 mJ/cm^2 and 37 mJ/cm^2 some type of change occurs within the film, as evidenced by the abrupt change in the slope of the capacitance curve. It is believed that this sudden change in the shape of the curve is the point at which the base quencher has been completely neutralized by acid and normal photoacid production and detection resumes. Thus, it would appear that at a dose between 29 and 37 mJ/cm^2 an amount of photoacid has been produced that is proportional on a molar basis to the amount of base loaded into the film. This amount of acid (and hence base) can be readily calculated using the Dill C parameter.

This exact methodology was carried out for the data presented in Figure 6.8 for a DBU loaded TPS-Tf/PHOST film. The C value of $0.031cm^2/mJ$ was used to calculate the normalized photoacid concentration (i.e. $[Acid]/[PAG_0]$) at doses of 29 and 37 mJ/cm^2. Values of 0.18 and 0.22 were calculated. An average value of 0.20 was assumed since the true "titration point" is likely somewhere between the two dose values utilized. Thus, 20% of the original moles of PAG have converted to photoacid at this point, and been neutralized by the base quencher. Assuming 1:1 stoichiometric neutralization, a similar number of moles of DBU must be present. As mentioned earlier, the CAR films used in these experiments were initially loaded with 0.30 moles of DBU per mole of PAG. Therefore, there is a discrepancy between the number of moles of

DBU measured experimentally and the number that was initially loaded. Two potential reasons for this discrepancy exist. First, it might be possible that a 1:1 stoichiometric neutralization does not take place[114]. Some of the DBU quencher may not participate in a reaction with the photoacid. Thus, more DBU would be present than indicated by the neutralization. The second idea for the discrepancy between the two base amounts is that perhaps the DBU is volatile enough that some of it is lost during the soft bake step. A soft bake of 115°C for 60 seconds is performed following the spin coating step to remove residual casting solvent. It is quite possible that some of the DBU is removed during this baking step, leading to the smaller measured content of base quencher. More work must be done to determine exactly how accurately IDE capacitance measurements can measure base loading.

6.4 Results and Discussion – Effects of Polymer Protecting Groups

As mentioned in the introductory section of this chapter (section 6.1.1), the reactive protecting groups that are typically synthesized onto the CAR matrix polymer have the potential to introduce additional confounding variables to the IDE Dill C analysis technique. In a typical CAR system, a post exposure bake at elevated temperatures is required in order for enough energy to be supplied to the resist for the acid catalyzed deprotection reactions to take place and alter the resist solubility. For this reason, the IDE Dill C capacitance measurements are taken at room temperature so that complications due to deprotection are avoided. If, however, the protecting group deprotects, or deblocks at room temperature in the presence of the photoacid, a new variable is introduced into the Dill C data analysis routine. The deprotection results in a

change in the net chemical makeup of the CAR film, possibly resulting in changes in the film's net dielectric constant, which can alter the measured IDE capacitance. If these changes are significant enough, they could potentially render the linear mixing relationships used to obtain Dill's C invalid, and cause the need for a new analytical approach. For this reason, the effects of protecting groups upon the IDE sensor based technique have been studied. In particular, two separate types of protecting groups have been examined: high activation energy protecting groups that should remain stable at room temperature and low activation energy groups that have the potential to react in the presence of photoacid even at room temperature. Tert-butyloxycarbonyl[5,9-11,115] protected PHOST was the high activation energy group that was studied while tetrahydropyranyl[117-124] ether protected PHOST was the low activation energy group examined. The results of this study are presented in the remainder of this chapter. Initially, FTIR measurements designed to determine whether or not the protecting groups are reactive at room temperature will be presented. Following this determination of their reactivity, IDE sensor capacitance measurements of such systems will be discussed.

6.4.1 FTIR Results: t-BOC/PHOST

The first resist polymer studied using FTIR spectroscopy was the t-BOC protected PHOST resin. t-BOC is known to be a high activation energy protecting group[122,125], meaning thermal energy must be provided in order for the acid catalyzed deprotection reaction to take place. At room temperature, essentially nothing should take place in a high activation system, even in the presence of photoacid. FTIR spectroscopy was used to prove that this is in fact the case for t-BOC. Figure 6.11 below illustrates an FTIR

spectrum taken of the t-BOC/PHOST film following spin coating onto the ZnSe crystal. No exposure has been performed at this point.

There are several peaks of interest in the FTIR spectra that can be monitored to follow deprotection[115]. The first of these is the broad OH stretch ranging from 3200 to 3500 cm^{-1} (close up view provided in Figure 6.11 b). As mentioned in section 6.2.2, as the t-BOC protecting group is removed from the polymer, OH groups take their place in the para position of the benzene ring to form the hydroxystyrene mer unit. Thus, the OH peak should increase in size with deprotection. For this particular polymer, this change may not be easily noticed. This t-BOC protected polymer is 26.4% protected, meaning that 73.6% of the polymer already contains hydroxyl groups. Thus, any change in the OH peak in the IR spectrum will be much more subtle than for a completely protected polymer such as the THP protected PHOST discussed earlier. The second peak that can indicate deprotection is located near 1755 cm^{-1} and is indicative of the carbonyl bond located on the t-BOC protecting group. When deprotection occurs, this carbon/oxygen double bond disappears as CO_2 is formed and liberated. Thus, the peak at 1755 cm^{-1} should decrease in size, or disappear if deprotection has taken place. Finally, a third set of peaks that can indicate t-BOC deprotection are located in the range from 1148 cm^{-1} to 1276 cm^{-1}. These peaks correspond to the C-O bond on the t-BOC group that disappears during deprotection. Thus, like the carbonyl peak, this peak should also shrink in size after deprotection. All three peaks that can be followed during deprotection are highlighted in Figures 6.11 a-c.

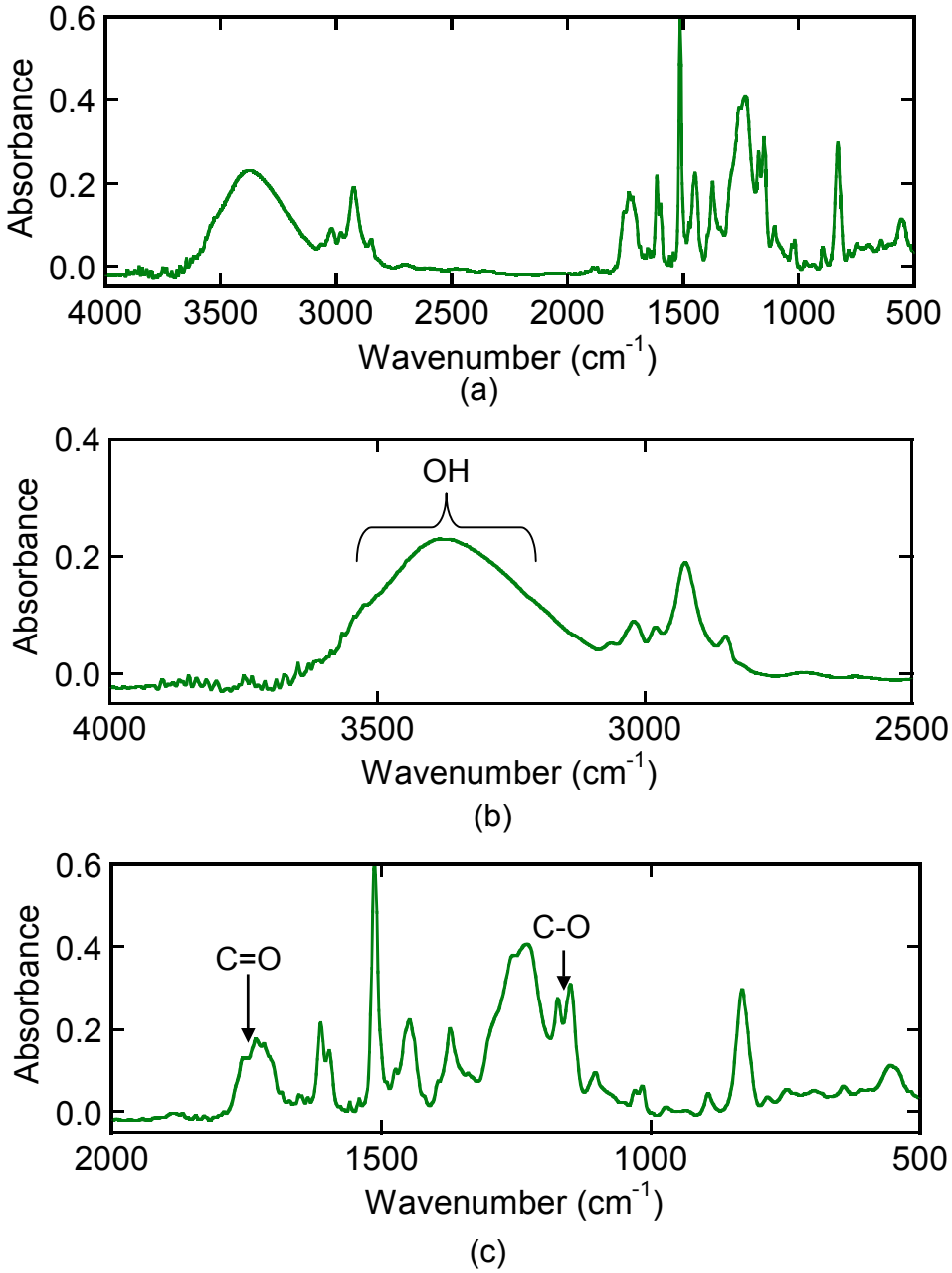

Figure 6.11 FTIR spectrum for t-BOC protected PHOST following spin coating onto ZnSe crystal (a) complete spectrum (b) close-up of high wavenumber region (c) close-up of low wavenumber region.

To determine the stability of the t-BOC group at room temperature, several FTIR scans were taken of the sample at different times. First, a scan was performed immediately after coating the resist onto the ZnSe crystal (Figure 6.11). No acid is present at this time and so the IR scan should represent a protected polymer that has experienced zero deprotection, providing a nice baseline to go from. Second, a scan was performed following several different exposure doses (Figure 6.12). These scans were designed to determine if the presence of different amounts of acid would initiate deprotection at room temperature. Once the desired total exposure dose was reached, FTIR scans were taken periodically over the course of an hour with the sample at room temperature to determine if any room temperature deprotection was occurring in the presence of a large quantity of photoacid (Figure 6.13). Finally, the sample was baked at 130ºC for 3.5 minutes to initiate deprotection. An FTIR scan was performed immediately following this PEB step. Figures 6.12 through 6.14 below illustrate the results of these scans.

Essentially no difference was observed between the post coat scan and the scans taken after the various exposure doses (Figure 6.12) indicating that increasing acid content does not initiate room temperature deprotection. None of the three peaks indicative of t-BOC deprotection were altered in any way. A total exposure time of 500 seconds was used giving the resist a total dose of 700 mJ/cm^2 at this point. The only difference that can be seen among the spectra is an odd change in absorbance located near 2300 cm^{-1}. This area of the absorbance spectrum changes absorbance from scan to scan in no logical manner, and has been observed to do so in all scans taken for all

samples. It has been suggested that this area of the spectrum is likely an anomaly that is instrument related, and not sample related[128]. Fortunately, no peaks of interest are located in this region.

Once 700 mJ/cm^2 dose was reached, the resist coated ZnSe disks were allowed to sit at room temperature for a total time of 61 minutes (Figure 6.13). Once again, no significant changes (other than increased noise in the water bands) were observed between spectra recorded at various points during this time period, indicating that no deprotection was occurring at room temperature, even in the presence of a significant quantity of photoacid. The time period of the delay studied here is important. A typical set of Dill C capacitance measurements usually takes on the order of 30 minutes to complete. Thus, it would appear that a high activation energy protecting group, such as t-BOC, should be capable of remaining stable during the course of an IDE sensor Dill C measurement.

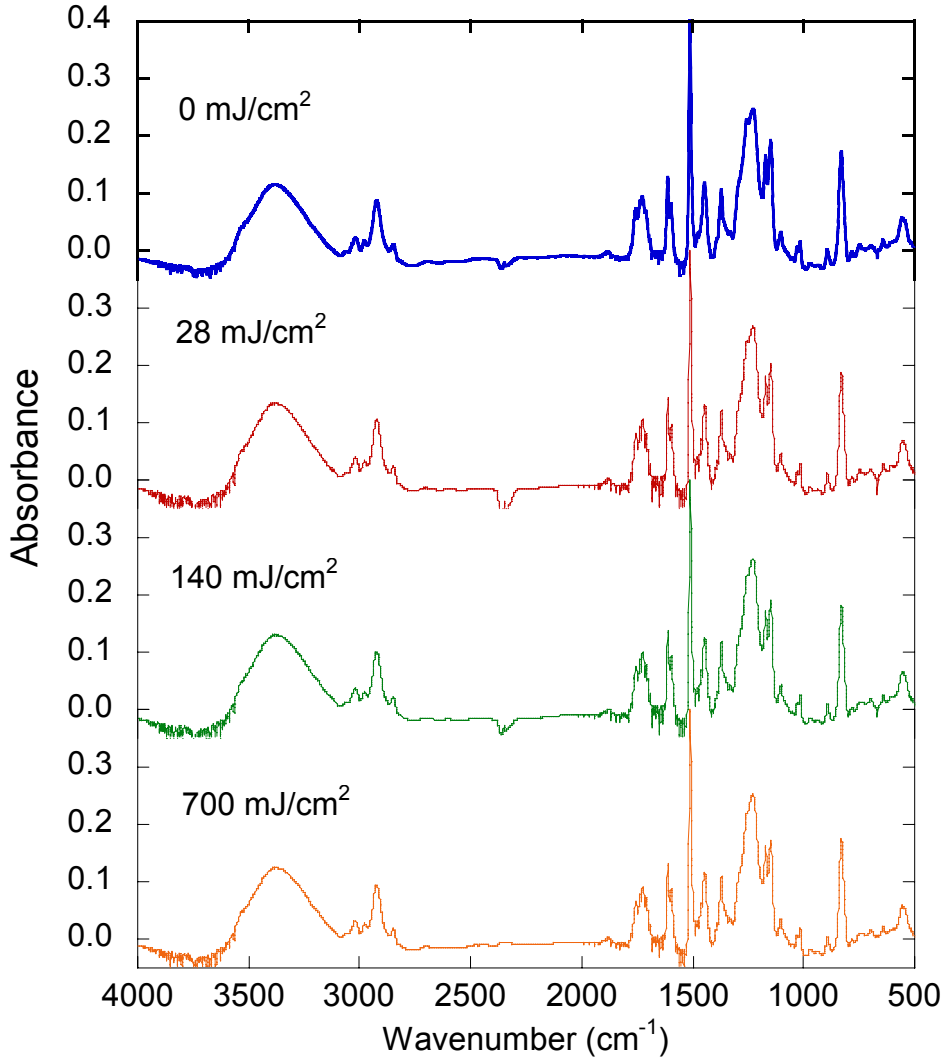

Figure 6.12 FTIR spectra of t-BOC protected PHOST following 0, 28, 140, and 700 mJ/cm^2 exposures.

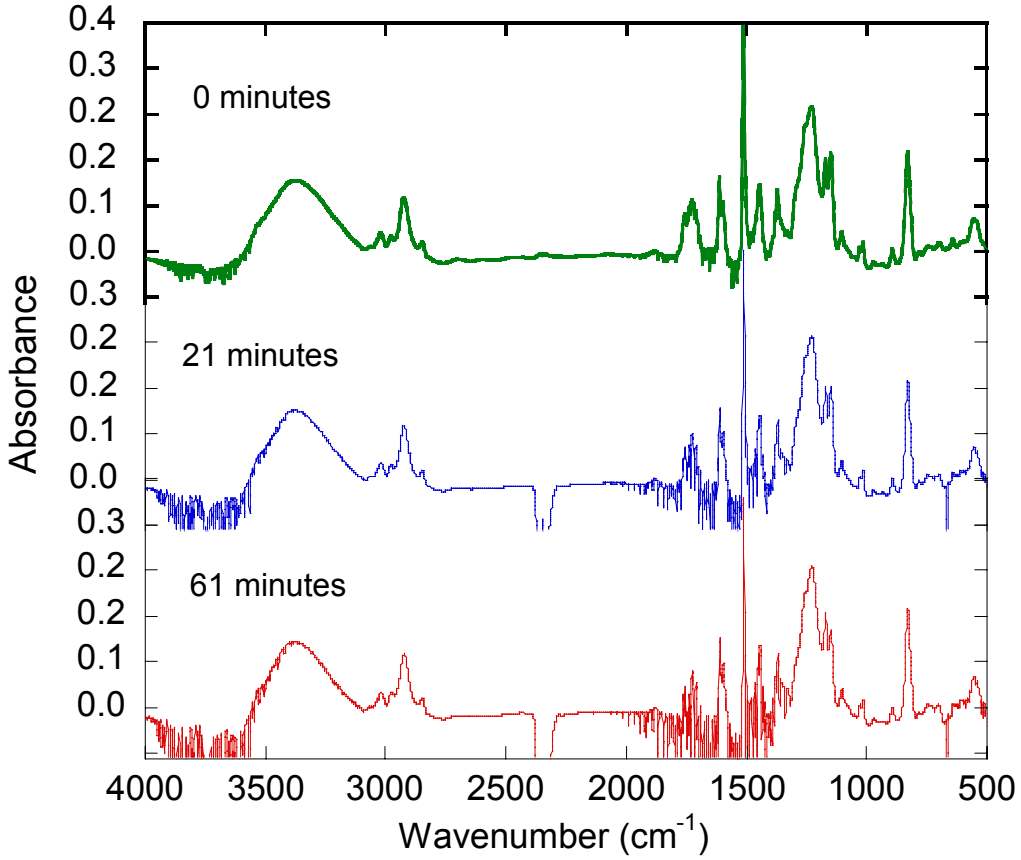

Figure 6.13 FTIR spectra of a t-BOC protected PHOST film 0, 21, and 61 minutes after exposure to 700 mJ/cm^2 of 248 nm radiation.

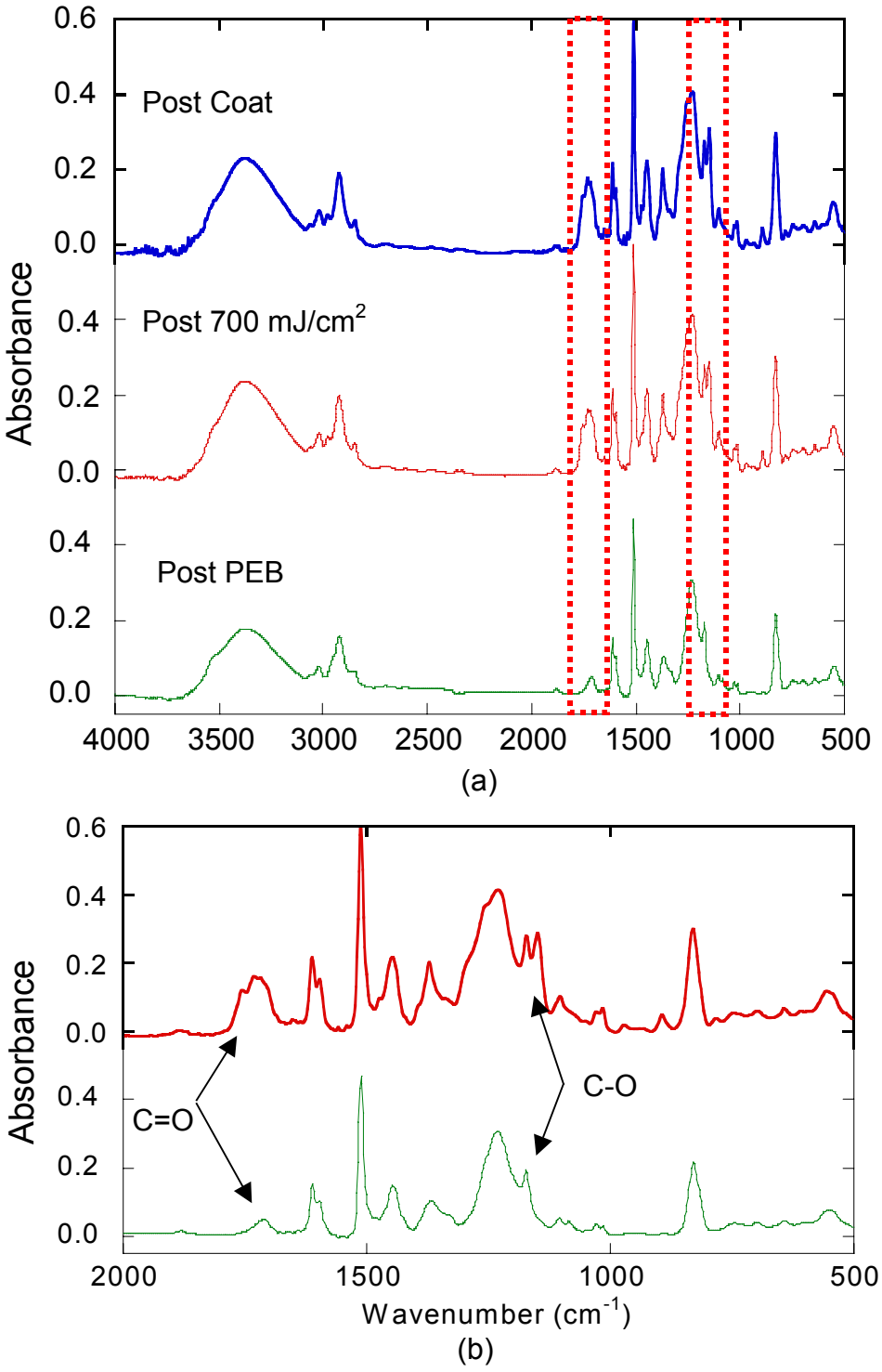

Figure 6.14 FTIR spectra of t-BOC protected PHOST at (a) post coat, post 700 mJ/cm^2 exposure, and post PEB at 130ºC for 3.5 minutes (b) close-up view of low wave number peaks indicating deprotection has taken place.

To prove that the t-BOC protected PHOST polymer is truly reactive, and will in fact deprotect when properly processed, the last steps taken were to subject the resist coated ZnSe crystal to a post exposure bake at 130 ºC for 3.5 minutes. The FTIR scans taken before and after this PEB step are shown in Figure 6.14 above. From the spectra, there is no easily discernable difference between the hydroxyl peaks before and after bake. However, the deprotection is easily observed in the two peaks that indicate the carbonyl and C-O bonds. The carbonyl peak at 1755 cm^{-1} decreases dramatically in size following the post exposure bake. Likewise, the peak in the range 1148 – 1276 cm^{-1} decreases as well. A close up view of this region of the FTIR spectrum is shown in Figure 6.14 b with these particular peaks highlighted.

Based on the FTIR results, it appears that a high activation energy protecting group, such as the t-BOC studied here, will remain stable at room temperature in the presence of significant quantities of photoacid, and thus present no complicating variables to the IDE Dill C analysis. This conclusion will be put to the test later in this chapter when the IDE sensor measurements of t-BOC protected PHOST are presented.

6.4.2 FTIR Results: THP Protected PHOST

The second resist polymer studied using FTIR spectroscopy was the THP protected PHOST resin. THP is known to be a low activation energy protecting group, meaning very little, if any thermal energy must be provided in order for the acid catalyzed deprotection reaction to take place. At room temperature, it is quite likely that deprotection will take place in the presence of the photoacid catalyst[124]. FTIR spectroscopy was used to determine if deprotection actually would take place at room

temperature. Figure 6.15 below illustrates an FTIR spectrum taken of the THP/PHOST film following spin coating onto the ZnSe crystal. No exposure has been performed at this point.

There are several peaks of interest in the THP FTIR spectra that can be monitored to follow deprotection[118,120,121,123,124]. The first of these is once again the broad OH stretch ranging from 3200 to 3500 cm^{-1} (close up view provided in Figure 6.15 b). Just as with the t-BOC protected polymer, as the THP protecting group is removed from the polymer, OH groups take their place in the para position of the benzene ring to form the hydroxystyrene mer unit. Thus, the OH peak should increase in size with deprotection. For the THP protected polymer used here, this change should be quite easily observed. As shown in Figure 6.15, the polymer synthesized in this work is nearly 100% protected, and thus very few hydroxyl groups are present. Thus, the OH stretch from 3200 cm^{-1} to 3500 cm^{-1} is not present in the spectrum recorded immediately following spin coating. As the polymer deprotects, the increased presence of this stretch should be easily identifiable. The other peaks that are commonly used to monitor deprotection in THP protected PHOST are located near 921 cm^{-1} and 969 cm^{-1}. These peaks represent the C-O bonds that disappear during deprotection and should therefore shrink during deprotection.

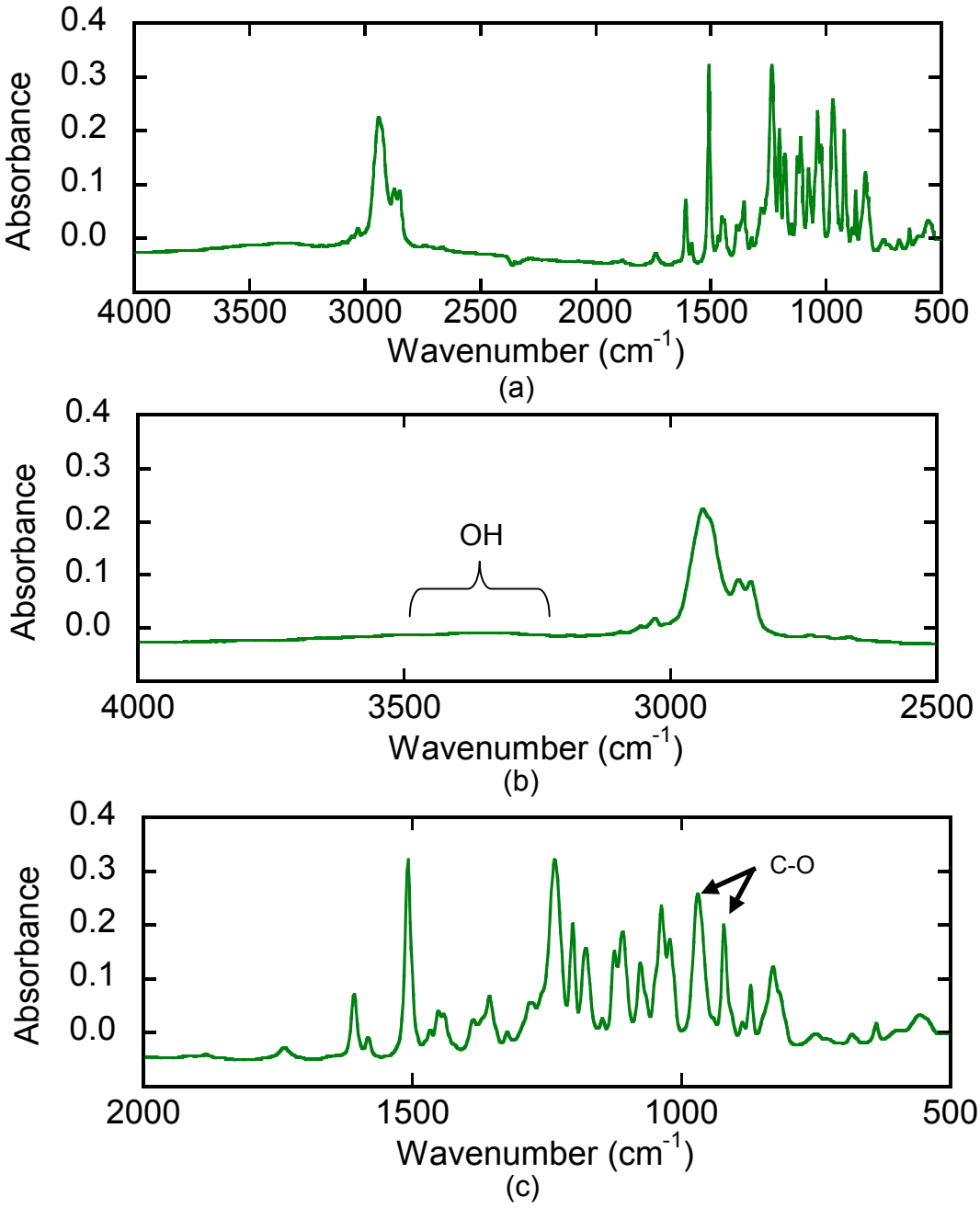

Figure 6.15 (a) FTIR spectra of THP protected PHOST immediately following spin coating (b) close – up view of high wavenumber region of THP/PHOST spectrum (c) close – up view of low wavenumber region of THP/PHOST spectrum.

To determine the stability of the THP group at room temperature, several FTIR scans were taken of the sample at different times, similar to those recorded for the t-BOC sample. First, a scan was performed immediately after coating the resist onto the ZnSe crystal (Figure 6.15). No acid is present at this time and so the IR scan should represent a protected polymer that has experienced zero deprotection, providing a nice baseline to go from. Second, a scan was performed following various exposure doses to determine the effects of increasing acid content at room temperature. Finally, a set of scans were recorded over time to determine if deprotection can occur with THP sitting at room temperature with a constant amount of photoacid present.

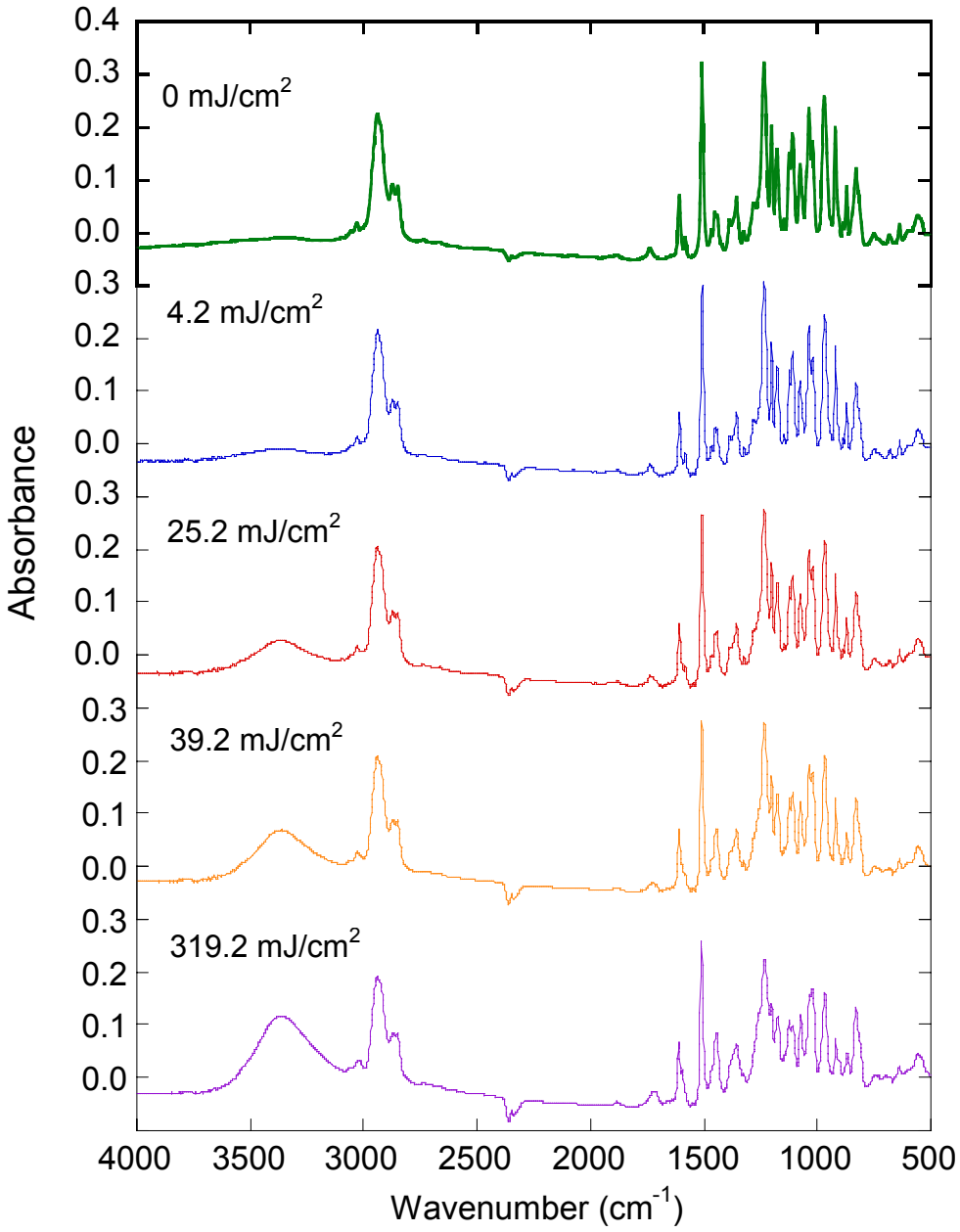

Figure 6.16 FTIR spectrum of THP protected PHOST following exposure doses of 0 mJ/cm^2, 4.2 mJ/cm^2, 25.2 mJ/cm^2, 39.2 mJ/cm^2, and 319.2 mJ/cm^2

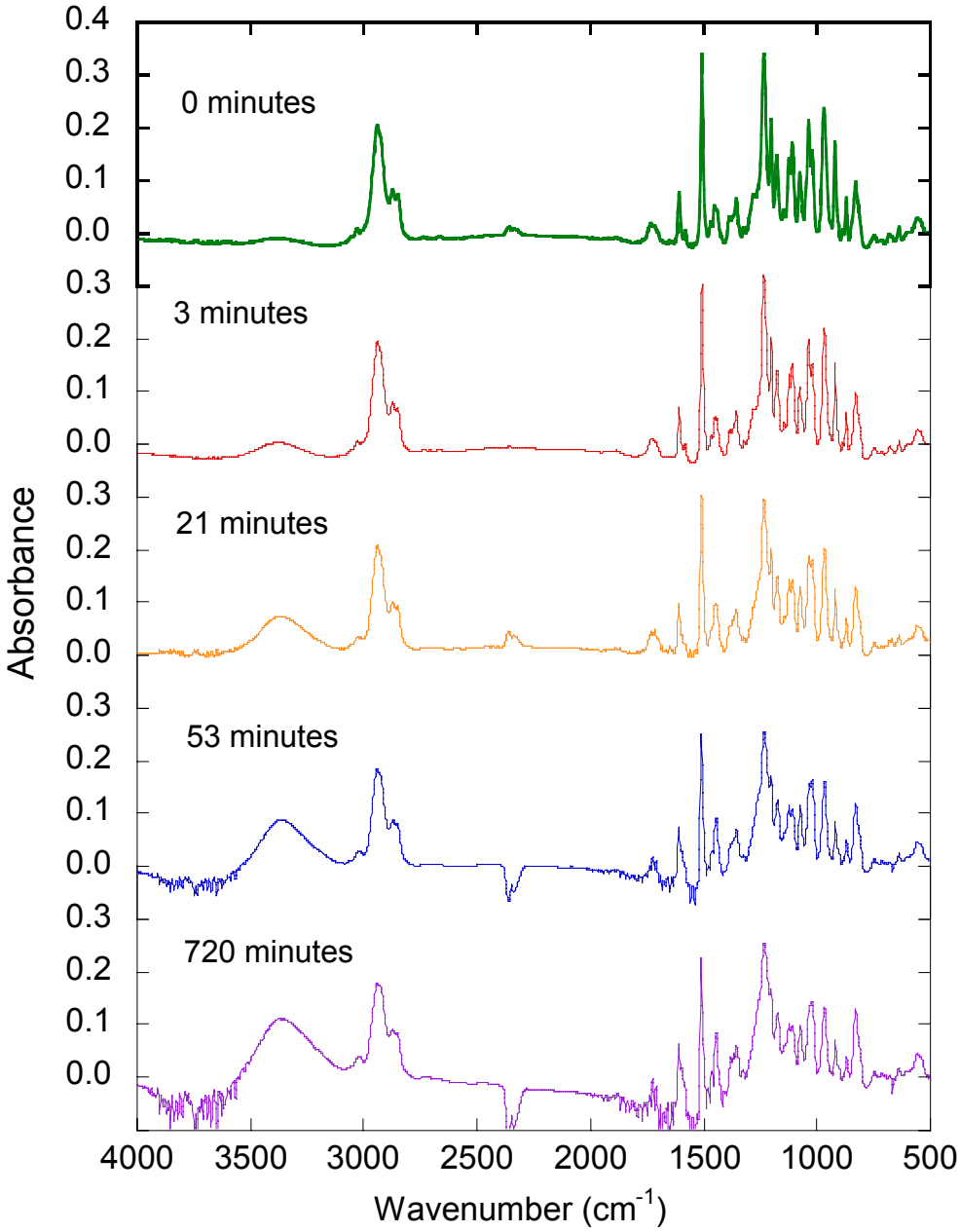

Figure 6.17 FTIR spectra of THP protected PHOST at various times following an exposure dose of 14 mJ/cm^2. Immediately after exposure 3 minutes following exposure 21 minutes following exposure 53 minutes following exposure and 720 minutes following exposure.

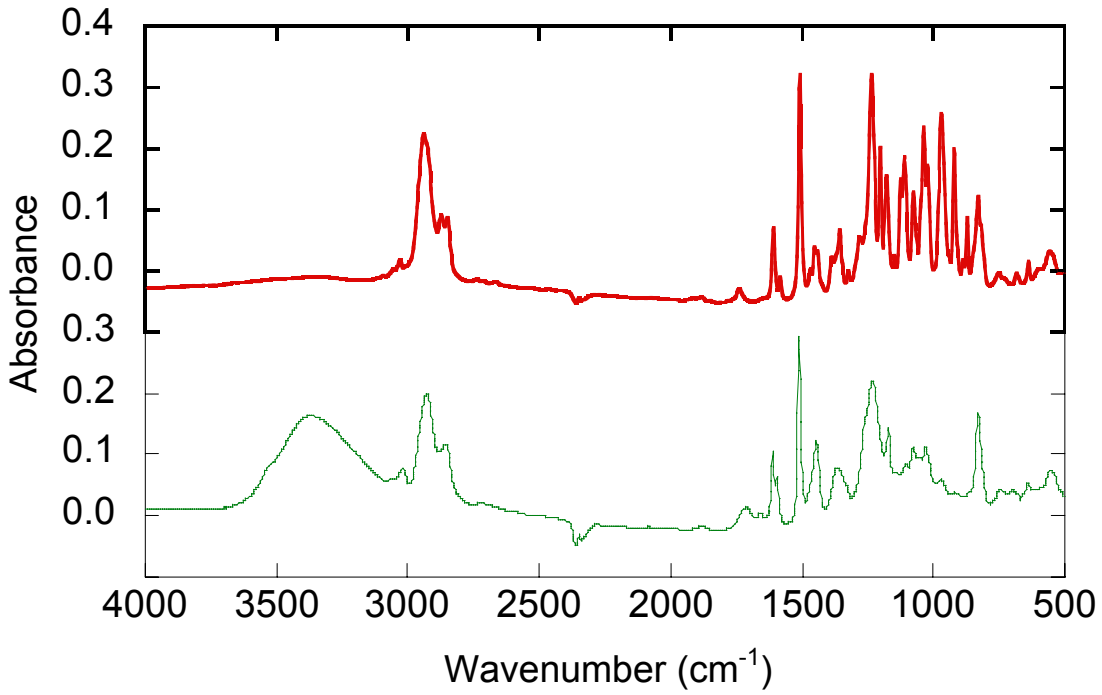

Figure 6.18 FTIR spectra of THP protected PHOST ■ post spin coat and ■ post PEB at 130 °C for 2 minutes.

As can be seen in Figures 6.16 and 6.17, the THP protecting group is not stable at room temperature in the presence of photoacid. In Figure 6.16, the THP protected film was exposed to several different exposure doses ranging from 0 to over 300 mJ/cm^2 over the course of 20 minutes. Significant deprotection is obviously occurring as indicated by the dramatic increase in the OH stretch from 3200 to 3500 cm^{-1}. It also would appear that the rate of deprotection may be dependent upon the quantity of photoacid present. Figure 6.17 takes another approach at examining the deprotection of THP. In this figure, the THP protected film was first exposed to 14 mJ/cm^2, and then FTIR scans were recorded at various times after this exposure as the sample sat at room temperature. As is easily observed from the OH stretch again, deprotection takes place over time in the presence of

a constant, reasonably small amount of photoacid. In fact, in the first 21 minutes, considerable deprotection has taken place. Thus, once again the THP appears to be quite unstable at room temperature in the presence of photoacid. More importantly, Figures 6.16 and 6.17 indicate that on the time scale involved with a Dill C measurement significant deprotection can take place at room temperature, adding a potentially confounding variable to the capacitance data analysis. Figure 6.18 provides the FTIR spectra of a THP protected film following a post exposure bake of 130°C for 2 minutes for comparison to the room temperature spectra. As in the room temperature spectra, the OH stretch changes dramatically with deprotection. However, it is interesting to note that the stretches near 921 and 969 cm^{-1} demonstrate a more dramatic decrease for the PEB processed film versus the room temperature films. It is thought that perhaps this difference is due to differences in the extent of deprotection that occur at PEB conditions versus room temperature.

Based upon the data collected via FTIR spectroscopy, it would appear that the THP protected PHOST polymer would not be an ideal subject for a Dill C measurement via IDE capacitance measurements. The deprotection that occurs immediately upon the generation of photoacid would cause changes in the chemical structure of the matrix polymer (and thus likely changes in the net k value of the polymer) leading to changes in measured capacitance that are difficult to deconvolute from the changes that are occurring due to photoacid production. More will be said regarding THP's effects upon IDE capacitance in the next section.

6.4.3 IDE Sensor Results for Protected PHOST Measurements

Having determined, as expected, that a high activation energy protecting group will remain stable at room temperature in the presence of photoacid and that a low activation energy group will become quite unstable and deprotect at room temperature, the next logical step was to see what effect this behavior would have upon the IDE electrical measurements.

A standard Dill C measurement routine was performed using IDEs coated with both the t-BOC and THP protected PHOST polymers. Dramatically different results were obtained. For the t-BOC protected polymer, normal capacitance behavior was observed. Following the post coat baseline capacitance measurement, this resist film was subjected to incremental doses of 248 nm radiation and capacitance measurements were recorded following each exposure dose to monitor the decomposition of the TPS-Tf PAG. Because this protecting group is stable and will not deprotect at room temperature, steady, unchanging capacitance values were observed following each exposure. Figure 6.19 below illustrates both the raw capacitance curves collected at various measurement frequencies, as well as the resulting model fits used to obtain Dill's C for the t-BOC system. As can be seen, normal capacitance versus exposure dose curves were obtained that were easily fit using the standard normalized Dill C analytical approach discussed in previous chapters. For this system, an average Dill C of 0.031 cm^2/mJ was measured with a 95% confidence interval of +/- 0.006.

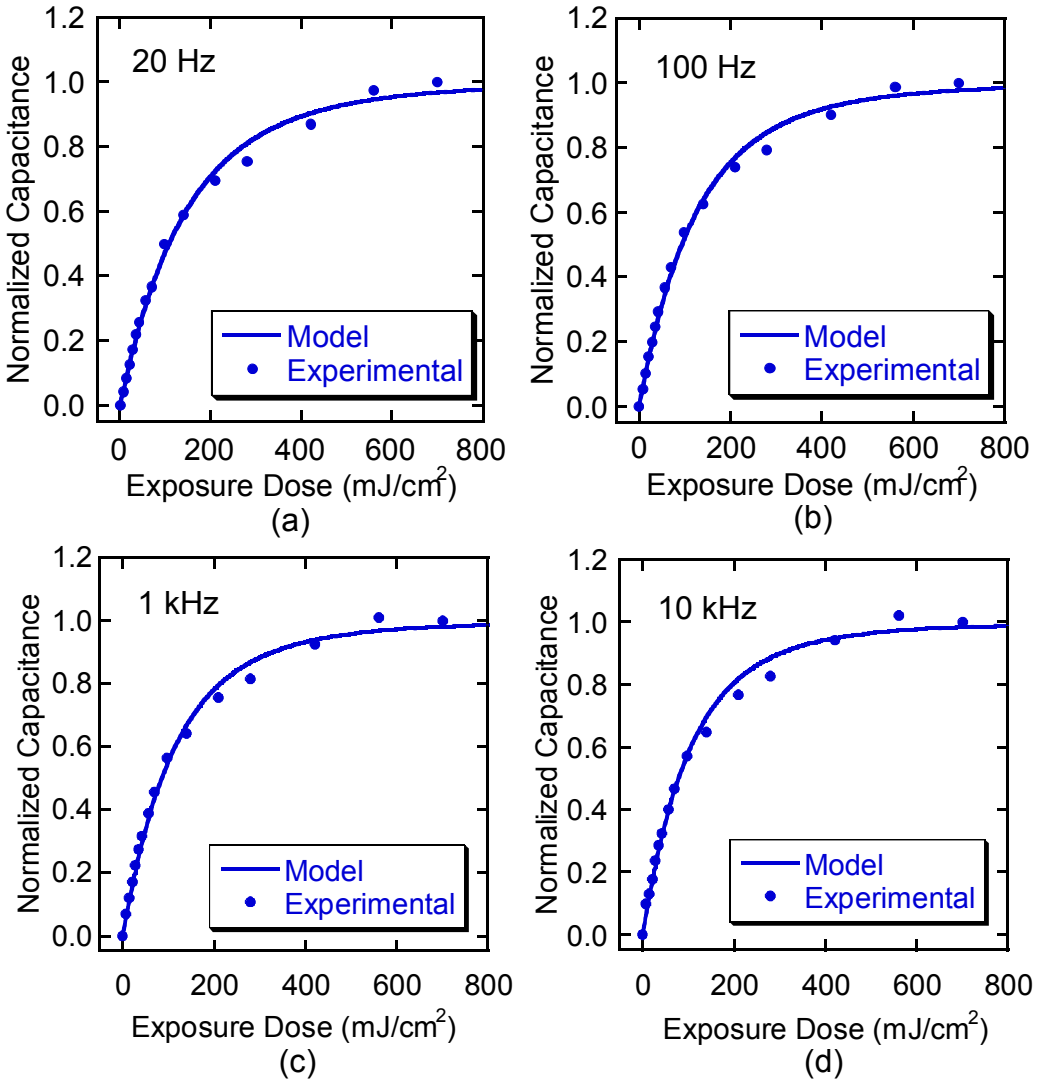

Figure 6.19 Capacitance versus exposure dose and model curve fits for TPS-Tf in a t-BOC protected PHOST film measured at (a) 20 Hz, (b) 100 Hz, (c) 1 kHz, and (d) 10 kHz.

The Dill C value of 0.031 cm^2/mJ is somewhat lower than that measured in the plain PHOST film of 0.045 cm^2/mJ. However, due to the presence of the protecting group, it is quite likely that the transfer mechanisms used to transfer exposure energy from the matrix to the PAG are somewhat different that those found in an unprotected matrix. The exact effect of this difference is unknown, but it could possibly be one reason for the lower Dill C value.

Unlike the t-BOC protected polymer, PAG decomposition in the THP protected PHOST film was not easily measured using the IDE sensors. Initially, a steady baseline capacitance value was measured prior to exposure. However, the capacitance values measured following exposure were less than desirable. Due to the deprotection that was occurring in the presence of the photoacid, a constantly changing capacitance value was observed following each exposure. This change was in the form of a slow, steady increase in the capacitance being measured. Essentially, the chemical changes that were occurring with the deprotection were resulting in a constantly changing baseline capacitance value. This constant change made it impossible to determine what capacitance change was the result of photoacid production and what capacitance could be attributed to the deprotection. Thus, it was impossible to attempt to create a model capacitance versus dose curve using the existing analytical approach, and the Dill C parameter for this system was not obtained.

It appears based upon the FTIR data presented earlier and the results of the capacitance measurements discussed here that a low activation energy protecting group presents a serious challenge to anyone wishing to measure PAG decomposition in such a

matrix using IDE sensors. In fact, measuring the Dill C parameter in such a matrix may prove to be one of the major limitations of using an IDE sensor measurement technique. Nevertheless, it is in theory still possible to measure such a system using IDE capacitance measurements. A new analytical technique would have to be developed that required significantly more experimental work. First, real time capacitance versus exposure dose measurements would have to be recorded. In the present form of the technique, the IDE's are exposed, and then subsequently measured. In order to measure a low activation energy matrix, the capacitance would have to be measured simultaneously with exposure dose so that there would be no time delay between exposure and measurement in which deprotection could take place. Second, detailed FTIR experiments would have to be performed to determine the precise kinetics of deprotection for any given loading of photoacid and measurement temperature. Detailed IDE measurements would then have to be performed to determine a mixing relationship between IDE capacitance and extent of deprotection. In addition, ellipsometry would have to be performed to determine the changes in film absorbance that result due to deprotection so that the proper exposure dose could be calculated versus depth within the film. Finally, once all of this information was obtained, the user would have to attempt to model the capacitance versus dose curve using a dynamic model that simultaneously accounts for: 1. the changes in deprotection rate that occur due to increasing acid production as well as increasing reaction time, 2. the changes in exposure dose received by the PAG molecules due to deprotection, 3. the change in baseline capacitance due to deprotection, and ultimately, 4. the change in capacitance due to the presence of photoacid. Needless to say, modeling such as system would be a challenging endeavor that opens up many potential sources of

experimental error and dramatically increase the experimental time and effort required to measure the Dill C parameter.

6.5 Conclusions and Recommendations

The work presented in this chapter was designed to demonstrate the versatility and applicability of the IDE sensor Dill C measurement technique to systems that more closely resemble true commercial resists. Specifically, it was designed to show that IDE capacitance measurements could be utilized in the presence of reactive matrices that contain acid labile protecting groups, as well as in the presence of base quenchers often used to minimize line width spread due to acid diffusion. A common base quencher used in commercial resists, 1,8-Diazabicyclo[5.4.0]undec-7-ene (1,5-5) (DBU), was added to a PHOST film loaded with TPS-Tf PAG and the results of this addition upon the measured IDE capacitance were observed. It was found that an initial lag, or even drop in capacitance was measured due to the neutralization of the photoacid that is initially produced upon exposure. An analytical approach was developed for dealing with such capacitance data that utilizes the normalization technique developed in Chapter 5 starting with an exposure dose immediately following the initial capacitance lag. A Dill C value of 0.031 cm^2/mJ was measured for the TPS-Tf PAG in the base loaded matrix. The ability to measure base loaded films provides an important advantage of the IDE based technique over the standard addition technique. The standard addition technique already requires base to be loaded into the film in order to measure C. Thus, determining the effect of a base quencher upon PAG kinetics is very difficult to do using this technique. In the IDE technique, due to its ability to measure C without requiring additives, it is

quite easy to compare the C parameter measured for a base loaded film to that measured in a plain matrix to determine the effects of a particular base quencher upon the C parameter for a PAG.

To understand the effects of using reactive matrices, protecting groups from two different classes of protecting groups were examined: a high activation energy group in the form of tert-butyloxycarbonyl and a low activation energy group in the form of tetrahydropyranyl. FTIR spectroscopy indicated that the t-BOC group was very stable at room temperature over long periods of time in the presence of large quantities of photoacid. In addition, the IR data also indicated that the THP group was highly unstable and deprotected quite easily at room temperature in the presence of photoacid. IDE sensor capacitance measurements further confirmed these results. Steady, unchanging capacitance values were obtained following exposure for the t-BOC protected system, indicating that the matrix was not changing and a steady, baseline chemical structure was present. A Dill C value of 0.031 cm^2/mJ was measured for a system composed of the t-BOC protected PHOST loaded with TPS-Tf PAG. The THP capacitance measurements, on the other hand, were found to constantly increase once photoacid was produced. This steady change made it impossible to measure the Dill C parameter for TPS-Tf in this system.

Based upon the results discussed in this chapter, the following recommendations are suggested for IDE Dill C measurements. First, in a base quencher loaded system, a standard normalized Dill C analytical technique should be utilized starting with the capacitance data and exposure dose immediately following the initial lag in capacitance that is observed. No other significant modifications are required to measure the C

parameter in a base loaded resist. Second, for Dill C measurements performed in a high activation energy protected matrix, a standard Dill C measurement technique can be utilized. The high activation energy reactive matrix should remain stable as photoacid is produced, and thus no new variables must be analyzed and no modifications to the existing technique are required. For low activation energy protected matrices, care must be taken to account for changing deprotection kinetics with increasing photoacid content, changing baseline capacitance due to deprotection, and changes in resist absorbance due to deprotection. Significantly more work is required to further investigate the potential use of IDEs to measure the C parameter in low activation energy systems.

CHAPTER 7

SUMMARY

7.1 Summary of Achievements

In the work presented in this thesis, a new technique for measuring photoacid generator (PAG) decomposition kinetics in chemically amplified photoresists (CARs) was developed. In this technique, capacitance measurements from photoresist coated interdigitated electrode (IDE) sensors are used as a means for monitoring the presence of photoacid within the resist's polymer matrix. The following bullets highlight the major accomplishments achieved during this work:

- A class 1000 "base free" cleanroom was constructed to provide a space for chemically amplified resist research.

- The spin coating characteristics of the IDE sensors were studied via SEM micrographs.

- The water sorption properties of novolac, PHOST, and HFAPNB were examined via quartz crystal microbalance techniques:
  - Diffusion coefficients of water in the polymers were calculated.
  - Equilibrium water content versus water partial pressure was measured.

- The effects of water content upon IDE capacitance measurements were examined.

- The basic IDE photoacid generation measurement procedure as well as the capacitance data analysis routine required to obtain Dill's C were developed:
  - IDE sensor sensitivity to photoacid was established

- An iterative approach to measuring Dill's C that requires fitting model capacitance versus dose curves to the experimental curves was developed.
- A linear mixing relationship was established between IDE capacitance and resist film contents.
- A multiple thin layer technique was developed for dealing with non-homogeneous photoacid distributions within the resist film.
- The effects of the exposure optical model upon the quality of model capacitance curves obtained was examined.

- The use of multiple measurement frequencies was examined as a potential tool for improving the capacitance response of the IDE sensor.

- A normalized capacitance expression and data analysis technique was derived that provides many advantages over the original technique.

- The effects of loading base quenchers into the resist matrix upon the IDE Dill C technique were examined.

- The effects of low and high activation energy protecting groups upon the IDE Dill C measurement technique were examined.

A short discussion of these accomplishments now follows.

7.2 Summary of IDE Technique and its Advantages

In the work presented in this thesis, a new technique for measuring photoacid generator (PAG) decomposition kinetics in chemically amplified photoresists (CARs) was developed. In this technique, capacitance measurements from photoresist coated interdigitated electrode (IDE) sensors are used as a means for monitoring the presence of photoacid within the resist's polymer matrix. Initially, the photoresist film of interest is spin coated onto the IDE sensor and a baseline capacitance measurement is recorded.

Following this initial measurement, the resist coated IDE is exposed to a small dose of UV light to decompose a small quantity of the PAG molecules. A second capacitance measurement is now recorded. Due to the presence of photoacid molecules within the polymer matrix following this exposure, the net dielectric constant of the photoresist film is now different than it was initially, leading to a change in the measured capacitance. The process of exposing the resist coated IDE to small doses of UV light and then measuring the IDE capacitance is repeated until no further change in capacitance is observed. This lack of change should indicate that essentially 100% of the initial PAG molecules have converted to their photoproducts. The raw capacitance versus exposure dose data collected during these measurements is then plotted and analyzed to determine the kinetic rate constant for PAG decomposition, otherwise known as the Dill C parameter. The analytical technique used to obtain the Dill C parameter involves creating model capacitance versus exposure dose curves and then fitting these model curves to the experimental curves using the Dill C parameter as the fitting function.

The use of electrical measurements from IDE sensors to measure PAG decomposition kinetics provides many advantages over previously used techniques. First, the IDE based technique is simple to perform and requires very little experimental time or raw materials. Previously used techniques, such as the standard addition technique or the absorbance/fluorescence based techniques, require lengthy experiments that involve significant amounts of wet chemistry as well as large volumes of materials. In the standard addition technique, multiple resist solutions must be formulated with varying amounts of base, and then each of these solutions must be spin coated onto a full size wafer, exposed, and developed in order to determine the dose to clear value. In the

absorbance/fluorescence based techniques, multiple resist solutions must again be formulated with additive molecules whose absorbance or fluorescence properties are pH sensitive. Then, in the solution based version of this method, the exposed films must be washed off of the wafers and collected in cuvettes for absorbance or fluorescence measurements. The experiments required for these two techniques require a large amount of time and effort! The IDE technique presented here requires only enough CAR resist solution to coat an area approximately 1 to 2 cm^2 in area. Then, following this coating, the only experimental work required is exposing the coated IDE and measuring its capacitance. A complete capacitance versus exposure dose experiment can be completed in 30 minutes, or often times less. In addition, because no wet chemistry is required, the IDE technique is very fab friendly, meaning the technique can easily be performed in a typical wafer fabrication facility using equipment that is typically already present.

The second advantage the IDE technique offers over previous methods is the non-invasive nature of the technique. In all of the previous techniques used to measure the Dill C parameter, some form of chemical indicator must be added to the resist solution. In the standard addition technique, this indicator is present in the form of the base that is added to neutralize photoacid. In the absorbance/fluorescence methods, chemicals whose absorbance or fluorescence properties change in the present of photoacid are added to the resist solutions. Adding such chemicals to the resist solutions introduces potentially complicating variables to the PAG kinetics analysis. Often times these chemicals alter the absorbance properties of the photoresist, meaning the exposure dose energy actually received by the PAG molecules may not be as perceived. In addition, adding such chemicals to the CAR solutions may also alter the ability of the polymer matrix to

transfer exposure energy from the matrix to the PAG molecules, or they may potentially participate in the reaction mechanism responsible for PAG decomposition. In the IDE based technique, no foreign chemicals are added to the resist film. Thus, the PAG decomposition observed through the IDE capacitance measurements is a more accurate representation of the PAG's ability to decompose in the polymer matrix being studied.

The third major advantage of the IDE technique over previous techniques is the ability of the IDE technique to measure the Dill C parameter for an unknown PAG in a resist solution whose composition is unknown. Previous techniques require specific knowledge of the amounts of PAG, base quencher, other indicator molecules, etc. in order to perform the technique to completion. Thanks to the ability of the IDE technique to utilize normalized capacitance data, this technique can be performed with no prior knowledge of the resist's composition. This is a key attribute for commercialization of this technique as often times the exact chemical composition of a commercial resist is a closely guarded secret.

Finally, the last advantage of the IDE technique is its ability to potentially characterize other aspects of the chemically amplified photoresist behavior. The work in this thesis discusses only measurement of the Dill C rate constant that describes PAG decomposition kinetics. As will be discussed in the future work section of this thesis, the IDE sensors can also potentially be used to study deprotection kinetics, photoacid diffusion, PAG/photoacid volatility, and even for characterizing CAR solution composition. This allows for the possibility of having a complete CAR characterization tool in the form of a tiny IDE sensor.

Four major areas of study were examined in this work and will be summarized in the next few paragraphs. First, external factors that could potentially introduce confounding variables into the IDE Dill C technique were examined. This area included looking at things such as resist water sorption, IDE spin coating capabilities, and environmental base contamination. Second, the development of the basic Dill C analytical routine was developed. This area focused on taking raw capacitance versus exposure dose data and using this data to produce an accurate Dill C parameter for PAG decomposition. The third area of work focused on improving upon the original IDE technique through the use of multiple frequency measurements and normalized capacitance data. Finally, the fourth area of work examined the applicability of the IDE technique to various situations that may be experienced with true commercial CAR solutions. In particular, the effects of base quenchers and protecting groups upon the technique were examined.

7.3 Study of Potentially Confounding Variables

Chapter 3 in this thesis presented the results of a study aimed at examining three potentially complicating issues associated with the IDE technique. First, ambient base contamination was addressed. It has long been known that base molecules found in the ambient environment can neutralized photoacid produced in a chemically amplified photoresist and cause problems with the quality of images produced through photolithography. Thus, to produce a suitable "base-free" environment to perform the IDE Dill C measurements, a 16' x 8' class 1000 cleanroom structure was erected and equipped with base filters to remove over 99.9% of the ambient base from the incoming

cleanroom air flow. A simple stability test was performed to determine that these filters were effective in removing the incoming base. Two wafers were spin coated with a chemically amplified photoresist and then their "dose to clear" value was measured after two different processing sequences: one wafer was immediately processed through the post exposure bake step following exposure while the second wafer was allowed to sit inside the room for over 1 hour following exposure prior to the post exposure bake, allowing this wafer to absorb any base present within the room. The dose to clear values measured for both wafers were identical, indicating that no significant quantities of base are present inside the cleanroom structure.

Once a "base-free" environment was established, the ability of the IDE sensors to be spin coated by a resist film was evaluated. Cross-section SEM micrographs of resist coated IDE's were taken to determine that three critical criteria were met by the spin coating process. First, the PHOST film used to coat the IDE filled the inter-finger spaces uniformly with no noticeable voids between the fingers. Second, the resist film surface over the IDE fingers was very planar, with very little or none of the underlying topography transferred to the film surface. This quality is important as it simplifies the calculations used to predict exposure intensity within the resist film. Finally, the film thickness over the IDE fingers was determined to be sufficient to capture essentially all of the fringe electric fields over the top of the fingers, simplifying the capacitance analysis required for calculating the Dill C parameter.

Finally, the last subject matter examined in this section of work was the ability of photoresist films to absorb water, how this ability changes with relative humidity, and what effect absorbed water has upon the IDE capacitance that is measured. The

relationship between environmental relative humidity and water uptake in three common resist polymers were studied using the frequency response of a quartz crystal microbalance: novolac, poly(p-hydroxystyrene), and bis-trifluoromethylcarbinol substituted poly(norbornene). All three polymer types exhibited linear relationships between water partial pressure in the ambient and total water uptake, and were found to be capable of absorbing significant quantities of water at saturation with PHOST absorbing the most at 9.8 wt%, 94,159 M_w HFAPNB at 7.7 wt%, 8,882 M_w HFAPNB at 5.6 wt%, 22,000 M_w novolac at 2.9 wt%, and 1,615 M_w novolac at 2.2 wt%. In addition, all three polymer types absorbed water rapidly with the majority of the water uptake occurring within the first few minutes of exposure to the saturated environment. Diffusion coefficients were estimated to be $1.8x10^{-9}$ cm^2/s for PHOST, $1.9x10^{-9}$ cm^2/s for the 94,159 M_w HFAPNB, $3.5x10^{-9}$ cm^2/s for the 8,882 M_w HFAPNB, $0.28x10^{-9}$ cm^2/s for the 22,000 M_w novolac, and $0.31x10^{-9}$ cm^2/s for the 1,615 M_w novolac. The effect of water partial pressure (i.e. relative humidity) upon the IDE capacitance measurements was also determined for the same three polymer types. Once again, linear relationships were observed between water partial pressure and the capacitance measured from the IDE sensors. Water absorbed into the resist film coating the IDE sensor greatly influences the net dielectric constant of the resist film, as shown by tremendous changes in measured IDE capacitance. The PHOST coated IDE's capacitance varied from 9 nF to over 16 nF from 0 to 100% relative humidity. Likewise, the HFAPNB coated sensor vaired from 6.8 nF to near 10 nF and the novolac coated sensor varied from 7.6 nF to over 8 nF. Finally, a common power law mixing rule was used to model the effects of resist film water content upon the net dielectric constant of the resist films.

Based upon the results obtained from the work summarized in this section and discussed in detail in Chapter 3, it can be concluded that of the three potentially confounding external variables studied, water sorption is potentially the most damaging. The effects of ambient base contamination have been essentially eliminated through the construction of a "base-free" cleanroom, while the IDE sensors were proven easily capable of being spin coated with uniform resist films. Relative humidity, on the other hand, cannot be completely eliminated from consideration. Relative humidity is known to vary considerably from day to day, and even hour to hour in certain locations of the world. Thus, anyone using IDE sensors for Dill C measurements must be mindful of the potential for relative humidity to skew capacitance measurements being recorded. The effects of water sorption can be minimized by performing all experiments in a short time period to minimize any fluctuations in environmental relative humidity. In addition, the normalization technique discussed in Chapter 5 can be utilized to eliminate any baseline capacitance fluctuations due to water sorption.

7.4 Development of the Basic Dill C Measurement Routine

The next major area of work discussed in this thesis focused on the development of the analytical routine that is used to calculate the Dill C parameter from the raw capacitance versus exposure dose data that is recorded from the IDE sensors. This work, presented in Chapter 4, addressed five main topics: IDE sensitivity to photoacid, creation of a calculation algorithm, developing a mixing relationship between capacitance and photoacid content, working with non-homogeneous photoacid distributions, and selecting the appropriate optical model for use in predicting exposure intensity throughout the

resist film. For the work discussed in Chapter 4 a model chemically amplified resist system composed of triphenylsulfonium triflate PAG mixed in a poly(p-hydroxystyrene) matrix was used.

The IDE sensors were proven to be extremely sensitive and quite capable of detecting the presence of photoacid with a capacitance change of over 50% of the baseline value in response to the generation of 4.56 wt% TPS-Tf PAG photoproducts. Using varying loadings of PAG (and hence photoacid after exposure), a linear capacitance mixing relationship was then developed that allows the IDE user to determine the amount of PAG and photoacid within the resist film based upon the capacitance that is measured from the IDE sensor. This linear mixing relationship made it possible to then develop the actual algorithm to be used in the Dill C calculation.

The algorithm is centered upon the premise of attempting to create model capacitance versus exposure dose curves and then fitting the model curves to the experimentally obtained curves using the Dill C parameter as the sole fitting function. Initially, a Dill C parameter is selected. Next, photoacid and PAG concentrations within the resist film are calculated using first order exposure kinetics and an appropriate optical model for the exposure intensity. Then, the linear capacitance mixing relationship is utilized to determine the capacitance that should be measured from the IDE sensor based upon the concentration values. After an entire capacitance versus exposure dose curve is generated using this approach, the model curve is compared to the experimental curve using an appropriate measure of fit, such as sum squared error (SSE). If the model curve is not a good match, a new Dill C is selected and a new model curve is generated. This process is repeated in an iterative fashion until the SSE value is minimized.

To properly use the analytical approach discussed above, two further areas of investigation were required. First, due to optical phenomena such as absorbance, standing waves, etc., a wide range of exposure intensities are experienced throughout the resist film. Thus, concentration gradients are formed. To deal with these gradients, a multi-layered approach was developed. In this approach, the resist film and the IDE fingers are divided into many very thin layers. The exposure intensity, PAG/photoacid concentrations, and capacitance contribution are calculated for each tiny layer, and then summed together appropriately to determine the overall output from the IDE sensor. Finally, in order to calculate the proper exposure intensity at each point within the resist film thickness, the appropriate exposure intensity model must be determined for a resist coated IDE sensor on a silicon dioxide substrate. It was determined through the case study of TPS-Tf in PHOST that a comprehensive intensity model that calculates standing wave intensities for each of the exposure wavelengths that are passed through the band pass 248 nm filter used for our exposures must be used. Each of these standing waves is appropriately weighted based on the particular wavelength's contribution to the total transmission spectrum and then summed together to determine the true intensity spectrum. TPS-Tf was found to have a Dill C of 0.045 cm^2/mJ at 248 nm wavelength in a PHOST matrix, which is in excellent agreement with values reported in the literature using other Dill C measurement techniques.

7.5 Improved IDE Dill C Measurements

Once the basic Dill C measurement routine was established, the third major area of work performed focused on improving this technique. Two major improvements were

achieved. First, the IDE sensitivity to PAG decomposition was increased through the use of multi-frequency measurements. In the original work used to develop the basic measurement routine a measurement frequency of 1 kHz was used only. For some PAGs measured later, smaller changes in capacitance that were more difficult to interpret were observed at this measurement frequency. It was shown in Chapter 5 that by using a range of measurement frequencies (in this case from 20 Hz up to 100 kHz) it is possible to increase (using lower frequencies) or decrease (using higher frequencies) the capacitance value measured from the IDE sensors due to the frequency dependence of the film's net dielectric constant. In addition, it was shown that the Dill C values calculated from capacitance measurements recorded at different frequencies were statistically the same. Thus, using multiple measurement frequencies is an acceptable tool for increasing IDE sensitivity.

The second improvement discussed in Chapter 5 was the development of a normalization scheme. Starting with the linear mixing relationships between IDE capacitance and resist film contents, a normalized capacitance expression that is equivalent to the normalized photoacid concentration within the resist was derived that can be used to calculate the Dill C parameter. Using this normalized expression offers many advantages over the original form of the technique. First, the normalized expression eliminates the need to measure the linear mixing relationships. Thus, the amount of time and raw materials required are greatly diminished. Second, by eliminating the need for the linear mixing relationships, improved curve fitting and Dill C accuracy is attained. Third, because the capacitance is normalized, shifts in baseline capacitance due to environmental changes, or due to IDE variations from sensor to sensor

no longer influence the ability of the IDE user to create model curves that properly fit the experimental curves. Finally (and perhaps most importantly), the use of normalized capacitance permits the measurement of PAG decomposition kinetics in resists of unknown composition.

It was shown through data collected for triphenylsulfonium triflate (TPS-Tf), triphenylsulfonium perfluoro-1-butanesulfonate (TPS-Nf), bis(4-tert-butylphenyl)iodonium triflate (TBI-Tf), bis(4-tert-butylphenyl)iodonium perfluoro-1-butanesulfonate (TBI-Nf), and N-hydroxy-5-norbornene-2,3-dicarboximide perfluoro-1-butanesulfonate (HND-Nf) that improved curve fits were obtained. In addition, by comparing data collected for these PAGs using both the original form of the technique as well as the normalized technique, it was shown that both techniques predict the same behavior and result in the same Dill C values. A 248 nm Dill C value of 0.046 cm^2/mJ was found for TPS-Tf in PHOST, 0.040 cm^2/mJ for TPS-Nf in PHOST, 0.055 cm^2/mJ for TBI-Tf in PHOST, 0.056 cm^2/mJ for TBI-Nf in PHOST, and 0.018 cm^2/mJ for HND-Nf in PHOST using the normalized technique.

7.6 Applicability of the IDE Technique to Commercial Resist Systems

The last major area of work discussed in this thesis focuses on the use of the IDE Dill C technique to measure PAG decomposition kinetics in resist systems that more closely resemble true commercial resists. In particular, two major studies were performed. First, the effects of an added base quencher (1,8-diazabicyclo[5.4.0]undec-7-ene (DBU)) upon the capacitance response of the resist coated IDE was examined. An initial lag in the capacitance response of the DBU loaded film was observed for the first

30 mJ/cm^2 of exposure. This lag is believed to be due to the neutralization of the generated photoacid by the DBU base quencher molecules. A means for analyzing this capacitance data using the normalized capacitance expression was discussed. It was shown that by starting with an exposure dose following the initial capacitance lag, and adjusting all exposure doses accordingly, it is possible to still obtain the Dill C parameter with the standard measurement procedure. A C value of 0.031 cm^2/mJ was obtained for TPS-Tf in PHOST loaded with DBU.

The second area of work presented in Chapter 6 focused upon the effects of protecting groups on the capacitance response measured using IDE sensors. A high activation energy protecting group (tert-butyloxycarbonyl (t-BOC)) and a low activation energy group (tetrahydropyranyl (THP)) were studied using the IDE technique. FTIR spectroscopy proved that the t-BOC protected PHOST film was quite stable at room temperature in the presence of photoacid while the THP protected PHOST was just the opposite. Significant deprotection of the THP protected polymer occurred at room temperature in the presence of triflic acid generated from the TPS-Tf PAG as indicated by a large increase in the size of the OH peak present in the FTIR spectrum. IDE sensor measurements confirmed these results. The low activation energy THP protected PHOST was very unstable with capacitance measurements demonstrating a steady increase as deprotection was occurring, making it impossible to measure the Dill C parameter from the data collected with such a system using the current analytical technique. The t-BOC protected PHOST sample was quite stable with steady capacitance values following each exposure. Using the capacitance data collected for the t-BOC protected sample, a Dill C of 0.031 cm^2/mJ was measured for TPS-Tf in the t-BOC protected PHOST matrix.

CHAPTER 8

RECOMMENDATIONS FOR FUTURE WORK

8.1 Improvements and Revisions to the Existing Technique

Despite the successes the IDE Dill C measurement technique has had in measuring PAG decomposition kinetics, there still remain several areas of future work that should be performed in order to further refine this technique and allow for even better measurements of a PAG's Dill C parameter. The suggestions discussed in this section focus on items that should be performed in order to improve the measurement of photoacid generation kinetics. In following sections, suggestions for work designed at probing other potential uses of IDE sensors will be discussed. The following recommendations for future work are suggested:

[1] All of the experimental work presented thus far has utilized a poly(p-hydroxystyrene) (PHOST) matrix that is loaded with one of several different PAGs. The primary purpose for using this matrix material has been the compatibility of this matrix polymer's absorbance with 248 nm wavelength exposures, and the fact that PHOST is readily available in our laboratory. In general, there is no reason why any number of polymer films could not serve as a matrix material for a PAG decomposition study. The matrix polymer simply has to remain inert to the particular exposure source so that a steady baseline capacitance is obtained. This concept should be tested by measuring PAG decomposition in several other common resist polymer matrices. Suggested resist polymers include novolac (a common 365 nm resist

polymer), poly(methyl methacrylate) (a common e-beam resist and 193 nm resist), and a fluorinated norbornene polymer, such as bis-trifluoromethylcarbinol substituted poly(norbornene) (a potential 157 nm resist). This study will prove the versatility of the IDE technique, as well as allow for the understanding of the matrix polymer's affect upon PAG decomposition for a common PAG.

[2] Along similar lines, additional PAGs other than those measured here should be studied. Five different PAGs are mentioned throughout this thesis: two sulfonium salt ionic PAGs, two iodonium salt ionic PAGs, and one non-ionic norbornene-based PAG. The range of PAGs studied in this thesis was intentionally limited to the more commonly used PAG molecules due to a limited number of IDE sensors available for experiments. In reality, countless photoacid generators, both ionic and non-ionic can be used in a chemically amplified photoresist. In addition, interest in polymeric PAGs that are actually bound to the resist matrix polymer has recently surfaced. A wider survey of PAG performance and compatibility with the IDE capacitance-based Dill C measurement technique should be performed to further test the bounds of the IDE sensors.

[3] All Dill C rate constants measured in this thesis were measured for PAG photolysis during 248 nm wavelength (or Deep UV) exposures. Recently, the semiconductor industry transitioned into 193 nm wavelength exposure sources, and in future years will likely move on to other wavelength exposure

sources as well. In order for the IDE Dill C technique to be useful, it must be shown that the IDE sensors can be used for PAG decomposition studies at these other exposure wavelengths, and that the increased energy contained in such exposures will not cause unwanted side effects in terms of sensor performance. Thus, it is suggested that IDE Dill C measurements be conducted using exposure sources other than 248 nm. In particular, 193 nm and 157 nm wavelength exposure sources should be tested as 193 nm sources are the current production tools and 157 nm sources are a potential candidate for next generation lithography exposure sources. 365 nm (i-line) exposure should probably also be studied as i-line exposures are still used from time to time for special applications. In addition to proving the versatility of the IDE sensors, this exposure source study will also allow for a comparison of PAG performance at multiple wavelengths.

[4] Building upon the protecting group work presented in Chapter 6 of this thesis, more work should be done with low activation energy protecting groups. It was shown in Chapter 6 that a low activation energy protecting group presents a unique challenge to anyone who wishes to monitor PAG decomposition in such a protected matrix. Room temperature deprotection can cause changes in the films baseline dielectric constant leading to a capacitance response that is very difficult to interpret. The analytical technique and experimental work that would be required to interpret capacitance data for such a protecting group were discussed in Chapter 6, but not actually performed. It is suggested that a set of experiments be

performed to determine if it truly is feasible to measure the Dill C parameter in a low activation energy reactive matrix. This experiment would entail performing detailed studies of deprotection kinetics versus temperature using FTIR spectroscopy. In addition, mixing relationships between IDE capacitance and degree of deprotection would have to be measured. Modifications to the exposure tool also need to be performed to allow for real time measurement of IDE capacitance during exposure. These exposure tool modifications may actually make it possible to perform a set of capacitance versus dose measurements quickly enough that the slow deprotection of a low activation energy system would not significantly affect the shape of the capacitance curve. This would be a very challenging set of experiments, but if successful, this particular suggested work item would add significantly to the IDE sensors usefulness as a resist characterization tool.

[5] The next suggested area of future work relates to the thin film approximations discussed in Chapter 4. In particular, the method use for dealing with the top fringe fields' capacitance contribution needs to be further refined. At this time, an area weighted average concentration and capacitance value is utilized for this region due to the curved shape of the fringe electric fields. This curved shape means that the electric fields are influenced by many different PAG/acid concentrations that vary spatially within the resist. The multiple thin layer approximation used for the inter-electrode finger spaces is not sufficient for this region. Finite element analysis should be performed to determine if the averaging technique utilized here is sufficient, or if a more

rigorous analytical technique must be used. Conformal mapping equations are one likely candidate for a means of more rigorously calculating the top fringe field's capacitance contribution to the net IDE capacitance.

[6] Continued work with base quenchers is also suggested. It was mentioned in Chapter 6 that the C parameter measured for TPS-Tf in a base loaded PHOST film was quite a bit lower than that measured in a plain PHOST matrix. It was suggested that perhaps the base quencher is responsible for this decrease, and that perhaps the base participates in the complex chemistry that takes place during PAG decomposition. No further investigation of this phenomenon was made due to a limited number of IDE sensors. To further explore this area, and to prove if base is truly the culprit for the lower C values, experiments that examine the effects of base loading upon the C parameter should be conducted. If the base is truly affecting C, then the response of C should scale with base loading. Likewise, the C parameter for other PAGs should be measured in the presence of base in order to see if their C values show a similar decrease in the presence of base.

8.2 Other Potential Resist Characterization Applications for IDE Sensors

The suggested future work discussed in the previous section centered upon work that could potentially improve, or increase the knowledge base associated with measuring photoacid generator decomposition kinetics via the IDE sensors. These sensors have been proven quite capable of measuring PAG decomposition. There are, however, many

other potential uses of these sensors as chemically amplified photoresist characterization tools. The following future work items are suggested to investigate some of these potential applications:

[1] Knowledge of the volatility of PAG/photoacid in CAR matrices is often an important piece of information in terms of understanding a CAR's performance. Many PAGs and/or photoacid molecules are volatile enough that significant quantities of the material diffuse out of the resist matrix during either the post apply bake, or during the post exposure bake process. With CAR deprotection performance so heavily dependent upon the photoacid that is present in the matrix, it is important that precise knowledge of the amount of photoacid present within the resist be obtained. This is especially important for CAR simulation applications. In Chapter 3 it was demonstrated that the polymer coated IDE sensors were capable of monitoring water entering and leaving the polymer matrix due to changes in the net k of the polymer. Similar IDE capacitance studies should be performed with photoacid to determine if the IDE sensors can monitor photoacid diffusion out of the resist matrix during a bake sequence. The studies should be performed in a dry environment to minimize the effects of water sorption and desorption. It should in theory be possible to accurately monitor how much photoacid has left the resist matrix for a given bake process based on the capacitance changes that occur as the sensor is baked. Thus, the data collected here could

be used to develop relationships that describe photoacid volatility and film content as a function of resist bake time and temperature.

[2] In Chapter 6, the effects of deprotection upon IDE capacitance measurements were discussed. It was mentioned that as a protecting group was removed from the matrix, the net dielectric constant of the polymer changed and was reflected in a change in the measured IDE capacitance. In terms of measuring the Dill C parameter, this change in capacitance is unwanted. However, this capacitance response could potentially be exploited for positive purposes. If a constant, known quantity of photoacid was generated, and then the protected resist was no longer subjected to any exposures, it should be possible to study deprotection kinetics using the IDE capacitance measurements. Detailed studies of the t-BOC (or other) protecting group should be performed to determine the feasibility of using the IDE sensors as deprotection characterization tools. Experiments should be performed in conjunction with FTIR spectroscopy to determine a relationship between extent of deprotection and IDE capacitance, so that one can observe capacitance and know exactly how much deprotection has occurred. Then, real time capacitance measurements can be performed as the resist film is baked at various temperatures. The capacitance versus time data can be converted to deprotection versus time to yield kinetics information.

[3] The potential for using IDE sensor structures for in-situ process monitoring should be investigated. Once a CAR film is characterized, precise knowledge

of the expected capacitance response for a given exposure dose is available. The IDE sensors could then be used in a reverse role as an in-situ performance monitor for lithography tools. IDE structures could easily be fabricated onto a pilot wafer that often accompanies production lots in a fabrication facility. As this pilot wafer is processed through a lithography stepper tool and exposed, the capacitance could easily be measured in-line and used to determine the exact exposure dose the film received. In addition, multiple sensors could be spread out over the pilot wafer's surface to investigate the uniformity of the exposure. The in-situ capacitance measurements could serve many purposes including stepper performance monitor and exposure source lifetime monitor. In addition, the in-line measurements could be fed forward to other automated processes to allow for in-line adjustments to be made (such as developer conditions, bake conditions, etc.)

8.3 IDEs for Measuring Photoacid Diffusivity

As one last recommended item of future work, the use of IDE sensors and impedance spectroscopy (IS) as a means for measuring photoacid diffusion coefficients should be investigated. As integrated circuit features have continuously shrunk in size, the impact of photoacid diffusion upon the quality of printed features has continuously increased. This concept was discussed in detail in Chapter 6 section 1.2 and shown in Figure 6.2. As the photoacid diffuses outside of the initially exposed region, it deprotects the matrix polymer as it travels resulting in an unwanted widening of the developed region. Because photoacid diffusion can potentially have such a significant impact upon

CAR performance, a great deal of effort has been poured into developing ways to measure the diffusion coefficient of photoacid molecules in resist matrices[126,127,129-138]. If the IDE sensors used in this thesis for Dill C measurements could be used to also measure photoacid diffusion coefficients, then a complete, all-in-one CAR characterization tool could be realized.

Fedynyshyn and coworkers[131], Itani and coworkers[132-135], and Nakamura and coworkers[136], have previously demonstrated that it may be possible to measure the diffusion coefficient of a photoacid through the use of the Nernst-Einstein equation and knowledge of the resist film's ionic conductivity. It should, in theory, be possible to utilize impedance spectroscopy[139-144] of the resist coated IDE structures used here for Dill C measurements to measure the resist film's ionic conductivity and therefore obtain the photoacid diffusion coefficient from the Nernst-Einstein equation shown below[131-136,141].

$$D = \frac{\sigma \cdot k \cdot T}{[H^+] \cdot q^2} \qquad [8.1]$$

Here, D is the diffusion coefficient of the ionic species of interest, σ is the ionic conductivity, k is the Boltzman constant, T is the measurement temperature, $[H^+]$ is the acid concentration, and q is the ionic charge of the diffusing species.

Impedance spectroscopy (IS) has often been used as a means for understanding the behavior of ionic species in a variety of media. Situations where IS has been employed have included measuring the conductive properties of lithium ions in battery or fuel cell electrolytes[140,143,144], measuring corrosion rates of a variety of substrates[139], and understanding the behavior of various salts in soil or concrete[142]. IS can be used in a

similar manner with the IDE structures used in this work to measure the ionic conductivity of the acid loaded CAR film. The PAG loaded CAR film can be exposed to generate a known quantity of photoacid within the matrix polymer. Then, the impedance modulus |Z| and phase angle φ of the resist coated IDE sensor are measured over a wide range of frequencies with a constant AC signal amplitude[139]. The impedance modulus and phase angle data can then be used to generate Nyquist plots of the real and imaginary impedance components. From the shape of the Nyquist plots, the ionic conductivity of the resist film can be determined for use in calculating the photoacid diffusion coefficient in equation 8.1[139-144].

This basic methodology has already been put to the test for a simple system consisting of TPS-Tf PAG loaded into a PHOST matrix. Three samples with different loadings of TPS-Tf were flood exposed for an extended period of time to fully convert the PAG to photoacid and then impedance spectroscopy scans from 20 Hz to 1 MHz were performed to measure the ionic conductivity of the films. The resulting Nyquist plots obtained from this preliminary work are shown below in Figure 8.1.

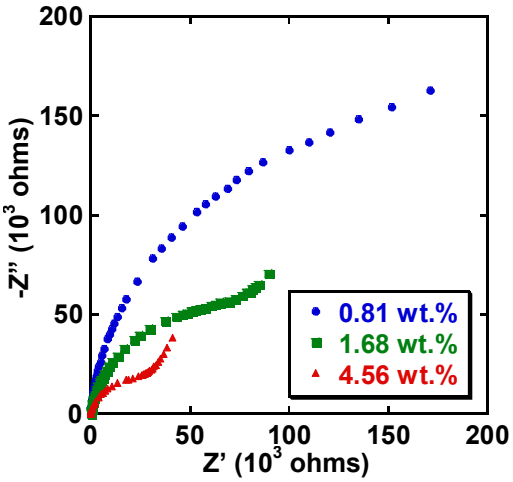

Figure 8.1 Nyquist plots resulting from impedance spectroscopy scans of TPS-Tf loaded PHOST films.

The initial semicircle shaped portion of the Nyquist plots shown in Figure 8.1 was used to obtain the ionic conductivity of the acid loaded PHOST film, which was subsequently used in equation 8.1 to calculate the photoacid diffusion coefficient. Essentially, if the initial semicircle is extended down to the Z' axis, the diameter of this semicircle corresponds to the resist film's bulk resistance, which can be used to obtain conductivity[139-144]. As shown in Figure 8.1 by the diameters of these semicircles, as acid loading increased, the film resistance decreased (the semicircle diameters shrank). This trend makes perfect sense, as the increased presence of photoacid enables better charge transport from one electrode finger to another.

To determine the best estimate of the resistance values for each resist film, the raw impedance data was fit to an equivalent circuit using LEVM complex nonlinear least

squares (CNLS) curve fitting software[145]. The equivalent circuit used to fit the TPS-Tf impedance curves presented here is displayed in Figure 8.2 below.

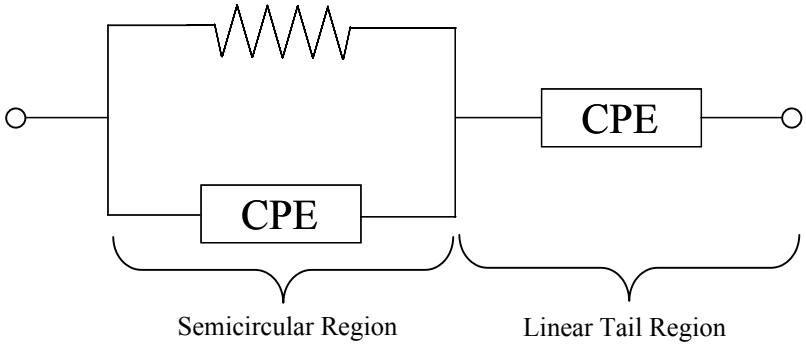

Figure 8.2 Equivalent circuit utilized for fitting experimental impedance curves with LEVM software.

As shown in Figure 8.2, the equivalent circuit used to fit the data using LEVM consisted of a resistor in parallel to a constant phase element (CPE) (providing the high frequency semicircle) all in series with another CPE (providing the low frequency linear tail). In a perfect case, the semicircular portion of the impedance data would be described by a resistor parallel to a capacitor, yielding a perfect semicircle with its center residing upon the x axis. Unfortunately, such perfect scenarios are rarely encountered in impedance studies. Typically, the semicircles measured have their centers displaced below the x axis, possibly due to the presence of a distribution of dielectric relaxation times centered around a mean value, as opposed to a single relaxation time for the material being studied[139]. The impedance curves collected for TPS-Tf were no exception. To account for the center displacement, a constant phase element is used in parallel with a resistor, rather than a capacitor. For a more thorough discussion of impedance data analysis,

equivalent circuit fitting, and constant phase elements, the reader is strongly encouraged to consult the impedance text by Macdonald[139].

Using the equivalent circuit shown in Figure 8.2 and the LEVM software, estimates for the resistance of the TPS-Tf loaded films whose impedance curves are displayed in Figure 8.1 were obtained. Resistance values of 2.07×10^5, 8.32×10^4, and 2.54×10^4 ohms were obtained for the 0.81, 1.68, and 4.56 wt% TPS-Tf films respectively at 23ºC and 24% relative humidity. Using the ionic conductivity values calculated from these resistance numbers, an average diffusion coefficient of 4.3×10^{-12} cm^2/s was calculated for triflic acid in PHOST at room temperature.

Unfortunately, this D value is far too large to be in agreement with values measured for triflic acid in PHOST at room temperature using other techniques[126,129,130]. It is believed that water absorbed into the resist film due to relative humidity plays a large role in the proton conduction mechanism and may be causing the measured D values to be too large. To test this hypothesis, a resist coated IDE was placed in the environmental chamber used to perform the relative humidity tests discussed in Chapter 3 and exposed to various relative humidity values as impedance scans were performed. Figure 8.3 below demonstrates the impact relative humidity (and hence film water content) can have upon the ionic conductivity of the resist film.

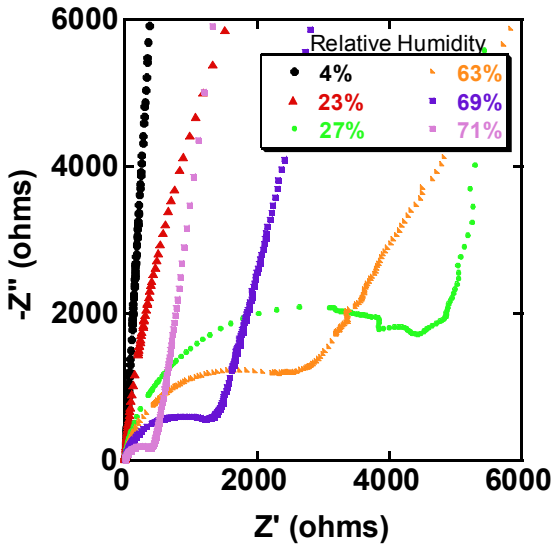

Figure 8.3 The effects of relative humidity upon the impedance scans obtained for TPS-Tf loaded PHOST.

Obviously, the water content of the film can lead to dramatically different values of ionic conductivity for the film, which can lead to large differences in the diffusion coefficient measured for photoacid at one relative humidity versus another. As relative humidity increased, the diameter of the semicircle shrank, indicating that the resistance of the resist film was also shrinking, or that the ionic conductivity of the resist film was increasing. Based on this dramatic dependence upon relative humidity (and armed with knowledge of resist water sorption capabilities discussed in Chapter 3), it is believed at this time that the water contained in the film facilitates proton conduction from one electrode finger to another, increasing the perceived diffusion coefficient calculated through the Nernst-Einstein equation. However, it is not presently clear exactly what the nature of the relationship between the sorbed water and photoacid is that causes the increase in

conductivity. More work needs to be performed to determine the exact nature of this relationship before an accurate photoacid diffusion coefficient can be obtained. Based on the preliminary findings shown here, the following future work is suggested for investigating the use of IDEs as photoacid diffusion coefficient measurement tools:

[1] Determine the true nature of the proton conduction mechanism in a water containing CAR film so that a better understanding of the origins of the ionic conductivity values measured from such a film can be had. This study will likely involve performing multiple impedance scans over a wide range of relative humidity values so that a solid relationship can be established between relative humidity, or water partial pressure and measured film resistance. This relationship can then be used to extrapolate back to a resist film with zero water content so that one can see the calculated diffusion coefficient of the photoacid without the aid of any water. A new impedance meter will likely need to be purchased as the film impedance is too large at very low humidities for our current instrument to make reliable measurements.

[2] Once the conduction mechanism is better understood, determine the appropriate conductivity value (i.e. conductivity for a wet film, dry film, or intermediate) to use for calculating the photoacid diffusion coefficient. In production photoresist films, it is quite likely that a small quantity of water exists in the resist films utilized. Thus, it may be necessary to intentionally

measure resist film's exposed to a specific relative humidity in order to obtain an accurate diffusion coefficient.

[3] Investigate the use of IDE sensors to measure diffusion coefficients at elevated temperatures, where due to increased polymer chain mobility, the photoacid becomes very mobile. The room temperature measurements conducted thus far are suitable for establishing the impedance technique as a viable option for measuring diffusion coefficients, however it is during the post exposure bake at elevated temperatures where the photoacid can seriously degrade resist performance.

[4] Benchmark the diffusion coefficients for specific photoacids obtained using the IDE sensor technique against those obtained using more traditional techniques.

BIBLIOGRAPHY

[1] Shockley W, *The path to the conception of the junction transistor,* IEEE Trans. Elec. Devices **ED-23(7)**, 597 – 620, 1976.

[2] Bardeen J, Brattain W, *The Transistor, A Semi-Conductor Triode,* Phys. Rev. **74**, 230 - 231, 1948.

[3] Brattain W, Bardeen J, *Nature of the Forward Current in Germanium Point Contacts* Phys. Rev. **74**, 231 – 232, 1948.

[4] Reid T, *The Chip: How Two Americans Invented the Microchip and Launched a Revolution*, Simon and Schuster, New York, 1984.

[5] Thompson L, Willson C, Bowden M, *Introduction to Microlithography, 2nd edition*, American Chemical Society, Washington DC, 1994.

[6] *International Technology Roadmap for Semiconductors,* Executive Summary, 2003.

[7] Semiconductor Industry Association (SIA) Fact Sheet http://www.semichips.org/pre_facts.cfm

[8] R. Jaeger, *Introduction to Microelectronic Fabrication*, Addison-Wesley Publishing, Reading, Mass., 1993.

[9] Willson C, Dammel R, Reiser A, *Photoresist Materials: A Historical Perspective*, Proceedings of SPIE, **3049**, 28 – 41, 1997.

[10] Reichmanis E, Thompson L, *Polymer Materials for Microlithography*, Chem. Rev., **89**, 1273 – 1289, 1989.

[11] MacDonald S, Willson C, Frechet J, *Chemical Amplification in High-Resolution Imaging Systems*, Acc. Chem. Res., **27(6)**, 151 – 158, 1994.

[12] Smith G, Bonham J, U.S. Patent 3,779,778, 1973.

[13] *International Technology Roadmap for Semiconductors,* 2003.

[14] Henderson C, *Advances in Photoresist Characterization and Lithography Simulation,* PhD Dissertation, 1998.

[15] Crivello J, Dietliker K, *Photoinitiators for Free Radical Cationic & Anionic Photopolymerisation, 2nd ed*., John Wiley and Son, New York, 1998.

[16] Dektar J, Hacker N, *Photochemistry of Triarylsulfonium Salts,* J. Am. Chem. Soc., **112**, 6004 – 6015, 1990.

[17] Dektar J, Hacker N, *Photochemistry of Diaryliodonium Salts,* J. Org. Chem., **55**, 639 – 647, 1990.

[18] Petersen J, Mack C, Thackeray J, Sinta R, Fedynyshyn T, Mori T, Byers J, Miller D, *Characterization and Modeling of a Positive Acting Chemically Amplified Resist,* Proc. SPIE, **2438**, 153 – 165, 1995.

[19] Pawloski A, Nealey P, *A Standard Addition Technique to Quantify Photoacid Generation in Chemically Amplified Photoresist,* Chem. Mater., **13**, 4154 – 4162, 2001.

[20] Croffie E, Yuan L, Cheng M, Neureuther A, Houlihan F, Cirelli R, Watson P, Nalamasu O, Gabor A, *Modeling influence of structural changes in photoacid generators on 193 nm single layer resist imaging,* J. Vac. Sci. Technol. B, **18(6)**, 3340 – 3344, 2000.

[21] Szmanda C, Kavanaugh R, Bohland J, Cameron J, Trefonas P, Blacksmith R, *A Simple Method for Measuring Acid Generation Quantum Efficiency at 193nm,* Proc. SPIE, **3678**, 857 – 866, 1999.

[22] Szmanda C, Brainard R, Mackevich J, Awaji A, Tanaka T, Yamada Y, Bohland J, Tedesco S, Dal'Zotto B, Brueneger W, Torkler M, Fallmann W, Loeschner H, Kaesmaier R, Nealey P, Pawloski A, *Measuring Acid Generation Efficiency in Chemically Amplified Resists with All Three Beams,* J. Vac. Sci. Technol. B, **17(6)**, 3356 – 3361, 1999.

[23] Cameron J, Fradkin L, Moore K, Pohlers G, *Comparison of Methods for Acid Quantification: Impact of Resist Components on Acid Generating Efficiency,* Proc. SPIE, **3999**, 190-203, 2000.

[24] Sohn Y, Oh H, An I, *Parameter Extraction for 193nm Chemically Amplified Resist from Refractive Index Change,* J. Vac. Sci. Technol. B, **19(6)**, 2077 – 2081, 2001.

[25] Sekiguchi A, Mack C, Isono M, Matsuzawa T, *Measurement of Parameters for Simulation of Deep UV Lithography Using a FT-IR Baking System,* Proc. SPIE, **3678**, 985 – 1000, 1999.

[26] Ziger D, Mack C, Distasio R, *The Generalized Characteristic Model for Lithography: Application to Negatively Chemically Amplified Resists,* Proc. SPIE, **1466**, 270 – 282, 1991.

[27] Jakatdar N, Bao J, Spanos C, Niu X, Bendik J, Hill S, *A Parameter Extraction Framework for DUV Lithography Simulation,* Proc. SPIE, **3677**, 447 – 456, 1999.

[28] Byers J, *Advance Resist Models (LITG106) Final Report,* SEMATECH Internal Report.

[29] Dill F, Hornberger W, Hauge P, Shaw J, *Characterization of Positive Photoresist,* IEEE Trans. Elect. Dev., **ED-22(7)**, 445 – 452, 1975.

[30] McKean D, Schaedeli U, MacDonald S, Polym. Mater. Sci. Eng., **60**, 45 – 48, 1989.

[31] Takeyama N, Ueda Y, Kusumoto K, Ueki H, Hanabata M, *Novel Analytic Method of Photoinduced Acid Generation and Evidence of Photosensitization via Matrix Resin,* ACS Symp. Ser., **537**, 53 – 63, 1994.

[32] Pawloski A, Szmanda C, Nealey P, *Evaluation of the Standard Addition Method to Determine Rate Constants for Acid Generation in Chemically Amplified Photoresist at 157 nm*, Proc. SPIE, **4345**, 1056-1065, 2001.

[33] Pawloski A, Nealey P, *Micromolar Concentrations of Base Quenchers Impact the Apparent Efficiency of Photoacid Generation in Chemically Amplified Resists*, J. Vac. Sci. Technol. B, **20(5),** 2162 – 2168, 2002.

[34] Pohlers G, Scaiano J, *A Novel Photometric Method for the Determination of Photoacid Generation Efficiencies Using Benzothiazole and Xanthene Dyes as Acid Sensors*, Chem. Mater., **9**, 3222 – 3230, 1997.

[35] Lu B, Dentinger P, Taylor J, *Evaluation of Photoacid Generators in Chemically Amplified Resists for X-ray Lithography using an On-wafer Photoacid Determination Technique*, Proc. SPIE, **3676**, 466 – 472, 1999.

[36] Pohlers G, Virdee S, Scaiano J, *Aromatic Monoazines as Fluorescent Sensors for Photoacid Generation in Thin Polymer Films*, Chem. Mater., **8(11)**, 2654 –2658, 1996.

[37] Okoranyanwu U, Byers J, Cao T, Webber S, Willson C, *Monitoring Photoacid Generation in Chemically Amplified Resist Systems,* Proc. SPIE, **3333**, 747-757, 1998.

[38] McKean D, Allen R, Kasai P, Schaedeli U, MacDonald S, *Acid Generation and Acid Diffusion in Photoresist Films,* Proc. SPIE, **1672**, 94-103, 1992.

[39] Cameron J, Chan N, Moore K, Pohlers G, *Comparison of Acid Generating Efficiencies in 248 and 193 nm Photoresists*, Proc. SPIE, **4345**, 106 – 118, 2001.

[40] Feke G, Grober R, Pohlers G, Moore K, Cameron J, *On-Wafer Spectrofluorometric Method for Determination of Relative Quantum Yields of Photoacid Generation In Chemically Amplified Resists,*"Anal. Chem., **73(14)**, 3472-3480, 2001.

[41] Morgan D, *Surface-Wave Devices for Signal Processing*, Elsevier, Amsterdam, 1985.

[42] Averine S, Chan Y, Lam Y, *Geometry Optimization of Interdigitated Schottky-barrier Metal-Semiconductor-Metal Photodiode Structures*, Solid-State Electronics, **45**, 441 – 446, 2001.

[43] Kollakowski S, Schade U, Bottcher E, Kuhl D, Bimberg D, Ambree P, Wandel K, *Silicon Dioxide Passivation of InP/InGaAs Metal-Semiconductor-Metal Photodetectors,* J. Vac. Sci. Technol. B, **14(3),** 1712 – 1718, 1996.

[44] Seto M, Rochefort C, de Jager S, *Leakage Current Reduction of Metal-Semiconductor-Metal Photodetectors by Using a Thin Interfacial Silicon Dioxide Layer,* Proc. SPIE, **3630**, 222 – 230, 1999.

[45] den Otter M, *Approximate Expressions for the Capacitance and Electrostatic Potential of Interdigitated Electrodes*, *Sensors and Actuators A*, **3165**, 1-5, 2002.

[46] Laureyn W, Van Gerwen P, Suls J, Jacobs P, Maes G, *Characterization of Nanoscaled Interdigitated Palladium Electrodes of Various Dimensions in KCl Solutions*, *Electroanalysis*, **13(3)**, 204 – 211, 2001.

[47] Van Gerwen P, Laureyn W, Laureys W, Huyberechts G, Op De Beeck M, Baert, Suls J, Sansen W, Jacobs P, Hermans L, Mertens R, *Nanoscaled Interdigitated Electrode Arrays for Biochemical Sensors*, Sensors and Actuators B, **49**, 73 – 80, 1998.

[48] Hofmann T, Schroder K, Zacheja J, Binder J, *Fluid Characterization Using Sensor Elements Based on Interdigitated Electrodes*, Sensors and Actuators B, **37**, 37 – 42, 1996.

[49] York T, Evans I, Pokusevski Z, Dyakowski T, *Capacitance Sensor for Micro Imaging*, Proc. SPIE, **4188**, 251 – 260, 2001.

[50] Chandran L, Baltes H, Korvink J, *Three-Dimensional Modelling of Capacitive Humidity Sensors*, Sensors and Actuators A, **25-27**, 243-247, 1991.

[51] Patel K, Kohl P, Allen S, *Dual Capacitor Technique for Measurement of Through-Plane Modulus of Thin Polymer Films,* J. Polym. Sci. Part B Polym. Phys., **38**, 1634-1644, 2000.

[52] Park S, Kang J, Park J, Mun S, *One-bodied humidity and temperature sensor having advanced linearity at low and high relative humidity range*, Sensors and Actuators B, **76,** 322-326, 2001.

[53] Matsuguchi M, Umeda S, Sadaoka Y, Sakai Y, *Characterization of Polymers for a Capacitive-Type Humidity Sensor Based on Water Sorption Behavior*, Sensors and Actuators B, **49**, 179 – 185, 1998.

[54] Lee C, Rhee H, Gong M, *Humidity Sensor Using Epoxy Resin Containing Quaternary Ammonium Salts*, Sensors and Actuators B, **73**, 124 – 129, 2001.

[55] Roman C, Bodea O, Prodan P, Levi A, Cordos E, Manoviciu I, *A Capacitive-Type Humidity Sensor Using Crosslinked poly(methyl methacrylate-co-(2 hydroxypropyl)-methacrylate)*, Sensors and Actuators B, **24-25**, 710 – 713, 1995.

[56] Berggren C, Bjarnason B, Jahansson G, *Capacitive Biosensors*, Electroanalysis, **13(3)**, 173 – 180, 2001.

[57] Pan Z, Hesketh P, Maclay G, *Novel Embedded Capacitive Sensors for Monitoring the Cure of Polyimide in Multichip Modules*, J. Vac. Sci. Technol. A, **11(4)**, 1396 – 1400, 1993.

[58] Boltshauser T, Chandran L, Baltes H, Bose F, Steiner D, *Humidity Sensing Properties and Electrical Permittivity of New Photosensitive Polyimides*, Sensors and Actuators B, **5,** 161 –164, 1991.

[59] Deutsch A, Swaminathan M, Ree M, Surovic C, Arjavalingam G, Prasad K, McHerron D, McAllister M, Kopcsay G, Giri A, Perfecto E, White G, *Measurement of Dielectric Anisotropy of BPDA-PDA Polyimide in Multilayer Thin-Film Packages"* IEEE Trans. Comp. Pack. Man. Techn. B, **17(4)**,486 – 492, 1994.

[60] Perry R, Green D, *Perry's Chemical Engineers' Handbook, 7th Edition*, McGraw-Hill, New York, 1997.

[61] Brydson J, *Plastics Materials, 5th Edition*, Butterworth Heinemann, Oxford, Chapter 6, 1989.

[62] Lu C, Czanderna A, *Applications of Piezoelectric Quartz Crystal Microbalances*, Elsevier, New York, Chapter 2, 1984.

[63] Kishkovich O, Kinkhead D, Higley J, Kerwin R, Piatt J, *Real-Time Methodologies for Monitoring Airborne Molecular Contamination in Modern DUV Photolithography Facilities,* Proc. SPIE, **3677**, 348 –376, 1999.

[64] MacDonald S, *Airborne Chemical Contamination of a Chemically Amplified Resist*, Proc. SPIE, **1446**, 2-12, 1991.

[65] Conley W, Babcock C, Lilygren J, Sandstrom C, Farrar N, Piatt J, Kincad D, Goodwin B, Kishkovich O, Higley J, Cate P, *Real Time Amine Monitoring and its Correlation to Critical Dimension Control of Chemically Amplified Resists for sub-0.25 um Geometry's,* Proc. SPIE, **3333**, 924 – 930, 1998.

[66] Yoshino H, Timko A, Itani T, Tanabe H, Houlihan F, Nalamasu O, *Environmental Stability of 193-nm Single Layer Chemically Amplified Resists,* NEC Res.& Develop.,**40(3),** 345 – 349, 1999.

[67] Kinkhead D, *The Value of Airborne Base Contamination Measurement in DUV Lithography*, Microlithography World, **Autumn**, 22 – 25, 1999.

[68] Higley J, Joffe M, *Airborne Molecular Contamination: Cleanroom Control Strategies,* Solid State Technol., **July**, 211 – 214, 1996.

[69] Private communication with David Ruede of Extaction Systems, Inc.

[70] Dammel R, *Diazonapthoquinone-based Resists, Vol. TT 11,* SPIE Optical Engineering Press, Bellingham, Washington, pp.12-26, 41-48, 1993.

[71] Hoskins T, Chung D, Agrawal A, Ludovice P, Henderson C, Seger L, Rhodes L, Schick R, *Bis(trifluoromethyl)carbinol-Substituted Polynorbornenes: Dissolution Behavior,* Macromolecules, **37(12)**, 4512-4518, 2004.

[72] Hall D, Osborn B, Patterson K, Burns S, Willson C, *Dissolution behavior of fluoroalcohol substituted polystyrenes*, Proc. SPIE, **4345**, 1066-1072, 2001.

[73] Ahmed S, Ludovice P, Kohl P, *Microstructure of 2,3 erythro di-isotactic polynorbornene from atomistic simulation*, Comput. Theor. Polym. Sci., **10**, 221-233, 2000.

[74] Han H, Seo J, Ree M, Pyo S, Gryte C, *Water sorption and diffusion behaviours in thin films of photosensitive polyimides*, Polymer, **39**(13), 2963-2972, 1998.

[75] Vieth W, *Diffusion In and Through Polymers: Principles and Applications*, Hanser, New York, pp. 19-47, 1991.

[76] Comyn J, *Polymer Permeability*, Elsevier, New York, pp. 7, 345 – 350, 1985.

[77] Hines A, Maddox R, *Mass Transfer: Fundamentals and Applications*, Prentice-Hall, Englewood Cliffs, Chapter 4, 1985.

[78] Mueller K, Koros W, Wang Y, Willson C, *Diffusivity Measurements in Polymers, Part III: Quartz Crystal Microbalance Techniques,* Proc. SPIE, **3049,** 871-878, 1997.

[79] Despond S, Espuche E, Domard A, *Water Sorption and Permeation in Chitosan Films: Relation Between Gas Permeability and Relative Humidity,* J. Polym. Sci., Part B: Polym. Phys. **39,** 3114 – 3127, 2001.

[80] Seo J, Cho K, Han H, *Dependence of Water Sorption in Polyimides on the Internal Linkage in the Diamine Component,* Polym. Degrad. Stab., **74,** 133-137, 2001.

[81] Nogueira P, Ramirez C, Torres A, Abad J, Cano J, Lopez J, Lopez-Bueno I, Barral L, *Effect of Water Sorption on the Structure and Mechanical Properties of an Epoxy Resin System*, J. Appl. Poly. Sci. **80,** 71-80, 2001.

[82] Krtil P, Trojanek A, Samec Z, *Kinetics of Water Sorption in Nafion Thin Films - Quartz Crystal Microbalance Study*, J. Phys. Chem. B., **105**, 7979-7983, 2001.

[83] Lehar O, Spak M, Meyer S, Dammel R, Brodsky C, Willson C, *Resist Re-Hydration During Thick Film Processing*, Proc. SPIE, **4345**, 463-474, 2001.

[84] Sebillote F, Weill A, Paniez P, *Cinetique de la diffusion de l'eau dans un film mince de photoresist*, Makromol. Chem., **186**, 1695-1699, 1985.

[85] Shibayama Y, Saito M, *Influence of Water on Photochemical Reaction of Positive-Type Photoresist*, Jpn. J. Appl. Phys., **29(10)**, 2152-2155, 1990.

[86] Zakri T, Laurent J, Vauclin M, *Theoretical Evidence for 'Lichtenecker's Mixture Formulae' Based on Effective Medium Theory,* J. Phys. D: Appl. Phys., **31**, 1589-1594, 1998.

[87] Karkkainen K, Sihvola A, Nikoskinen K, *Effective permittivity of mixtures: numerical validation by the FDTD method*, IEEE Trans. Geosci. Rem. Sensing, **38(3)**, 1303-1308, 2000.

[88] Cogdell J, *Foundations of Electrical Engineering, 2nd Edition,* Prentice Hall, Upper Saddle River, New Jersey, p 109, 1996.

[89] Askeland D, *The Science and Engineering of Materials, 3rd Edition,* PWS Publishing, Boston, Chapter 18, 1994.

[90] Rao Y, Qu J, Marinis T, Wong C, *A Precise Numerical Prediction of Effective Dielectric Constant for Polymer-Ceramic Composite Based on Effective-Medium Thoery*, IEEE Trans. Comp. Pack. Technol., **23(4)**, 680 – 683, 2000.

[91] Schweitzer R, Morris J, *Improved Quantitative Structure Property Relationships for the Prediction of Dielectric Constants for a Set of Diverse Compounds by Subsetting of the Data Set,* J. Chem. Inf. Comput. Sci.,**40**, 1253 – 1261, 2000.

[92] Wakino K, *A New Proposal on Mixing Rule of the Dielectric Constant of Mixture*, Proc. Ninth IEEE Int. Symp Appl. Ferro., 33 – 38, 1994.

[93] Sareni B, Krahenbuhl L, Beroual A, Brosseau C, *Effective Dielectric Constant of Random Composite Materials*, J. Appl. Phys., **81(5)**, 2375 – 2383, 1997.

[94] Goncharenko A, Lozovski V, Venger E, *Lichtenecker's Equation: Applicability and Limitations*, Optics Communications, **174**, 19 – 32, 2000.

[95] Martin J, Marquina J, Bottreau A, *Application of Permittivity Mixture Laws to Carbon Black Dielectric Characterization by Time Domain Reflectometry*, Proc. 16th Int. Meet. Hertz. Opt. Diel., 2001.

[96] Hayakawa T, Adachi K, *Miscibility of Poly(n-butyl acrylate)/Poly(propylene glycol) Blends. 2. Dielectric Study of Local Heterogeneity*, Macromolecules, **33**, 6840 – 6848, 2000.

[97] Neelakanata P, Subramaniam K, Gu C, *Permittivity and Permeability of Chiralic Mixture: Application of Logarithmic Law of Mixing,* Electronics Letters, **27(6)**, 496 – 497, 1991.

[98] Chylek P, Srivastava V, *Effective Dielectric Constant of a Metal-Dielectric Composite*, Physical Review B, **30(2)**, 1008 – 1009, 1984.

[99] Gao L, Gu J, *Effective Dielectric Constant of a Two-Component Material with Shape Distribution*, J. Phys. D:Appl. Phys., **35**, 267 – 271, 2002.

[100] Sareni B, Krahenbuhl L, Beroual A, Brosseau C, *Effective Dielectric Constant of Periodic Composite Materials*, J. Appl. Phys., **80(3)**, 1688 – 1696, 1996.

[101] Liu C, Wu H, *Computation of the Effective Dielectric Constant of Two-Component, Three-Dimensional Mixtures Using a Simple Pole Expansion Method*, J. Appl. Phys, **82(1)**, 345 – 350, 1997.

[102] Zeng H, Juang J, Lin J, Wu K, Uen T, Gou Y, *Temperature Dependence of the Penetration Depth and Effective Dielectic Constant Measured by $YBa_2Cu_3O_{7-\delta}$ Microstrip Ring Resonators*, Physica C, **351**, 97 – 102, 2001.

[103] Frost N, McGrath P, Burns C, *Effect of Fillers on the Dielectric Properties of Polymers,* Proc. IEEE Int. Symp. Elect. Insul., 300 – 303, 1996.

[104] Lim Y, Moore R, *Properties of Alternately Charged Coplanar Parallel Strips by Conformal Mappings*, IEEE Trans. Elec. Dev., **ED-15(3)**, 173 – 180, 1968.

[105] Farnell G, Cermak I, Silvester P, Wong S, *Capacitance and Field Distributions for Interdigital Surface-Wave Transducers*, IEEE Trans. Son. Ultrason., **SU-17(3)**, 188 – 195, 1970.

[106] Heavens O, *Optical Properties of Thin Solid Films,* Dover Publications, New York, 1991.

[107] Dill F, *Optical Lithography*, IEEE Trans. Elect. Dev., **ED-22(7)**, 440-444, 1975.

[108] Dill F, Neureuther A, Tuttle J, Walker E, *Modeling Projection Printing of Positive Photoresists,* IEEE Trans. Elect. Dev., **ED-22(7)**, 456 – 464, 1975.

[109] Widmann D, *Quantitative Evaluation of Photoresist Patterns in the 1-μm Range,* Applied Optics, **14(4),** 931 – 934, 1975.

[110] Cuthbert J, *Optical Projection Printing,* Solid State Tech., **August**, 59 – 69, 1977.

[111] Mack C, *Analytical Expression for the Standing Wave Intensity in Photoresist,* Applied Optics, **25(12),** 1958 – 1961, 1986.

[112] Mack C, *Standing Waves in Photoresist,* Microlithography World, **Spring**, 22 – 24, 1994.

[113] Mack C, *PROLITH: A Comprehensive Optical Lithography Model,* Proc. SPIE, **538,** 207 – 220, 1985.

[114] Pawloski A, Nealey P, *The Multifunctional Role of Base Quenchers in Chemically Amplified Photoresists,* Chem. Mater., **14**, 4192 – 4201, 2002.

[115] Frechet J, Eichler E, Ito H, Willson C, *Poly(p-tert-butoxycarbonyloxystyrene): A Convenient Precursor to p-hydroxystyrene Resins,* Polymer, **24,** 995 – 100, 1983.

[116] Private Communications with Matthew Romberger of Dupont Electronic Materials.

[117] Shiraishi H, Hayashi N, Ueno T, Sakamizu T, Murai F, *Novolak Resin-Based Positive Electron-Beam Resist System Utilizing Acid-Sensitive Polymeric Dissolution Inhibitor with Solubility Reversal Reactivity,* J. Vac. Sci. Technol. B **9(6)**, 3343 – 3347, 1991.

[118] Hattori T, Schlegel L, Imai A, Hayashi N, Ueno T, *Chemical Amplification Positive Deep UV Resist Using Partially Tetrahydropyranyl-Protected Polyvinylphenol,* Proc. SPIE, **1925,** 146 – 154, 1993.

[119] Watanabe O, European Patent Specification #EP 0 494 792 B1

[120] Hayashi N, Ueno T, Hesp S, Toriumi M, Iwayanagi T, *Tetrahydropyranyl Potected Polyhydroxystyrene for a Chemically Amplified Deep UV Resist,* Polymer, **33(8),** 1583 – 1588, 1992.

[121] Schlegel L, Ueno T, Shiraishi H, Hayashi N, Iwayanagi T, *Highly Sensitive Positive Deep-UV Resist Utilizing a Sulfonate Acid Generator and a Tetrahydropyranyl Inhibitor,* Microelectronic Engineering, **14,** 227 – 236, 1991.

[122] Malik S, Blakeney A, Ferreira L, Maxwell B, Whewell A, Sarubbi T, Bowden M, Van Driessche V, Fujimori T, Tan S, Aoai T, Uenishi K, Kawabe Y, Kokubo T, *Lithographic Properties of Novel Acetal-Derviatized Hydroxy Styrene Polymers,* Proc. SPIE, **3678**, 388 – 400, 1999.

[123] Hayashi N, Schlegel L, Ueno T, Shiraishi H, Iwayanagi T, *Polyvinylphenols Protected with Tetrahydropyranyl Group in Chemical Amplification Positive Deep UV Resist Systems,* Proc. SPIE, **1466,** 377 – 383, 1991.

[124] Hesp S, Hayashi N, Ueno T, *Tetrahydropyranyl- and Furanyl-Protected Polyhydroxystyrene in Chemical Amplification Systems,* J. Appl. Polym. Sci., **42**, 877 – 883, 1991.

[125] Lewellen J, Gurer E, Lee E, Chase L, Dulmage L, *Effect of PEB Temperature Profile on CD for DUV Resists,* Proc. SPIE, **3882,** 45-54, 1999.

[126] Stewart M, Somervell M, Tran H, Postnikov S, Willson C, *Study of acid transport using IR spectroscopy and SEM*, Proc. SPIE, **3999**, 665 – 674, 2000.

[127] Mueller K, Koros W, Mack C, Willson C, *Diffusivity Measurements in Polymers, Part IV: Acid Diffusion in Chemically Amplified Resists,* Proc. SPIE, **3049,** 706 – 711, 1997.

[128] Private Communications with Bruker Optics, Inc.

[129] Stewart M, Tran H, Schmid G, Stachowiak T, Becker D, Willson C, *Acid catalyst mobility in resist resins*, J. Vac. Sci. Technol. B, **20(6)**, 2946 – 2952, 2002.

[130] Postnikov S, Stewart M, Tran H, Nierode M, Medeiros D, Cao T, Byers J, Webber S, Willson C, *Study of resolution limits due to intrinsic bias in chemically amplified photoresists*, J. Vac. Sci. Technol. B, **17(6)**, 3335 – 3338, 1999.

[131] Fedynyshyn T, Thackeray J, Georger J, Denison M, *Effect of Acid Diffusion on Performance in Positive Deep Ultraviolet Resists*, J. Vac. Sci. Technol. B, **12(6)**, 3888 – 3894, 1994.

[132] Itani T, Yoshino H, Fujimoto M, Kasama K, *Photoacid bulkiness effect on dissolution kinetics in chemically amplified deep ultraviolet resists*, J. Vac. Sci. Technol. B, **13(6)**, 3026 – 3029, 1995.

[133] Itani T, Yoshino H, Hashimoto S, Yamana M, Samoto N, Kasama K, *Acid and base diffusion in chemically amplified DUV resists*, Microelectronic Engineering, **35**, 149 – 152, 1997.

[134] Itani T, Yoshino H, Hashimoto S, Yamana M, Samoto N, Kasama K, *Polymer structure effect on dissolution characteristics and acid diffusion in chemically amplified deep ultraviolet resists*, J. Vac. Sci. Technol. B, **15(6)**, 2541 – 2544, 1997.

[135] Itani T, Yoshino H, Hashimoto S, Yamana M, Samoto N, Kasama K, *A study of acid diffusion in chemically amplified deep ultraviolet resist*, J. Vac. Sci. Technol. B, **14(6)**, 4226 – 4228.

[136] Nakamura J, Ban H, Deguchi K, Tanaka A, *Effect of acid diffusion on resolution of a chemically amplified resist in X-ray lithography*, Jpn. J. Appl. Phys., **30(10)**, 2619 – 2625, 1991.

[137] Jessop J, Goldi S, Scranton A, Blanchard G, Rangarajan B, Capodieci L, Subramanian R, Templeton M, *Characterizing Acid Mobility in Chemically Amplified Resists via Spectroscopic Methods,* Proc. SPIE, **3678,** 914 – 922, 1999.

[138] Richter E, Hien S, Sebald M, *Acid Diffusion Analysis in the Chemically Amplified CARL Resist,* Microelectronic Engineering, **53**, 479 – 483, 2000.

[139] MacDonald J, *Impedance Spectroscopy: Emphasizing Solid Materials and Systems*, John Wiley & Sons, New York, 1987.

[140] Esteghamatian M, Xu G, *Effect of lithium doping on the conductivity of poly(p-phenylene vinylene)*, Synthetic Metals, **63**, 195-197, 1994.

[141] Atkins P, *Physical Chemistry,* 5th edition, W.H. Freeman and Company, New York, 835 – 838, 1994.

[142] Buchwald A, *The ion mobility of deteriorating salts in masonry materials of different moisture content*, Materials for Buildings and Structures, Euromat, **99(6)**, 157-162, 2000.

[143] Borkowska R, Reda A, Zalewska A, Wieczorek W, *Composite polyether electrolytes with Lewis acid type additives*, Electrochimica Acta, **46**, 1737 – 1746, 2001.

[144] Abe T, Gu N, Iriyama Y, Ogumi Z, *Lithium-ion-conductive polyethylene oxide based polymer electrolytes containing tris(pentafluorophenyl)borane*, J. Flourine Chemistry, **123**, 279 – 282, 2003.

[145] LEVM curve fitting software downloaded from the homepage of J. Ross Macdonald, http://www.physics.unc.edu/~macd/

VITA

The author, Cody M. Berger, was born on November 26, 1975 in Pasadena, Texas. A graduate of Sherman High School in Sherman, Texas, Cody attended The University of Texas at Austin from August 1994 until December of 1998 in pursuit of a B.S. in Chemical Engineering. After obtaining his bachelor's degree, Cody worked for 1.5 years as a plasma etch process engineer at a Texas Instruments, Inc. wafer fabrication facility in Sherman, Texas. Following his love for microelectronics, Cody returned to graduate school in August of 2000 to obtain his PhD. For the last four years, Cody has worked on photoresist characterization projects under the direction of Dr. Clifford L. Henderson in the School of Chemical & Biomolecular Engineering at Georgia Tech in Atlanta, Georgia. After obtaining his PhD, Cody will soon be returning to Texas to continue his career in microelectronics as a process development engineer for Texas Instruments, Inc.